Design and synthesis of antimycobacterial agents targeting the mycobacterial electron transport chain and the cell wall synthesis, and *in vitro* testing against different mycobacterial species

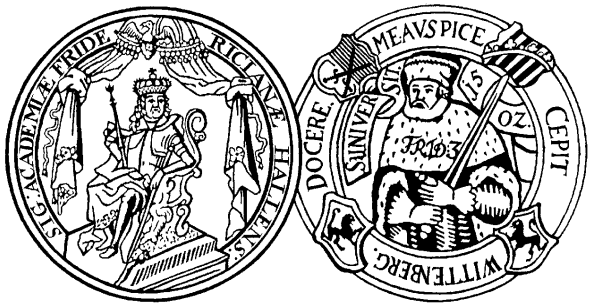

Dissertation

zur Erlangung des Doktorgrades

der Naturwissenschaften (*Doctor rerum naturalium*)

der Naturwissenschaftlichen Fakultät I-Biowissenschaften

der Martin-Luther-Universität Halle-Wittenberg

vorgelegt von

MSc.- Rana Abdelaziz

Halle (Saale),
June 2023

This thesis is based on the work done in Prof. Peter Imming's working group at Martin-Luther University and Prof. John Rubinstein's research lab at the Hospital for Sick Children, Toronto, Canada.

Part of the work reported here has been accepted for publication in ACS omega (April 2023).

Gutachter:

Prof. Dr. Peter Imming, Halle

Prof. Dr. Wolfgang Sippl, Halle

Prof. John Rubinstein, Toronto (Canada)

Datum der Disputation: 28.06.2023

Table of Contents

ACKNOWLEDGEMENTS **VI**

LIST OF FIGURES **VIII**

LIST OF TABLES **X**

LIST OF SCHEMES **X**

LIST OF ABBREVIATIONS **XI**

1. INTRODUCTION **1**

1.1. Mycobacterial infections **1**

1.1.1. Tuberculosis prevalence and treatment challenges 1

1.1.2. Infections caused by non-tuberculous mycobacteria (NTM) 2

1.2. Drug targets and Ligands **3**

1.2.1. Oxidative phosphorylation 4

1.2.1.1. Mitochondrial ETC 5

1.2.1.2. Mycobacterial ETC complexes and ATP synthase 6

1.2.1.2.1. $CIII_2CIV_2$ 8

1.2.1.3. Role in drug efflux 9

1.2.2. Mycobacterial cell wall synthesis 10

2. RESEARCH OBJECTIVES **14**

2.1. IPA analogues **14**

2.2. EMB analogues **15**

3. RESULTS AND DISCUSSION **16**

3.1. Synthesis 16

3.1.1. Imidazopyridine amides (IPAs) 16

3.1.1.1. Previously reported imidazopyridines 16

3.1.1.2. Synthetic schemes 19

3.1.1.3. Synthesis of the imidazo[1,2-a]pyridine-3- carboxylic acids (Scheme 1A) 21

3.1.1.4. Synthesis of the 2-substituted-benzoxazole tail (Scheme 1B) 23

3.1.1.5. Amide coupling (Scheme 1C, Scheme 2 and Scheme 3iii) 25

3.1.1.6. Synthesis of farnesyl and geranyl amines[127] (Scheme 3) 26

3.1.1.7. Imidazo[1,2-a]pyridine-3-carboxamide analogues (IPAs 1-30) 26

3.1.1.8. Solubility assay for IPAs[128, 129] 27

3.1.2. Cytochrome *bd*-inhibitor (31) 29

3.1.3. Ethambutol (EMB) analogues 31

3.1.3.1. Previously reported EMB analogues 31

3.1.3.2. Synthetic schemes 33

3.1.3.3. Symmetrical EMB analogues having N-atoms as substituents on aromatic system (Scheme 5 and Scheme 6) 34

3.1.3.4. Synthesis of EMB analogues with alkyl side chains (37-40) 36

3.2. *In silico* studies 38

3.2.1. Structure-activity relationship (SAR) of Q203-$CIII_2CIV_2$ IPAs 38

3.2.2. SAR of EMB 42

3.3. Biological evaluation 49

3.3.1. IPAs 49

3.3.1.1. Biochemical assays 49

3.3.1.1.1. *Msmeg* $CIII_2CIV_2$ activity assay 49

3.3.1.1.2. Mitochondrial CIII activity assay 59

3.2.2.1. In vitro growth inhibition assays 62

3.2.2.1.1. Screening against *Mtb* 63

3.2.2.1.2. Screening against *Msmeg and M. abscessus* 64

3.2.2.1.3. Screening against *M. intracellulare* 65

3.2.2.1.4. Screening against *M. intracellulare and Msmeg* in glucose-free medium 68

3.2.2.2. Minimum bactericidal concentration (MBC) in *Msmeg* 70

3.3.2. EMB analogues 71

3.2.2.3. In vitro growth inhibition assays 71

4. CONCLUSIONS AND SUGGESTIONS FOR FUTURE WORK 74

4.1. IPAs 74

4.2. EMB analogues 76

5. SUMMARY 78

6. ZUSAMMENFASSUNG 80

7. EXPERIMENTAL PROCEDURES 83

7.1. Chemistry 83

7.1.2. General 83

7.1.3. Procedures 84

7.1.3.1. Imidazopyridine amides (IPA) 84

7.1.3.1.1. Synthesis of Imidazo[1,2-a]pyridine-3-carboxylic acid Scaffold (1-15c) 84

7.1.3.1.2. Synthesis of 2-substituted 1,3-benzoxazole-5-methylamine (Scheme 1B) 89

7.1.3.1.3. General procedure for the synthesis of alkyl amines[127] (Scheme 3) 91

7.1.3.1.4. Synthesis of imidazopyridine amide analogues (1-30) 93

7.1.3.2. Cytochrome bd inhibitor 109

7.1.3.2.1. Synthesis of ethyl 2-heptylacetoacetate (1h) 109

7.1.3.2.2. Synthesis of 3-Heptyl-2-methylquinolin-4(1H)-one (31) [131, 132, 187] 109

7.1.3.3. EMB analogues 110

7.1.3.3.1. Synthesis of symmetric EMB analogues having N-atoms as substituents on aromatic systems (Scheme 5 and Scheme 6). 110

7.1.3.3.2. Synthesis of EMB analogues with alkyl side chains (Scheme 7) [142] 111

7.2. Solubility assays for IPAs 114

7.3. *In silico* 115

7.3.1. Structure-activity relationship (SAR) of Q203-*Msmeg* $CIII_2CIV_2$ 115

7.3.2. SAR of EMB and synthesized analogues 116

7.4. Biological evaluation 117

7.4.1. Biochemical assays for IPAs 117

7.4.1.1. *M. smegmatis* growth, cell lysis, and protein purification 117
7.4.1.2. NDH-2 purification from *Caldalalibacillus thermarum* strain TA2.A1 118
7.4.1.3. Sub-mitochondrial particle (SMP) preparation 118
7.4.1.4. Oxygen Consumption assays 119
7.4.1.5. NDH-2 activity assay 120
7.4.1.6. *Bos taurus* complex I activity assay 120
7.4.1.7. *Candida albicans* complex III activity assay 121
7.4.2. *In vitro* mycobacterial growth inhibition assays (IPAs and EMB) 121
7.4.2.1. *M. tuberculosis* 121
7.4.2.1.1. Testing of IPAs 121
7.4.2.1.2. Testing of EMB analogues 122
7.4.2.2. *M. intacellulare, M. smegmatis* and *M. abscessus* 123
7.4.2.2.1. Bacterial cells and culture media 123
7.4.2.2.2. MIC determination 123
7.4.2.2.3. MBC determination 124

8. REFERENCES 126

CURRICULUM VITAE (CV) 148

LIST OF PUBLICATIONS 151

CONFERENCE PRESENTATIONS 152

Acknowledgements

I would like to thank Prof. Dr. Peter Imming, Faculty of Natural Sciences I- Biosciences, Institute of pharmacy, Martin-Luther-University, Halle-Wittenberg, Germany for suggesting and supervising this research project. I express my deepest thanks for his endless support during my PhD. I am grateful for his trust and encouragement that helped me throughout the project. His constructive feedback has helped me learn a lot.

I would like to express my gratitude to our collaborator Prof. John L. Rubinstein, Departments of Medical Biophysics and Biochemistry, The University of Toronto, Toronto, Canada for the opportunity to do the biochemical assays and learn how to build a protein model and his supervision during my stay in Canada.

I am grateful to my dear colleagues Lea Mann, Adrian Richter, Markus Lang, Ruth Feilcke, Paul Palme, Andreas Beuchel, Christoph Lehmann, for the pleasant working atmosphere, our endless laughs, food gatherings, outings, events, and memorable trips. I would also like to acknowledge our technicians Ilona Fritsche, Julia Seiser and the diploma student Jan köhne. I would like to also thank Dr. Dina Robaa for dedicating time to introduce me to the Schrödinger software and her help with the docking.

Thanks to Prof. Rubinstein's working group (Gautier Courbon, Yingke Liang, Thamiya Vasanthakumar, Sarah Bickers, Hanlin Wang and Stephanie Bueler) at the Hospital for Sick Children for making my stay in Toronto unforgettable. Special thanks to Dr. Justin Di Trani, for his help in the biochemical assays and for teaching me the process of protein isolation to running biochemical assays. I had so much fun working with him in the lab. I would also like to acknowledge David J. Yanofsky for the electron cryomicroscopy structures of *Msmeg* $CIII_2CIV_2$.

I would like to thank Dr. Norbert Reiling, Head of the Division of Microbial Interface Biology, Research Center Borstel for his cooperation performing the assays on *Mtb* for testing the activity of EMB analogues and Dr. Henok Asfaw, Departments of Medicine and Microbiology and Immunology, Life Sciences Institute, University of British Columbia, Vancouver, Canada for testing the activity of IPAs in *Mtb.*

I would like to thank my colleagues Dr. Adrian Richter and Lea Mann for performing the assays on *Msmeg*, *M. abscessus* and *M. intracellulare*.

I wish to thank my friends Sara Atwa, Salma elShamy, Nouran Emad, Menna Mohamed, Fatma Ismail, Dina Ismail, Yara Nawwar, Sherif Reda, Ahmed Osama, Abdelrahman Nagi Hazem Shawkat, Mariam Khaled, Shahir Morcos, Carine Magued for their support and encouragement.

Finally, I must express my very profound gratitude to my mother and sister for providing me with unfailing support and continuous encouragement throughout my years of study and through the process of researching and writing this thesis. This accomplishment would not have been possible without them. Thank you.

List of Figures

Figure 1. Examples of anti-mycobacterial drug targets and their inhibitors. Adapted from [43, 44]. 4
Figure 2. Mitochondrial ETC. Adapted from[49]. 5
Figure 3. Summary of electron flow in the mycobacterial ETC. Adapted from[50, 51].....6
Figure 4. Mycobacterial ETC under aerobic conditions. 7
Figure 5. Schematic diagram of CIICIV (half of the supercomplex). Adapted from[48]. 9
Figure 6. Examples of efflux pumps in mycobacteria. Adapted from[47].....10
Figure 7. Simplified diagram of mycobacterial cell envelope. Adapted from[44, 78]. 11
Figure 8. Structure of *Msmeg*-EmbB bound to di-arabinose. 12
Figure 9. Diagram showing the catalytic reaction of Emb proteins. Adapted from[80]. 13
Figure 10. *Msmeg* EmbA catalytic site. 13
Figure 11. Examples of drugs on the market with the IP-scaffold. 16
Figure 12. Structures of **ND-008454** and **ND-09759**. 17
Figure 13. Structures of the lead compound (**1**) and **Q203**. 17
Figure 14. IPA analogue with a benzoxazole ring system. 18
Figure 15. *N*-(2-phenoxyethyl)-IP-3-carboxamides. The analogues displayed are examples of IPA analogues that have different targets from that of Q203. 18
Figure 16. Structures of IPA analogues with alkaline fused ring systems. Both analogues have shown high potency against MDR-*Mtb*, similar to Q203.[111] 19
Figure 17. Bromination of ethyl 3-oxo-pentanoate with NBS and ammonium acetate (NH_4OAc) as a catalyst.[105, 86] 22
Figure 18. Radical initiation by AIBN.[116, 117] 22
Figure 19. Mechanism of imidazo[1,2-a]pyridine formation.[114] 22
Figure 20. Cyclization of the amide intermediate using pyridinium p-toluenesulfonate as a catalyst. [86] 23
Figure 21. Mechanism of benzoxazole formation using $MeSO_3H$ as a catalyst.[121] 24
Figure 22. By-products from the amide coupling using HATU. 26
Figure 23. HSQC spectrum of compound **4.** 27
Figure 24. Q203 graph as an example of the graph output from the nephelometry solubility assay. 28
Figure 25. Left: analytical RP-HPLC traces of **1h**. **Right:** NMR spectra of the two peaks after being separated by preparative HPLC.. 30
Figure 26. Proposed reaction mechanism[134] of **1h** with aniline to form compound **31.** 30
Figure 27. *N*,*N*-diisopropylenediamine (lead compound, **1**), (+)-(2S,2S')-2,2'-(ethylenediamino)di(butan-1-ol) (EMB, **2**). **3** and **4** are examples of reported EMB analogues with weak activity against *Msmeg*.[145] 31

Figure 28. Examples of EMB analogues.....32
Figure 29. Tripartite hybrid compounds with a broad antimicrobial spectrum.[144].....32
Figure 30. Structures of EMB analogues**.**.....34
Figure 31. Positive mode MS-spectra. **(A)** APCI-MS **(B)** ESI-HRMS of **33**.....35
Figure 32. Structures of EMB and SQ109 compared to **38**, **39** and **40**.....37
Figure 33. **(A)** Q_o site of *Msmeg* $CIII_2CIV_2$. **(B)** Structures of MK and MKH_2.....38
Figure 34. Q203 binding site interactions. 40
Figure 35. 2D representations of compounds **24** (**A**) and **27** (**B**)......41
Figure 36. EMB interactions at *Mtb*-EmbB active site.....43
Figure 37. 2D representations of compounds **32** (**A**) and **33** (**B**)**.**.....46
Figure 38. 2D representations of compounds **34** (**A**) **and 35** (**B**)......47
Figure 39. 2D representations of compounds **36** (**A**) **and 37** (**B**).....48
Figure 40. Examples of MKH_2 analogues used in $CIII_2CIV_2$ activity assays**.**.....50
Figure 41. Possible by-products from DMW chemical reduction. 50
Figure 42. Oxygen consumption assay. 51
Figure 43. NADH oxidation monitored by absorption at λ= 340 nm. NDH-2 activity was monitored spectrophotometrically by following the oxidation of NADH. 52
Figure 44. Average % activity against *Msmeg* $CIII_2CIV_2$ **(**Q203 and compounds **24-27**).....53
Figure 45. Average % activity against *Msmeg* $CIII_2CIV_2$ (**1-8**, R^1= Br). 54
Figure 46. IC_{50} of Q203 (**A**) and compound **27** (**B**). 58
Figure 47. Sub-mitochondrial membrane (SMP). Adapted from[49].....59
Figure 48. NADH oxidation in SMP at [10 µM]. **27** and **Q203** do not bind to complex I. 60
Figure 49. Comparison of the activity in sub-mitochondrial particles.....61
Figure 50. $CIII_2$ activity assay.....62
Figure 51. The structure of compounds **24** and **26**. R^1 is coloured in red.....64
Figure 52. Superimposition of the QcrB subunit of *M. abscessus* with *Mtb* and *Msmeg*. 65
Figure 53. MSA of the QcrB orthologs in mycobacterial species. 66
Figure 54. Overlay of an AlphaFold model of *M. intracellulare* QcrB subunit with *Mtb* QcrB subunit 68
Figure 55. Bactericidal activity of Q203+**31** against *Msmeg* which was grown in a medium supplemented with oleic acid.....71
Figure 56. % Growth of EMB and **34** (**A**), **33** and **35** (**B**). 72
Figure 57. % Growth of compounds **36** and **37**. 73
Figure 58. Summary of the SAR of IPAs. 74

List of Tables

Table 1. Solubilities of Q203 and IPAs in PBS buffer. 28
Table 2. Average % inhibition (µM) of *Msmeg* $CIII_2CIV_2$ by Q203 and IPA analogues. 55
Table 3. A brief comparison between *Mtb*, *Msmeg*, *M. abscesuus* (*Mabs*) and *M. intracellulare* (*M. intra*). 63
Table 4. The minimum inhibitory concentrations (MIC_{90}) in µM of the tested IPAs against *Mtb*, *Msmeg*, *M. abscessus* (*Mabs*) and *M. intracellulare*. 67
Table 5. Comparison of MIC_{90} against *Msmeg* and *M.intracellulare* in glucose-rich (ADS) and glucose-free (oleic acid) media. 70
Table 6. MIC_{95} (µM) of the tested EMB analogues against *Mtb*, *Msmeg*, *M. abscessus* and *M. intracellulare* 73

List of Schemes

Scheme 1. General synthetic scheme, (A) Synthesis of imidazo[1,2-a]pyridine-3-carboxylic acids, (B) Synthesis of 2-substitutedbenzo[d]oxazole-5-methylamine, (C) Synthesis of **1-24**, and **26**[a] 20
Scheme 2. Synthesis of **25**, **29** and **30**[a] 21
Scheme 3. Synthesis of **27** and **28**[a] 21
Scheme 4. Synthesis of cytochrome bd-inhibitor **(31)**[130] 29
Scheme 5. Synthesis of compounds **32** and **33**. 33
Scheme 6. Synthesis of compound **35.** 33
Scheme 7. Synthesis of compounds **37-40.**[142] 34

List of Abbreviations

ABC	ATP-binding cassette
ACN	Acetonitrile
ADP	Adenosine diphosphate
AftA,B,C and D	Arabinosyl transferases A, B, C and D
AG	Arabinogalactan
AIBN	Azobisisobutyronitrile
AIDS	Acquired immunodeficiency syndrome
AOX	Alternative oxidase
APT NMR	Attached Proton Test NMR
AraTs	Arabinosyl transferase family
ATP	Adenosine triphosphate
BBr_3	Boron tribromide
BDQ	Bedaquiline
CC_{50}	Cytotoxic concentration inhibiting 50% growth
CI	Complex I, NADH dehydrogenase (NDH-1)
CII	Complex II, succinate dehydrogenase (SDH)
CIII	Complex III, cytochrome bc_1 complex
CIV	Complex IV, cytochrome *c* oxidase, cytochrome aa_3 oxidase
$CIII_2CIV_2$	Cytochrome bc-aa_3 supercomplex / supercomplex
$CDCl_3$	Deuterated chloroform
CD_3OD	Deuterated methanol
$CHCl_3$	Chloroform
Cryo-EM	Cryogenic electron microscopy
CSF	Cerebrospinal fluid
CytCO	Cytochrome *c* Oxidase
Cyt.	Cytochrome
DBE	Dibromoethane
DCM	Dichloromethane
DDM	n-Dodecyl-β-maltoside
DIAD	Diisopropyl azodicarboxylate
DIPEA	*N*,*N*-Diisopropylethylamine

DME	1,2-dimethoxyethane
DMF	*N*,*N*-Dimethylformamide
DMSO	Dimethyl sulfoxide
DMW	2,3-dimethyl[1,4]naphthoquinone
$DMWH_2$	2,3-dimethyl[1,4]naphthoquinol
DP	Decaprenyl phosphophate
DPA	Decaprenyl-phosphoryl-D-arabinose
EDC.HCl	1-(3-dimethylaminopropyl)-3-ethylcarbodiimide hydrochloride
EMB	Ethambutol
EP	Efflux pump
ESI-HRMS	High-resolution electrospray ionization mass spectrometry
EtOAc	Ethyl acetate
EtOH	Ethanol
ETC	Electron transport chain
FR	Fumarate reductase
FQ	Fluoroquinolones
GDN	Glyco-diosgenin
GT-C	Glycosyl transferases C superfamily
GTBS	GDN-Tris buffered saline
H-bond	Hydrogen bond
HATU	1-[Bis(dimethylamino)methylene]-1*H*-1,2,3-triazolo[4,5-b]pyridinium-3-oxide hexafluorophosphate
HCO	Heme-copper oxidase
HOBt	1-hydroxybenzotriazole
HPLC	High-performance liquid chromatography
HRMS	High-resolution mass spectrometry
HSQC NMR	Heteronuclear single quantum correlation experiment
Hz	Hertz
INH	Isoniazid
IP	Imidazopyridine
IPA	Imidazopyridine amide/ Imidazo[1,2-a]pyridine-3-carboxamide
J	Coupling constant
LAM	Lipoarabinomannan

M.	*Mycobacterium*
M.intra	*M. intracellulare*
m.p.	Melting point
MAC	*Mycobacterium avium complex*
mAGP	Mycolyl-arabinogalactan-peptidoglycan
MAI	*Mycobacterium avium intracellulare*
MDR	Multi-drug resistant
MeOH	Methanol
$MeSO_3H$	Methane sulfonic acid
MFS	Major facilitator family
MIC	Minimum inhibitory concentration
MK / MK-9 (II-H_2)	Menaquinone
MKH_2	Menaquinol
MOPS	(*N*-morpholino)propanesulfonic acid
MSA	Multiple sequence alignement
Msmeg	*Mycobacterium smegmatis*
Mtb	*Mycobacterium tuberculosis*
$NaHCO_3$	Sodium bicarbonate
NBS	N-bromosuccinamide
NDH	NADH dehydrogenase
NH_4OAc	Ammonium acetate
NR	Nitrate reductase
NTM	Non-tuberculous mycobacteria
PBS	Phosphate buffered saline
PD	Periplasmic carbohydrate-binding domains
PG	Peptidoglycan
PMF	Proton motive force
PMSF	Phenylmethylsulfonyl fluoride
ppm	Parts per million
PyBOP	Benzotriazole-1-yl-oxy-tris-pyrrolidino-phosphonium hexafluorophosphate
PZA	Pyrazinamide
PL	Periplasmic loop
$\Delta\psi$	Membrane potential

ΔpH	Transmembrane proton gradient
Q	Ubiquinone
QH_2	Ubiquinol
RIF	Rifampicin
rmsd	Root mean square deviation
RND	Resistance nodulation division
RNS	Reactive nitrogen species
RNU	Relative nephelometric units
ROS	Reactive oxygen species
SAR	Structure activity relationship
SDH	Succinate dehydrogenase
SMP	Sub-mitochondrial particle
SMR	small multidrug resistance
SOD	Superoxide dismutase
SP	Standard precision
TBDPSiCl	*Tert*-butyldiphenylsilylchloride
TFA	Trifluoracetic acid
THF	Tetrahydrofuran
TLC	Thin layer chromatography
TM	Trans-membrane
XDR	Extended-drug resistant
XP	Extra precision

1. Introduction

1.1. Mycobacterial infections

1.1.1. Tuberculosis prevalence and treatment challenges

Tuberculosis (TB) is one of the oldest and most pervasive respiratory diseases and remains one of the leading causes of death worldwide.[1, 2, 3, 4, 5] In 2021, 10.6 million new TB infections and 1.6 million deaths were reported.[2] The majority of cases and deaths occur in low- and middle-income countries, particularly in Africa and Asia.[2,5] In these countries, poverty, malnutrition, poor living conditions, and limited access to healthcare can all contribute to the high incidence and prevalence of TB. The disease is caused by *Mycobacterium tuberculosis* (*Mtb*), a slow-growing acid-fast bacterium that can be transmitted by air droplets. It primarily affects the lungs, but can also infect other areas in the body, such as lymph nodes, the skeleton, skin and soft tissues. TB bacilli can adapt to the high oxidative stress levels in human macrophages and survive for years by down-regulating their metabolism and entering a state of dormancy until the host's immune status weakens and they become active.[6] Long-term combination therapy, most commonly a combination of isoniazid (INH), rifampicin (RIF), pyrazinamide (PZA), and ethambutol (EMB), and problems with patient compliance with the prescribed regimen, lead to the continuous emergence of multidrug-resistant (MDR) and extensively drug-resistant (XDR) *Mtb.* The lack of rapid, cheap, point-of-care diagnostics to diagnose MDR-TB and insufficient second-line drug options add to the challenges of TB treatment.

The COVID-19 pandemic has had a significant impact on TB control efforts, leading to disruptions in diagnosis and treatment and a potential increase in TB cases and deaths.[7] The pandemic has led to reduced access to healthcare services for many people with TB, due to fear of exposure to COVID-19, as well as economic and travel restrictions.[8] Social distancing, lockdowns and travel restrictions are likely to reduce the risk of TB spreading outside the household, but increase the risk of TB transmission within the household and are outweighed by the increase in TB deaths in the last three years compared to 2019 (20% increase in 2021).[1, 2, 9] Moreover, the COVID-19 pandemic has also negatively affected TB research and development, with delays in clinical trials and a reduction in funding for TB research. The global health communities continue to work towards reducing the burden of TB through increased investment in research, improved diagnostic and treatment approaches, and expanded

access to care for all those in need. The goal is to ensure that progress made in the fight against TB is not lost and that TB remains a priority on the global health agenda.[1, 7, 8, 9]

1.1.2. Infections caused by non-tuberculous mycobacteria (NTM)

Non-tuberculous mycobacteria (NTM) are a group of bacteria in the genus *Mycobacterium* which are not *Mtb* and *Mycobacterium leprae*. They are ubiquitous in the environment and can cause infections in humans. NTM infections in general are becoming more common and are recognized as a growing public health concern.

NTM infections can cause a variety of diseases, including lung infections, skin infections, and infections in other parts of the body such as the lymph nodes, bones, and joints. Similar to *Mtb*, immunocompromised individuals are at increased risk of developing NTM infections. Additionally, people who are exposed to contaminated water sources, such as hot tubs or poorly maintained swimming pools, may also be at increased risk of NTM infection.[10, 11] NTM infections can be difficult to diagnose and treat because they may not respond to traditional TB treatments and antibiotics. Treatment of NTM infections typically involves a combination of a three-drug regimen of either clarithromycin or azithromycin, plus RIF and EMB, and may take up to 12 months to complete. In some cases, surgical intervention may be required to treat the infection.[12] In some populations, such as those with cystic fibrosis, the prevalence of NTM infections is estimated to be up to 20%.[13]

Among the ~200 different NTM species identified, pulmonary infections are caused mostly by *Mycobacterium avium* complex (MAC) and *Mycobacterium abscessus* complex (MABC). [14]

M. abscessus complex (MBC)

M. abscessus and its subspecies *abscessus*, *bolletii*, and *massiliense* are by far the most common causative agents of pulmonary disease due to rapidly growing mycobacteria.[15] They are found in two morphotypes, smooth and rough. The smooth variant infects humans and can survive intracellularly in macrophages for years without symptoms. Certain factors, as yet unknown, induce a morphological change to the rough variant which is more virulent. It can aggregate extracellularly to form colonies that induce a proinflammatory response, with the result being massive tissue destruction. Phagocytosis is prevented by the large size of these aggregated colonies. [16, 17, 18] They can be found in water, soil, and dust. They can also be a source of contamination for medications and products, including medical devices. *M. abscessus* infections are typically difficult to treat and can cause serious health problems, particularly in people with cystic fibrosis.[19] It is resistant to most anti-mycobacterial agents, including

macrolides [20, 21] highlighting the need of discovering new antibiotics that target *M. abscessus* infections.

***M. avium* complex (MAC)**

MAC are slowly growing NTM which consist of 12 separate species.[22] Pulmonary infection in humans is caused commonly by *M avium, M. intracellulare and M. chimera*. MAC species are also known to show considerable variations in the morphology of their colonies, ranging from smooth, thin, transparent, to smooth and opaque, to rough.[22] *M avium* and *M. intracellulare* are collectively referred to as *Mycobacterium avium-intracellulare* (MAI) due to the difficulty in differentiating between them.[22, 23] MAC are the frequently isolated NTM in clinical cystic fibrosis, and immunodeficiency diseases, such as AIDS in China and USA.[24] Transmission to humans occurs via inhalation, contact, or smear infection.[25] Reports have shown that with *M. intracellulare* lung infections disease prognosis is worse than in *M. avium* lung infections.[26] The international guidelines recommended treatment with three-drug combination therapy consisting of a macrolide (azithromycin or clarithromycin), EMB, RIF. In case of severe or macrolide-resistant MAC pulmonary infections parenteral amikacin or streptomycin are added to the drug regimen.[12, 25] With prolonged treatment, 65% of the patients achieve culture conversion and some patients even relapse.[27]

1.2. Drug targets and Ligands

Mycobacterial (*Mtb* and NTM) drug targets include cell wall synthesis, nucleic acid synthesis, protein synthesis, and oxidative phosphorylation. There are several drugs on the market and under development for the treatment of mycobacterial infections. The first-line anti-TB drugs are examples of drugs that are already on the market: RIF (RNA polymerase inhibitor)[28], PZA (membrane potential disruption)[29], INH (mycolic acid synthesis inhibitor)[30] and EMB (arabinogalactan and lipoarabinomannan synthesis inhibitor).[31] In addition, there are protein synthesis inhibitors such as streptomycin and kanamycin (aminoglycosides) and macrolides such as azithromycin and clarithromycin (protein synthesis inhibitors).[32] The third-generation fluoroquinolones (FQ) such as moxifloxacin and gatifloxacin act as DNA gyrase inhibitors. [32] The cell wall synthesis inhibitors PBTZ169 and BTZ043[33], the protein synthesis inhibitors sutezolid and AZD5847[34, 35], the ATP synthase inhibitor TBAJ-587[36] and the cytochrome *bc-aa*$_3$ supercomplex inhibitor telacebec[37] (Q203) are examples of anti-TB drugs in clinical

trials.[38] Pretonamid (PA-824)[39], delamanid[40, 41] and SQ109[42] are examples of drug candidates with multiple targets (**Figure 1**).

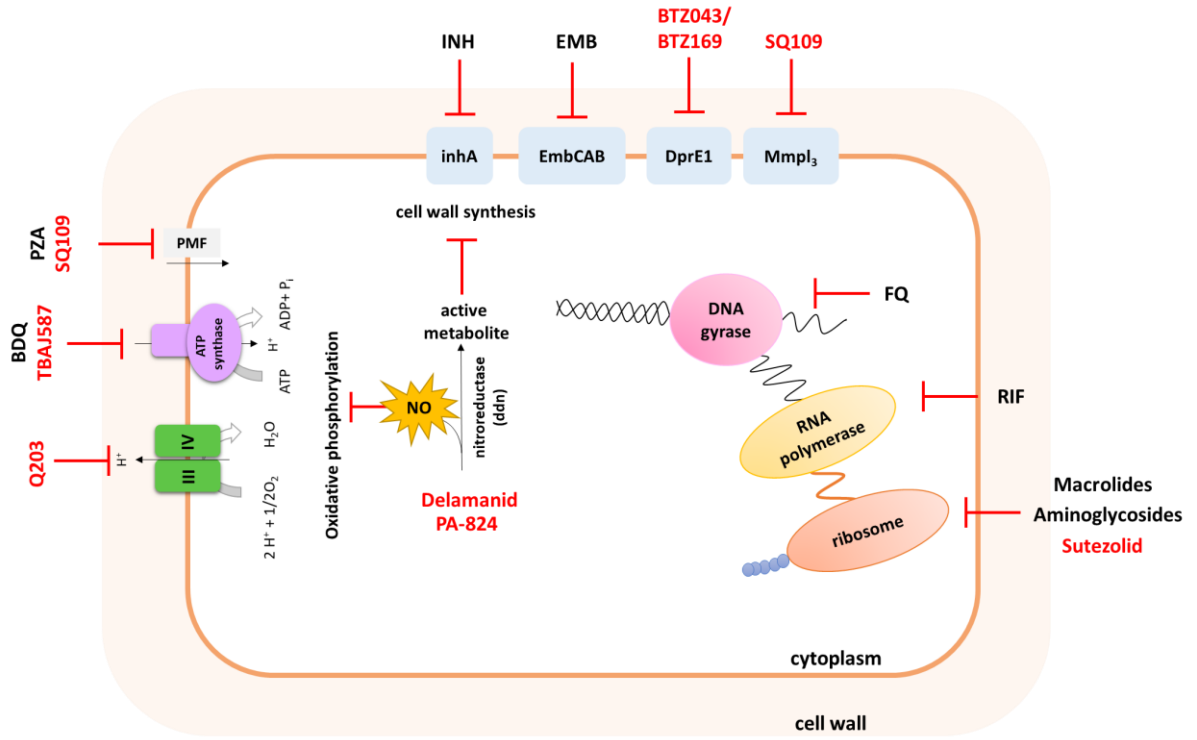

Figure 1. Examples of anti-mycobacterial drug targets and their inhibitors. Drugs on the market are coloured in black, while the drug candidates in clinical trials are coloured in red. Adapted from [43, 44].

The long duration of treatment, the continuous emergence of resistant TB strains and the resistance of NTM to most anti-TB drugs necessitate the search for new drug candidates and the understanding of the mechanism of action of the drug targets and the mycobacterial rescue mechanisms.

In the following sections, we are going to discuss oxidative phosphorylation and mycobacterial cell wall synthesis in more detail.

1.2.1. Oxidative phosphorylation

Mycobacterial cellular respiration is a promising target for TB treatment.[45,46] Cellular respiration results in the production of adenosine triphosphate (ATP), the chemical energy currency in cells, using energy from the oxidation of nutrients. Cellular respiration needs the combined activities of the electron transport chain (ETC) and ATP synthase. The ETC is a series of membrane-embedded protein complexes that establish a transmembrane proton motive force (PMF), using energy from a series of redox reactions. The PMF drives ATP

synthesis by the F_1F_o-ATP synthase.[47] Structural and mechanistic differences between mycobacterial ETC complexes compared to ETC complexes from eukaryotic mitochondria and other bacteria allow selective inhibition of mycobacterial respiration.

1.2.1.1. Mitochondrial ETC

The human mitochondrial ETC consists of four complexes (I to IV) embedded in the inner mitochondrial membrane. As shown in **Figure 2**, electrons from the oxidation of NADH and succinate by complexes I and II are transported to complex III (cytochrome bc_1) via ubiquinone (Q), a membrane-embedded electron carrier. Complex III transfers electrons from the oxidation of ubiquinol to ubiquinone to soluble cytochrome *c*, which in turn transfers electrons to complex IV (cytochrome *c* oxidase or cytochrome aa_3) where oxygen is reduced to water.[48,49]

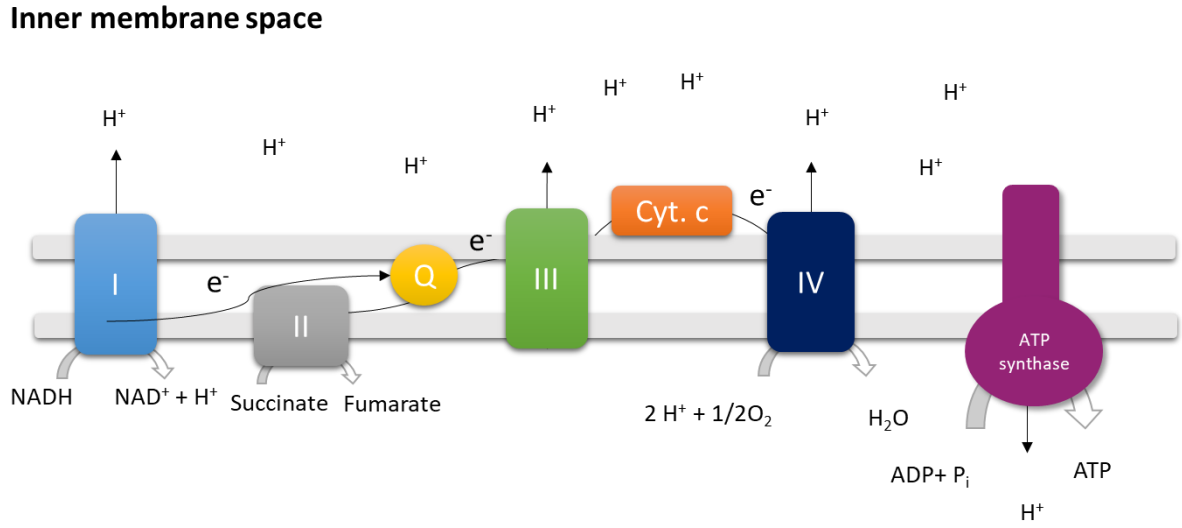

Figure 2. Mitochondrial ETC. Adapted from[49].

1.2.1.2. Mycobacterial ETC complexes and ATP synthase

The mycobacterial ETC can utilize various electron donors and acceptors depending on its microenvironment (**Figure 3**).

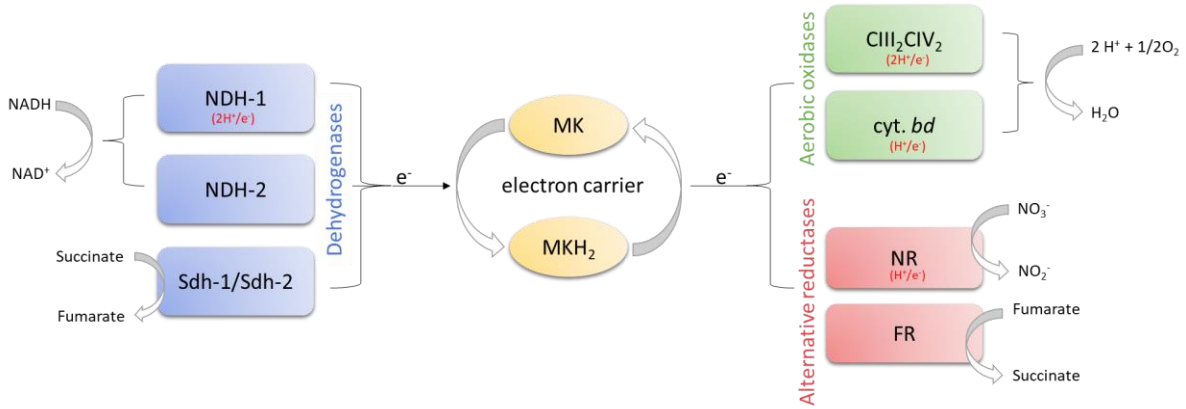

Figure 3. Summary of electron flow in the mycobacterial ETC. Electrons are transported via MK (electron carriers) from dehydrogenases (electron donors) to aerobic oxidases or anaerobic reductases (electron acceptors). Nitrate reductase (NR) and fumarate reductase (FR) are examples of alternative electron acceptors under anaerobic conditions. Adapted from[50, 51].

Electrons produced during metabolic reactions are transferred to the ETC mainly through the oxidation of NADH to NAD^+ via NADH dehydrogenases (NDH).[52] Mycobacteria have two types of NADH dehydrogenases, a proton-pumping NDH-1 (complex I, the homologue of complex I in mitochondria)[53] and a nonproton-pumping NDH-2 (**Figure 3**). There are two types of NDH-2 in *Mtb*, Ndh and NdhA. While Ndh is common among all mycobacteria, some mycobacteria such as *M. smegmatis (Msmeg)*, *M. abscessus* and *M. leprae* lack the NdhA enzyme. It has been reported that NDH-2 is essential for mycobacterial growth (Ndh)[47, 54] while NDH-1 may have an important role in virulence, for example in *Mtb*.[54] The nonproton-pumping NDH-2 is important for maintaining the electron flux (maintains PMF and replenishes [NAD^+] pool) in the absence of growth.[55] In *Mtb*, for example, the electron transfer is not affected by the back pressure of the PMF in the absence of growth and high rates of ATP synthesis due to the coupling of NDH-2 to cytochrome *bd* oxidase.[51]

Succinate dehydrogenase (SDH, complex II) is an electron donor that couples oxidative phosphorylation to carbon metabolism. SDH catalyzes the oxidation of succinate to fumarate in the TCA cycle (citric acid cycle in the cytoplasm), leading to the reduction of menaquinone (MK) to menaquinol (MKH_2, **Figure 3)**.[56] Most mycobacteria express two types of SDH: sdh-

1 and sdh-2. Sdh-1 is the primary aerobic SDH and its inhibition under hypoxic conditions leads to the accumulation of succinate.[57] The oxidation of succinate is taken over by Sdh-2 or the fumarate reductase[58] (FR, absent in *Msmeg*[56]). Previous studies have shown that sdh-2 is essential for growth and the generation of membrane potential under hypoxia.[56, 59, 60]

Electrons from redox reactions in NDH-1, NDH-2, and SDH are transported via menaquinone[61] (MK-9 (II-H_2)[55], electron carrier) to one of the mycobacterial respiratory terminal oxidases, the cytochrome *bc-aa*$_3$ supercomplex ($CIII_2CIV_2$) or the cytochrome *bd* complex[62] under aerobic conditions (**Figure 4**).[50, 51]

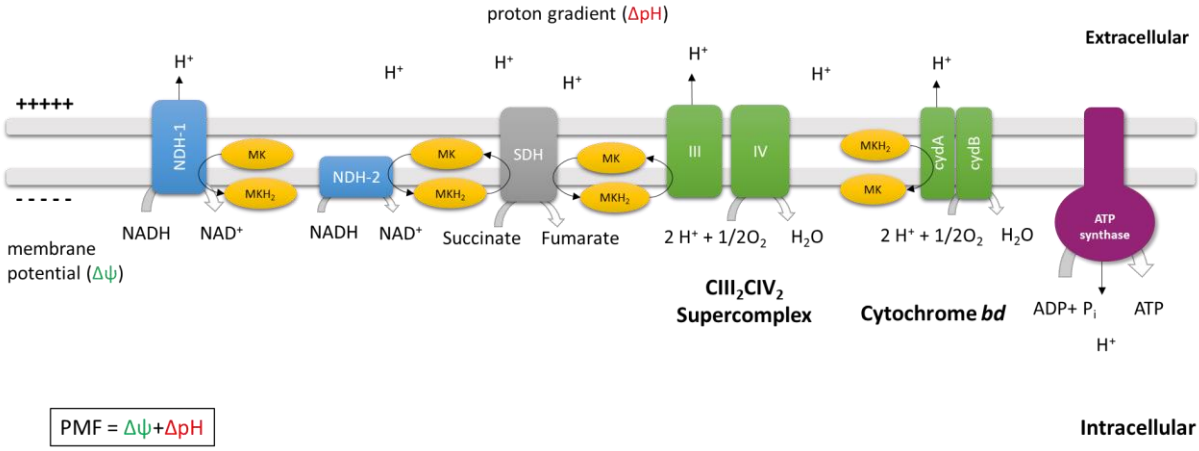

Figure 4. Mycobacterial ETC under aerobic conditions. ‘‘Adapted with permission from [Abdelaziz, R.; Di Trani, J. M.; Sahile, H.; Mann, L.; Richter, A.; Liu, Z.; Bueler, S. A.; Cowen, L. E.; Rubinstein, J. L.; Imming, P. Imidazopyridine Amides: Synthesis, *Mycobacterium Smegmatis* $CIII_2CIV_2$ Supercomplex Binding and in Vitro Antimycobacterial Activity. *ACS Omega* **2023**. https://doi.org/https://doi.org/10.1021/acsomega.3c02259]. Copyright [2023] American Chemical Society’’

The cytochrome *bd* oxidases[62] are a type of terminal oxidase that helps mycobacteria survive under stress conditions, i.e. hypoxia, RNS or ROS production as a defence mechanism of the host cell.[63] They are structurally different from other terminal oxidases, like Heme-copper oxidase (HCO) and alternative oxidases (AOX, cyanide insensitive oxidases)[64]. They can oxidize MKH_2 to MK and reduce O_2 to H_2O, functioning as an alternative pathway when $CIII_2CIV_2$ is inhibited. Alternative electron acceptors that can operate under anaerobic conditions are nitrate and fumarate via nitrate reductases (NR) and fumarate reductases (FR)[58] (**Figure 3**).[55]

The movement of electrons across the ETC generates a membrane potential ($\Delta\psi$)[65] which leads to the development of a transmembrane proton gradient (ΔpH) and eventually the PMF. The PMF is essential for ATP synthesis via F_1F_o-ATP synthases, where the electrochemical

potential energy generated by the PMF is converted into chemical energy (ATP). ATP can also be synthesized by substrate-level phosphorylation.[53] Energy produced during metabolic steps is used for ATP synthesis. This method provides rapid ATP regardless of whether the ETC is functional. However, mycobacteria mainly depend on ATP produced by oxidative phosphorylation.[53, 66]

1.2.1.2.1. $CIII_2CIV_2$

Mycobacteria lack soluble cytochrome *c*, and thus the transfer of electrons from complex III to IV occurs differently than in mitochondria. Complexes III and IV in mycobacteria form an obligatory supercomplex ($CIII_2CIV_2$), rather than existing as two separate entities (**Figure 4**).[48,67] Instead of Q, mycobacteria use MK as an electron carrier. Complex III has three subunits: QcrA, QcrB, and an anchored QcrC domain with two c-type hemes that transfer electrons to complex IV.

Complex III: The QcrA subunit contains FeS protein ([2Fe-2S], Rieske protein) which is homologous to the FeS protein in the canonical cytochrome bc_1 (complex III). In mitochondrial complex III, the FeS protein head domain moves away from the electron donor (QH_2) to the electron acceptor cytochrome c_1. However, electron cryomicroscopy data showed that in mycobacteria FeS center is fixed while the diheme cytochrome cc (cyt. cc, QcrC) head domain adopts two conformations: open and closed, allowing the transfer of electrons between the FeS center and complex IV.[48] A superoxide dismutase subunit (SOD) in contact with the QcrA and/or QcrC subunits in *Msmeg* $CIII_2CIV_2$ is thought to detoxify the reactive oxygen species (ROS) generated as a defence mechanism in the host phagolysosomes of macrophages. [48,67] The QcrB subunit contains heme b_L, and heme b_H. It has two menaquinone binding sites: Q_o, where MKH_2 is oxidized to MK and Q_i where MK is reduced to MKH_2 in a process known as the Q cycle (**Figure 5**).

Complex IV: The cytochrome c oxidase (CytcO), like its mitochondrial counterpart, belongs to the type A heme-copper oxidase A1 subfamily (HCO). It consists of CtaC (homologous to subunit I) which contains 2 Cu_A ions, CtaD (subunit II homologue) which contains heme *a*, heme aa_3 and Cu_B, CtaE (subunit III), CtaF, CtaI and CtaJ. [68] Similar to mitochondrial Complex IV, it has two proton transfer pathways (K and D pathways).[69]

The diagram below (**Figure 5**) explains the flow of electrons (blue arrows) in one-half of $CIII_2CIV_2$ where oxygen is partially reduced into water ($½\ O_2 + 2e^- + 2H^+ \rightarrow H_2O$). One

electron from MKH_2 oxidation in the Q_o site is transferred to FeS (QcrA) and then via the cyt. c_I and cyt. c_{II} (QcrC) to Cu_A; the primary electron acceptor in complex IV. Cu_A transfers the electron via heme *a* to the catalytic site (heme aa_3 and Cu_B) where oxygen is reduced.

The second electron is transferred to heme b_L and then to heme b_H where MK is reduced to MK^- (semiquinone). This cycle is repeated twice to fully reduce MK to MKH_2 and a total of 4 H^+ are pumped to the periplasm. The full reduction of oxygen requires a total of eight protons and four electrons.[48, 68] Q203 (telacebec, discussed in section **3.1.1.1**) binds at the Q_o site, preventing the oxidation of MKH_2 to MK, thus blocking the transfer of electrons to complex IV.

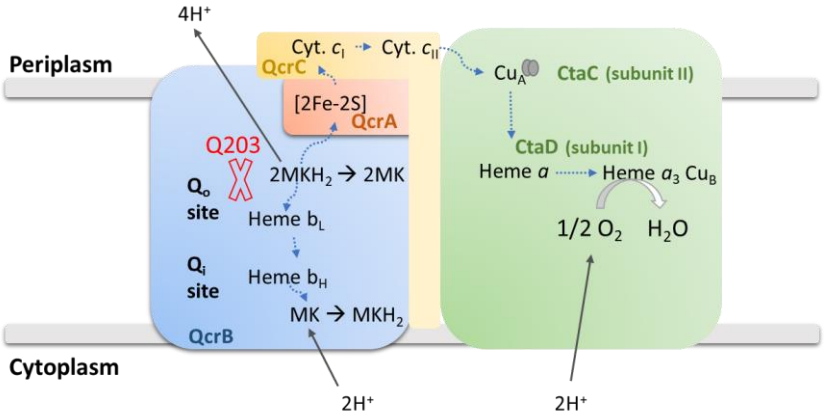

Figure 5. Schematic diagram of CIICIV (half of the supercomplex). The blue arrows represent the flow of electron. Adapted from[48].

1.2.1.3. Role in drug efflux

Oxidative phosphorylation is important for the function of efflux pumps (EP).[70] The major facilitator family (MFS), the small multidrug resistance family (SMR) and the resistance nodulation division (RND) are examples of EPs that depend on the PMF (**Figure 6**). ATP binding cassette family (ABC), such as P-glycoprotein, are ATP-dependent efflux pumps (**Figure 6**).[47] EPs are one of the reasons behind the mycobacterial resistance to drug treatments. Mycobacteria in the human host or during drug treatment can induce the expression of efflux pumps for detoxification.[71] For example, WhiB7 (a redox-sensitive transcriptional activator) plays a major role in mediating intrinsic drug resistance, sometimes through the direct regulation of efflux pumps.[72]

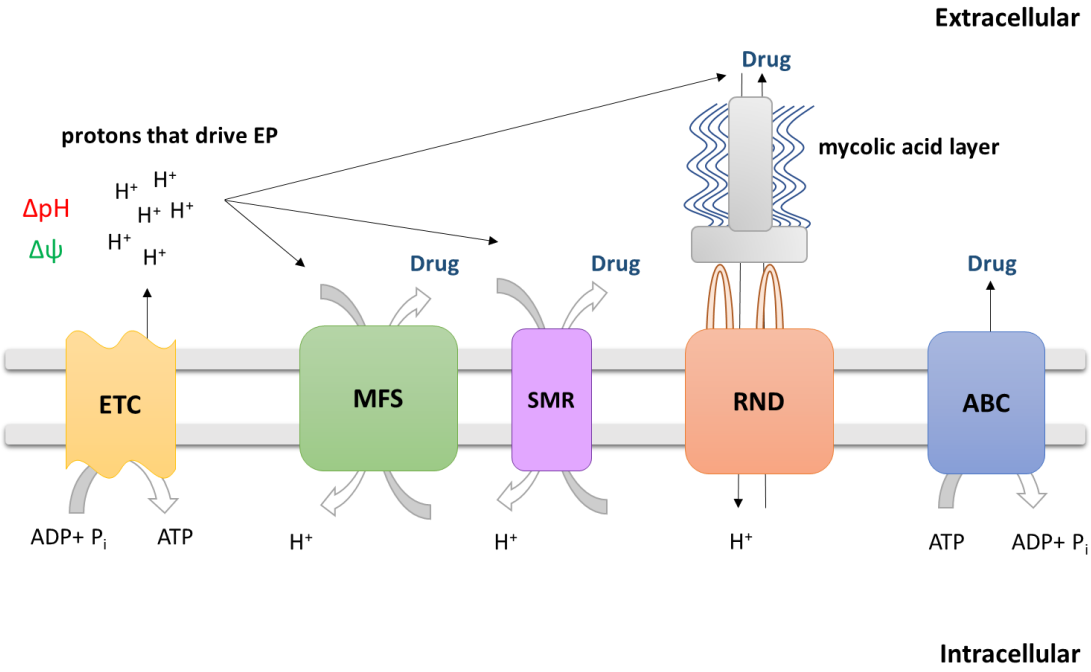

Figure 6. Examples of efflux pumps in mycobacteria. Adapted from[47].

1.2.2. Mycobacterial cell wall synthesis

The mycobacterial cell envelope is important for growth and virulence. It is more complex than the cell wall of Gram-negative or Gram-positive bacteria. It is also a major contributor to mycobacterial resistance against common antibiotics due to its low permeability to drugs. The lipid-rich cell envelope also protects mycobacteria against different environmental stressors, such as temperature, disinfectants, changes in pH and osmotic pressure.

The main component is the mycolyl-arabibinogalactan-peptidoglycan complex (mAGP) which is composed of a cross-linked network of peptidoglycan (PG), highly branched arabinogalactan (AG), and long chain mycolic acids. They are covalently bonded together forming the core structure of the cell envelope.[73] Another key component of the cell wall is a phosphatidyl-*myo*-inositol-derived glycolipid containing mannan and arabinan domains called lipoarabinomannan (LAM, **Figure 7**).[74] LAM acts as a virulence factor playing a key role in modulating host-immune response by binding to Toll-like receptors. [75, 76, 77]

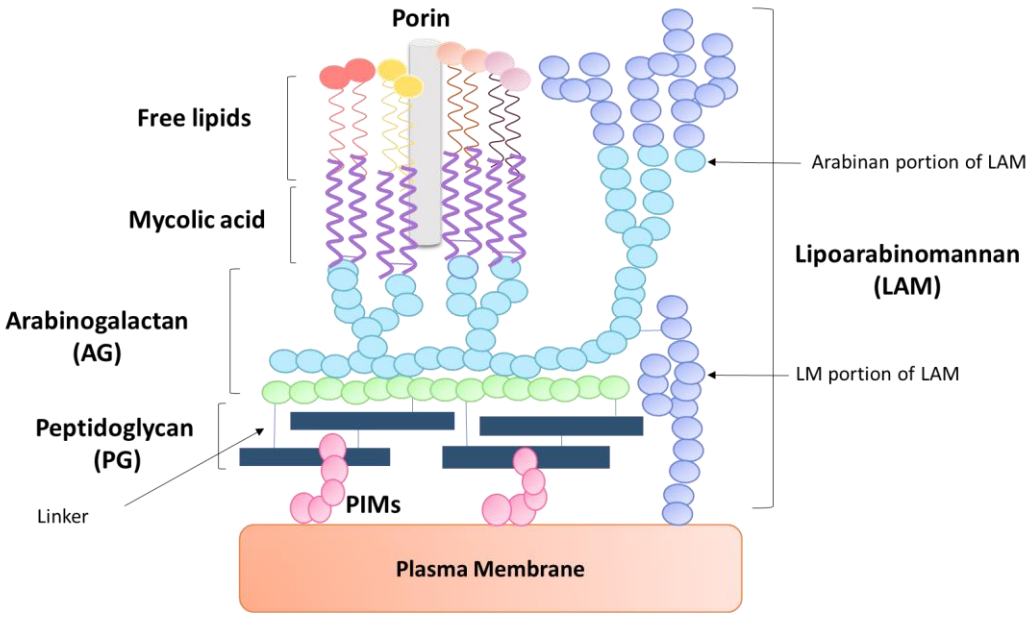

Figure 7. Simplified diagram of mycobacterial cell envelope. PIMs = phosphatidylinositol mannosides. Adapted from[44, 78].

The importance of the mycobacterial cell wall for survival, its unique structure and unique biosynthetic pathways, made it an attractive target for many antimicrobial drugs. For example, EMB targets Emb proteins which belong to the arabinofuranosyl transferases family (AraTs). They are trans-membrane (TM) proteins that add D-arabinofuranose sugar moiety from decaprenyl-phosphoryl-D-arabinose (DPA) to the growing AG and LAM. [79, 80] They are named Emb after their inhibitor EMB.

Other AraTs also add arabinofuranose moieties to either the galactan of AG or the mannan core of the LAM.[81] They include arabinosyl transferases A (AftA), B (AftB), C (AftC) and D (AftD). AftA starts the AG synthesis by adding D-arabinofuranose to C5 of the D-galactofuranose 8,10,12 of the existing galactan. AftB adds terminal β-(1→2) D-arabinofuranose to AG and LAM. AftC and AftD have been reported to be responsible for α-(1→3) and α-(1→5) branching.[82] All of these pathways, however, are not fully characterized yet.

The recently reported electron cyromicroscopy structures of EmbA, EmbB and EmbC proteins in *Mtb* and *Msmeg*, have shown that they consist of 15 TM helices, 11 of which are shared with other members of the glycosyl transferases C (GT-C) superfamily, and *N*- and *C*-terminal periplasmic carbohydrate-binding domains (*N*-PD and *C*-PD, **Figure 8**) which are anchored to the TM helices. Periplasmic (PL) and cytoplasmic (CL) loops connect the TM helices and acyl carrier proteins (ACpM) were found bound to EmbA, EmbB and EmbC at the cytoplasmic site.[79, 80] The structures have also shown that the catalytic site is located in a cavity in the junction between the TM helices and the PD domains. The site consists of an acceptor binding site (A_o-site), a donor binding site (D-site) and a negatively charged Aspartate residue (part of the DDX motif in PL2). (**Figure 8**).

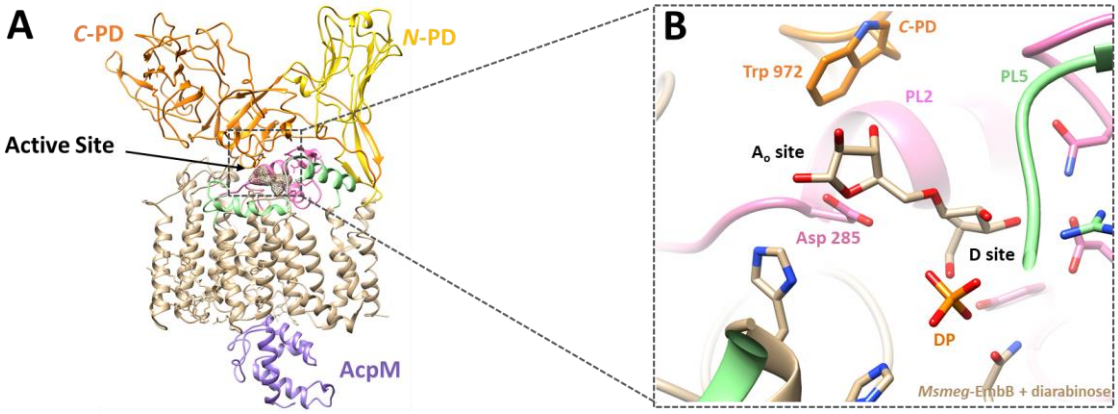

Figure 8. Structure of *Msmeg*-EmbB bound to di-arabinose. **(A)** Overall structure of *Msmeg*-EmbB-AcpM. **(B)** Di-arabinose at the active site. The active site consists of an acceptor binding site (A_o-site), a donor binding site (D-site) and a negatively charged Aspartate residue (part of the DDX motif in PL2).The figure was generated using UCSF Chimera software version 1.15.[83]

Emb proteins catalyze the same reaction, however, have different substrate affinities. EmbA-EmbB catalyzes the α-(1→3) linkage on the terminal hexarabinofuranosyl motif of AG, followed by the addition of β-(1→2) D-arabinofuranose by AftB enzyme. It has been reported to catalyze the α-(1→5) linkage in AG as well.[74, 79, 81] EmbC catalyzes α-(1→5) glycosidic linkage leading to linear elongation of LAM (**Figure 9**).

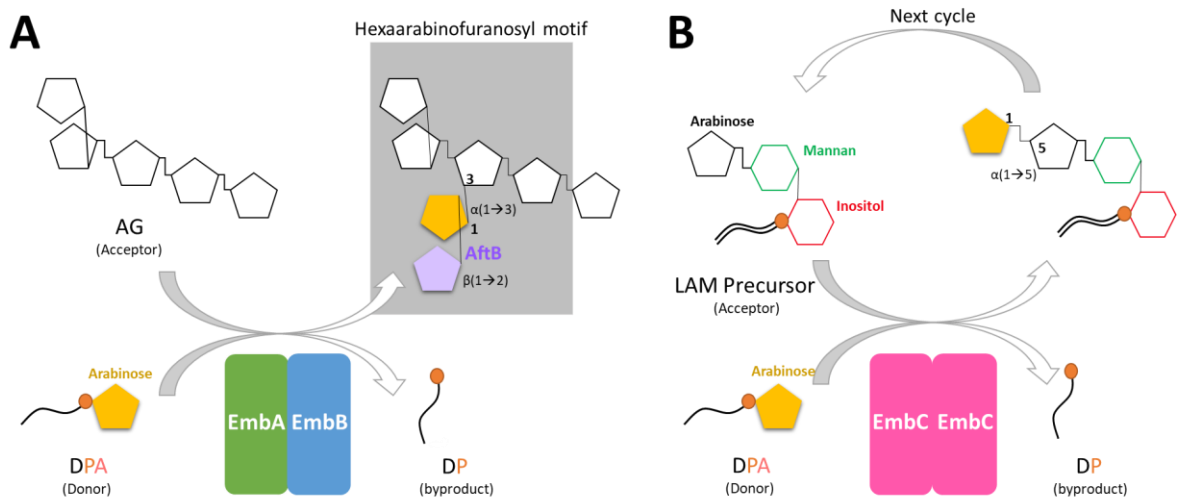

Figure 9. Diagram showing the catalytic reaction of Emb proteins. (A) EmbA-EmbB catalyzes the branching of AG (B) $EmbC_2$ catalyzes the synthesis of LAM. Adapted from[80].

Electron cryomicroscopy structures of *Mtb* and *Msmeg* EmbA-EmbB-$AcpM_2$ heterodimers and $EmbC_2$-$AcpM_2$ homodimers bound to EMB have shown that EMB binds to EmbB and EmbC, whereas no density for EMB was observed in EmbA. An additional loop in EmbA, which normally blocks the acceptor entry into the catalytic site (**Figure 10**), also appears to block the entry and binding of EMB.[80] Furthermore, active site mutations in EmbB and EmbC have been proven to lead to EMB resistance, but not in EmbA.[84]

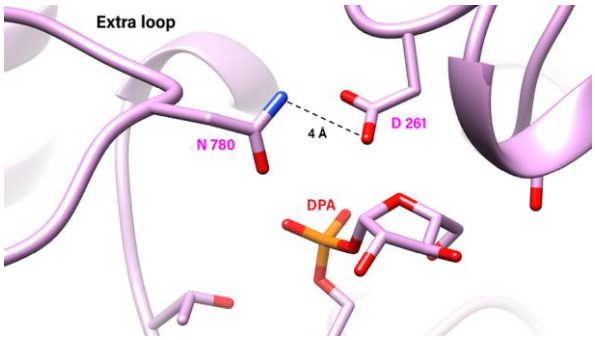

Figure 10. *Msmeg* EmbA catalytic site. Asn 780 residue in the extra loop interacts with the catalytic residue Asp 261. The figure was generated using UCSF Chimera software version 1.15.[83]

EMB acts as a competitive inhibitor which binds at the catalytic site of EmbB and EmbC instead of both substrates (the growing AG/LAM and DPA) inhibiting the arabinose transfer. This inhibition leads to the inhibition of branching of the terminal hexaarabinofuranosyl motif of AG and the LAM synthesis, thus disrupting the cell wall synthesis. EMB has been reported to have stronger binding affinities to *Mtb* EmbB compared to *Msmeg* EmbB and $EmbC_2$.[80]

2. Research objectives

The thesis aimed to investigate two different antimycobacterial compound classes, both of which the molecular details of their targets were recently reported.

2.1. IPA analogues

Q203, a member of the imidazopyrdine amide (IPA) class of compounds, is currently in phase 2 clinical trials (clinicaltrials.gov identifier NCT03563599).[37] Despite having high potency (MIC_{50} 2.7 nM[85]) in *in vitro* growth inhibition assays, its high lipophilicity and poor solubility[86], leading to an extended half-life of 321.12 ± 227.29 h[87], necessitate searching for IPAs with comparable *in vitro* activity and improved pharmacokinetic (PK) parameters. Q203 is given in doses up to 300 mg/d in clinical trials (NCT03563599), similar to INH standard dose in adults[88] with active TB infection.

The goal of my project was to establish the synthesis of IPAs analogues for the investigation of their molecular interaction with the target, QcrB subunit of $CIII_2CIV_2$ in mycobacteria. The IPAs were devised for an improved understanding of the molecular mechanism of action, making use of the molecular assay facilities in our laboratories and in particular trying to approach the long-term goal of targeting problematic mycobacteria that are not sensitive to Q203. These mycobacteria include *M. abscessus* and *M. intracellulare*, NTM of emerging importance.[89] The insensitivity may be due to pharmacokinetic differences IPAs display in different mycobacteria or differences in target binding and inhibition.

We designed and synthesized a set of 30 IPA analogues, 25 of which were benzoxazole IPA analaogues to explore the details of binding to $CIII_2CIV_2$. The benzoxazole ring system has the advantage of decreasing the high lipophilicity of Q203 and being hydrophobic enough to allow the compound's membrane penetration.[86] The synthesized compounds and Q203 were tested in enzyme inhibition assays against the *Msmeg* $CIII_2CIV_2$, as well as in whole-cell growth inhibition assays *in vitro* against *Mtb*, *Msmeg*, *M. abscessus* and *M. intracellulare*.

We collaborated on this project with Prof. John Rubinstein, Departments of Biochemistry and Medical Biophysics, University of Toronto, Canada, and Dr. Henok Sahile, Departments of

Medicine and Microbiology and Immunology, Life Sciences Institute, University of British Columbia, Vancouver, Canada.

2.2. EMB analogues

The recently published electron cryomicroscopy structural models of the arabinofuranosyl transferases (EmbCAB)[79, 80] in *Mtb* and *Msmeg* encouraged us to synthesize new EMB analogues to further investigate the binding site. We designed symmetric and asymmetric analogues and tested their activity against *Mtb*, *Msmeg*, *M. abscessus* and *M. intracellulare*.

3. Results and Discussion

3.1. Synthesis

3.1.1. Imidazopyridine amides (IPAs)

3.1.1.1. Previously reported imidazopyridines

The imidazopyridine (IP) heterocycle is an important scaffold [90, 91, 92] in medicinal chemistry that can be found in many natural and synthetic drug substances. Drug substances that incorporate this moiety possess a wide range of pharmacological activities such as antiviral, antifungal, anticancer[93], antibacterial, antiulcer (Zolmidine), anti-osteoporotic (Minodronic acid) $GABA_A$ receptor agonist (Zolpidem) and anti-inflammatory (Miroprofen) activities. (**Figure 11**) [94, 95]

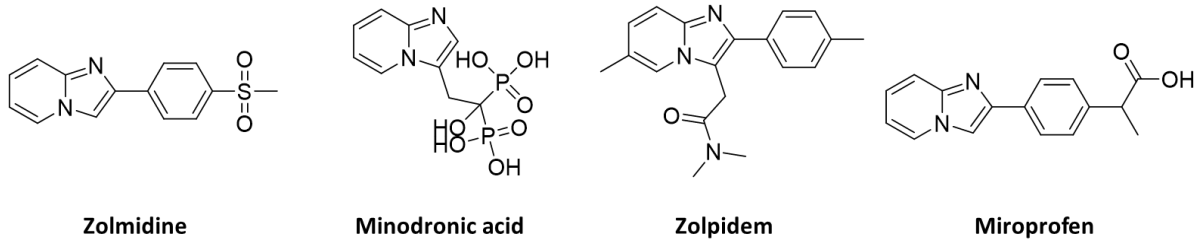

Figure 11. Examples of drugs on the market with the IP-scaffold.

The anti-mycobacterial activity of imidazopyridines has been investigated by many research groups. Imidazo[1,2-a]pyridine-3-nitroso derivatives were reported in 2004 to have significant anti-TB activity, however, were non-selective to mycobacteria and had high cell toxicity.[96] In 2009, 3-amino-imidazo[1,2-a]pyridines were reported as *Mtb* glutamine synthetase inhibitors but without assessment of the *in vitro* activity against *Mtb* H37Rv.[97, 98]

Imidazo[1,2-a]- pyridine-3-carboxamides (IPAs) with very good efficacy against *Mtb* H37Rv, MDR-*Mtb* and XDR-*Mtb* strains and without cytotoxicity were first reported in 2011 by the group of Marvin Miller at the University of Notre Dame (Indiana, USA).[99, 100] They originated from their research on antibacterial sideromycins[101] which led to the discovery of the hit compound, ethyl-7-diaminoethylimidazo[1,2-*a*]pzridine-3-carboxylate. Optimization of this hit resulted in a series of IP analogues with improved minimum inhibitory concentration (MIC; µM) and pharmacokinetics. *N*-Benzyl-2,7-dimethylimidazo[1,2-*a*]pyridine-3-carboxamide (ND-008454, **Figure 12**) was the most potent analogue with $MIC_{90} \leq 1$ µM against H37Rv *Mtb* as well as MDR and XDR strains. [99, 100]

Additionally, (ND-008454) was tested against NTM like *M. avium* which showed MIC close to that of *Mtb*. *M. abscessus* and *Msmeg* showed MIC values > 50 µM. Some of the analogues were tested against NTM, Gram-positive *S. aureus*, Gram-negative *E. coli* and the fungus *Candida albicans*. None of them showed activity, suggesting the specificity of these agents against mycobacteria.[99]

Further modifications on the lead ND-008454 led to a series of analogues with improved MIC values (five compounds of this series were in the nM range) and pharmacokinetic parameters.[102] An example is shown in **Figure 12**.

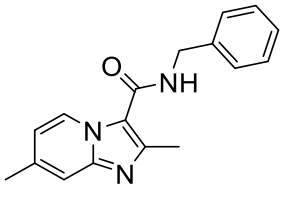

ND-008454

MIC_{99} = 1.25 µM against *Mtb* $H_{37}Rv$

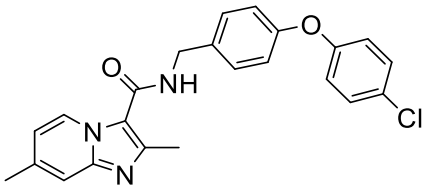

ND-09759

MIC_{99} = 0.006 µM against *Mtb* $H_{37}Rv$

Figure 12. Structures of **ND-008454** and **ND-09759**.

Institute Pasteur Korea reported hundreds of IPAs in two patents.[103, 104] They started by screening 120,000 compounds and out of 96 active hits, one IP-carboxamide was chosen for lead optimization. These optimizations finally resulted in Q203 (**Figure 13**).

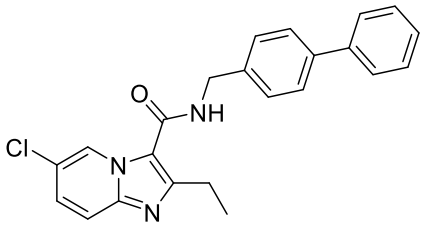

1

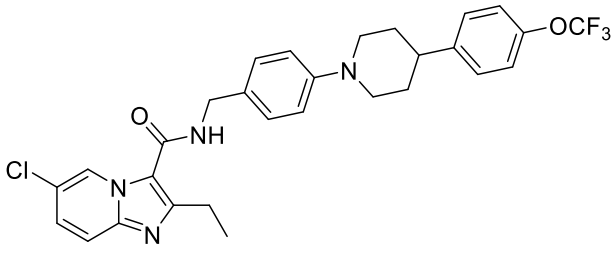

Q203

Figure 13. Structures of the lead compound (**1**) and **Q203**.

Q203[105], INN: telacebec, showed MIC_{50} against *Mtb* in the nM range, both outside (2.7 nM) and inside (0.28 nM) macrophages.[85] It targets the mycobacterial cytochrome *bcc-aa*$_3$, known as the $CIII_2CIV_2$ supercomplex. Q203 has been and is still being tested in clinical studies: a first-in-human trial (clinicaltrials.gov identifier NCT02530710); a phase 1 ascending multiple-dose study (NCT02858973); and a phase 2a multiple-dose trial for the evaluation of early bactericidal activity (NCT03563599), where it showed a dose-dependent reduction in the load

of viable mycobacteria in the sputum. It has also been tested for its effect on an inflammatory biomarker in coronavirus patients (NCT04847583).[37, 48, 106, 107]

The high potency, low cardiotoxicity (hERG patch clamp IC_{50} > 30 µM)[85] and activity of Q203 against MDR-TB strains made it suitable for further development. The research group at Institute Pasteur Korea synthesized several IPA analogues with modified side chains aiming to reduce lipophilicity (LogP) and the length of the side chain.[86, 108] They designed analogues with fused ring systems, which led to the discovery of another promising IPA analogue (**Figure 14**) with a benzoxazole heterocycle in its side chain. This compound has shown high potency against *Mtb* H37Rv strain both extracellularly (MIC_{80} = 27 nM) and intracellularly (MIC_{80} = 9 nM) as well as reduced AlogP of 6.97 compared to 7.88 in Q203.[86]

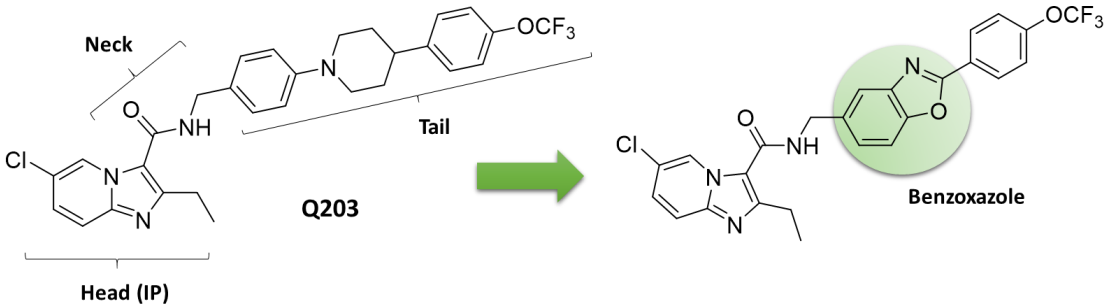

Figure 14. IPA analogue with a benzoxazole ring system.

A series of novel IPAs were reported by Lv et al., 2017. Modifications in their lead compound IMB-1402 [109] led to two compounds that showed good potency against drug-sensitive and drug-resistant *Mtb* strains with good safety indices (**Figure 15**). However, molecular docking analysis suggested that they bind to a different target than Q203 and the above-mentioned analogues. Docking studies showed strong interactions with the pantothenate synthetase enzyme (PDB ID- 3IVX).[95, 110]

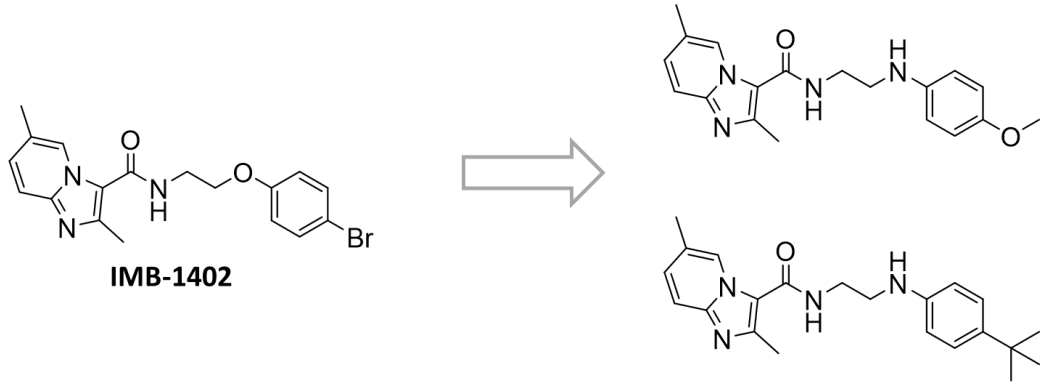

Figure 15. *N*-(2-phenoxyethyl)-IP-3-carboxamides. The analogues displayed are examples of IPA analogues that have different targets from that of Q203.

IPA analogues with basic fused ring systems were later designed by the same group in China aiming to reduce the lipophilicity of Q203. Most of the synthesized compounds showed high potency against *Mtb* H37Rv strain (MIC < 0.25 μM). Twelve compounds showed MIC values of < 0.035 μM - similar to Q203- against MDR-*Mtb* strains. Most of the compounds showed low cytotoxicity similar to Q203 at the same concentration (CC_{50} > 64 μg/mL). Furthermore, all of the compounds reported had lower LogP values (ranging from 5.10 to 6.93) than Q203 (7.64), but no clear correlation between LogP and potency could be deducted (**Figure 16**).[111]

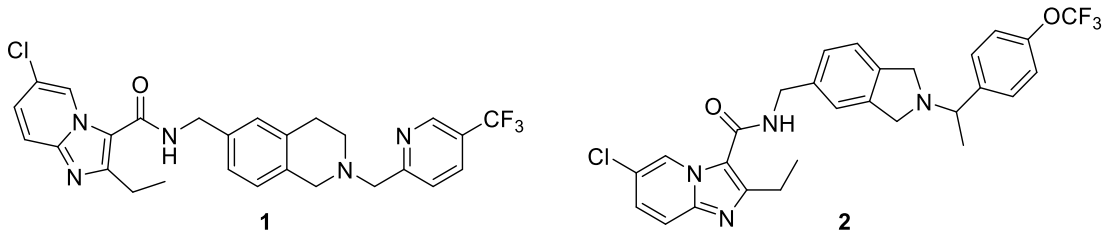

Figure 16. Structures of IPA analogues with alkaline fused ring systems. Both analogues have shown high potency against MDR-*Mtb*, similar to Q203.[111]

We designed and synthesized a set of IPA analogues to explore the details of binding to $CIII_2CIV_2$. The benzoxazole IPA shown in **Figure 14** was chosen as the lead compound since it showed high intracellular (MIC_{80} = 9 nM) and extracellular (MIC_{80} = 27 nM) activities. The benzoxazole ring system has the advantage of decreasing the high lipophilicity of Q203 and being hydrophobic enough to allow the compound's membrane penetration. [86]

3.1.1.2. Synthetic schemes

Through a 7-step synthetic scheme, a series of 30 IPA analogues were synthesized, 25 of which were benzoxazole IPA analogues. The general scheme was divided into three major parts; synthesis of the imidazopyridine scaffold (**Scheme 1A**), synthesis of the benzoxazole tail (**Scheme 1B**), and amide coupling (**Scheme 1C, Scheme 2, Scheme 3iii**). The synthesis of compounds **27** and **28** (**Scheme 3**) was slightly different from the general scheme.

Scheme 1. General synthetic scheme, **(A)** Synthesis of imidazo[1,2-a]pyridine-3-carboxylic acids, **(B)** Synthesis of 2-substitutedbenzo[d]oxazole-5-methylamine, **(C)** Synthesis of **1-24**, and **26**[a] *

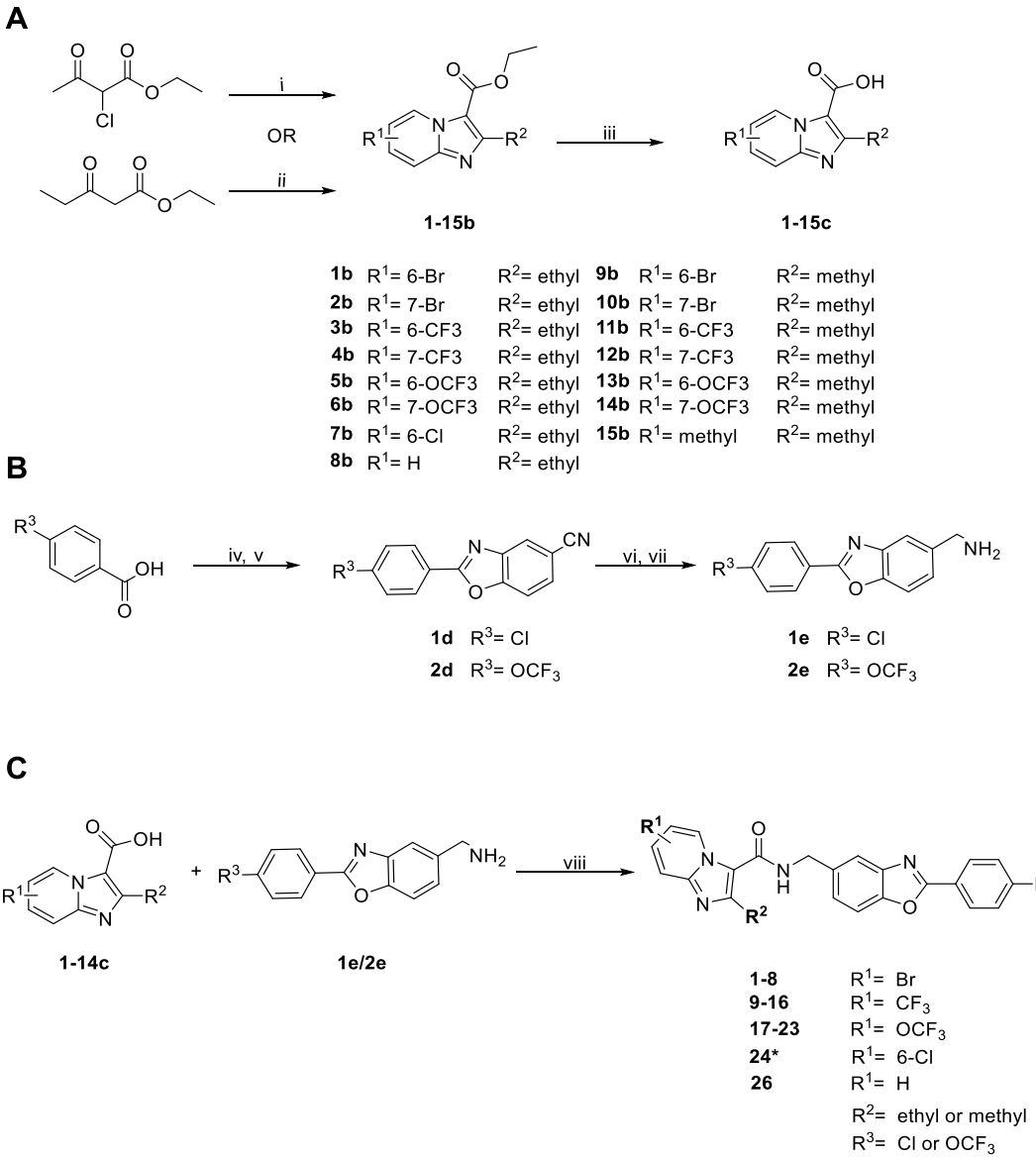

[a]Reaction conditions: **(A)** (i) 2-aminopyridine, EtOH, reflux overnight; overnight. (ii) NBS, H_2O, 30 min, 80 °C; 2-aminopyridine, 30 min-1 h, 80 °C. (iii) Ester hydrolysis:LiOH, EtOH/H_2O (3:1, v/v), reflux overnight. **(B)** (iv) thionyl chloride, DCM/DMF, room temperature, 1 h; (v) 3-amino-4-hydroxybenzonitrile, methanesulfonic acid, dioxane, 100 °C. (vi) di-*tert*-butyl-dicarbonate, $NiCl_2.6H_2O$, $NaBH_4$, MeOH, 0 °C to room temperature, overnight; (vii) 4 M HCl in dioxane, 2 h. **(C)** (viii) Amide coupling: HATU, DMF, DIPEA, room temperature, 1 h.

* Compound previously described in the literature. [86]

* ''Reprinted with permission from [Abdelaziz, R.; Di Trani, J. M.; Sahile, H.; Mann, L.; Richter, A.; Liu, Z.; Bueler, S. A.; Cowen, L. E.; Rubinstein, J. L.; Imming, P. Imidazopyridine Amides: Synthesis, *Mycobacterium Smegmatis* $CIII_2CIV_2$ Supercomplex Binding and in Vitro Antimycobacterial Activity. *ACS Omega* **2023**. https://doi.org/https://doi.org/10.1021/acsomega.3c02259]. Copyright [2023] American Chemical Society''

Scheme 2. Synthesis of **25, 29** and **30**[a] ‡

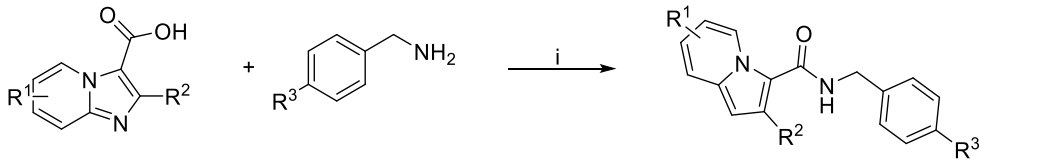

25*	R^1= 7-CH_3	R^2= methyl	R^3= H
29	R^1= 6-Cl	R^2= ethyl	R^3= H
30*	R^1= 6-Cl	R^2= ethyl	R^3= Cl

[a] Reaction conditions: HATU, DIPEA, DMF, room temperature, 1 h.

* Compounds previously described in the literature. [103, 112]

Scheme 3. Synthesis of **27** and **28**[a]

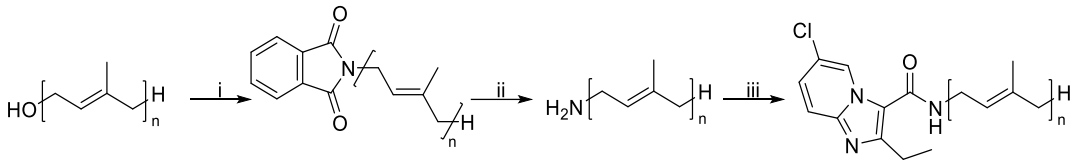

1f n= 3	**1g** n= 3	**27** n= 3
2f n= 2	**2g** n= 2	**28** n= 2
3f n= 2 (saturated alkyl)*	**3g** n= 2 (saturated alkyl)	

[a]Reaction conditions: (i) phthalimide, DIAD, Ph_3P in dry THF, room temperature, 4 h. (ii) hydrazine (50% w/w in H_2O), MeOH, overnight, room temperature. (iii) (1) **7c**, DIPEA, dry DMF, 10 minutes; (2) HATU, stir 20 min; (3) **1g** or **2g**, room temperature, 1 h.

* **3f** was synthesized from 3,7-dimethyl-1octanol.

3.1.1.3. Synthesis of the imidazo[1,2-a]pyridine-3- carboxylic acids (Scheme 1A)

A common approach for the synthesis of imidazo[1,2-a]pyridine is through the condensation of substituted 2-aminopyridines with compounds like β-ketoesters that have good leaving groups.[99, 86, 113, 114] The first attempt was to carry out α-bromination of ethyl-3-oxo-pentanoate separately and then the condensation reaction as reported by the group in Institut Pasteur Korea.[105, 86] They carried out the bromination step in diethyl ether using *N*-bromosuccinamide (NBS) as a brominating agent and ammonium acetate as a catalyst (**Figure 17**). However, their procedure was not reproducible. The reaction was successful in *tert*-butylmethyl ether and using AIBN (azobisisobutyronitrile) as a radical initiator (**Figure 18**).[115] The reaction of the β-ketoester with Br_2 in water or chloroform[105] was successful as well. However, the highly

‡ ''Reprinted with permission from [Abdelaziz, R.; Di Trani, J. M.; Sahile, H.; Mann, L.; Richter, A.; Liu, Z.; Bueler, S. A.; Cowen, L. E.; Rubinstein, J. L.; Imming, P. Imidazopyridine Amides: Synthesis, *Mycobacterium Smegmatis* $CIII_2CIV_2$ Supercomplex Binding and in Vitro Antimycobacterial Activity. *ACS Omega* **2023**. https://doi.org/https://doi.org/10.1021/acsomega.3c02259]. Copyright [2023] American Chemical Society''

reactive α-brominated β-ketoester formed could not be isolated in good yields, which affected the yield of the next step.

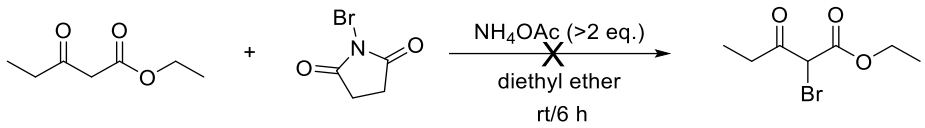

Figure 17. Bromination of ethyl 3-oxo-pentanoate with NBS and ammonium acetate (NH_4OAc) as a catalyst.[105, 86]

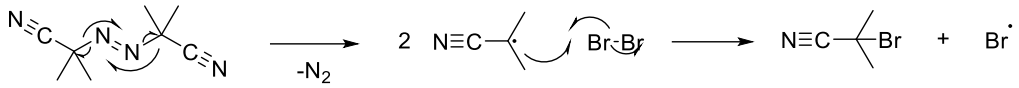

Figure 18. Radical initiation by AIBN.[116, 117]

We, therefore, opted for a one-pot reaction in water involving the halogenation of the β-ketoester and intramolecular cyclization (condensation) in the same reaction vessel to synthesise imidazo[1,2-a]pyridine-3-carboxylic acid. Ethyl-3-oxopentanoate and NBS were stirred in water for 30 min, then substituted 2-aminopyridine was added and stirred for a further 30 min before the 2-ethylimidazo[1,2-a]pyridine-3-carboxylic acid ester (**1-8b**) was extracted and purified. The advantage of this method is that the highly reactive brominated product can react directly with the nucleophile (2-aminopyridine) once it is formed. Intramolecular cyclization finally leads to the desired esters (**Figure 19**). [114] The yields were ≤ 30%, much lower than those reported by[114]. However, in their scheme, they mostly used unsubstituted 2-aminopyridines. An electron-withdrawing group on the pyridine, as in our case, would make the amino group less nucleophilic. Increasing the reaction time did not lead to better yields.

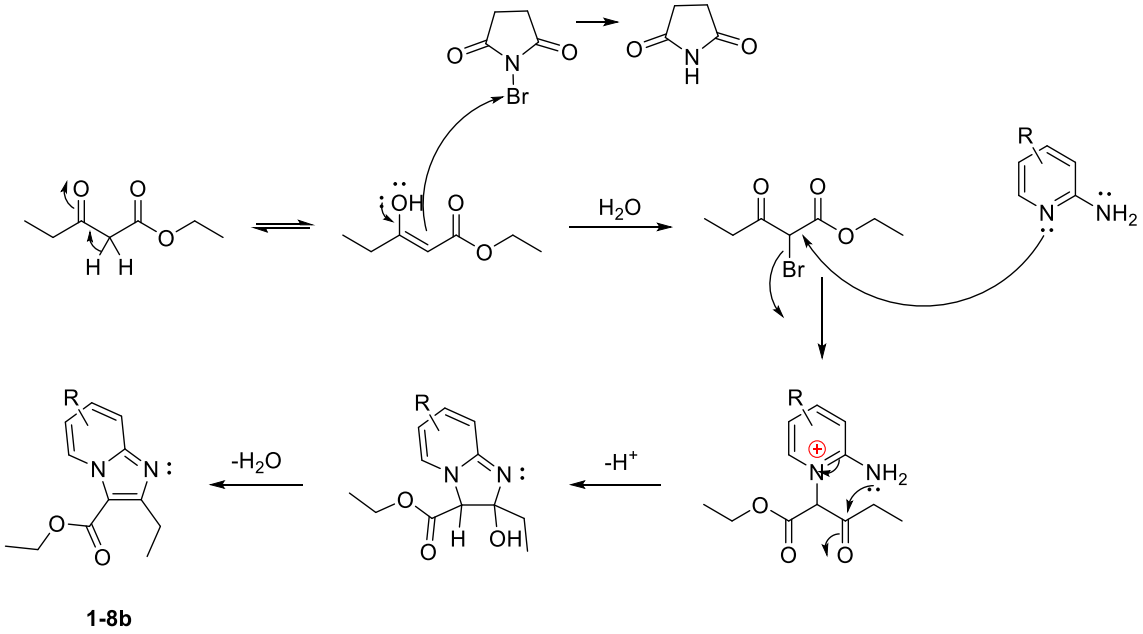

Figure 19. Mechanism of imidazo[1,2-a]pyridine formation.[114]

Alternatively, ethyl 2-chloroacetoacetate and 2-aminopyridine were stirred in EtOH under reflux overnight to form 2-methylimidazo[1,2-a]pyridine-3-carboxylic acid ester (**9-15b**).[105] Both methods gave similar yields, but the reaction in water was faster. The same procedure has been reported in a patent by Marvin Miller's research group in 2011, however, they used DME as the solvent instead of EtOH.[100]

The formed esters were hydrolysed with hydrated LiOH in EtOH:H_2O (3:1, v/v) mixture to give imidazo[1,2-a]pyridine-3-carboxylic acids (**1-15c**).[105]

In our experiments, we observed that the synthesis of ethyl 2-bromo-3-oxo-pentanoate from NBS or Br_2 worked best with water as a solvent compared to chloroform, ether and DMSO. The reaction did not need a catalyst, was fast and gave better yields. Similar to the bromination reaction, the rate of the cyclization reaction was faster in water (~30 min.-1 h) compared to a separate cyclization reaction in EtOH (overnight). Water has been reported to accelerate reaction rates due to the hydrophobic effect and hydrogen bonding between water molecules and reactants. Furthermore, even with insoluble reactants, the hydrophobic effect can increase the rate and selectivity of reactions.[118, 119]

3.1.1.4. Synthesis of the 2-substituted-benzoxazole tail (Scheme 1B)

Due to their importance as scaffolds for compounds with diverse pharmacological activities, various synthetic methods have been reported for benzoxazoles.[120] They are often synthesized by condensation of *o*-aminophenol and benzoic acid or benzoic acid derivatives. The protocol reported by Kang et al.[86] started with the reaction of *p*-substituted benzyl chlorides with *o*-aminophenol in dioxane under reflux overnight. After evaporation of dioxane, the amide formed was cyclized by the addition of pyridinium *p*-toluenesulfonate and xylene to the intermediate amide and the mixture was stirred again under reflux overnight to give the 2-substituted benzoxazole. In our experiments, the previously reported cyclization with xylene and pyridinium *p*-toluenesulfonate as a catalyst did not work (**Figure 20**).

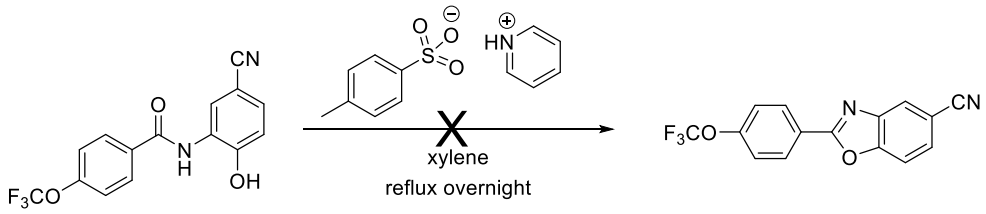

Figure 20. Cyclization of the amide intermediate using pyridinium *p*-toluenesulfonate as a catalyst. [86]

After several trials, we were able to obtain the benzoxazole tail (**1d and 2d**) in good yields using methanesulfonic acid as a catalyst. It was added to a mixture of 3-amino-4-hydroxybenzonitrile and *p*-substituted benzyl chloride in dioxane[121] and stirred overnight under reflux. The product was recrystallized from isopropanol to give reddish-brown crystals (30-70% yield). The proposed mechanism is explained in the figure below (**Figure 21)**.

The nucleophilic amine attacks the carbonyl carbon and replaces the chlorine. The amide intermediate (**a**) formed undergoes amide-imine tautomerism catalyzed by methanesulfonic acid ($MeSO_3H$). The iminol (**b**) in turn reacts with $MeSO_3H$ to form the corresponding mesylate (**c**). The hydroxyl group substitutes the formed mesylate by an intramolecular nucleophilic substitution, eventually forming the benzoxazole ring.[121]

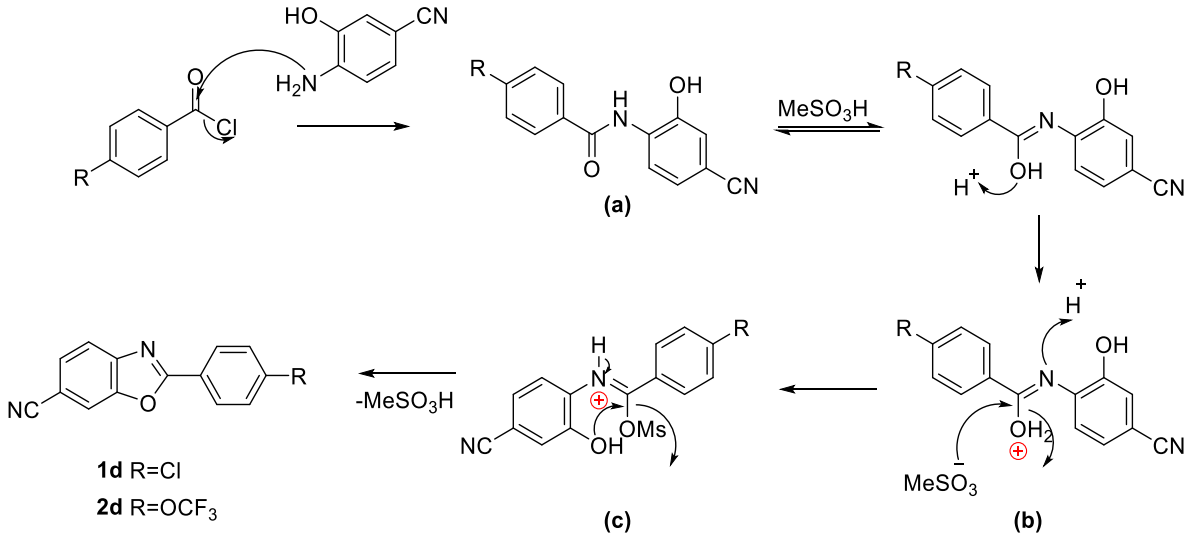

Figure 21. Mechanism of benzoxazole formation using $MeSO_3H$ as a catalyst.[121]

The selective reduction of the benzonitrile to the primary benzylamine was a challenging step. Borane dimethylsulfide and $LiAlH_4$ reduced the imine functional group of the benzoxazole ring together with the nitrile group, leading to ring opening. Starting with the reduction of the educt, 3-amino-4-hydroxybenzonitrile, to avoid ring opening was not successful. This is because the nitrile group is attached to an electron-rich aromatic system, which reduces the partial positive charge on the carbon atom, making it more difficult to reduce. To selectively reduce the nitrile without affecting the benzoxazole ring, $NaBH_4$ was used as the reducing agent with $NiCl_2.6H_2O$ as a catalyst. This reaction has been reported in EtOH and the primary amine produced could be isolated by filtration on celite.[86]

However, we were unable to isolate the primary amine from the reaction mixture. The masses of a methyl ester a secondary amine, a primary amide and benzoxazole ring opening (loss of

CH_3) were also detected in ESI-MS. To overcome this problem, we modified the protocol by adding di-*tert*-butyl-dicarbonate to the reaction mixture.[122, 123] In the workup, first diethylenetriamine was added as a coordinating ligand to remove nickel boride. Then MeOH was evaporated and the reaction mixture was dissolved in EtOAc and washed with 10% citric acid, saturated $NaHCO_3$ and brine to neutralize excess unreacted $NaBH_4$. The *boc*-protected primary amine (**1eBoc/2eBoc**) was separated from the remaining **1d/2d** by column chromatography. Finally, stirring **1eBoc/2eBoc** in 4M HCl in dioxane for 1 h was sufficient to precipitate **1e/2e** as a hydrochloride salt (73-90% yield).

The combination of excess $NaBH_4$ with a catalytic amount of $NiCl_2.6H_2O$ leads to the *in-situ* formation of nickel boride, a catalyst[124], which activates nitriles towards reduction into the primary amine by $NaBH_4$.[122, 125, 126] Trapping the primary amine with di-*tert*-butyl-dicarbonate helps in isolating it from the reaction mixture and prevents side reactions such as dimerization.

3.1.1.5. Amide coupling (Scheme 1C, Scheme 2 and Scheme 3iii)

Coupling of the imidazo[1,2-a]pyridine carboxylic acids (**1-15c**) to the amine counterparts (**1e**,**2e**,**1g** or benzylamines) was achieved by using coupling agents such as 1-[Bis(dimethylamino)methylene]-1H-1,2,3-triazolo[4,5-b]pyridinium-3-oxid-hexafluoro-phosphate (HATU) and Benzotriazole-1-yl-oxy-tris-pyrrolidino-phosphonium hexafluorophosphate (PyBOP).

With HATU, the amide formation was faster than with PyBOP, leading to a complete conversion after 1 h. It is noteworthy that the order of addition of the reactants in this reaction made a difference in the yield. First, the acid and DIPEA were dissolved in DMF. HATU was then added and the mixture was stirred for 20 min. before the amine was added. This sequence allowed sufficient time for the activated ester to form before adding the amine. After 1 h, brine was added to precipitate the product. Washing thoroughly with brine helped remove DMF and DIPEA. Finally, washing with a small amount of MeOH removed the remaining impurities.

The coupling reagents 1-(3-dimethylaminopropyl)-3-ethylcarbodiimide hydrochloride (EDC.HCl) and 1-hydroxybenzotriazole (HOBt) have also been reported to be successful. Although reported by several groups, the conversion of the imidazo[1,2-a]pyridine carboxylic acids to acid chlorides with thionyl chloride[105] or oxalyl chloride[100] and subsequent reaction with the benzylamine counterpart was not successful.

3.1.1.6. Synthesis of farnesyl and geranyl amines[127] (Scheme 3)

The tail of compounds **27** and **28** consists of isoprene units (3 and 2), instead of a 2-substituted benzoxazole heterocycle. Compound **27**, as an example, was synthesized via coupling of **7c** with *E*-farnesyl amine (**2g**), which was synthesized from *E*-farnesol in two steps. The first step was the synthesis of *N*-farnesylphthalimide (**1f**) from farnesol. This reaction is a variation of the Mitsunobu reaction. The second step was the deprotection of the *N*-farnesylpthalimide to farnesyl amine (**1g**) with hydrazine hydrate (70% yield).[127] The conversion of farnesyl bromide to farnesyl amine following Gabriel's synthesis was also successful, but with much lower yields.

3.1.1.7. Imidazo[1,2-a]pyridine-3-carboxamide analogues (IPAs 1-30)

The poor solubility of the IPAs in organic solvents made their purification challenging. Compounds **1-24** were mainly purified by dissolving impurities in the least possible amount of MeOH followed by vacuum filtration until sufficient HPLC purity was reached. The problem with this method is that the product itself was partially soluble in MeOH, resulting in the loss of some product and ultimately lower yields. Compounds **25-30** had better solubility in organic solvents. **27** and **28** did not need further purification after thorough washing with brine. Compounds **25**, **29** and **30** were purified by column chromatography. The impurities filtered or removed by column chromatography were excess unreacted acid or amine and by-products of the coupling reaction (**Figure 22**).

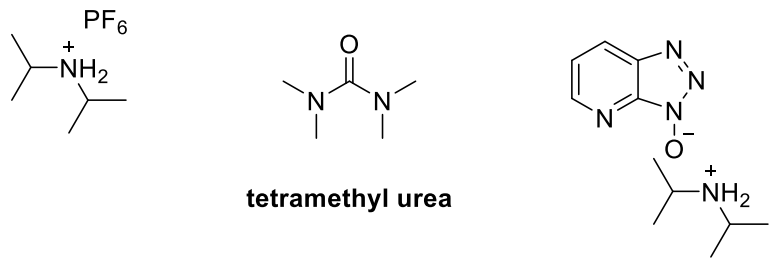

Figure 22. By-products from the amide coupling using HATU.

In some cases, a dimer of **2e** was detected by ESI-MS. For example, the HPLC-HRMS spectra of compounds **7** and **8** showed a peak with a mass corresponding to that of the **2e** dimer. In this case, these compounds were purified by preparative HPLC.

Furthermore, the solubility problem affected the concentration of the prepared NMR samples. In most cases, the sample was dissolved in $CHCl_3$ at a concentration of 1 mg/mL. The low sample concentration affected mainly ^{13}C and APT NMR spectra where quaternary carbon

atoms could not all be identified in all spectra. HSQC NMR was done, for some compounds, to identify the signals of quaternary carbon atoms and help confirm the structure (**Figure 23** as an example). Finally, the product formation was confirmed by combining the data from the ESI-HRMS, ^{1}H and ^{13}C NMR spectra.

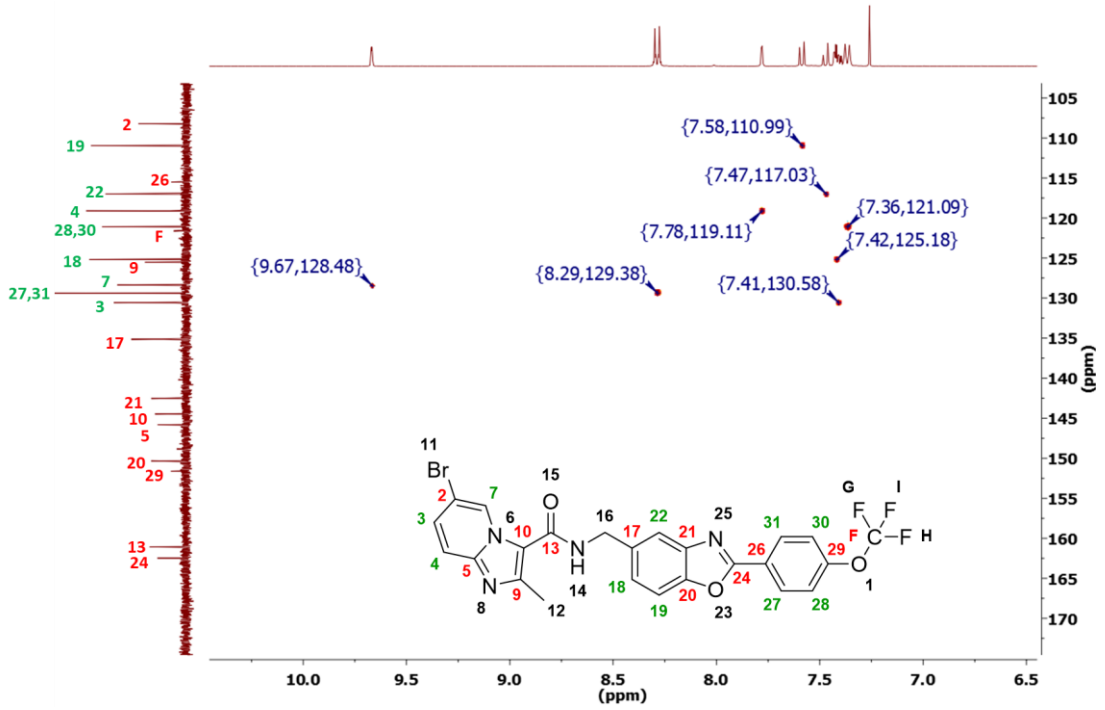

Figure 23. HSQC spectrum of compound **4.** In this compound, all C-atoms were detected in ^{13}C NMR. The figure is a zoomed-in view of the aromatic tertiary (CH, green) and quaternary (red) carbons. CH_2 and CH_3 are not shown here). The assignments were predicted by Mestrenova software. The assignments of the quaternary carbons are tentative.

3.1.1.8. Solubility assay for IPAs[128, 129]

The solubility of Q203 and the prepared IPA analogues was determined using a microplate-based laser nephelometry (NEPHELOstar^{plus}). 10 mM or 2.5 mM stock solutions were prepared in DMSO, depending on the solubility of the compound. From these stocks, serial dilutions were prepared in DMSO/PBS buffer. The concentration of DMSO in the sample was kept constant (2%) to avoid solubility enhancement by a gradual increase in DMSO. The machine measured the intensity of scattered light as a function of the concentration of insoluble particles. The higher the concentration of the precipitate, the higher the intensity of the signal detected by the nephelometer detector (RNU, relative nephelometric units). The generated graphs showed two linear fittings for soluble and insoluble phases. The point of intersection between the lines is taken as the kinetic solubility point. (**Figure 24**) Most of the compounds

showed solubilities < 54 µM (**Table 1**). Lower solubilities cannot be determined as 54 µM has been reported as the limit of detection for this method.[129]

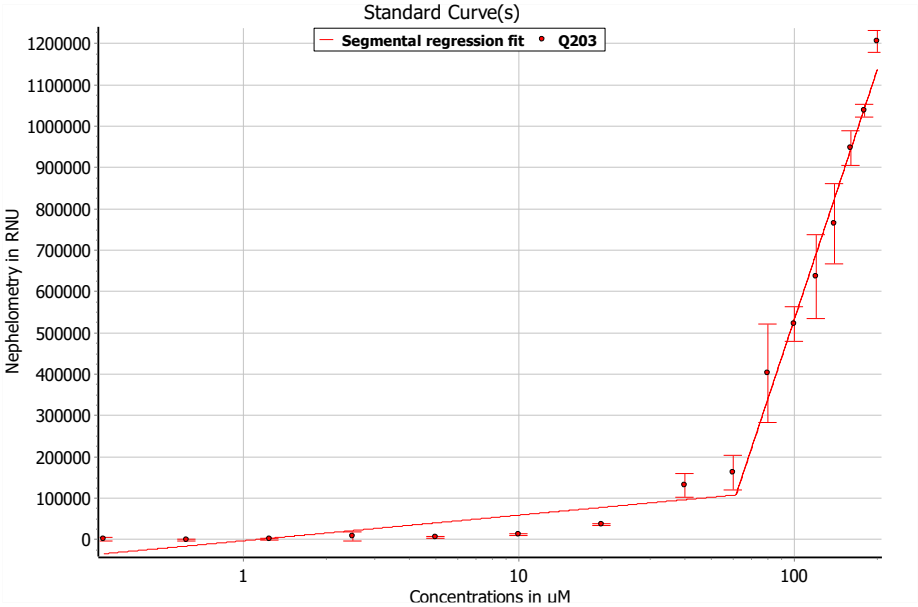

Figure 24. Q203 graph as an example of the graph output from the nephelometry solubility assay. The x-axis concentration values are shown in a log scale. The point of intersection between the two fitted lines represents the solubility of Q203.

Table 1. Solubilities of Q203 and IPAs in PBS buffer.

Code	Solubility* (µM)	Code	Solubility* (µM)
Q203	61	**16**	< 54
1	< 54	**17**	n.d.
2	< 54	**18**	n.d.
3	< 54	**19**	< 54
4	< 54	**20**	< 54
5	<54	**21**	< 54
6	n.d.	**22**	< 54
7	< 54	**23**	< 54
8	< 54	**24**[86]	< 54
9	< 54	**25**[112]	< 54
10	< 54	**26**	< 54
11	< 54	**27**	73
12	< 54	**28**	< 54
13	< 54	**29**	65
14	n.d.	**30**	< 54
15	< 54		

* 54 µM has been reported as the nephelometric detection limit for compounds with a molecular weight of 500.[129]

3.1.2. Cytochrome *bd*-inhibitor (31)

Scheme 4. Synthesis of cytochrome *bd*-inhibitor **(31)**[130]

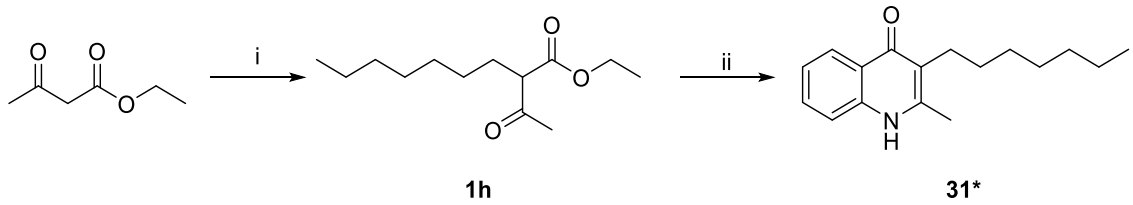

[a]Reaction conditions: (i) (1) NaH, dry THF, 30 min.; (2) heptyl bromide, 12 h. (ii) (1) Aniline, toluene, glacial acetic acid, Dean-Stark trap (100 °C), 3-24 h; (2) biphenyl ether, reflux (250 °C).

[*] This compound was previously described in the literature. *(*AD7-1)[130, 131]

Compound **31** (3-heptyl-2-methylquinolin-4(1H)-one), a previously reported cytochrome *bd*-inhibitor, was synthesized in two steps (**Scheme 4**).[130, 132] The first step was the synthesis of ethyl 2-heptylacetoacetate (**1h**) from ethyl acetoacetate and heptyl bromide under basic conditions (nucleophilic substitution). The purification of **1h** was done using column chromatography. When the purified **1h** was dissolved in acetonitrile:water mixture (ACN:H_2O, 9:1) two signals appeared in the analytical RP-HPLC traces at 215 nm, one of which showed absorption at 254 nm as well (**Figure 25**). The two peaks were separated by preparative RP-HPLC using ACN:H_2O (15-85 % gradient) solvent system. The ^{1}H NMR spectra (**Figure 25**) were identical, as well as their masses, which implied that in ACN:H_2O mixture, both the keto and enol isomers could be detected, and not in deuterated chloroform (solvent used for NMR).

The second step was the condensation of aniline with **1h** to form 3-heptyl-2-methylquinolin-4(1*H*)-one (**31**) through an imine intermediate (Schiff base, **Figure 26**). Heating of the Schiff base at 250 °C was necessary for ring closure. Biphenyl ether was chosen as a solvent because of its high boiling point.[133] The ^{1}H and ^{13}C NMR spectra were similar to those reported in the literature[132], but the yield (14%) was much lower than reported (69%). This procedure followed the standard Conrad-Limpach reaction for the synthesis of 4-hydroxyquinolines.[134]

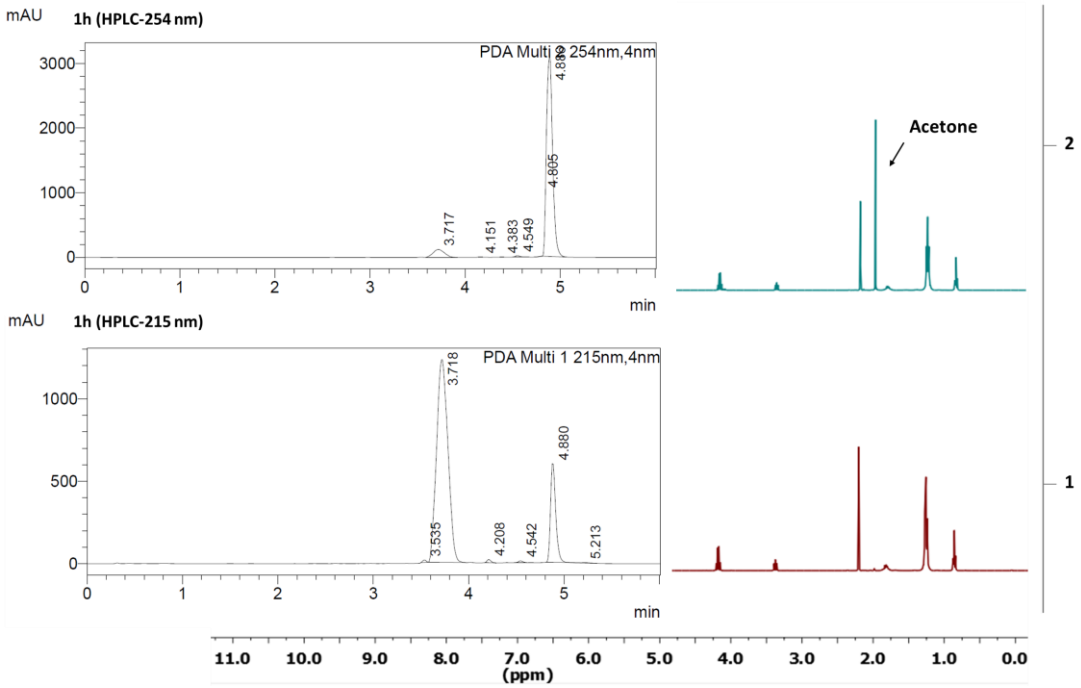

Figure 25. Left: analytical RP-HPLC traces of **1h**. The upper trace shows peaks detected at λ = 254 nm, and the lower trace show peaks at λ = 215 nm. **Right:** NMR spectra of the two peaks after being separated by preparative HPLC. The solvent peak (green spectrum) corresponds to acetone.

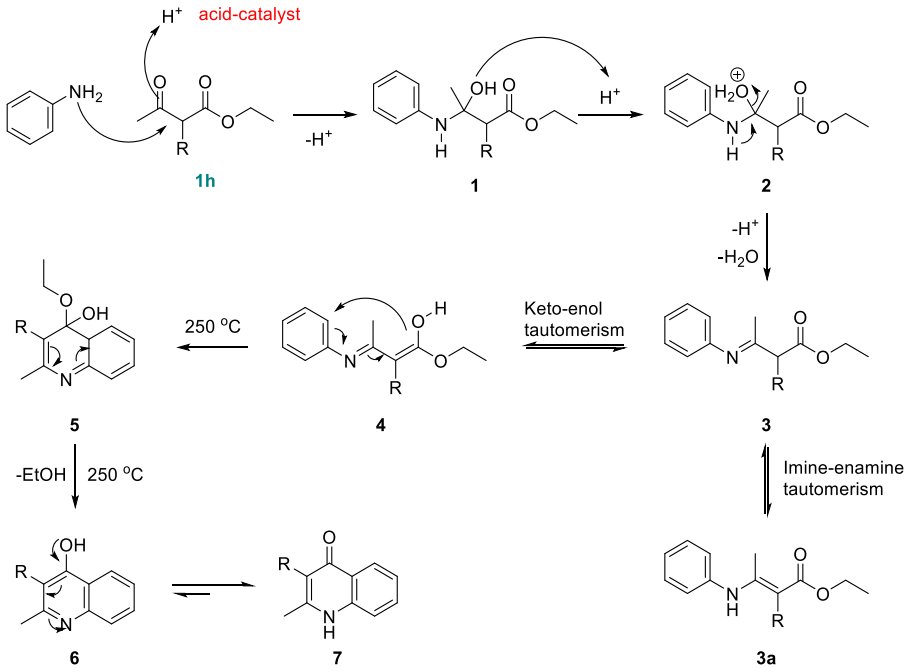

Figure 26. Proposed reaction mechanism[134] of **1h** with aniline to form compound **31.** The reaction starts with a nucleophilic attack on the ketone in an acidic medium. The formed hemiaminal (**1**) is unstable and the hydroxyl group is lost as water (**2**) leading to the formation of an imine intermediate (Schiff base, **3**). Heating to 250 °C allows the cyclization of the imine-enol tautomer to the desired 4-quinolone (**7**). This step requires high activation energy because it breaks the aromaticity of the phenyl ring (**5**). The aromaticity is regenerated by the loss of EtOH (**6**). 4-Quinolone scaffold (**7**) is formed by keto-enol tautomerism.[134]

3.1.3. Ethambutol (EMB) analogues

3.1.3.1. Previously reported EMB analogues

Ethambutol (EMB) was developed in the early 1960s from the lead compound *N,N*-diisopropylenediamine (**Figure 27**).[135, 136] It is still included in first-line drug regimens for TB and NTM infections such as those caused by *M. avium* complex (MAC).[12, 25, 137, 138] The *dextro-S,S* isomer is the active isomer, while the meso isomer is 16 times less active[139] and the *levo* isomer is almost inactive (500 times less active).[136] It was found to be active against INH- and streptomycin-resistant strains, however, it is always used in combination. It is given in doses of 15-25 mg/kg/day for adults and 10-15 mg/kg/day for children aged 6-12 years old.[139] EMB should not be given to children under 5 years of age due to potential ocular toxicity and difficulty testing their visual acuity. The toxicity may be due to EMB's ability to chelate metals such as copper and zinc. This chelation depletes their levels and leads to visual impairments.[140, 141]

Several symmetric and asymmetric EMB analogues have been reported.[135, 136, 139, 142, 143, 144] For example, compounds **3** and **4** in **Figure 27** were among a panel of asymmetric analogues which were tested for activity against *Msmeg*, *as* a model of *Mtb*. They showed weak activity against *Msmeg* compared to EMB.[145] These compounds were not tested against *Mtb*.

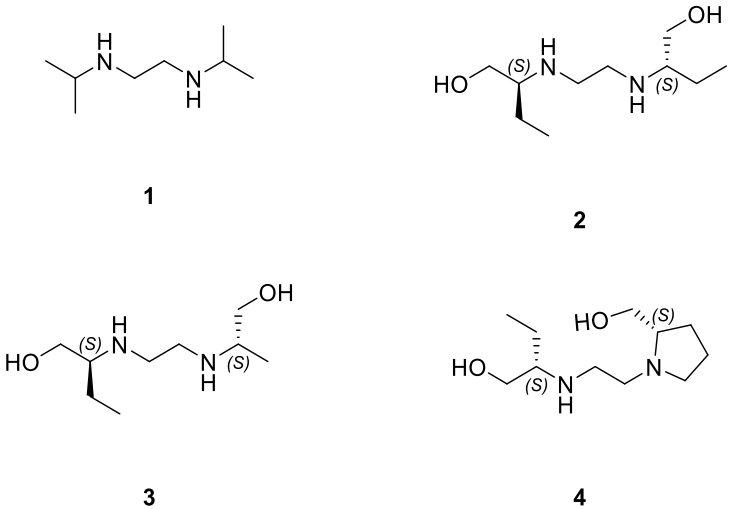

Figure 27. *N,N*-diisopropylenediamine (lead compound, **1**), (+)-(*2S,2S'*)-2,2'-(ethylenediamino)di(butan-1-ol) (EMB, **2**). **3** and **4** are examples of reported EMB analogues with weak activity against *Msmeg*.[145]

Richard Lee's group reported analogues of higher predicted Clog*P* values but less active than EMB (**Figure 28**). They suggested that these analogues may have better PK profiles such as absorption and serum half-life, leading to better cerebrospinal fluid (CSF) penetration. A better CSF penetration than EMB would make them good candidates for the treatment of CSF infections. However, they have not been further tested to confirm if they retain *in vivo* activity and have better PK profiles.[142] Another series of analogues from Lee's group showed higher *in vitro Mtb* activity compared to EMB (**Figure 28**). The 1,2-diamine backbone of EMB was retained in these analogues, but the side chain was changed to cyclic (bulkier) side chains in addition to the removal of the hydroxyl groups. The most active compound was SQ109, which was later reported to target, among other targets, a trehalose monomycolate transporter (MmpL3), important for cell wall biosynthesis.[42, 143]

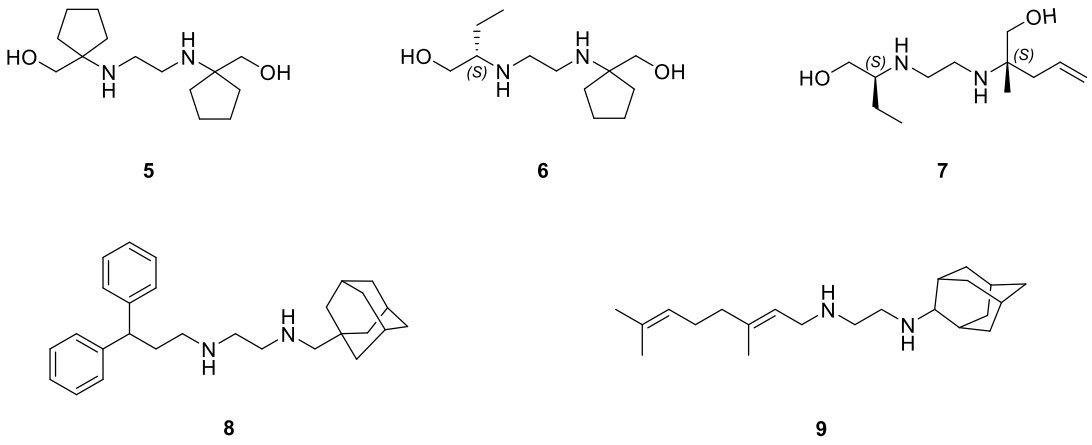

Figure 28. Examples of EMB analogues. Compounds **5-7** are examples of the set of analogues of lower potency than EMB, while **8** and **9** are examples of analogues that showed higher potency. Compound **9** is SQ109.[142, 143]

In another investigation, the ethylenediamine backbone was combined with the chloroquine pharmacophore and the isoxyl bioisostere (urea) to synthesize a short series of compounds with broad antimicrobial activity (**Figure 29**). These compounds were active against protozoa and *Mtb*. Compound **10** was found to be twice as potent as EMB and isoxyl (known as thiocarlide)[146] which is a thiourea anti-TB drug targeting mycolic acid synthesis.[144]

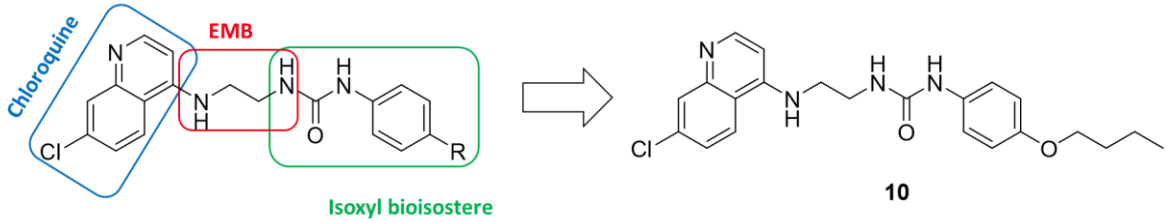

Figure 29. Tripartite hybrid compounds with a broad antimicrobial spectrum.[144]

Based on the reported EMB analogues, it can be hypothesized that modifications in EMB lead to weak or loss of activity. The modifications that deviate from the original EMB structure could result in potent analogues with a different target such as the multi-target SQ109 in **Figure 28**.

3.1.3.2. Synthetic schemes

To further investigate the above hypothesis, we designed and synthesized a series of EMB analogues with symmetric (**Scheme 5**, **Scheme 6** and compound **38** in **Scheme 7**) and asymmetric (**Scheme 7**) side chains attached to the ethylenediamine moiety, following up on the panel of EMB analogues previously synthesized during my master's thesis[44]. We aimed to test the activity of the synthesized analogues against *Mtb* as well as *M. abscessus* and *M. intracellulare.*

The synthetic details are discussed in the next sections, **3.1.3.3** and **3.1.3.4**.

Scheme 5. Synthesis of compounds **32** and **33**.

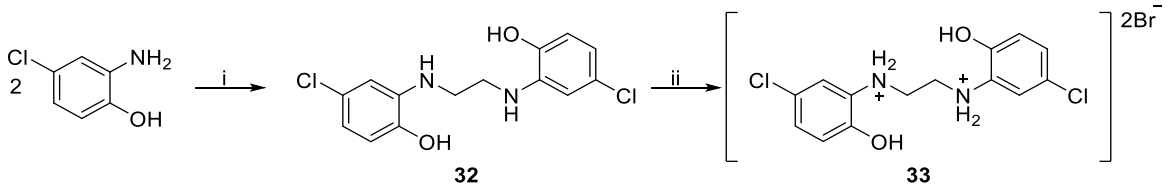

[a]Reaction conditions: (i) dibromoethane (DBE), DMF, 100 °C, 2 h, inert atmosphere. (ii) BBr_3, 0 °C-room temperature, 5 h.

Scheme 6. Synthesis of compound **35.**

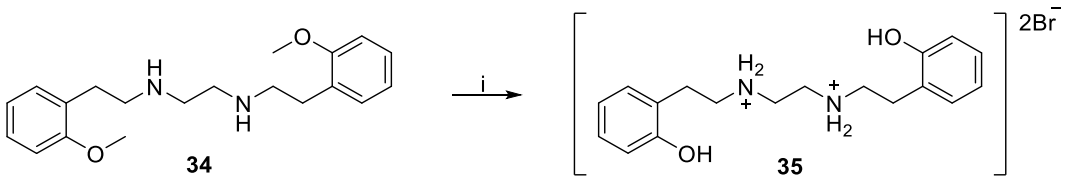

[a]Reaction conditions: (i) HBr aqueous solution (48%), 130 °C, 3 h, room temperature, overnight.

Scheme 7. Synthesis of compounds **37-40.**[142]

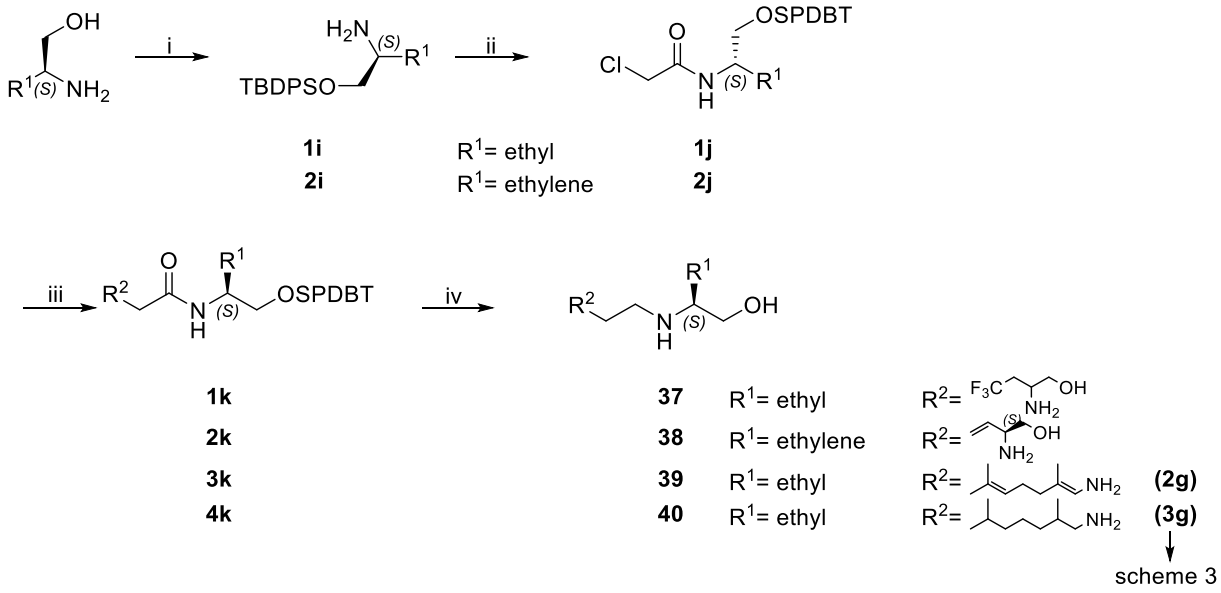

[a]Reaction conditions: (i) (s)-(+)-2-amino-1-butanol, TBDPSiCl, imidazole, dry DCM, room temperature, overnight. (ii) chloroacetylchloride, DIPEA, DCM, room temperature, 16 h. (iii) **nK (n=1-4)**, DIPEA, DMF, 14 h, 70 °C. (iv) $LiAlH_4$, dioxane, reflux, overnight.

3.1.3.3. Symmetrical EMB analogues having N-atoms as substituents on aromatic system (Scheme 5 and Scheme 6)

Compounds **32** and **33** (**Scheme 5**) are analogues to the previously reported EMB analogue 2-({2-[(2-hydroxyphenyl)amino]ethyl}amino)phenol[136] (**Figure 30**). They were synthesized to study the effect of a *p*-Cl substituent and an ether instead of a hydroxyl group on the aromatic ring on activity.

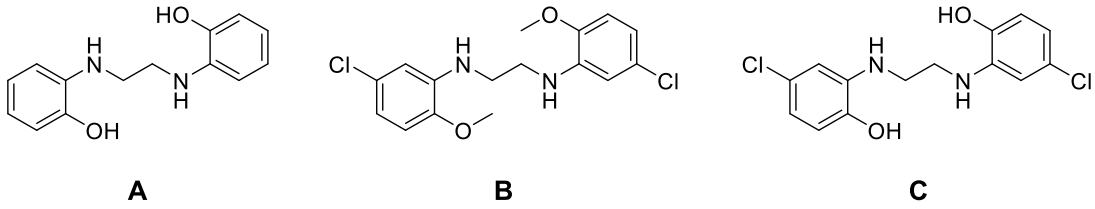

Figure 30. Structures of EMB analogues**. A=** 2-({2-[(2-hydroxyphenyl)amino]ethyl}amino)phenol[136], B= **31** and C= **32**.

First, dibromoethane (DBE) was added to a solution of excess 5-chloro-2-methoxyaniline in DMF.[147] $CaCO_3$ was added as a basic salt to the reaction mixture. The reaction was refluxed for 2 h, followed by extraction and purification using column chromatography to yield **32** as a white solid.

The *O*-demethylation of **32** was done using excess boron tribromide (BBr_3). After five hours of stirring at room temperature, the reaction was quenched with MeOH. Commonly, water or a basic aqueous solution (Na_2CO_3) could be used to quench the reaction, giving boric acid and HBr or NaBr as by-products.[148] Using MeOH, however, would give trimethyl borate and HBr, which could be easily removed from the reaction mixture by evaporation under vacuum. The product is obtained as a dibromide salt. Interestingly, $[M+Br]^+$ peak was observed both in APCI-MS and ESI-HRMS spectra of compound **33** (**Figure 31**). It has been reported that anions could be stabilized by dicationic centers[149, 150, 151, 152], which may be the case here.

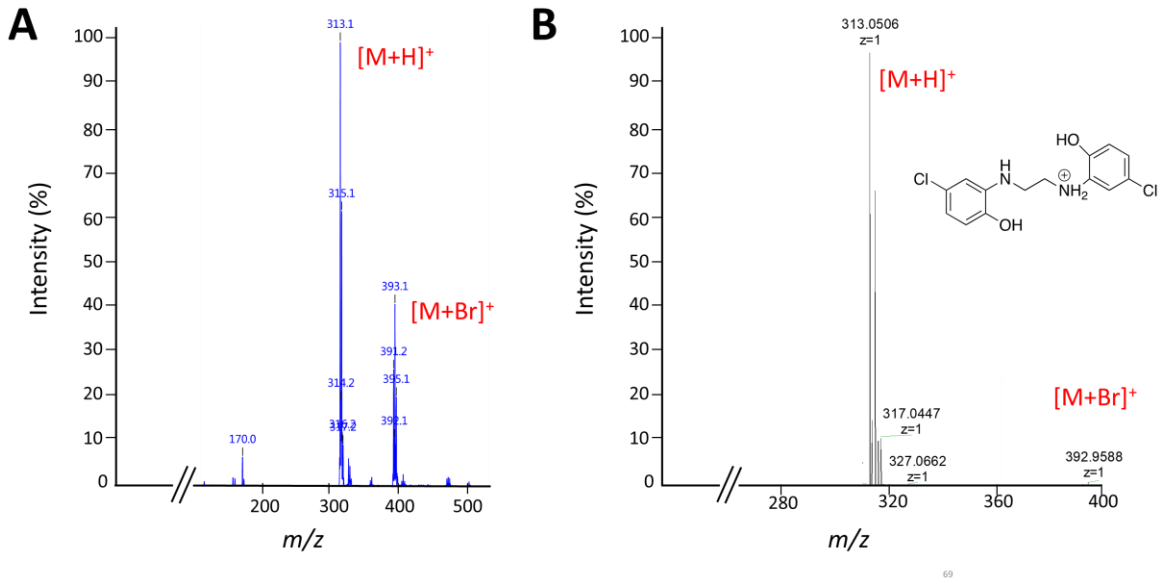

Figure 31. Positive mode MS-spectra. **(A)** APCI-MS **(B)** ESI-HRMS of **33**.

The 2-methoxy group in compound **34** was cleaved at 130 °C using a 48% aqueous HBr solution (**Scheme 6**) to give **35** as a salt.[148] The obtained salt was purified using preparative HPLC. The hydrolysis could also be carried out with BBr_3 as compound **33.**

Compound **35** is an analogue of the previously synthesized 2-methoxyphenylethyl EMB analogue, compound **34**, which showed 40% inhibition against *Mtb* at 10 µg/mL (25µM) compared to 67% inhibition of EMB at the same concentration.[44]

3.1.3.4. Synthesis of EMB analogues with alkyl side chains (37-40)

The synthetic scheme (**Scheme 7**) mostly followed a previously reported protocol.[142] The first step was the protection of the hydroxyl group in the aminoalcohol with *tert*-butyldiphenylsilyl chloride (TBDPSiCl). Imidazole and TBDPSiCl were stirred for 15 min before the addition of the amino alcohol. This allowed the formation of the activated butyldiphenylsilyl imidazole; a stronger silylating agent. In this reaction, imidazole acted as a catalyst as well as a base to help remove produced HCl.[153, 154] During work up, pH was kept <12 to avoid cleavage of the silyl group.[154] After purification by column chromatography, the yield obtained ranged from 67-99% yield (**1-2i**). We observed that a second addition of imidazole after the addition of the amino alcohol, helped improve the yield. This could be due to excess HCl in the reaction, hindering the regeneration of the catalyst. This was especially observed when the amino alcohol was in the form of a hydrochloride salt (**2i**). Auxiliary bases such as triethylamine could be added in this case to help in the regeneration of the catalyst.[153, 154]

The next step was adding the ethylene group of EMB through amide coupling with chloroacetyl chloride (**1-2j**).[155] Then either a second amino alcohol or an alkyl amine (**2g** or **3g**) was added through a nucleophilic substitution reaction. The order of addition of the reactants affected the obtained yield when the second amino alcohol was a hydrochloride salt. Stirring the amino alcohol first with excess DIPEA allowed the deprotonation of the primary amine, and thus the free base (nucleophile) could react readily to give **2k**. The excess DIPEA helped in the removal of the produced HCl from the reaction as well. Several trials of purification of **2k** resulted in very low yields. The ^{1}H NMR spectrum could not confirm the purity of the compound. However, direct mass measurements of the TLC spots suggested that all the spots were isomers (same mass). **3k** and **4k** were synthesized from reacting **1j** with **2g** or **3g** respectively. The yields of this reaction ranged from 5-40%.

The final step was the reduction of the amide and deprotection of the silyl group using $LiAlH_4$ in dioxane. [44] **1-4k** was added to a mixture of $LiAlH_4$ in dry dioxane at 0 ^{o}C. The mixture was stirred overnight under argon at 100 ^{o}C. We used dioxane instead of tetrahydrofuran (THF)[142] which is commonly used as a solvent in reduction reactions with $LiAlH_4$. Alkyl amide reduction is challenging due to its low reactivity, which could be overcome by increasing the time of the reaction or increasing the temperature. Therefore, dioxane was the solvent of choice as it allowed heating at a higher temperature (101 ^{o}C) compared to THF, and thus helped move the reaction forward. The workup was done by carefully adding H_2O (H_2O:$LiAlH_4$, 1:1), then

NaOH 15% aqueous solution (H_2O:$LiAlH_4$, 1:1) and finally H_2O (H_2O:$LiAlH_4$, 3:1). This work up method help dissolve and break up the slurry into fine granules of Li^+ and Al^{3+} salts byproducts which are easily filtered.

After filtration, the solvent was evaporated and the pure **37** was obtained by recrystallization from a chloroform/heptane mixture**.** HPLC purity was 89% and was not further purified since did not show any *in vitro* activity.

Compounds **38, 39** and **40** shown in **Figure 32**, however, could not be purified by recrystallization nor by column chromatography. Trials to precipitate the pure **39** and **40** as hydrochloride salts were not successful as well. Preparative TLC for the purification of compound **38** was not successful. None of the collected bands showed the mass of the product.

SQ109[156], currently in clinical trials, has been reported to have pleiotropic effects which could explain its high potency and low resistance. Besides targeting the MmpL3 transporter[157], it inhibits MK biosynthesis by inhibiting MenA and MenG enzymes. Therefore, PMF in mycobacteria is disrupted and therefore ATP synthesis is inhibited.[42] Compound **39** was designed as a chimera of EMB and SQ109 to test the effect of the geranyl side chain on activity. Compound **40** is the saturated analogue of **39** (**Figure 32**). Unfortunately, both compounds could not be tested *in vitro* due to the failure of purification.

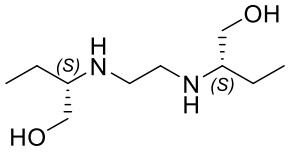

EMB

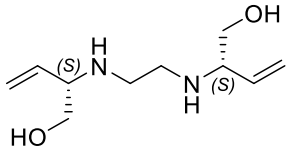

38

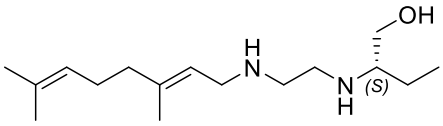

39

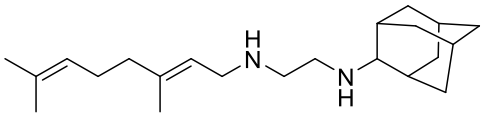

SQ109

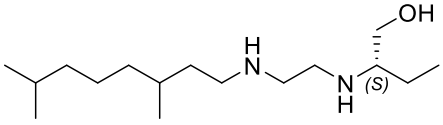

40

Figure 32. Structures of EMB and SQ109 compared to **38**, **39** and **40**.

3.2. *In silico* studies

3.2.1. Structure-activity relationship (SAR) of Q203-CIII$_2$CIV$_2$ IPAs

The recently published electron cryomicroscopy structures (3 Å) of the free (PDB:7rh5) and Q203-bound (PDB:7rh7) *Msmeg* CIII$_2$CIV$_2$[**] showed that Q203 binds at the oxidation site Q_o (Q_p) where MKH_2 is oxidized to MK and that there may be two binding positions of MKH_2 at the Q_o site. The first one is far from the redox center (**Figure 33A**), where MKH_2 is probably loosely bound to Phe 156. The second one is located deeper in the Q_o site and close enough to FeS and His 368 allowing for the transfer of electrons (redox reactions). Q203 blocks both positions by filling the binding pocket (**Figure 33A**). [107]

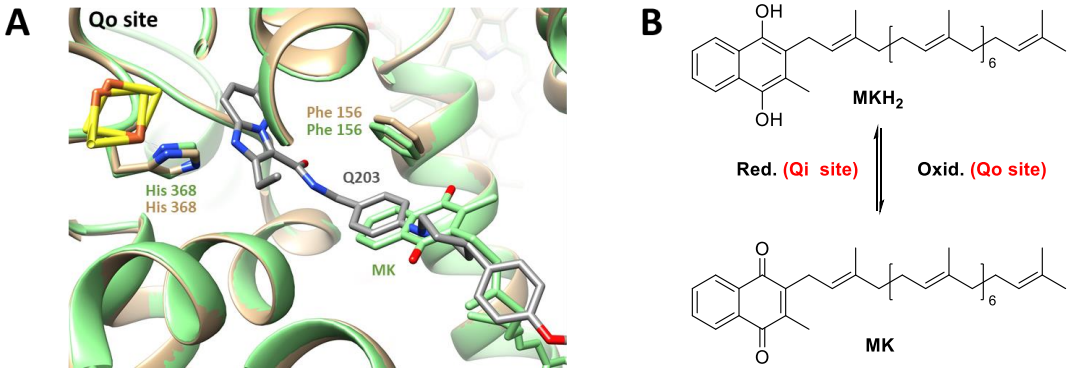

Figure 33. **(A)** Q_o site of *Msmeg* CIII$_2$CIV$_2$. The free (PDB:7rh5, green) and Q203-bound (PDB:7rh7, beige) *Msmeg* CIII$_2$CIV$_2$ models were superimposed using UCSF Chimera software.[83] MK is shown in one position, close to the Phe 156 residue. Q203 binds deeper in the pocket, blocking the two proposed binding positions of MK/MKH_2 at the Q_o site. **(B)** Structures of MK and MKH_2.

We used the generated model of Q203-bound *Msmeg* CIII$_2$CIV$_2$ to better understand the drug-target interactions. Our investigations showed three main interactions in the head region (IP) of Q203, namely a halogen bond between the chlorine at C6 and the backbone carbonyl of Leu 166 (QcrB subunit), a hydrogen bond between N1 of the IP and His 368 (QcrA subunit), and van der Waals interactions between the ethyl group and Ile 178 (QcrB subunit, **Figure 34A and C**).

The distance between the ethyl group and the Ile 178 alkyl side chain was ~ 4 Å, suggesting that a chain longer than the ethyl group is not favoured. The previously reported significant

[**] The electron cryomicroscopy *Msmeg* CIII$_2$CIV$_2$ structure was determined by David Yanofsky in the Lab of Prof. Rubinstein, Hospital for Sick Children, Toronto, Canada.

decrease in the activity of IPAs with propyl and isopropyl chains also supported this hypothesis.[105] A recently published *Mtb* $CIII_2$ model[158] reported an interaction between 6-Cl and Tyr 164 via a water molecule between the two residues. The water molecule formed a halogen bond with 6-Cl and a hydrogen bond with Tyr 164 simultaneously. Two possible hydrogen bonds between N1 of IP; one with His 375 and another with Glu 314 were reported. In *Msmeg*, an aspartate (Asp 309) replaces Glu 314 in *Mtb*. A hydrogen bond between N1 of IP and Asp 309 could not be detected in the *Msmeg* $CIII_2CIV_2$ model, however, the distance between Asp 309 and the IP (3.5 Å) suggested that a hydrogen bond was possible (**Figure 34A and C**).

In the neck (linker) region of Q203, a hydrogen bond between the amide and Thr 308 was found possible (**Figure 34A and C)**. Thr 308 is homologous to Thr 313 in *Mtb* which has been reported to be important for IPA binding. [85]Although an earlier study suggested that Thr 313 formed a hydrogen bond with N1 of the IPA, we found that Thr 308 was closer to the neck (<4 Å), thus suggesting that a hydrogen bond with the amide was more likely. In line with our findings, the recently published electron cryomicroscopy model of *Mtb* $CIII_2$ showed that Thr 313 formed a hydrogen bond with the amide linker (**Figure 34D)**.[158]

Finally, a π-π interaction was observed between Phe 156 and the benzyl group in the tail (~3.5 Å, **Figure 34A**).[107] This finding suggested that the importance of a long lipophilic tail was for better membrane penetration or improved metabolic stability rather than target interactions. Moreover, the long lipophilic tail would fill in the binding pocket, blocking the two binding positions of MKH_2.

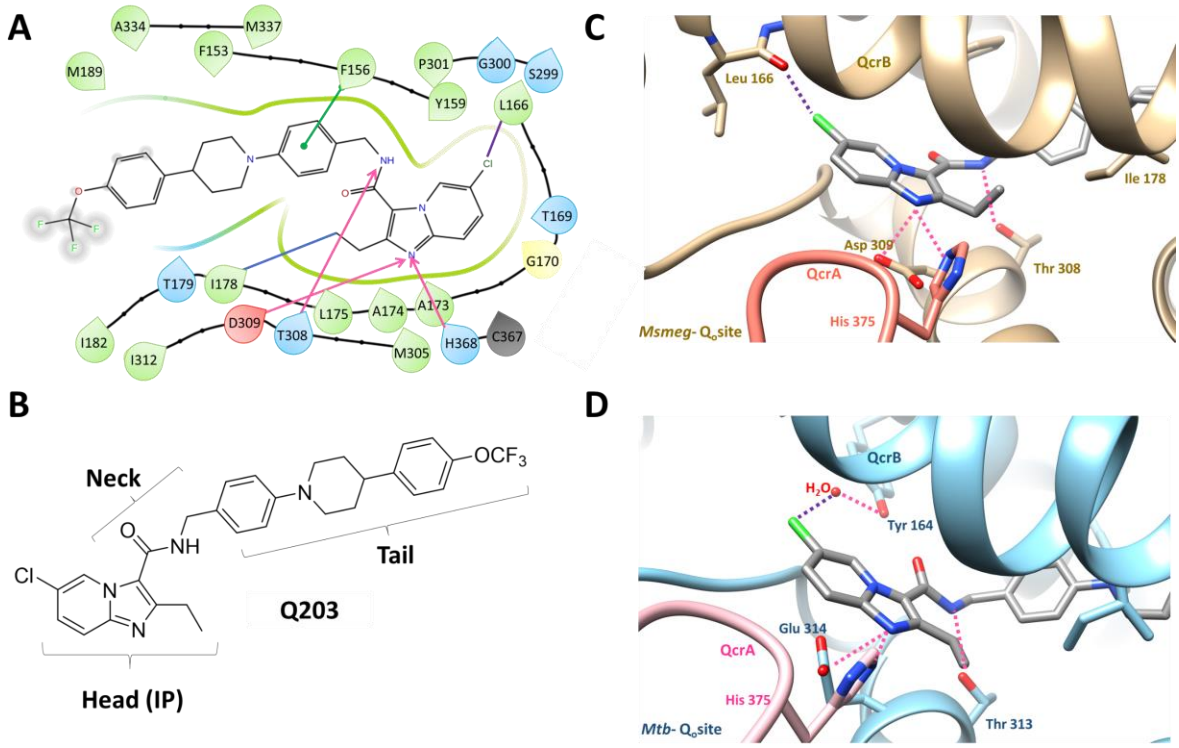

Figure 34. Q203 binding site interactions. **(A)** 2D diagram of Q203 interactions at the *Msmeg*-Qo site. Hydrogen bonds are shown in pink, halogen bonds in purple, π-π interactions in green and van der Waals interactions are shown in blue. (**B**) Structure of Q203. (**C**) 3D representation of *Msmeg*-Qo site. (**D**) 3D representation of *Mtb*-Qo site. **C** and **D** show a comparison between Q203 main interactions (head and neck) in *Msmeg*[107] and *Mtb*[158] models. The figures were generated using Schrödinger software (Schrödinger Suite 2022-3, Schrödinger, New York, USA, NY, 2021) (**A**) and UCSF Chimera software (**C-D**).[83]

Docking compound **24** in *Msmeg* $CIII_2CIV_2$ showed a second possible π-π interaction with Tyr 153 and the benzoxazole ring (**Figure 35A**). Compound **27** showed the main interactions in the head and neck. Hydrophobic interactions are also possible with its flexible tail (**Figure 35B**).

It is clear from the above-mentioned SAR and docking results that the main interactions lie in the head and neck regions, while a long tail helps in filling in the binding pocket. These observations were further investigated in the biological assays discussed in section **3.3.1**.

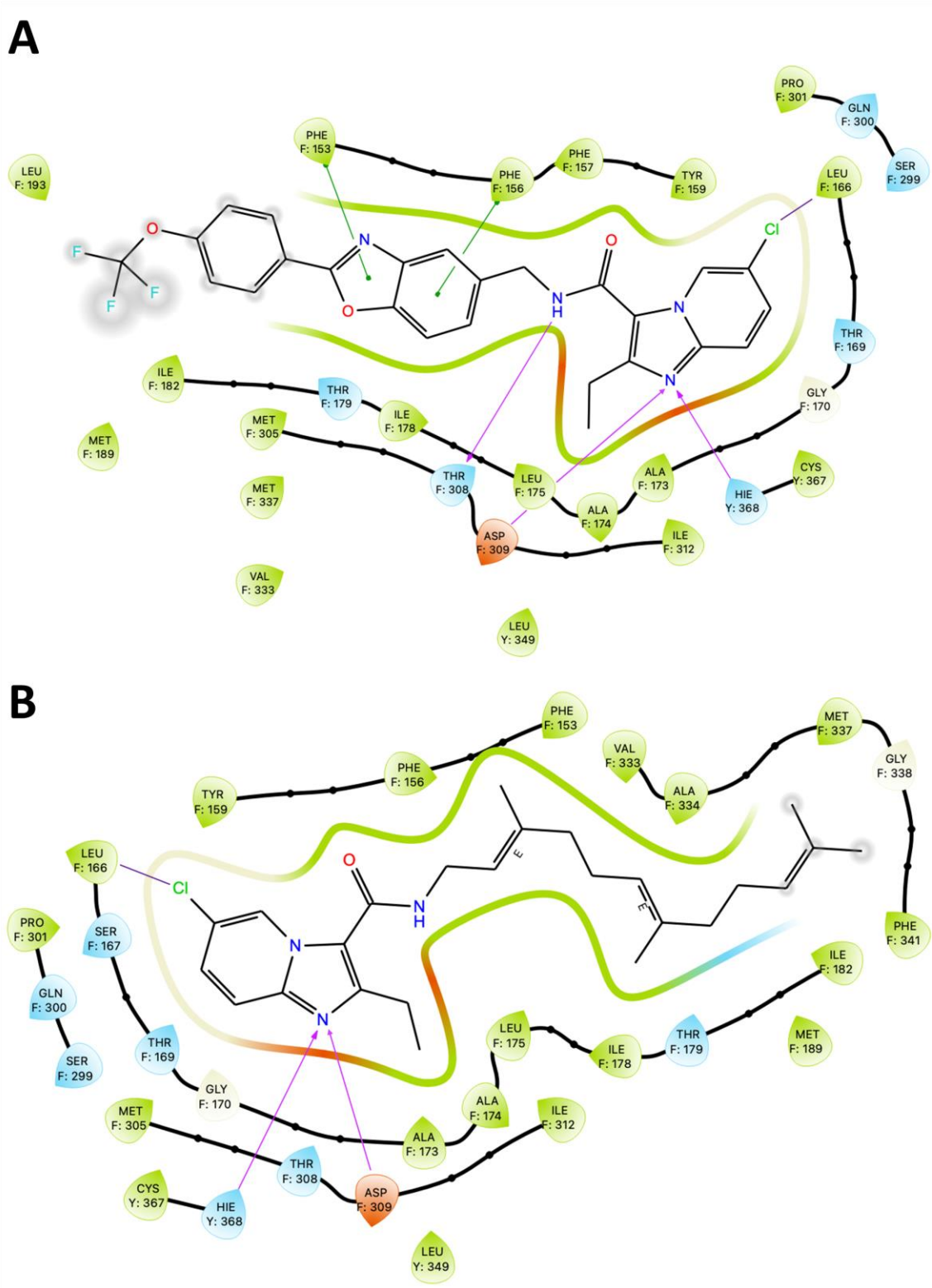

Figure 35. 2D representations of compounds **24 (A)** and **27 (B).** Hydrogen bonds are shown as magenta arrows, halogen bond is shown as purple line and green lines represent the π-π interactions.

3.2.2. SAR of EMB

The electron cryomicroscopic structure of *Mtb*-EmbB bound to EMB[80] (2.97 Å, PDB:7bvf) showed that two positively charged basic amines ($pKa_1 = 6.35$ and $pKa_2 = 9.3$)[159] are important for electrostatic interactions with the catalytic residues Asp 299 and the phosphate group of the decaprenylphosphate (DP, **Figure 36B**). They may also form cation-π interactions with Trp 988 and Tyr 302. The α-ethyl side chains could form hydrophobic interactions with Met 306, Ile 303, Trp 592 and Trp 1028. Finally, the two β-hydroxyl groups could form hydrogen bonds (H-bonds) with Glu 327 and His 594 residues in both Emb proteins (**Figure 36A**). The DP was found stabilized in place by interactions with Arg 403, Thr 590 and Trp 592. It could also form an electrostatic interaction with one of the nitrogen atoms (**Figure 36B**).

Mutations to Met 306[160], which is conserved in all EmbB proteins, have been reported to decrease the binding affinity to EMB without affecting the enzymatic activity. Met 306 normally interacts with the neighbouring Glu 327 and Tyr 302 and therefore mutations in Met 306 are thought to cause changes in the interaction and binding to EMB. Gly 406 and Gln 497 are also considered hotspots for resistance, despite the absence of direct interaction with EMB (10 Å away). Gln 497 interacts with Glu 328 which in turn interacts with Glu 327. Mutations to Gln 497 would lead to disruption of these interactions and consequently to EMB. It is hypothesized that Gly 406 mutation to a bulkier side chain, would lead to steric hindrance and thus conformational changes at the binding site.[80]

It has been reported that the *S*, *S* isomer is 500x more potent than the *R*, *R* isomer.[142] This may be due to the disruption of the H-bond and hydrophobic interactions of the side chain. A two-carbon spacer between the nitrogen atoms has been reported to be important for EMB activity.[136, 143] This hypothesis is supported by the 3D structure of EMB interactions at the active site, where a longer carbon spacer would lead to the loss of one or all of the crucial electrostatic interactions.

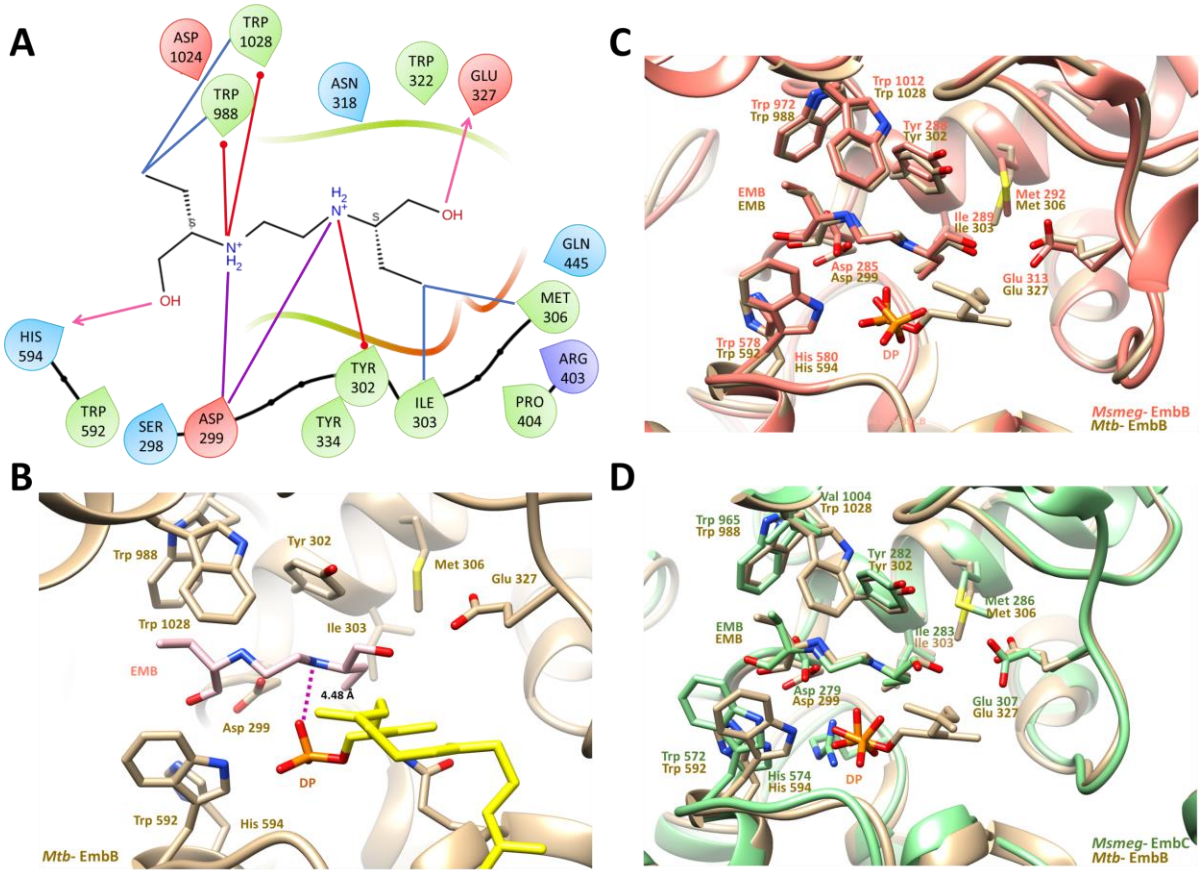

Figure 36. EMB interactions at *Mtb*-EmbB active site. **(A)** 2D diagram of EMB interactions. Hydrogen bonds are shown in pink, electrostatic interactions are in purple, red represents the cation-π interactions and Van der Waals interactions are represented in blue. **(B)** 3D representation of EMB at *Mtb*-EmbB active site. The line in magenta shows the distance between one of the oxygen atoms of the phosphate group and one nitrogen atom of EMB (4.48Å). **C** and **D** show *Mtb*-EmbB superimposed with *Msmeg*-EmbB (PDB:7bvc) and *Msmeg*-EmbC (PDB:7bve), respectively. The figures were generated using Schrödinger software (Schrödinger Suite 2022-3, Schrödinger, New York, USA, NY, 2021) (**A**) and UCSF Chimera software (**B-D**).[83]

As shown in **Figure 36C** and **D**, the active sites of *Mtb*-EmbB (PDB:7bvf) and *Msmeg*-EmbB (PDB:7bvc) and *Msmeg*-EmbC (PDB:7bve) are quite similar. In EmbC there is only one mutated residue (Trp 1028 to Val 1004). The structure of *Mtb*-EmbB was used for docking compounds **32-37** to investigate the possible interactions at the binding site.

The results of docking compounds **32** and **33** (**Figure 37**) showed three possible π-π interactions between the aromatic rings and Trp 988, Trp 1028 and Tyr 302. In compound **33** (**B**), one of the hydroxyl groups could form a hydrogen bond with the catalytic aspartate residue (Asp 299). Replacing the secondary alkyl amines with aniline resulted in hydrogen bonds instead of electrostatic interactions between Asp 299 and the two amino groups. This could affect the binding affinity of **32** and **33**. The predicted pKa values of nitrogen atoms were 2.64 and 4.73 (**32**) and 2.78 and 4.86 (**33**).[††]

The docking results of **34** (**Figure 38A**) showed that the two hydrogen bonds between the hydroxyl groups and Glu 327 and His 594 were lost, however, aromatic hydrogen bonds with Asp 1024, Glu 327, Tyr 334 and Asp 299 were found possible. Three possible cation-π interactions between one amino group and Trp 1028, Trp 988 and Trp 592 were observed, in addition to Tyr 302 and the second amino group. The electrostatic interactions between the two basic nitrogen atoms and Asp 299 were maintained. One of the phenoxymethyl groups is solvent exposed.

In compound **35** (**Figure 38B**), two hydrogen bonds between one hydroxyl group and Asp 1024, and between the second hydroxyl group and Asp 299 were observed. Four cation-π interactions were observed: two between one of the nitrogen atoms and Trp 1028 and Trp 592, and two between the second nitrogen atom and Tyr 302 and Trp 988. In addition to π-π interactions between one phenyl ring and Tyr 302. Electrostatic interactions with the catalytic residue Asp 299 were maintained. Despite the shown possible interactions, compound **35** did not show activity in the *Mtb* growth inhibition assays.

The docking results of compounds **36**[‡‡] and **37** showed clashes between the OCF_3 group Trp 1028 and Trp 988 (**Figure 39**). Electrostatic interactions with the Asp 299 and cation-π interactions with Tyr 302 were observed. The predicted pKa values were 5.67 and 8.45 for compound **36** and 5.83 and 9.28 for compound **37**.[§§] The CF_3 group decrease the basicity of the two nitrogen atoms, however, at least one of them can still be ionized at physiological pH

[††] Marvin Sketch version 21.3 was used for pKa predictions.

[‡‡] Compound **34** was previouslyreported in[44]**.**

[§§] Marvin Sketch version 21.3 was used for pKa predictions.

(pH = 7) or inside macrophages (acidic pH~5). In compound **36**, the two hydroxyl groups could form hydrogen bonds with Gln 445 and Asp 299.

The docking results showed that compounds **32** and **33** can still bind to the active site, despite the decrease in the nitrogen basicity. Compounds **34** and **35** showed similar interaction to EMB despite the extended side chain (phenoxyethyl side chain), which differs from the original EMB scaffold: The trifluoromethyl groups in compounds **36** and **37** showed possible interference with nearby Trp residues which might affect their activity. To evaluate these observations, the compounds were tested for *in vitro* growth inhibition in *Mtb. Msmeg, M. abscessus* and *M. intracellulare*. The results of the assays are discussed in section **3.2.2.3**.

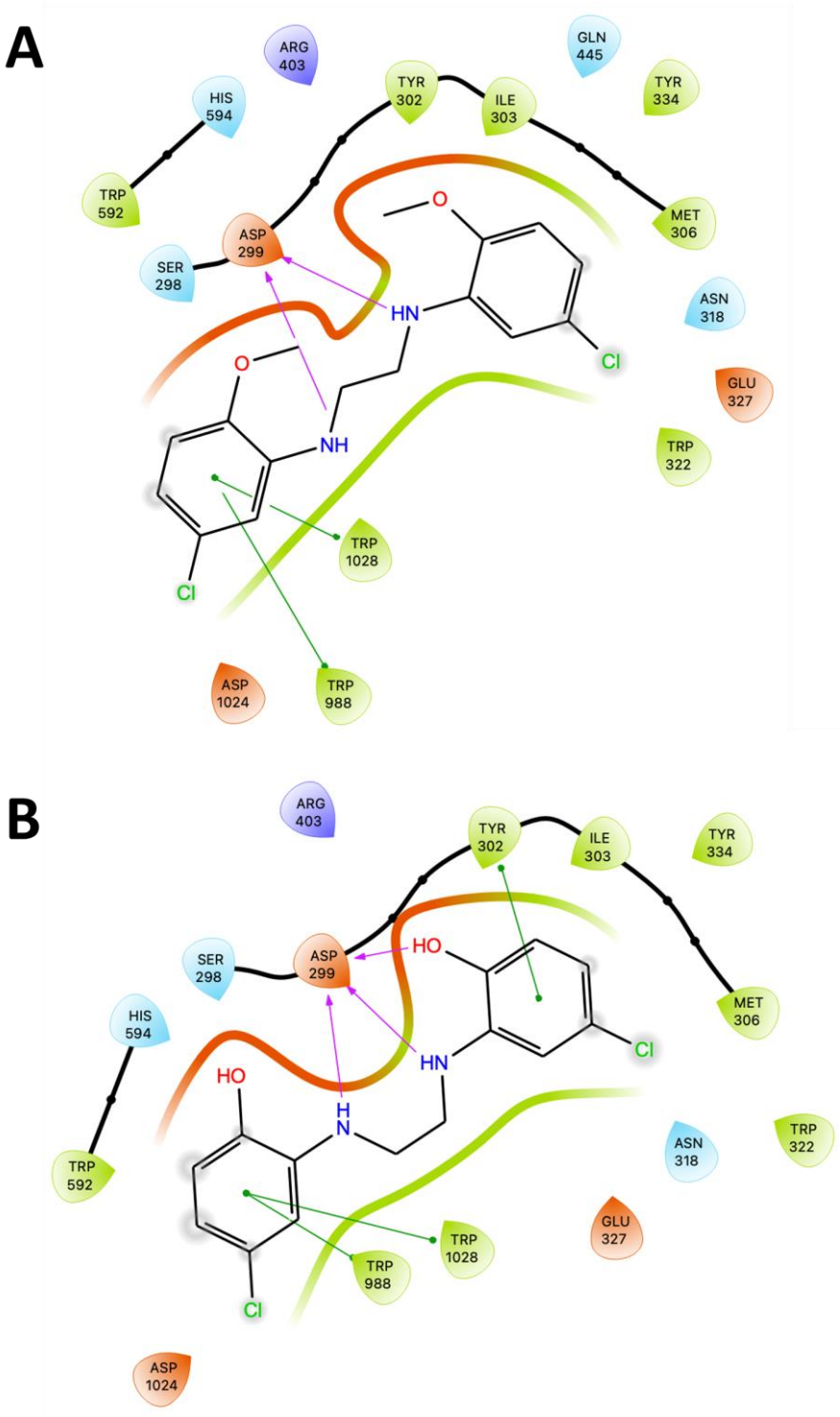

Figure 37. 2D representations of compounds **32 (A)** and **33 (B).** Hydrogen bonds are shown as magenta arrows and green lines represent the π-π interactions.

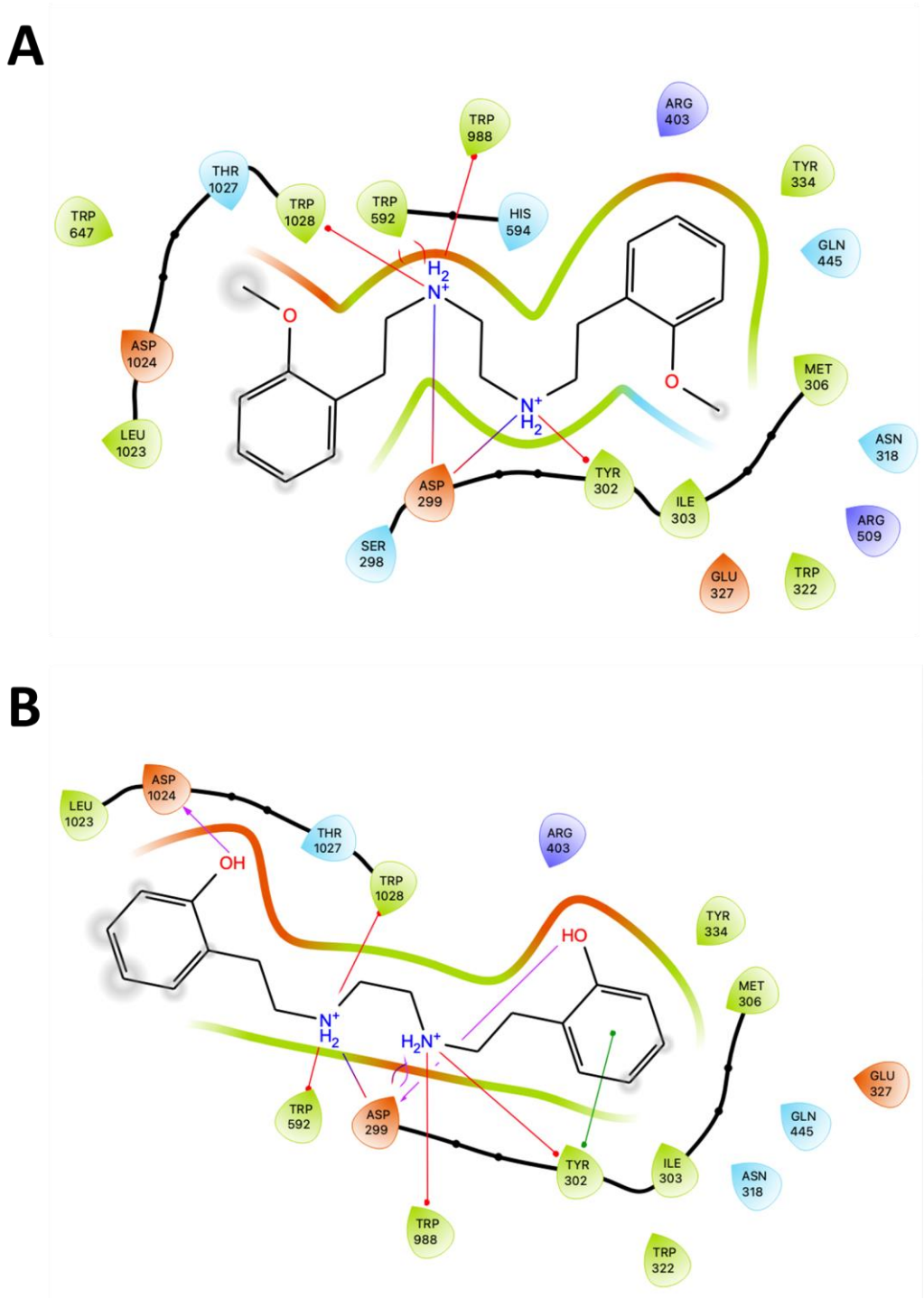

Figure 38. 2D representations of compounds **34 (A) and 35 (B)**. Hydrogen bonds are shown as magenta arrows, electrostatic interactions are in purple, and red lines represent the cation-π interactions.

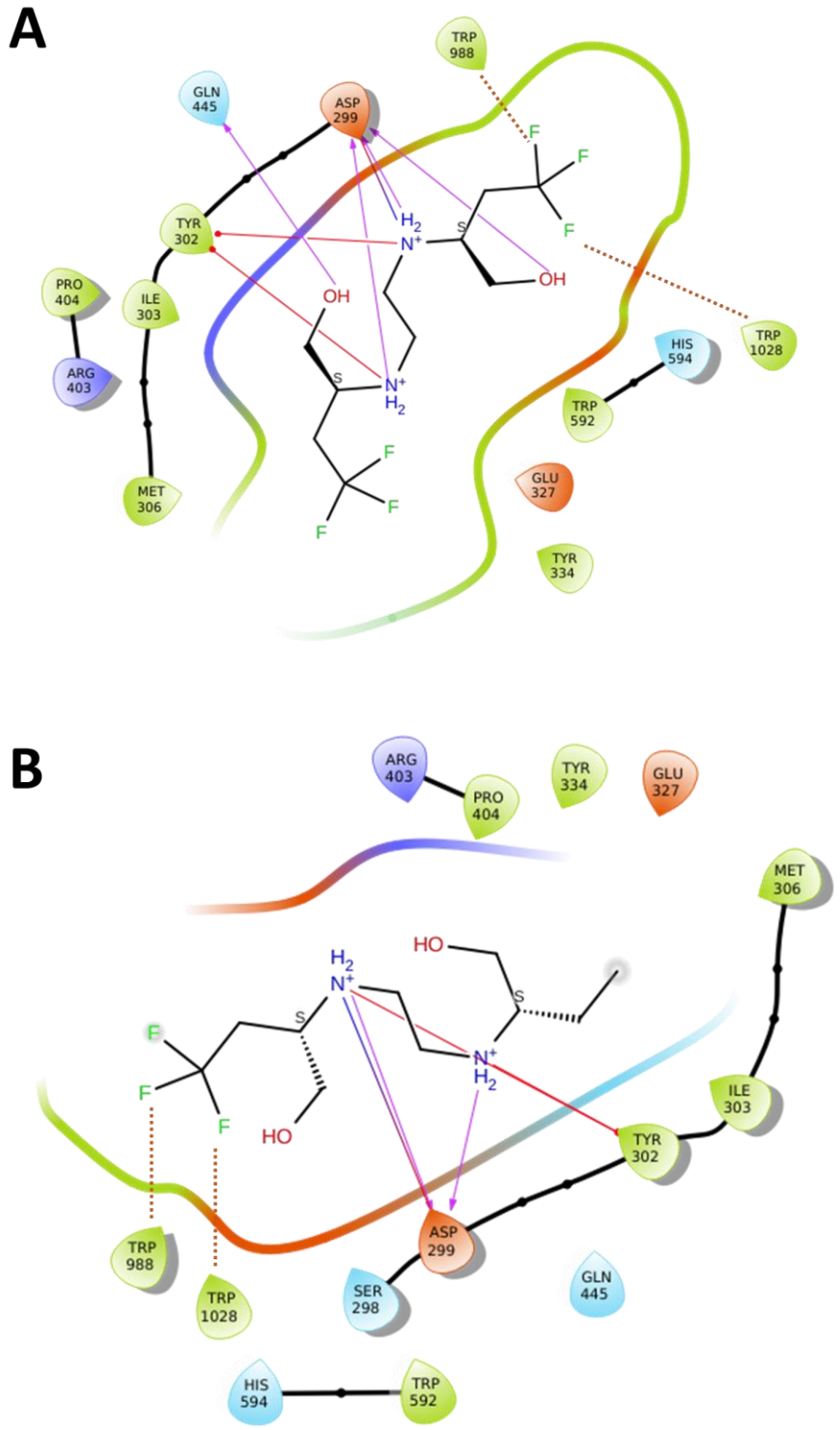

Figure 39. 2D representations of compounds **36 (A) and 37 (B)**. Hydrogen bonds and electrostatic interactions are shown as magenta arrows, red lines represent the cation-π interactions and clashes are represented in brown dashed lines.

3.3. Biological evaluation

3.3.1. IPAs

3.3.1.1. Biochemical assays

In this section, we will discuss the biochemical assays established and conducted in Prof. John Rubinstein's lab at the Peter Gilgan Centre for Research and Learning, the Hospital for Sick Children, Toronto, Canada. The assays were established to evaluate the inhibition of *Msmeg* $CIII_2CIV_2$ by the synthesized IPAs (**1-27**) compared to Q203 and to confirm their specificity to mycobacterial ETC. The fast-growing non-pathogenic *Msmeg* is often used as a model due to structural similarities with *Mtb* for known and putative drug targets.[161] Handling of *Msmeg* requires lower biosafety laboratories (BSL-2), easing assay conduction.[162,163]

3.3.1.1.1. *Msmeg* $CIII_2CIV_2$ activity assay

To quantify the inhibition of $CIII_2CIV_2$, we employed a $CIII_2CIV_2$ activity assay using a Clark-type oxygen electrode. Such assays typically use MKH_2 analogues as electron donors rather than mycobacterial MKH_2 or canonical mitochondrial QH_2, since neither is soluble in the assay's aqueous solution. QH_2 cannot be used in our assays to reduce *Msmeg* $CIII_2CIV_2$ due to the lower redox potentials of mycobacterial $CIII_2$ compared to the canonical $CIII_2$.[164] 2-Methyl[1,4]naphthoquinone (menadione) and 2,3-dimethyl[1,4]naphthoquinone (DMW) are examples of two MKH_2 analogues previously used (**Figure 40**).[48, 68] These analogues were reported to suffer from autoxidation which leads to O_2 reduction even in the absence of $CIII_2CIV_2$.[165] The enzyme catalyzed O_2 reduction could therefore be calculated by subtracting the background reduction from the observed reduction in the presence of $CIII_2CIV_2$. The rate of autoxidation of menadiol has been reported to be higher than $DMWH_2$ at neutral or basic pH. However, a recent study by our collaborators showed the rate autoxidation of $DMWH_2$ was higher at pH 7.5.[107] Nevertheless, both have relatively slow rates of autoxidation compared to other [1,4]naphthoquinone analogues.[165] We favoured the use of DMW over menadiol as it has been reported to show greater $CIII_2CIV_2$ activity and more favourable redox potentials than menadiol. [107, 68, 166] The addition of exogenous SOD was proven to suppress the quinol autoxidation[107, 165], thus, we added excess exogenous bovine C-type SOD (500 nM) in our assay to measure the $CIII_2CIV_2$ oxidoreductase activity with the suppression of quinol autoxidation.

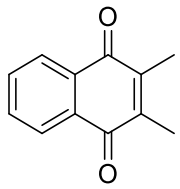

2,3-dimethyl-[1,4]naphthoquinone

(DMW)

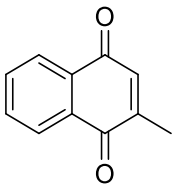

2-methyl-[1,4]naphthoquinone

(M**enadione)**

Figure 40. Examples of MKH_2 analogues used in $CIII_2CIV_2$ activity assays**.**

In contrast to our recent study where the electron donor DMW was reduced chemically[107], here we used an assay where DMW was reduced to $DMWH_2$ by adding the NADH dehydrogenase enzyme from *Caldalkalibacillus thermarum* (NDH-2) to the reaction mixture[52] DMW was reduced by NDH-2 using electrons from the oxidation of NADH. The reduced $DMWH_2$ was re-oxidized to DMW by the *Msmeg* $CIII_2CIV_2$ catalyzing the reduction of oxygen to H_2O (**Figure 42A**). The enzymatic reduction of DMW was found to be more reliable than chemical reduction. The concentration of the chemically reduced DMW varied from batch to batch. This variation could be due to the formation of by-products such as semi-reduced naphthoquinone or saturated diol (**Figure 41**).[167, 168] We could not identify the presence of such side products. However, it has been reported before in $NaBH_4$-mediated ketone reduction of α,β-unsaturated ketones.[167, 168]

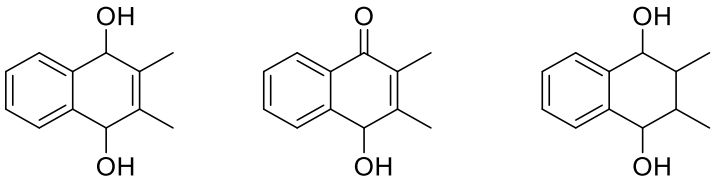

$DMWH_2$ **1** **2**

Figure 41. Possible by-products from DMW chemical reduction. (1) semi-reduced DMW, (2) 2,3-dimethyl-1,2,3,4-tetrahydronaphthalene-1,4-diol.[167, 168]

In the assay, NADH was added in excess to the chamber of the oxygen electrode to initiate the rapid reduction of all the DMW to $DMWH_2$, which then allowed a slower reduction of O_2 to H_2O by $CIII_2CIV_2$ (**Figure 42B**, *orange curve*). This reduction of oxygen proceeded until all oxygen in the chamber was consumed (**Figure 42B**, *orange curve*). The specific activity of $CIII_2CIV_2$ in this assay was found to be 340 ± 24 e^-/s (± s.e. from 5 separate measurements each from a different batch of protein), ~3 fold higher than measurements with chemically reduced DMW.[107] As in our previous study with chemically reduced DMW[107], there was residual $CIII_2CIV_2$ activity even at high concentrations of Q203 (**Figure 42B**, *green curve versus blue curve*). All compounds, including Q203, were tested for binding and inhibition of the purified *Msmeg* $CIII_2CIV_2$ via this assay.

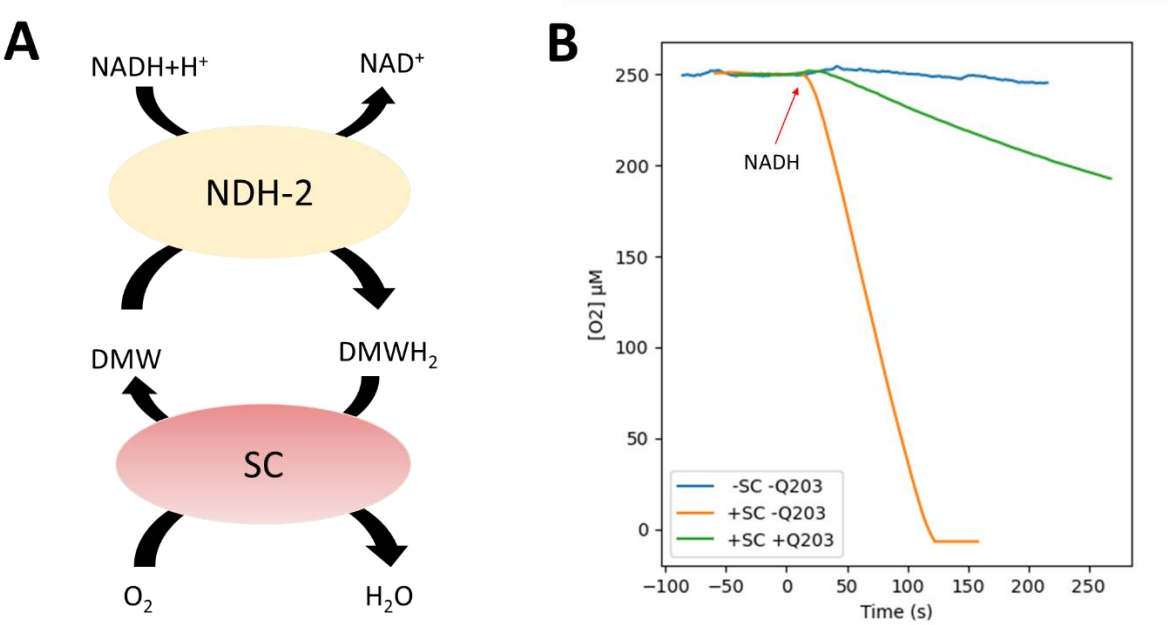

Figure 42. Oxygen consumption assay. (**A**) The assay principle. (**B**) The rate of oxygen consumption in case of no inhibitor '-Q203' (orange), with inhibitor '+Q203' (green), and baseline autoxidation in the absence of $CIII_2CIV_2$, '-SC -Q203' (blue). The red arrow represents the point where NADH was injected. ''Reprinted with permission from [Abdelaziz, R.; Di Trani, J. M.; Sahile, H.; Mann, L.; Richter, A.; Liu, Z.; Bueler, S. A.; Cowen, L. E.; Rubinstein, J. L.; Imming, P. Imidazopyridine Amides: Synthesis, *Mycobacterium Smegmatis* $CIII_2CIV_2$ Supercomplex Binding and in Vitro Antimycobacterial Activity. *ACS Omega* **2023**. https://doi.org/https://doi.org/10.1021/acsomega.3c02259]. Copyright [2023] American Chemical Society''

All of the compounds tested do not inhibit *Caldalkalibacillus thermarum* NDH-2.

NADH oxidation assays confirmed that all the compounds tested including Q203 did not inhibit NDH-2, supporting the validity of the oxygen consumption assay results. The concentration tested was 10 µM. The oxidation of NADH was monitored spectrophotometrically at λ = 340 nm. In **Figure 43**, the graphs **(A-C)** show that none of the tested compounds **1-26** binds to NDH-2, thus validating the oxygen consumption assay results. The baseline, where no NDH-2 was added to the reaction mixture, is shown in Black. Graph **D** shows that Q203 and compound **27** do not bind to NDH-2. The black line is blank, which is the NDH-2 in the absence of an inhibitor. Compound **27** is shown in magenta and Q203 is in green.

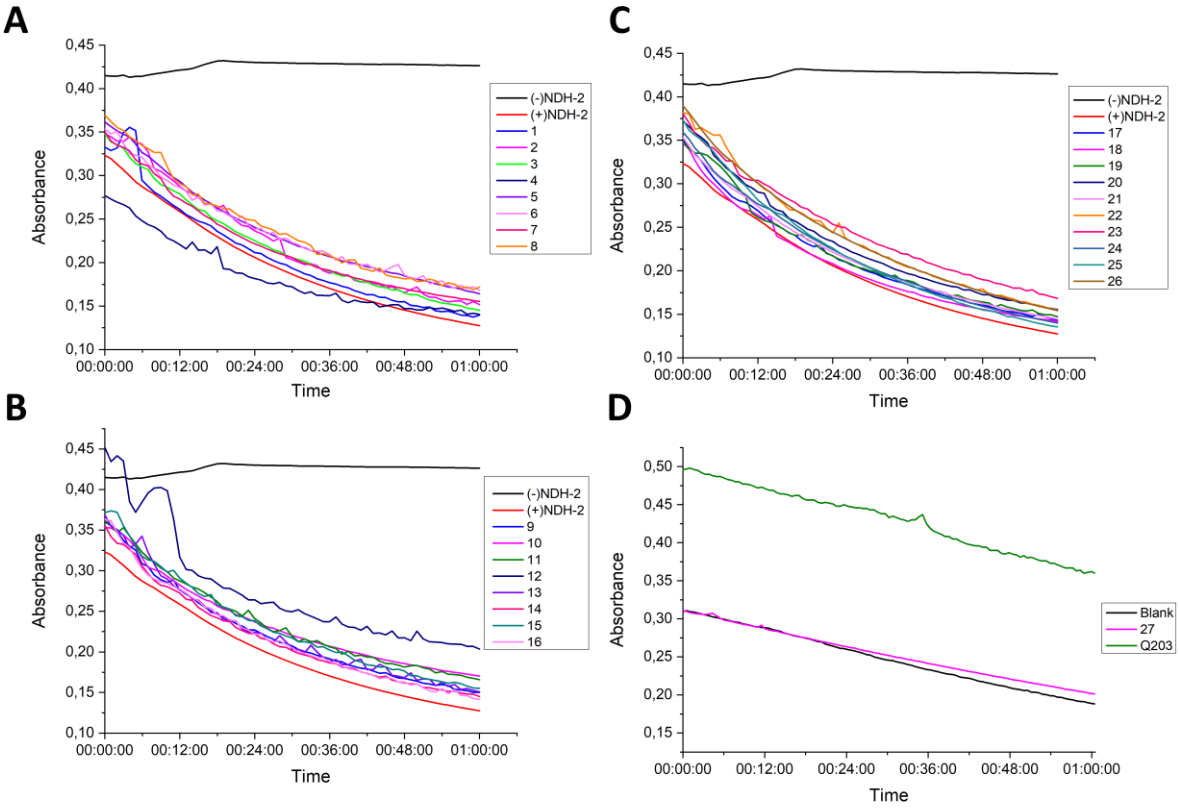

Figure 43. NADH oxidation monitored by absorption at λ= 340 nm. NDH-2 activity was monitored spectrophotometrically by following the oxidation of NADH. ‘‘Reprinted with permission from [Abdelaziz, R.; Di Trani, J. M.; Sahile, H.; Mann, L.; Richter, A.; Liu, Z.; Bueler, S. A.; Cowen, L. E.; Rubinstein, J. L.; Imming, P. Imidazopyridine Amides: Synthesis, *Mycobacterium Smegmatis* $CIII_2CIV_2$ Supercomplex Binding and in Vitro Antimycobacterial Activity. *ACS Omega* 2023. https://doi.org/https://doi.org/10.1021/acsomega.3c02259]. Copyright [2023] American Chemical Society’’

Compound 27 showed inhibition of $CIII_2CIV_2$ that was comparable to Q203.

Compound **27** was synthesized to test the effect of a tail that resembles MK on binding to the active site and electron transfer. This compound had the same head (2-ethyl, 6-Cl) and neck (amide linker) as Q203 and a short isoprene tail (**Table 2**), similar to the natural substrate (MK). At the tested concentration (10 µM), compound **27** showed 88 ± 1% inhibition of $CIII_2CIV_2$ activity, which is similar to inhibition by Q203 (85 ± 7 %, **Figure 44**). Unexpectedly, the substitution of the 6-Cl in the IP with a hydrogen atom showed better percentage inhibition despite the possibility of a halogen bond formation by the chlorine atom. Compound **24**[86] (R^1=Cl) showed only 20 % inhibition, while compound **26** (R^1=H) showed 50 % inhibition (**Figure 44**). The replacement of the halogen at C7 with a methyl group and the shortening of the tail (benzyl group) in compound **25**[102] resulted in very weak to no binding at the tested concentration (10 µM). This compound has been reported by Marvin Miller's research group (ND-008454, section **3.1.1.1**).[102]

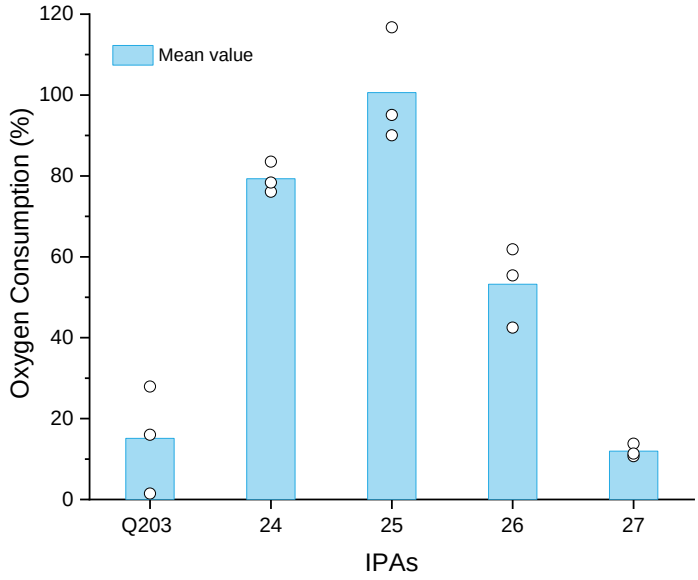

Figure 44. Average % activity against *Msmeg* $CIII_2CIV_2$. The graph shows the average % activity of Q203 and compounds **24-27**. (mean +/- s.d., n = 3 independent assays represented by o in the graph)

The above-mentioned differences support the SAR study from the electron cryomicroscopy *Msmeg*-Q203 model that the main binding interactions between the IPAs and $CIII_2CIV_2$ are between N1 of the imidazopyridine head with His 368 and between the amide bond in the neck with Thr 308 (**Figure 34,** section **3.2.1**). No significant inhibition was detected in compounds with methyl[112] (R^1=CH_3), trifluoromethyl (R^1=CF_3) or trifluoromethoxy (R^1=OCF_3) in the head region (**Table 2**). Bromo-substituted analogues (R^1=Br), however, showed approximately 50% inhibition (**Table 2** and **Figure 45**). 6-Br analogues (**1-4**) were more potent than the 7-Br analogues (**5-8**).

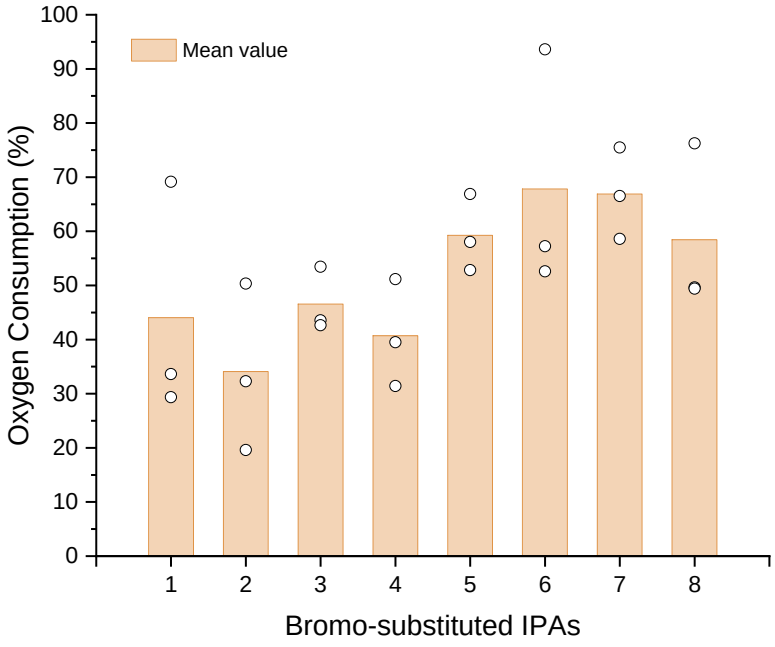

Figure 45. Average % activity against *Msmeg* $CIII_2CIV_2$. The graph shows the average % activity of the bromo-substituted analogues (1-8, R^1= Br) with approximately 50% inhibition. (mean +/- s.d., n = 3 independent assays represented by o in the graph) ''Adapted with permission from [Abdelaziz, R.; Di Trani, J. M.; Sahile, H.; Mann, L.; Richter, A.; Liu, Z.; Bueler, S. A.; Cowen, L. E.; Rubinstein, J. L.; Imming, P. Imidazopyridine Amides: Synthesis, *Mycobacterium Smegmatis* $CIII_2CIV_2$ Supercomplex Binding and in Vitro Antimycobacterial Activity. *ACS Omega* **2023**. https://doi.org/https://doi.org/10.1021/acsomega.3c02259]. Copyright [2023] American Chemical Society''

Table 2. Average % inhibition (μM) of *Msmeg* $CIII_2CIV_2$ by Q203 and IPA analogues**.** Experiments were done in triplicates to calculate the standard deviation (mean ± s.e., n=3 independent assays).

Code	Structure	Average % inhibition [10 μM] ± s.e.
Q203 **(telacebec)**	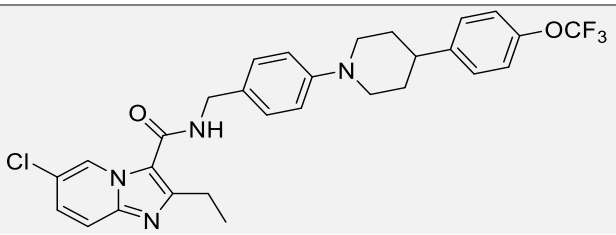	85 ± 7
1	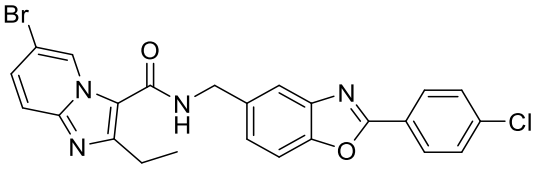	56 ± 13
2	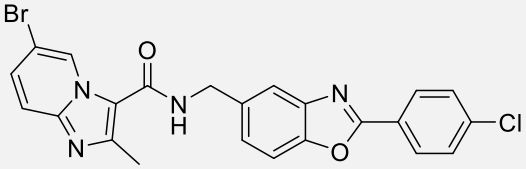	66 ± 9
3	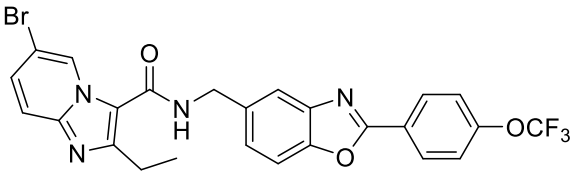	54 ± 3
4	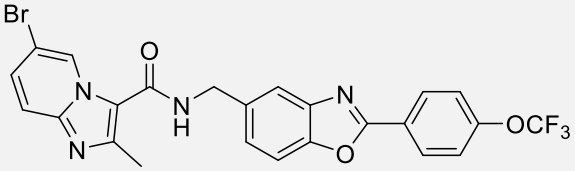	59 ± 6
5	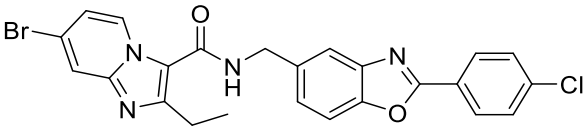	41 ± 4
6	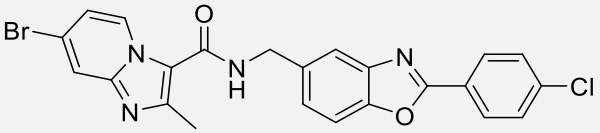	32 ± 13
7	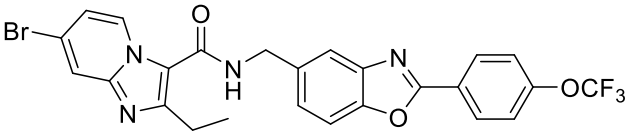	33 ± 5
8	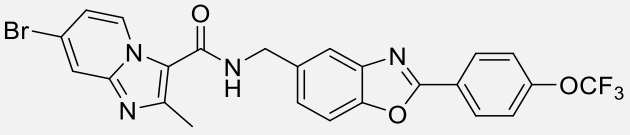	42 ± 9

9	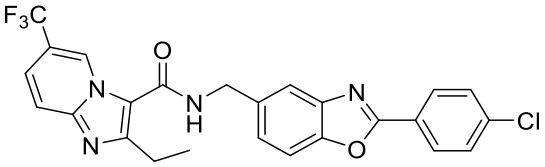	20 ± 23
10	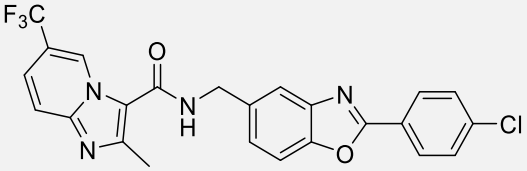	8 ± 6
11	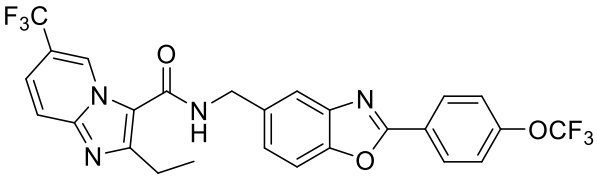	6 ± 7
12	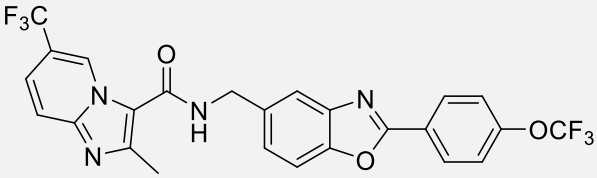	27 ± 7
13	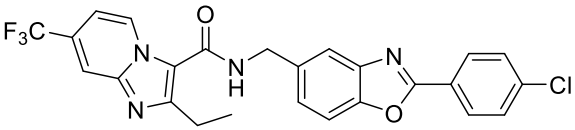	12 ± 8
14	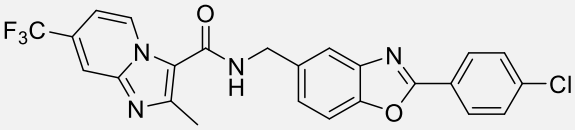	21 ± 4
15	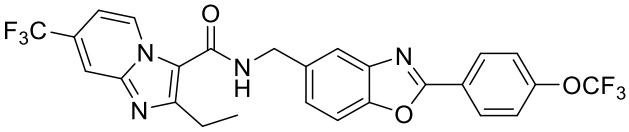	10 ± 14
16	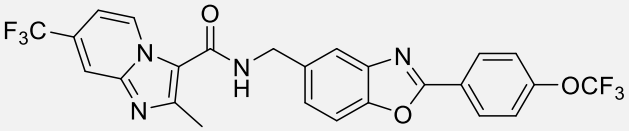	9 ± 8
17	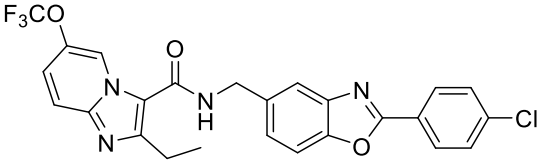	49 ± 13
18	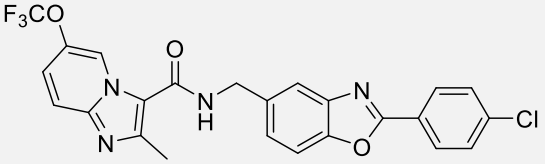	49 ± 18
19	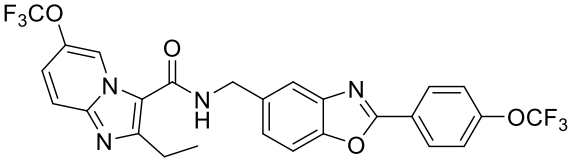	42 ± 17

20	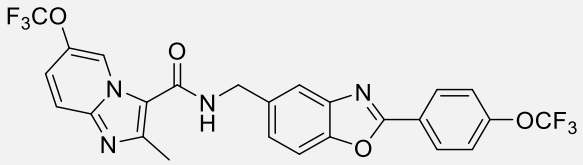	45 ± 10
21	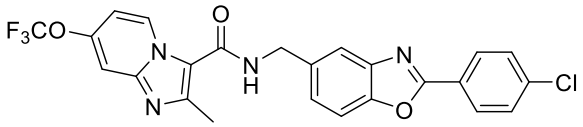	45 ± 15
22	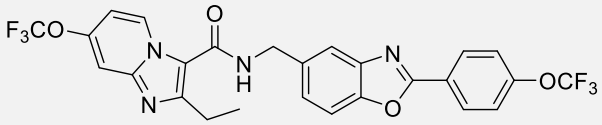	49 ± 22
23	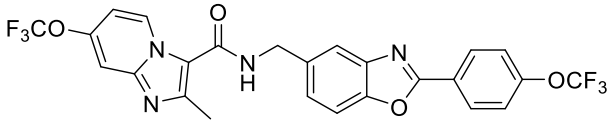	29 ± 3
24[86]	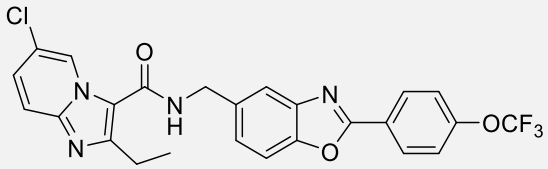	20 ± 2
25[112]	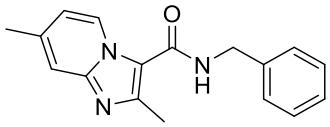	0 ± 8
26	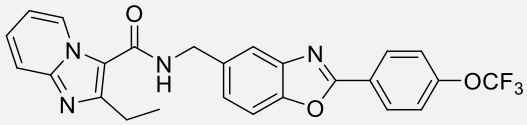	46 ± 6
27	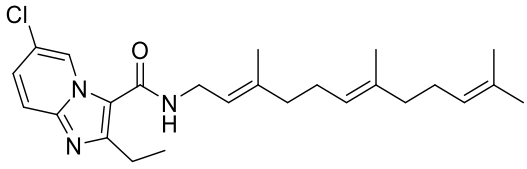	88 ± 1

''The table is adapted with permission from [Abdelaziz, R.; Di Trani, J. M.; Sahile, H.; Mann, L.; Richter, A.; Liu, Z.; Bueler, S. A.; Cowen, L. E.; Rubinstein, J. L.; Imming, P. Imidazopyridine Amides: Synthesis, *Mycobacterium Smegmatis* $CIII_2CIV_2$ Supercomplex Binding and in Vitro Antimycobacterial Activity. *ACS Omega* **2023**. https://doi.org/https://doi.org/10.1021/acsomega.3c02259]. Copyright [2023] American Chemical Society''

Q203 and compound 27 IC_{50} values are relatively similar.

The IC_{50} against *Msmeg* $CIII_2CIV_2$ of both Q203 and **27** was determined through the repetition of the oxygen consumption assay with different concentrations of test compounds (10 µM, 1 µM, 0.1 µM, and 0.01 µM). The IC_{50} values for Q203 and compound **27** were calculated as 99 ± 32 nM and 441 ± 138 nM respectively (mean +/- s.e., n=4 independent assays from biological triplicates, **Figure 46**). These values show that Q203 and **27** have relatively similar potencies, supporting the hypothesis that the tail has no significant effect on the binding but rather the penetration. The assays were repeated on different days and using different batches of $CIII_2CIV_2$, which could explain the high s.e. values. Nevertheless, these values show that compound **27** has relatively high potency, supporting the hypothesis that the tail has no significant effect on the binding but rather the penetration. The IC_{50} in our assay is higher than the IC_{50} reported in inverted membrane vesicles of *Msmeg* (IC_{50}= 20 nM).[169] This could be explained by the high binding affinity of $DMWH_2$ to $CIII_2CIV_2$ in our assays, the high concentrations of DMW (100 µM) and Q203 (10 µM) used, and by the presence of the complex being in detergent rather than in a lipid bilayer.

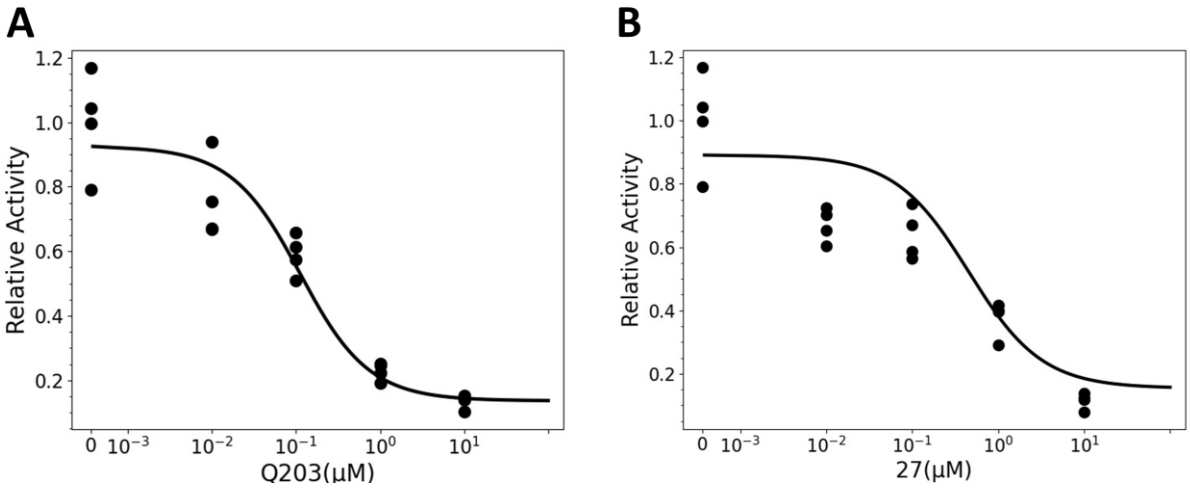

Figure 46. IC_{50} of Q203 **(A)** and compound 27 **(B)**. "Reprinted with permission from [Abdelaziz, R.; Di Trani, J. M.; Sahile, H.; Mann, L.; Richter, A.; Liu, Z.; Bueler, S. A.; Cowen, L. E.; Rubinstein, J. L.; Imming, P. Imidazopyridine Amides: Synthesis, *Mycobacterium Smegmatis* $CIII_2CIV_2$ Supercomplex Binding and in Vitro Antimycobacterial Activity. *ACS Omega* 2023. https://doi.org/https://doi.org/10.1021/acsomega.3c02259]. Copyright [2023] American Chemical Society"

3.3.1.1.2. Mitochondrial CIII activity assay

We tested the activity of some of the IPAs against *Bos taurus* mitochondrial cytochrome bc1 complex (CIII) to verify their specificity against mycobacterial $CIII_2CIV_2$. The IPAs chosen were those which showed strong binding in the above-mentioned *Msmeg* $CIII_2CIV_2$ activity assays.

First, we performed activity assays against sub-mitochondrial membrane particles (SMPs) using a Clark-type oxygen electrode. The SMPs were prepared by the sonication of previously isolated bovine mitochondria[†††] (**see section 7.4.1.3**). This inversion (**Figure 47**) exposed the respiratory complexes, allowing us to study their enzymatic activities. In this assay, Rotenone - a complex I (CI) inhibitor, Antimycin A - a CIII inhibitor, and KCN – a complex IV (CIV) inhibitor were used as positive controls.

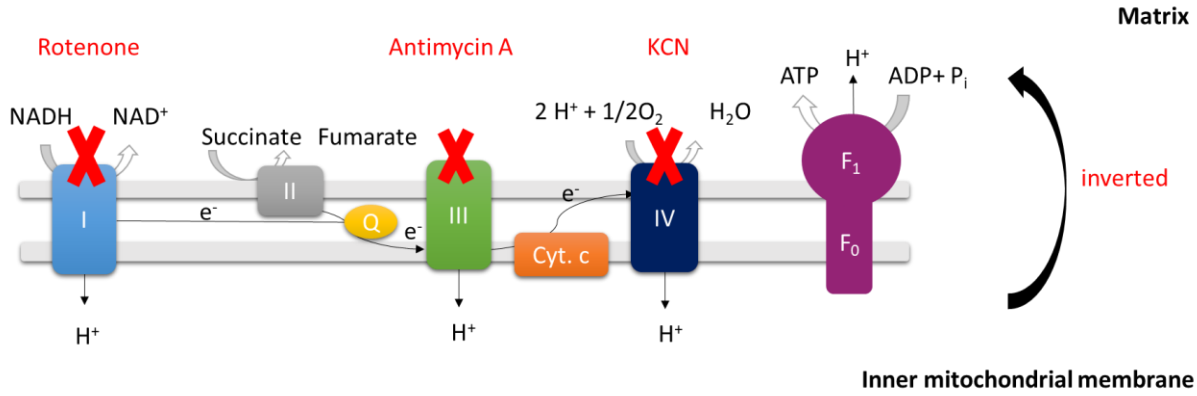

Figure 47. Sub-mitochondrial membrane (SMP). Rotenone, Antimycin A and KCN were used as positive controls. Adapted from[49].

Second, we sent the tested compounds to be tested for activity against purified mitochondrial $CIII_2$ from *Candida albicans* to further confirm the specificity of the IPAs.[‡‡‡] In this assay, the reduction of cytochrome *c* was monitored spectrophotometrically at $\lambda = 550$ nm to measure the activity of $CIII_2$. As the positive control Inz-5, a known inhibitor, was tested at different concentrations

[†††] The handling of bovine heart and harvesting mitochondria were done by colleagues in the group of Prof. John Rubinstein, Hospital for Sick Children, Toronto, Canada.

[‡‡‡] This assay was performed by Zhong Liu in the Lab of Leah E. Cowen, Department of Molecular Genetics, The University of Toronto, Toronto, Canada.

By monitoring the NADH oxidation at λ = 340 nm in the presence of SMPs, it was confirmed that at 10 µM, **27** and Q203 do not inhibit mitochondrial complex I (**Figure 48**). As positive controls in this assay, we used Rotenone and Antimycin A.

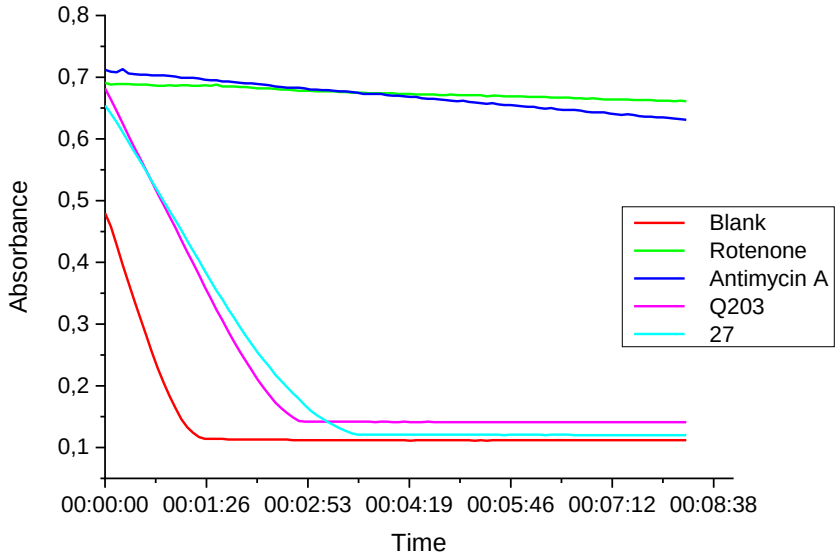

Figure 48. NADH oxidation in SMP at [10 µM]. **27** and **Q203** do not bind to complex I. Green: Rotenone. Blue: Antimycin A. Magenta: Q203. Cyan: compound **27**. Red: Blank, only SMP without positive control or test compound. ‘‘Reprinted with permission from [Abdelaziz, R.; Di Trani, J. M.; Sahile, H.; Mann, L.; Richter, A.; Liu, Z.; Bueler, S. A.; Cowen, L. E.; Rubinstein, J. L.; Imming, P. Imidazopyridine Amides: Synthesis, Mycobacterium Smegmatis $CIII_2CIV_2$ Supercomplex Binding and in Vitro Antimycobacterial Activity. ACS Omega **2023**. https://doi.org/https://doi.org/10.1021/acsomega.3c02259]. Copyright [2023] American Chemical Society’’

Q203, 24 and 27 do not inhibit mitochondrial cytochrome *bc*$_1$ (CIII).

Compounds (Q203 and **27**) that showed activity against *Msmeg* $CIII_2CIV_2$ did not show activity against *Bos taurus* mitochondrial cytochrome *bc*$_1$ (CIII) nor *Candida albicans* mitochondrial cytochrome *bc*$_1$, confirming their specificity against the mycobacterial $CIII_2CIV_2$. Although **24** did not show activity in the *Msmeg* $CIII_2CIV_2$ activity assay, it showed high potency in the *in vitro Mtb* growth inhibition assays.[86]

Oxygen consumption assays, where Q203, **24**[86], or **27** were incubated with SMPs at concentrations of 10 µM and 1 µM, were performed. The results showed some inhibition at 10 µM, while at 1 µM no inhibition was detected (**Figure 49**).

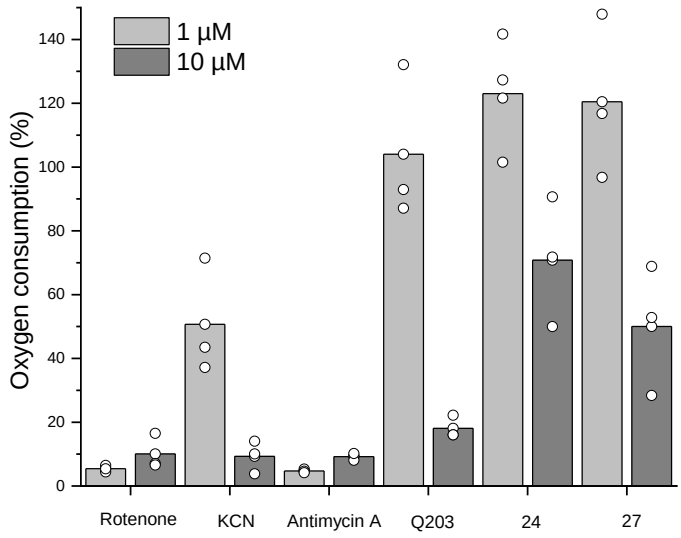

Figure 49. Comparison of the activity in sub-mitochondrial particles. Rotenone, KCN, and Antimycin A were used as positive controls. The graph shows that Q203, **24**, and **27** inhibit CIII at 10 µM; 80%, 30% and 50% inhibition respectively, while at 1 µM they show no inhibition. (mean +/- s.d., n = 3 independent assays). ''Reprinted with permission from [Abdelaziz, R.; Di Trani, J. M.; Sahile, H.; Mann, L.; Richter, A.; Liu, Z.; Bueler, S. A.; Cowen, L. E.; Rubinstein, J. L.; Imming, P. Imidazopyridine Amides: Synthesis, Mycobacterium Smegmatis CIII2CIV2 Supercomplex Binding and in Vitro Antimycobacterial Activity. *ACS Omega* **2023**. https://doi.org/https://doi.org/10.1021/acsomega.3c02259]. Copyright [2023] American Chemical Society''

Candida albicans $CIII_2$ activity assays confirmed the specificity of Q203, 24[86], and 27.[§§§]

The reduction of cytochrome c was monitored spectrophotometrically (absorption at $\lambda = 550$ nm) to measure the activity of purified mitochondrial $CIII_2$. No inhibition was observed at the concentrations tested (10 µM and 1 µM), confirming the specificity of Q203 and analogues to mycobacteria (**Figure 50A** and **B).** As the positive control, Inz-5 (**Figure 50D**) - a known inhibitor - was tested at different concentrations (**Figure 50C**: Black [0], no inhibition, while purple [2500 nM] almost complete inhibition). The experiment was done in triplicates.

[§§§] This assay was performed by Zhong Liu in the Lab of Leah E. Cowen, Department of Molecular Genetics, The University of Toronto, Toronto, Canada.

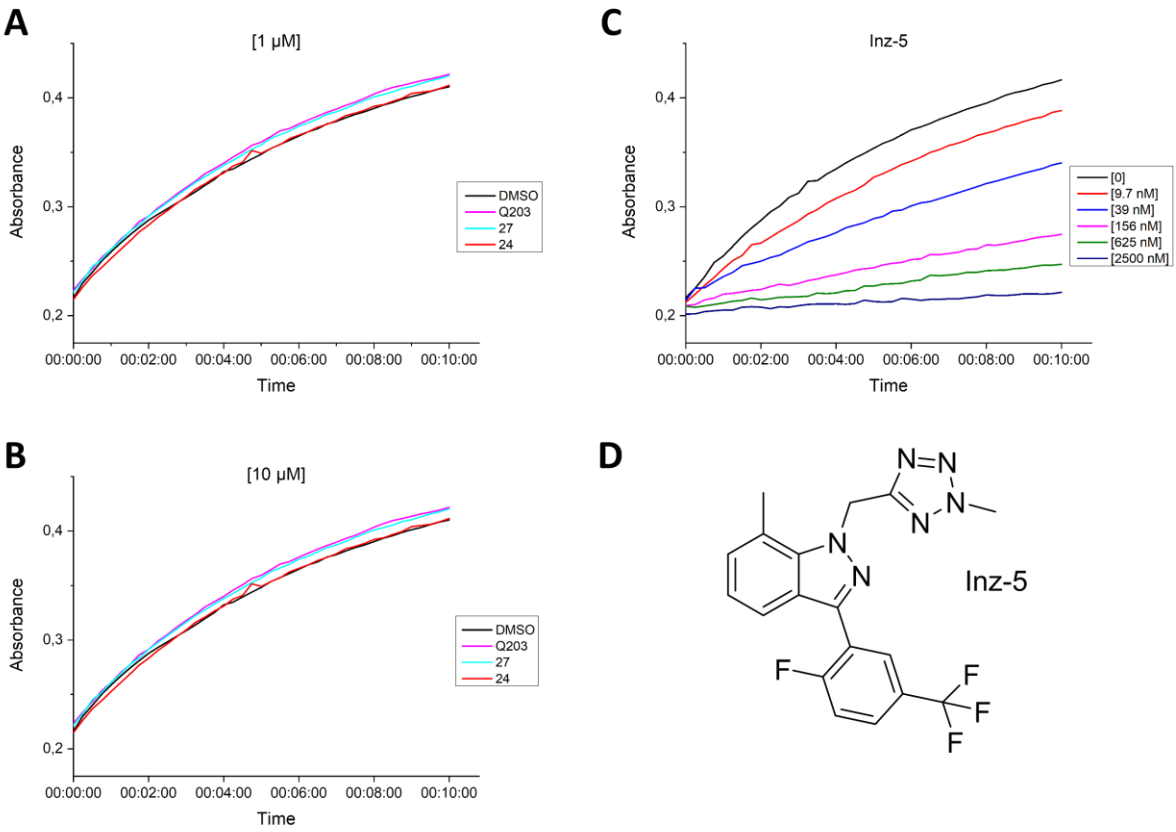

Figure 50. $CIII_2$ activity assay. Graphs **A** and **B** show the results of testing Q203, **24** and **27** at [1µM] and [10µM] respectively. Graph **C**: Black line represents the cytochrome c reduction in absence of Inz-5. At a conc of 2500 nM (navy blue line), Inz-5 completely inhibit the reduction. **D** shows the structure of Inz-5, a known $CIII_2$ inhibitor. ''Reprinted with permission from [Abdelaziz, R.; Di Trani, J. M.; Sahile, H.; Mann, L.; Richter, A.; Liu, Z.; Bueler, S. A.; Cowen, L. E.; Rubinstein, J. L.; Imming, P. Imidazopyridine Amides: Synthesis, *Mycobacterium Smegmatis* $CIII_2CIV_2$ Supercomplex Binding and in Vitro Antimycobacterial Activity. ACS Omega **2023**. https://doi.org/https://doi.org/10.1021/acsomega.3c02259]. Copyright [2023] American Chemical Society''

3.2.2.1. *In vitro* growth inhibition assays

In this section, we will discuss the results obtained from the screening of IPAs against different mycobacterial species. The screening of *M. abscessus*, *Msmeg* and *M. intracellulare* was done in our lab facilities by my colleagues Dr. Adrian Richter and Lea Mann.

As mentioned in section **1.1.2**, NTM are a growing health problem that is difficult to diagnose and treat. The majority of NTM pulmonary infections are caused by *M. abscessus*[15, 19] and the MAC complex (includes: *M. avium*, *M. intracellulare* and *M. chimera*).[14] *M. avium* and *M. intracellulare* are difficult to differentiate. However, the prognosis for *M. intracellulare* is worse than for M. avium.[26] **Table 3** shows a brief comparison between *Mtb*[6] and the NTM tested (*Msmeg*[161], *M. abscessus*[15, 19], *M. intracellulare*[13, 24]).

Table 3. A brief comparison between *Mtb*, *Msmeg*, *M. abscesuus* (*Mabs*) and *M. intracellulare* (*M. intra*).

	Mtb	***Msmeg***	***Mabs***	***M. intra***
Properties	• Slow-growing	• Fast-growing	• Fast-growing	• Slow-growing
Cultivation	• 7H9 medium • OADC* • 37 °C	• 7H9 medium • ADS or OA** • 37 °C	• 7H9 medium • ADS • 37 °C	• 7H9 medium • ADS or OA • 37 °C
Occurrence	• Humans • Animals	• Water sources • Soil	• Water sources • Soil • Humans • Animals	• Water sources • Soil • Humans • Animals
Highest Risk	• Immunocompromised individuals	• N/A	• Cystic fibrosis patients • Immunocompromised individuals	
Pathogenicity	• TB in humans • Mainly infects lungs	• Non-pathogenic*** • A model for pathogenic mycobacteria	• Growing public health problem • Pulmonary infections (most common) • Difficult to diagnose and treat	
Transmission	• Inhalation	• N/A	• Water • Indirect contact • Contaminated medical devices	• Inhalation • Water • Contact (direct/indirect)

*OADC = oleic acid- albumin-dextrose-catalase (growth supplement).
**ADS = albumin-dexrose-saline (growth supplement), OA = oleic acid.
****Msmeg* does not live in mammals and rarely causes infections in human (skin/soft tissue)[161].

3.2.2.1.1. Screening against *Mtb*[****]

In *Mtb in vitro* growth inhibition assays, Compounds **1-4** showed an MIC_{90} of 0.2 μM, while **24**[86] showed ~5× higher potency ($MIC_{90} \leq 0.04$ μM). Br-substitution at C-7 in compounds **5-8** led to a 50-fold decrease in activity (≥ 10μM). CF_3 and OCF_3 instead of bromine or chlorine led to a ~125-fold decrease in activity (**Table 4**). These results were rather consistent with the

**** The compounds were sent for screening against *Mtb* to the laboratory of Prof. Yossef Av Gay, Department of Medicine and Microbiology and Immunology, University of British Columbia, Vancouver, Canada.

results of the CIII2CIV2 activity assays, suggesting that a group bigger than bromine at C6 or C7 is not well tolerated.

Contradictory to the results of the oxygen consumption assays described above, replacing the halogen at C6 or C7 with a hydrogen atom led to a decrease in activity. For instance, compound **26** (R^1= H) showed a ~ 250-fold decrease in activity compared to **24**[86] (R^1= 6-Cl). In addition, compound **24** in the $CIII_2CIV_2$ activity assays did not show strong binding to the *Msmeg* $CIII_2CIV_2$ (**Table 2**), unlike its high *in vitro Mtb* activity. Compound **27** showed MIC_{90} > 10 µM contrary to its high activity in the binding assay. One explanation for this observation could be that the π-π interaction, found in the Q203-*Msmeg* model, increases the binding affinity in *Mtb*. Efflux mechanisms could also contribute to the high *in vitro* MIC of **27**.

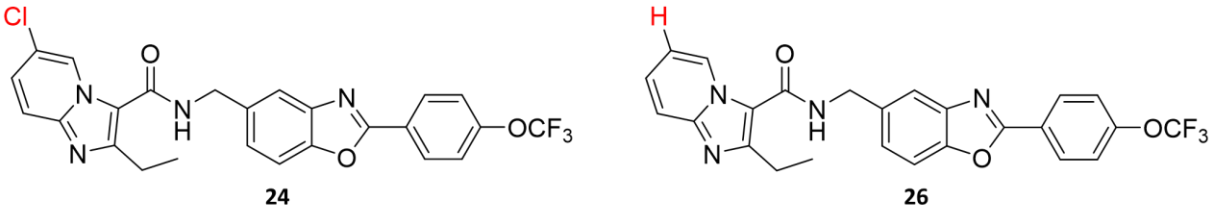

Figure 51. The structure of compounds **24** and **26**. R^1 is coloured in red.

3.2.2.1.2. Screening against *Msmeg and M. abscessus*††††

All compounds were inactive towards *Msmeg* and *M. abscessus* with MIC_{90s} > 25, 50 or 100 µM (**Table 4**). It has been reported that combining an efflux pump inhibitor such as verapamil (0.11 mM) with Q203 increases its potency *in vitro* and *ex vivo*.[170] However, no change in activity was detected when we combined verapamil with the test compounds in *Msmeg* assays.

Polymorphisms, namely S182G, E314D, A317L and A396C (highlighted in yellow **Figure 52**), in the QcrB subunit of *M. abscessus* has been reported to be the reason for its insensitivity to Q203.[171] However, superimposing the QcrB subunit of *Mtb* (PDB:7e1w, **Figure 52A blue**), *Msmeg* (PDB:7rh7, **Figure 52B beige**), and an AlphaFold model (UniProt: A0A0U1AIY2, **Figure 52A and B pink**)[172,173] of *M. abscessus* showed that these mutations do not affect the binding site. The highlighted residues in **Figure 52B** are the same in both *Msmeg* and *M. abscessus* models. The models were superimposed using UCSF Chimera software.[83]

†††† The screening of *Msmeg* and *M. abscessus* was done in our lab facilities by my colleagues Dr. Adrian Richter and Lea Mann.

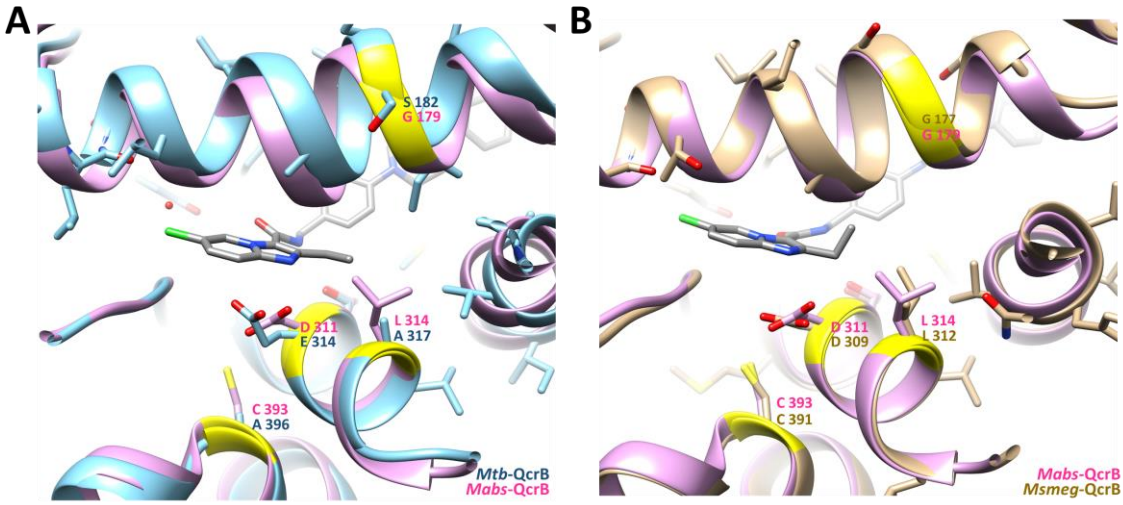

Figure 52. Superimposition of the QcrB subunit of *M. abscessus* with *Mtb* and *Msmeg.* An AlphaFold model[172,173] (**A** and **B** pink ribbon, UniProt: A0A0U1AIY2) of the QcrB subunit was downloaded and superimposed with *Mtb* (A blue, PDB:7e1w) and *Msmeg* (B, beige, PDB:7rh7) QcrB subunits using UCSF Chimera software .[83] (**A**) The figure displays the mutations S182G, E314D, A317L and A396C (highlighted in yellow) in *M. abscessus* compared to *Mtb*. It appears that these mutations do not affect the binding site. (**B**) The highlighted residues are the same in both *Msmeg* and *M. abscessus* models. ''Reprinted with permission from [Abdelaziz, R.; Di Trani, J. M.; Sahile, H.; Mann, L.; Richter, A.; Liu, Z.; Bueler, S. A.; Cowen, L. E.; Rubinstein, J. L.; Imming, P. Imidazopyridine Amides: Synthesis, *Mycobacterium Smegmatis* $CIII_2CIV_2$ Supercomplex Binding and in Vitro Antimycobacterial Activity. *ACS Omega* **2023**. https://doi.org/https://doi.org/10.1021/acsomega.3c02259]. Copyright [2023] American Chemical Society''

The Q203-bound to *Mtb* CIII model[174] showed that Q203 forms three hydrogen bonds compared to the two in *Msmeg*. A third hydrogen bond, however, with Asp 309 in *Msmeg* was found possible. The halogen in *Mtb* forms a halogen bond with a water molecule, which in turn forms a hydrogen bond with a Tyr 164.[174] In *Msmeg*, the halogen directly forms a halogen bond with the carbonyl of Leu 166 in QcrB (**Figure 34,** section **3.2.1**).[107]

These models suggest that the *in vitro* inactivity against *Msmeg* and *M. abscessus* is related to the compensatory mechanism by the cytochrome *bd* complex in mycobacteria, other unknown compensatory mechanisms or different binding affinities in different species.

3.2.2.1.3. Screening against *M. intracellulare*‡‡‡‡

The results of the *M. intracellulare in vitro* growth inhibition assay (**Table 4**) showed that it is more sensitive to IPAs than other mycobacteria tested, in addition to being a better model than

‡‡‡‡ The screening of *M. intracellulare* was done in our lab facilities by my colleague Lea Mann.

Msmeg for predicting the *in vitro* activity of IPAs against *Mtb*. Sequence alignment of QcrB orthologs in the tested mycobacterial species using Basic Local Alignment Search Tool (BLAST)[175] and *Mtb* as query sequence showed higher similarities between *M. intracellulare* (86.92% seq. identity) and *Mtb* compared to *Msmeg* (82.17% seq. identity) and *M. abscessus* (78% seq. identity). The QcrB sequences of *Mtb* (accession no.: WP_078447324.1), *M. intracellulare* (WP_054585160.1), *Msmeg* (WP_003895658.1) and *M. abscessus* (WP_074356503.1) were then used for multiple sequence alignment (MSA) using ClustalW[176] and the results were viewed with Jalview software[177] and shown in Figure 53. The amino acids that are important for interactions with Q203 in *Mtb* are highlighted with red boxes. F 158, I 178 and Y 164 are conserved in all species while E 314 is mutated to D 309 in *Msmeg* and *M. abscessus*.

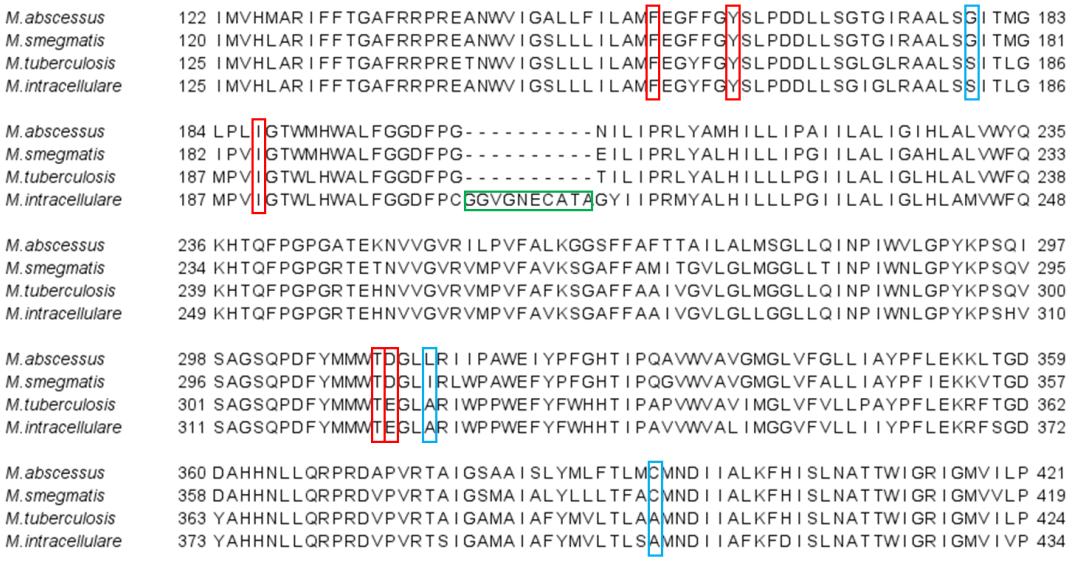

Figure 53. MSA of the QcrB orthologs in mycobacterial species. Red boxes represent the amino acids interacting with Q203, green represents 10 amino acids insertion in *M. intracellulare*[178] and blue boxes represent the previously reported mutations in *M. abscessus*. MSA was done using ClustalW[176] and viewed in Jalview software version 2.11.2.6.[177]

Similar to the results of the *Msmeg* $CIII_2CIV_2$ oxygen consumption assay and the *Mtb in vitro* growth inhibition assays, 6-Br analogues (**1-4**) were more potent than 7-Br (**5-8**). Compounds **1-4** showed MIC_{90} from 6 to 12 nM, while **5-8** had lower potencies (MIC_{90} in µM range). There was no pattern in the MICs of the analogues with R^1= CF_3. Compounds **9** (R^1= 6-CF_3, R^3= OCF_3), **11** (R^1= 6-CF_3, R^3= Cl) and **13** (R^1= 7-CF_3, R^3= OCF_3) showed activity: **9** was the most potent with MIC_{90}= 6 nM, **11** showed a ~ 100-fold decrease in potency and **13** showed a 65-fold decrease in potency. Compounds **10**, **12**, and **14-16** showed no activity (MIC_{90} >25 µM).

OCF_3 substituted IPAs (**17-23**) showed MIC_{90s} >25 µM, supporting the hypothesis that bulkier substituents are not well-tolerated. Compound **24** showed MIC_{90} = 5 nM. The substitution of the 6-Cl in **24** with an H-atom in compound **26** resulted in a slight decrease in activity (2-fold). 7-methyl and a shorter benzyl group in the tail led to a 1000-fold decrease in activity in compound **25**. Compound **27** showed a 200-fold decrease in potency compared to Q203 and compounds **1-4** and **9**. The lower activity is consistent with the result of the *Mtb in vitro* growth inhibition assay.

Table 4. The minimum inhibitory concentrations (MIC_{90}) in µM of the tested IPAs against *Mtb*, *Msmeg*, *M. abscessus (Mabs)* and *M. intracellulare*.

Code		*Mtb**	*Msmeg***	*Mabs***	*M. intracellulare***
1	R^1= Br	0.2	>50	>50	0.006
2		0.2	>50	>50	0.012
3		0.4	>50	>50	0.012
4		0.2	>50	>50	0.006
5		>10	>25	>25	>25
6		10	>100	>100	12.5
7		>10	>25	>25	0.8
8		>10	>25	>25	25
9	R^1= CF_3	>10	>100	>100	0.006
10		>10	>100	>100	>100
11		>25	>100	>100	0.8
12		>25	>100	>100	>25
13		>25	>50	>50	0.39
14		0.156	>100	>100	50
15		>25	>50	>50	>25
16		>25	>50	>50	>100
17	R^1= OCF_3	>10	>25	>25	>25
18		>10	>100	>100	100
19		>25	>50	>50	>25
20		>25	>50	>50	>25
21		>10	>100	>50	>100
22		>25	>50	>50	>25
23		>10	>50	>100	>25
24[86]	6-Cl	≤0.04	>100	>100	0.005
25[102]	7-Me	2.5	>100	>100	6.3
26	-	>25	>100	>100	0.01
27	6-Cl	>10	>100	>100	0.8
28	6-Cl	n.d	>100	>100	100
29	6-Cl	n.d	>100	>100	>100
30	6-Cl	n.d	>100	>100	>100
Q203	6-Cl	n.d	>100	>100	0.003

*OD-measurements.
**RFP-measurements, the maximum concentration tested differed depending on the solubility of the compounds.

Contrary to our results, a recent study suggested that the insertion of 10 amino acids in the linker between two TM helices near the binding site (**Figure 53**, green box and **Figure 54**) would lead to resistance of *M. intracellulare* to Q203.[178] However, the results of our assay (**Table 4**) showed that it is very sensitive to IPAs. In their assays, they used clinical isolates that may have developed resistance, explaining the difference in results. They also used a different method for testing growth inhibition, the Alamar blue assay, which depends on cellular respiration to reduce resazurin dye and show a colour change (blue to pink).[179, 180] Disruption of the ETC by Q203 could have affected the assay results. In contrast, we used *M. intracellulare* expressing a red fluorescent protein (RFP) called tdTomato.

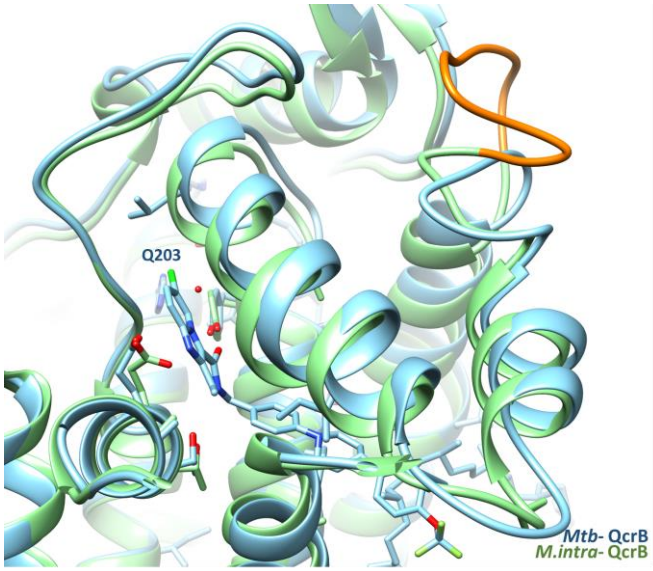

Figure 54. Overlay of an AlphaFold model of *M. intracellulare* QcrB subunit (UniProt: A0A220YBG8_MYCIT) with *Mtb* QcrB subunit (PDB: 7e1w). The models were superimposed using UCSF Chimera software.[83] The amino acid insertion in *M. intracellulare* is shown in orange colour.

3.2.2.1.4. Screening against *M. intracellulare and Msmeg* in glucose-free medium[§§§§]

As mentioned in section **1.2.1.2**, one of the alternative mechanisms of mycobacteria that are upregulated in anaerobic conditions or when the bc_1 complex is inhibited is the cytochrome *bd*-complex. A recent study[181] on the response of *Msmeg* to Q203 has shown that upon treatment of a wild type *Msmeg* and a cytochrome *bd* knock out (*bd*-KO) with Q203, both $CIII_2CIV_2$ as well as cytochrome *bd* complex are overexpressed. The level of $CIII_2CIV_2$ overexpression in *Msmeg bd*-KO was similar to the wild type, explaining the sensitivity of

[§§§§] The screening of *M. intracellulare* was done in our lab facilities by my colleague Lea Mann.

Msmeg bd-KO to Q203. The level of expression also varied from cell to cell. A putative second cytochrome *bd* complex has been reported based on genetic analysis, however, it is not known whether it can compensate for the inhibition of $CIII_2CIV_2$ and/or cytochrome *bd* complex.[181]

These findings could explain the insensitivity of *Msmeg* to IPAs in our assays (section **3.2.2.1.2**). Other factors could also contribute to resistance such as the overexpression of efflux pumps and the use of glucose in the growth medium as an energy source as an adaptation to the inhibition of the ETC. It has been reported that the bactericidal activity of BDQ, an inhibitor of F_1F_o ATP-synthase was significantly enhanced when mycobacteria were grown on non-fermentable energy sources, for example, oleic acid.[182, 183] The use of a lipid source instead of glucose deprives mycobacteria of producing ATP via glycolysis. Substrate-level phosphorylation (glycolysis) can rapidly provide ATP regardless of whether the ETC is functional and act as a rescue mechanism in case of inhibition of the ETC.

We, therefore, tested the activity of Q203 against *Msmeg* and *M. intracellulare* when grown in a glucose-free medium. The aim was to test the change in sensitivity to Q203 in the glucose-free medium (oleic acid) compared to the glucose-rich medium (ADS). In addition, the effect of a combination of compound **31**, a cytochrome *bd* inhibitor, and Q203 was tested under both growth conditions.

Msmeg

The results showed an 8-fold decrease in the MIC_{90} of Q203 when bacteria were grown in the medium supplemented with oleic acid (MIC_{90} = 12.5 µM, **Table 5**) compared to ADS (MIC_{90} >100 µM). These results suggest that *Msmeg* indeed uses glucose as an alternative source of energy in response to $CIII_2CIV_2$ inhibition. The combination of compound **31** and Q203 did not affect the MIC in ADS but showed an 8-fold decrease in MIC_{90} of Q203 in oleic acid (MIC_{90} = 6.25 µM, **Table 5**). The overexpression of both $CIII_2CIV_2$ and cytochrome *bd* complex in response to inhibition could explain the lack of effect of the cytochrome *bd* inhibitor (**31**) on the MIC of Q203 in ADS.

M. intracellulare

The results showed no major difference in the MIC_{90} of Q203 in oleic acid compared to ADS. The similarity in MICs could be because *M. intracellulare* is a slow-growing mycobacterium, and therefore the overexpression of $CIII_2CIV_2$ and cytochrome *bd* complex in response to inhibition is slower than in fast-growing mycobacteria such as *Msmeg*. We observed a ~ 8-fold decrease in MIC_{90} of **31** in oleic acid (MIC_{90} = 12.5 µM, **Table 5**), which suggests that *M. intracellulare* is less adaptable in an oleic acid medium. The combination of compound **31** and Q203 resulted in a 4-fold decrease in MIC_{90} of Q203 in the oleic acid medium (MIC_{90} = 0.0017 µM, **Table 5**). In ADS, the combination with **31** did not affect the MIC_{90} of Q203.

Table 5. Comparison of MIC_{90} (µM) against *Msmeg* and *M. intracellulare* in glucose-rich (ADS) and glucose-free (oleic acid) media.

Code	*M. intracellulare*		*Msmeg*	
	ADS	***Oleic acid***	***ADS***	***Oleic acid***
BDQ	0.02	0.06	0.03	0.25
Q203	0.003	0.007	>100	12.5
31	>100	12.5	>100	>100
Q203 + **31**	0.005 + 50	0.0017+ 1.6*	>50+50	6.25 + 6.25

3.2.2.2. Minimum bactericidal concentration (MBC) in *Msmeg*

It has been reported that the bactericidal activity of Q203 can be achieved in *Mtb* through the combination of Q203 with **31**, a cytochrome *bd* complex inhibitor.[169] To assess the effect of this combination in *Msmeg*, a concentration-dependent MBC was determined. Q203 combined with **31** were tested for bactericidal activity in *Msmeg* which was grown in a medium supplemented with oleic acid. Q203 alone was tested as a negative control. After 3 days of incubation, the results showed a bactericidal effect (MBC_{99}) at a concentration of 50 µM (8x MIC, **Figure 55**).

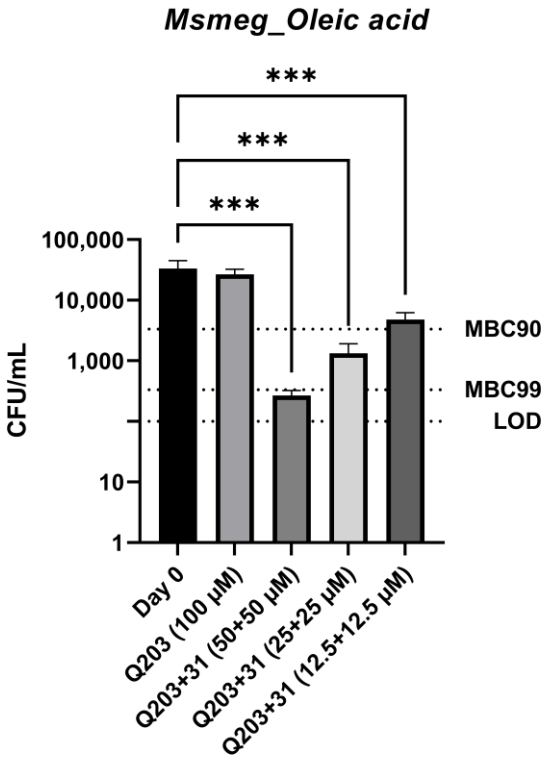

Figure 55. Bactericidal activity of Q203+**31** against *Msmeg* which was grown in a medium supplemented with oleic acid. LOD: limit of detection. Experiments were carried out in triplicates. The mean values are represented as bars with the standard deviations as error bars. A one-way analysis of variance (ANOVA) multiple-comparison test was performed using GraphPad Prism 9 software to compare treated groups with the inoculum (Day 0). ***: P = 0.0002.

3.3.2. EMB analogues

3.2.2.3. *In vitro* growth inhibition assays

The results of the *Mtb* growth inhibition assay[*****] showed that replacing the secondary alkyl amines with anilines in compounds **32** and **33** led to a decrease in activity. Compound **32** showed almost no inhibition at 8 µM. At higher concentrations, compound **32** was insoluble, and therefore not tested. Compound **33** showed ~80% inhibition at 64 µM (**Figure 56B**, green bars). These data are consistent with the reported SAR of EMB in terms of the ionization of the two nitrogen atoms. The decrease in the basicity of the nitrogen atoms in **32** and **33** would affect the electrostatic interactions with the catalytic Asp 299. At physiological pH, both nitrogen atoms are unionized and form hydrogen bonds instead. In addition, the orientation of

[*****] *Mtb* assays were done in the laboratory of PD Dr. Norbert Reiling, Research Center Borstel.

the oxygen atoms could affect the hydrogen bonding with residues Glu 327 and His 592, resulting in reduced binding affinity and thus loss of activity.

Compound **34** showed lower potency than EMB with MIC_{95} = 64 µM versus 16 µM in EMB (**Figure 56A**). The lower potency could be due to the loss of the hydrogen bond interactions with His 594 and Glu 327 in compound **34** (**Figure 39**) compared to EMB (**Figure 37A**). The free hydroxyl group in compound **35** led to an increase in MIC_{95} compared to the methyl ether in **34**. 64 µM was the highest tested concentration (**Table 6**). At this concentration, compound **35** only showed 9% inhibition (**Figure 56B**, blue bars). This finding is opposite to the *in silico* study that suggested that the free hydroxyl groups in compound **35** can form two hydrogen bonds with Asp 1024 and Asp 299 (**Figure 39**).

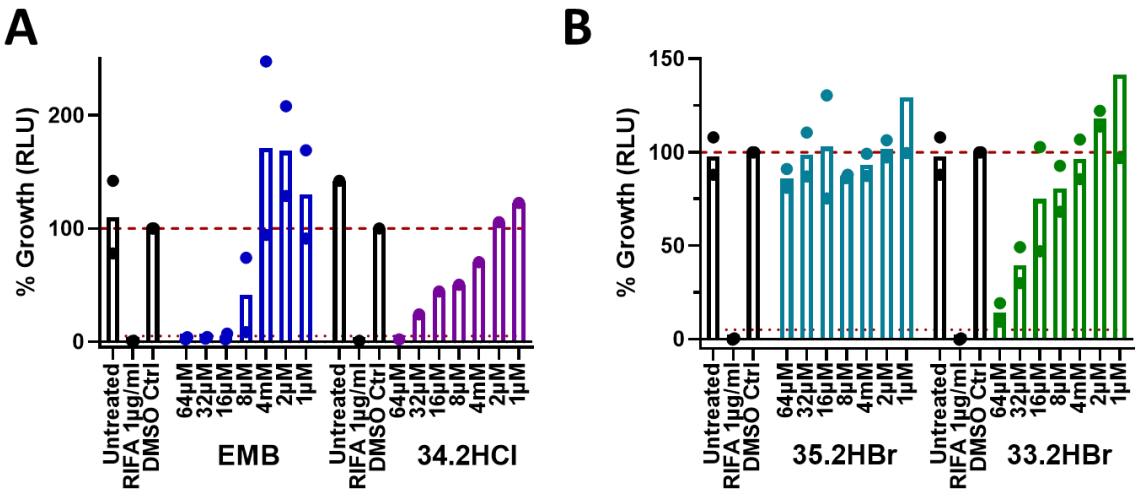

Figure 56. % Growth of EMB and **34** (**A**), **33** and **35** (**B**). (**A)** Almost no growth was observed at 16 µM concentration of EMB and at 64 µM of **34**. (**B) 35** (blue) showed almost no activity at the tested concentrations, while compound **33** (green) showed ~80% inhibition at 64µM. RLU= relative light unit.

The asymmetric EMB analogue **37** showed no inhibition at the tested concentrations, and neither did its symmetric analogue **36** (**Figure 57**). This inactivity could be due to possible steric clashes between the trifluoromethyl (CF_3) group and tryptophan amino acid in the active site. (Trp 1028 and Trp 988, **Figure 40**).

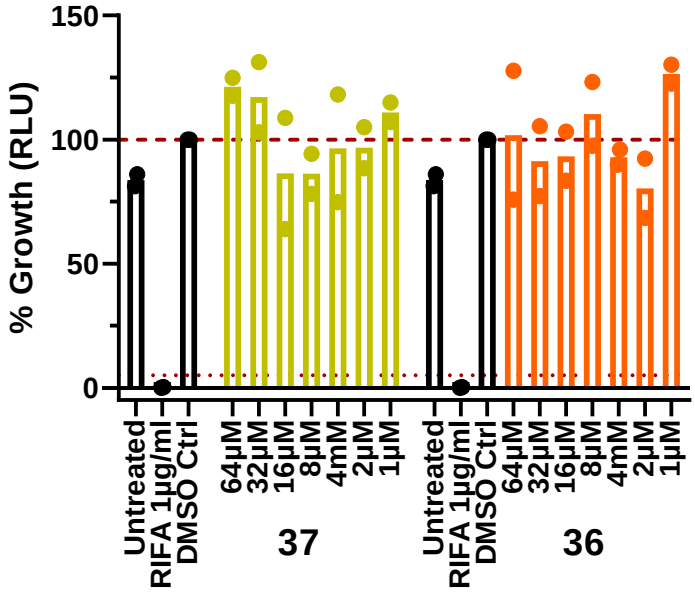

Figure 57. % Growth of compounds **36** and **37**. No inhibition was observed in both compounds at the tested concentrations.

None of the tested compounds showed activity against *Msmeg*, *M. abscessus* or *M. intracellulare* (MIC_{90} >100 µM).[†††††]

Table 6. MIC_{95} (µM) of the tested EMB analogues against *Mtb*, *Msmeg*, *M. abscessus* and *M. intracellulare.*

Code	***Mtb* (MIC_{95})**	***Msmeg***	***M. abscessus***	***M. intracellulare***
32	>8 µM**	>100	n.d.	>100
33	>64	>100	>100	>100
34	64	>100	>100	>100
35	>>64	>100	>100	>100
36*	>>64	>100	>100	>100
37	>>64	>100	>100	>100
EMB	16	1.6	150	4.7

*Synthesis was reported in RA's Master thesis.[44]
** 8 µM was the highest tested concentration due to compound's insolubility at higher concentrations.

[†††††] These assays were done in our lab facilities by my colleagues Lean Mann and Dr. Adrian Richter.

4. Conclusions and suggestions for future work

4.1. IPAs

With the panel of IPAs prepared and tested for this investigation, data were generated that allow some generalizations on the IPA-$CIII_2CIV_2$ interaction in *Msmeg*, tentative correlation with *in vitro* activities and extrapolation to other mycobacterial species.

As for SAR of the IPAs (**Figure 58**), a halogen substituent at C6/C7 of the IP moiety is important for $CIII_2CIV_2$ inhibitory activity. Substitution at C6 leads to a stronger effect than at C7. Electron cryomicroscopy data, corroborated by *in silico* models, show that a halogen bond[184] can be formed with Tyr 164[174] in *Mtb* and the carbonyl of Leu 166 in *Msmeg*.[107] A substituent bigger than bromine and incapable of halogen bonding at C6/C7 is not tolerated.

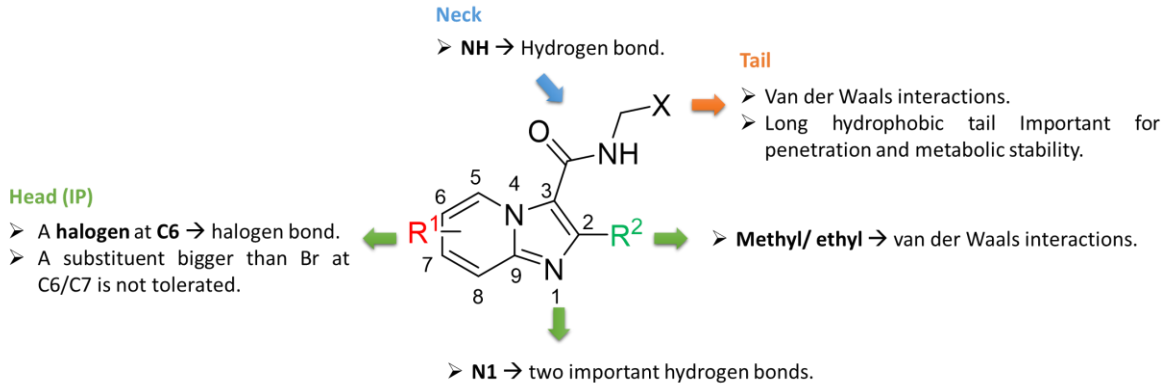

Figure 58. Summary of the SAR of IPAs.

The NADH oxidation assays for both the NDH-2 enzyme and the SMPs support that the head of the IPA, not the tail, leads to specificity. None of the compounds tested showed activity against bovine mitochondrial complex I or *Caldalalibacillus thermarum* NDH-2 despite both of these enzymes having a quinone binding site. The inactivity in these assays for compound **27**, which has an isoprene tail similar to the natural quinone substrate, thus allowing binding through the tail, further supports the hypothesis that binding and in particular specificity of binding to a mycobacterial $CIII_2CIV_2$ mainly rests in the head region.

Mostly, no generally applicable correlation could be made between the results in the *Msmeg* $CIII_2CIV_2$ oxygen consumption assay and the *Msmeg*, *Mtb* and *M. intracellulare* growth inhibition assays. For example, the strong inhibition by compound **27** in the *Msmeg* $CIII_2CIV_2$ binding assays did not translate to high potency in the *Mtb* or *M. intracellulare* assays. The

opposite was observed in the case of compound **24**: weak inhibition of $CIII_2CIV_2$ and strong growth inhibition of *Mtb* and *M. intracellulare*. However, for *Msmeg*, all compounds did not inhibit or only weakly inhibited growth, regardless of any inhibition in the $CIII_2CIV_2$ oxygen consumption assay or *Mtb* and *M. intracellulare* growth inhibition assays.

This lack of a general correlation pattern between assays implies that inhibition of $CIII_2CIV_2$ activity is not sufficient to translate into growth inhibition. This finding may be due to either efflux or alternative resistance mechanisms the mycobacteria can resort to, or the activity of the cytochrome *bd* terminal oxidase as a rescue mechanism when $CIII_2CIV_2$ is inhibited. The cytochrome *bd* oxidase in *Mtb* has been shown to prevent the bactericidal activity of Q203 despite its low MIC (nM). Bactericidal activity against *Mtb* can only be achieved through the combination of Q203 with a cytochrome *bd* inhibitor.[169] In *M. abscessus*, the cytochrome *bd* complex has been reported to not affect susceptibility to Q203 and other IPAs. Therefore, other yet unknown mechanisms must be the reason for the insensitivity of *M. abscessus* to Q203.[171] *Msmeg* overexpresses both $CIII_2CIV_2$ and cytochrome *bd* complex in response to Q203 treatment.[181] A putative second cytochrome *bd* complex has been proposed based on genetic analysis, however, it is not known yet whether it can compensate for the inhibition of $CIII_2CIV_2$ and/or cytochrome *bd* complex.[181] In addition, pharmacokinetic parameters such as solubility, permeation through human and bacterial cell membranes and bacterial metabolism of the IPAs could play a role.

The similarity of the binding sites of the *Msmeg* and *Mtb* $CIII_2CIV_2$ electron cryo-structures supports the hypothesis that the resistance could be due to one of the above reasons (**Figure 52**). Furthermore, the *Msmeg* $CIII_2CIV_2$ electron cryomicroscopy structure and *M. abscessus* AlphaFold QcrB model (**Figure 52B**) as well as MSA (**Figure 53**) displayed even higher similarity, but we did not observe growth inhibition of *M. abscessus* with any of the IPAs tested.

Additionally, the assay results against *Msmeg* in an oleic acid medium showed that the bacteria used the glucose in the growth medium as an energy source through glycolysis to compensate for the ETC disruption. Q203 activity (MIC_{90} =12.5 µM) in the oleic acid medium increased more than 8-fold compared to the ADS medium (MIC_{90} >100 µM, **Table 5**). In *Msmeg*, the bactericidal activity of Q203 was only observed in combination with **31** in the oleic acid medium (MBC_{99} = 50µM). The combination of Q203 with **31** and growing *Msmeg* in oleic

acid medium blocks two of the rescue mechanisms: glycolysis as an alternative ATP source and the cytochrome *bd* complex.

The results of the *M. intracellulare* growth inhibition assays showed that it is more sensitive to IPAs than other mycobacteria tested, in addition to being a better model than *Msmeg* for predicting the *in vitro* activity of IPAs against *Mtb*. For example, most of the compounds that showed activity against *M. intracellulare* were also active against *Mtb*, but with higher MIC values (**Table 4**). MSA also showed higher similarity between the slow-growing *Mtb* and *M. intracellulare* compared to the fast-growing *Msmeg* and *M. abscessus* (**Figure 53**). The role of the cytochrome *bd* complex in *M. intracellulare* appears to be less important than in *Msmeg*. The combination of Q203 and **31** showed no difference in the MIC of Q203 in both the ADS and the oleic acid media. Differences in the expression levels of the terminal oxidases ($CIII_2CIV_2$ and cytochrome *bd* complex) between the two mycobacteria could be an explanation. Adaptation of *M. intracellulare* to Q203 inhibition may also be slower than for *Msmeg*. An MBC assay is required to confirm whether or not a bactericidal effect is achieved. Macrophage infection assays are also planned to investigate the intracellular activities of IPAs. The results reported here highlight the need to evaluate the role of the cytochrome *bd* complex and the expression level of $CIII_2CIV_2$ for bacteriostatic or bactericidal activity in different mycobacterial species. In addition, the effect of different media on the inhibition of oxidative phosphorylation should be evaluated. Further improvement of the PK parameters of novel IPAs compared to Q203 is also required.

In future studies, it is crucial to investigate mycobacterial defense mechanisms in order to develop new drug candidates that can inhibit oxidative phosphorylation mycobacteria, such as *M. abscessus*.

4.2. EMB analogues

To date, not all mycobacterial arabinosyl transferases are well characterized, there is a lot to discover and understand about their structures and functions.[81, 82] The recently published 3D structure of the Emb proteins in *Mtb* and *Msmeg* helped in understanding the drug-target interactions. However, *in silico* studies could not predict the binding/activity of the tested EMB analogues. For example, compounds **32** and **33** with high docking scores did not show significant *in vitro* activity. In addition, docking could not explain the loss of activity in **35** compared to **34**.

The results of *in vitro* growth inhibition assays of the synthesized EMB, as well as the previously reported EMB analogues, suggest that modifications to EMB may reduce/abolish activity or lead to a shift in target, as in the case of SQ109.

Further investigations on the target such as enzymatic assays are recommended to confirm the activity of these compounds on the Emb proteins. Inactivity could be due to penetration problems, efflux pumps or rapid degradation (metabolism) by mycobacteria.

5. Summary

Tuberculosis (TB), caused by *Mycobacterium tuberculosis* (*Mtb*), is one of the oldest and most pervasive diseases. Death rates are decreasing over the years; however, it is still one of the leading causes of death worldwide. Non-tuberculous mycobacteria (NTM), such as *M. abscessus* and *M. avium* complex, are considered a growing public health problem, especially among patients with cystic fibrosis. The long duration of treatment, the continuous emergence of resistant TB strains and the resistance of NTM to most anti-TB drugs necessitate the search for new drug candidates and the understanding of the mechanism of action of the drug targets and the mycobacterial rescue mechanisms.

Among the attractive targets for TB treatment are mycobacterial cellular respiration and cell wall synthesis. The structural differences between mycobacterial electron transport chain (ETC) complexes, ETC complexes from eukaryotic mitochondria and other bacteria allow selective inhibition of mycobacterial respiration. Whereas, the importance of the mycobacterial cell wall for survival, its unique structure and unique biosynthetic pathways made it an attractive target for many antimicrobial drugs.

Q203, INN: telacebec, is an imidazopyridine amide (IPA) that targets the respiratory $CIII_2CIV_2$ supercomplex of the mycobacterial ETC. To gain a better understanding of the molecular mechanism of action of IPA, **30** analogues were prepared through a seven-step synthetic scheme. The inhibition of purified *M. smegmatis* $CIII_2CIV_2$ (*Msmeg* $CIII_2CIV_2$) was tested using an oxygen consumption assay. The IPAs reported here were devised for an improved understanding of the molecular mechanism of action, making use of the molecular assay facilities in our laboratories and in particular trying to approach the long-term goal of targeting problematic mycobacteria that are not sensitive to Q203. These mycobacteria include *M. abscessus* and the *M. avium* complex, NTM of emerging importance.

The oxygen consumption assay results generally supported structure-activity relationship information obtained from the electron cryomicroscopy structure of *Msmeg* $CIII_2CIV_2$ bound to the Q203 model. At a concentration of 10 µM, compound **27** showed 88 ± 1.15 % inhibition compared to 85 ± 7.5 % inhibition with Q203. None of the IPAs, including Q203, showed inhibition of mitochondrial ETC, proving their selectivity against mycobacteria. None of the tested compounds showed *in vitro* growth inhibition against *Msmeg* or *M. abscessus*. Most of

the compounds that showed activity against *M. intracellulare* were also active against *Mtb*, but with lower potency. For example, compounds **1-4** showed MIC_{90} = 200 nM against *Mtb* and MIC_{90} = 6-12 nM against *M. intracellulare*. There was not a perfect correlation between the *in vitro Mtb* growth inhibition and *Msmeg* $CIII_2CIV_2$. For example, compound **27** showed only 70% inhibition at 10 µM (Q203: MIC_{80} extracellular 4 nM). The results of the *M. intracellulare* growth inhibition assays showed that it is more sensitive to IPAs than other mycobacteria tested, in addition to being a better model than *Msmeg* for predicting the *in vitro* activity of IPAs against *Mtb*. Q203 activity in the *Msmeg* growth inhibition assay was observed when *Msmeg* was grown in a glucose-free medium (oleic acid) and bactericidal activity (MBC_{99} = 50µM) in *Msmeg* was achieved when Q203 was combined with **31**, a cytochrome *bd*-complex inhibitor. In contrast to *Msmeg*, the activity of Q203 in *M. intracellulare* was not significantly affected by the growth medium or the combination with **31.**

Ethambutol (EMB) is one of the first-line drugs used to treat *Mtb* and is also included in treatment regimens for NTM. It inhibits the Emb proteins, which are essential for the synthesis of arabinogalactan and lipoarabinomannan of the mycobacterial cell wall. To better understand the structure-activity relationship, a small panel of EMB analogues were designed to test their activity against *Mtb* and NTM. *In silico* studies and the *in vitro Mtb* growth inhibition assays did not correlate. Compound **34** showed activity against *Mtb*, but not NTM. Compounds **32**, **33**, **35**, **36** and **37** did not show activity against any of the tested species.

The results suggest that further investigation of resistance mechanisms in different mycobacterial species is urgently needed to understand the lack of correlation between enzymatic assays, *in silico* studies and cellular activity, and to design new effective antimycobacterial drug candidates. Enzymatic assays of EMB analogues against Emb proteins are also needed to confirm whether these analogues bind to the target or not.

6. Zusammenfassung

Die durch Mycobacterium tuberculosis (*Mtb*) verursachte Tuberkulose (TB) ist eine der ältesten und am weitesten verbreiteten Krankheiten. Obwohl die Sterblichkeitsraten in jüngster Zeit zurückgegangen sind, ist TB immer noch eine der häufigsten Todesursachen weltweit. Nicht-tuberkulöse Mykobakterien (NTM), wie *M. abscessus* und *M. avium*, gelten als wachsendes Problem für die öffentliche Gesundheit, insbesondere bei Patienten mit Mukoviszidose. Die lange Behandlungsdauer, das kontinuierliche Auftreten resistenter TB-Stämme und die Resistenz von NTM gegen die meisten Anti-TB-Medikamenten erfordern die Suche nach neuen Wirkstoffkandidaten und die Erforschung des Wirkmechanismus und der Resistenzmechanismen der Mykobakterien erforderlich.

Zu den attraktiven Zielstruckturen für die TB-Behandlung gehören die Zellatmung und die Zellwandsynthese von Mykobakterien. Die strukturellen Unterschiede zwischen den Komplexen der mykobakteriellen Elektronentransportkette (ETC), den ETC-Komplexen aus eukaryotischen Mitochondrien und anderen Bakterien ermöglichen eine selektive Hemmung der mykobakteriellen Zellatmung. Die Bedeutung der mykobakteriellen Zellwand für das Überleben, ihre einzigartige Struktur und ihre Biosynthesewege machen sie zu eine attraktiven Zielstruktur für antimikrobielle Wirkstoffe.

Q203, INN: Telacebec, ist ein Imidazopyridinamid (IPA), das auf den respiratorischen $CIII_2CIV_2$-Superkomplex der mykobakteriellen ETC abzielt. Um ein besseres Verständnis des molekularen Wirkmechanismus von IPA zu erlangen, wurden 30 Analoga durch ein siebenstufiges Syntheseschema hergestellt. Die Hemmung von gereinigtem *M. smegmatis* $CIII_2CIV_2$ (*Msmeg* $CIII_2CIV_2$) wurde mit einem Sauerstoffverbrauch Assay untersucht. Die hier vorgestellten IPAs wurden für ein besseres Verständnis des molekularen Wirkmechanismus entwickelt, wobei die molekularen Assay-Einrichtungen in unseren Labors genutzt wurden und insbesondere versucht wurde, das langfristige Ziel zu erreichen, problematische Mykobakterien, die nicht empfindlich auf Q203 reagieren, zu bekämpfen. Zu diesen resistenten Mykobakterien gehören *M. abscessus* und der *M. avium*.

Die Sauerstoffverbrauch Testergebnisse stützten im Allgemeinen die Informationen zur Struktur-Aktivitäts-Beziehung, die aus der Kryoelektronenmikroskopie-Struktur des an das Q203-Modell gebundenen *Msmeg* $CIII_2CIV_2$ gewonnen wurden. Bei einer Konzentration von

10 µM zeigte Verbindung **27** eine Hemmung von 88 ± 1,15 % im Vergleich zu einer 85 ± 7,5 %igen Hemmung durch Q203. Keine der IPAs, einschließlich Q203, zeigte eine Hemmung der mitochondrialen ETC, was ihre Selektivität gegenüber Mykobakterien beweist. Keine der getesteten Verbindungen zeigte *in vitro* eine Wachstumshemmung gegen *Msmeg* oder *M. abscessus*. Die meisten Verbindungen, die eine Aktivität gegen *M. intracellulare* zeigten, waren auch gegen *Mtb* aktiv, jedoch mit geringerer Wirksamkeit. Zum Beispiel zeigten die Verbindungen **1-4** MIC_{90} = 200 nM gegen *Mtb* und MIC_{90} = 6-12 nM gegen *M. intracellulare*. Es bestand keine eindeutige Korrelation zwischen der *In vitro*-Wachstumshemmung von *Mtb* und *Msmeg* $CIII_2CIV_2$. So zeigte beispielsweise Verbindung **27** bei 10 µM nur eine 70%ige Hemmung (Q203: MIC_{80} extrazellulär = 4 nM). Die Ergebnisse der Assays zur Wachstumshemmung von *M. intracellulare* zeigten, dass es empfindlicher auf IPAs reagiert als andere getestete Mykobakterien. *M. intracellulare* ist daher ein geeigneteres Model als *Msmeg* für die Vorhersage der *In vitro*-Aktivität von IPAs gegen *Mtb*. Die Aktivität von Q203 im *Msmeg*-Wachstumshemmungstest wurde beobachtet, wenn *Msmeg* in einem glukosefreien Medium (Ölsäure) gezüchtet wurde, zudem wurde bakterizide Aktivität (MBC_{99} = 50µM) in *Msmeg* beobachtet, wenn Q203 mit **31**, einem Cytochrom *bd*-Komplex-Inhibitor, kombiniert wurde. Im Gegensatz zu *Msmeg* wurde die Aktivität von Q203 in *M. intracellulare* durch das Wachstumsmedium oder die Kombination mit **31** nicht wesentlich beeinflusst.

Ethambutol (EMB) gehört zu den Medikamenten der ersten Wahl bei der Behandlung von Mtb Infektionen und wird auch zur Therapie von NTM Erkankungen genutzt. Es hemmt die Emb-Proteine, die für die Synthese von Arabinogalaktan und Lipoarabinomannan der mykobakteriellen Zellwand verantwortlich sind. Um die Struktur-Wirkungs-Beziehung besser zu verstehen, wurde eine kleine Gruppe von EMB-Analoga synthesiziert, um ihre Aktivität gegen *Mtb* und NTM zu testen. Die *In silico*-Studien und die *In vitro*-Tests zur Hemmung des *Mtb*-Wachstums korrelierten nicht. Verbindung **34** zeigte Aktivität gegen *Mtb*, aber nicht gegen NTM. Die Verbindungen **32**, **33**, **35**, **36** und **37** zeigten gegen keine der getesteten Spezies eine Wirkung.

Die Ergebnisse legen nahe, dass weitere Untersuchungen der Resistenzmechanismen bei verschiedenen Mykobakterienarten dringend erforderlich sind, um die fehlende Korrelation zwischen enzymatischen Tests, *In silico*-Studien und zellulärer Aktivität zu verstehen und neue wirksame antimykobakterielle Wirkstoffkandidaten zu entwickeln. Enzymatische Assays von

EMB-Analoga gegen Emb-Proteine sind ebenfalls erforderlich, um zu bestätigen, ob diese Analoga an das Ziel binden oder nicht.

7. Experimental procedures

7.1. Chemistry

7.1.2. General

Reagents obtained from Sigma Aldrich, abcr, TCI and Enamine were used without further purification. All organic solvents used were of pure analytical grade. Dioxane and THF were dried over 4 Å molecular sieves, while DCM was dried over 3 Å molecular sieves. Column chromatography was carried out using silica-gel 40-60 µm mesh with mobile phases such as heptane:EtOAc (or heptane:*tert*-butylmethylether) and $CHCl_3$:MeOH. Flash chromatography was performed on puriFlash® 430 (Interchim, Montluçon, France). Prepacked columns with silica gel of 30 µm pore size were used. Thin layer chromatography (TLC) was done using TLC silica gel 60 F_{254} plates (Merck). Mass spectrometry was performed on: APCI-MS (Advion expression^S CMS; Ithaca, NY, USA). The flow rate used was 10 µL/min and the super soft method was used to avoid fragmentation. The *m/z* range was from 100 to 1000 with an acquisition speed of 10,000 *m/z* units/sec. ESI-MS spectra were recorded on LCQ-Classic, Thermo Finnigan; direct injection. For the high-resolution mass spectrometry (HRMS) a Q ExactiveTM Plus Orbitrap mass spectrometer (Thermo Scientific, Bremen, Germany) was used. Melting points (m.p.) were measured on a Kofler bench apparatus. ^{1}H-NMR and ^{13}C-NMR spectra were recorded at 400 MHz, 500 MHz, and 126 MHz, 101 MHz respectively using a lampe-vnmrs400 spectrometer. ^{1}H shifts are referenced to the residual protonated solvent signal (δ 7.26 for $CDCl_3$, δ 3.31, 4.87 for CD_3OD and δ 2.5 for 11.5 TFA/DMSO) and ^{13}C shifts are referenced to the deuterated solvent signal (δ 77.0 for $CDCl_3$, δ 49.0 for CD_3OD and δ 164.2 for TFA/DMSO). Abbreviations: s= singlet, d= doublet, dd= double doublet, ddd= doublet of doublets of doublets, t= triplet, dt = doublet of triplets, q= quartet, tq= triplet of quartet, p= pentet, tp= triplet of pentet, m= multiplet. Assignments were proven by HSQC. Chemical shifts are given in parts per million (ppm), and all coupling constants (*J*) are given in Hz. In most ^{13}C NMR, some quaternary carbon atoms were covered by noise due to low concentrations and solubility in organic solvents. The purities of the tested compounds were determined by high-performance liquid chromatography (HPLC). The HPLC purity of the final compounds was 95% or higher. The instrument used was from Shimadzu (Kyoto, Japan). Pump: two LC-10AD pumps, Detector: SPD-M10A VP PDA detector, and Sampler: SIL-HT autosampler. Analytical HPLC: LiChrospher column RP-18, 5 µm particle size and 10 cm

length was used, and the solvent system was MeOH: H_2O, 5 to 95% + 0.05% TFA over 30 minutes. Preparative HPLC: NUCLEODUR 100-5 C18 ec column was used and, the used mobile phase was ACN:H_2O, 5 to 95% ACN + 0.1% formic acid over 30 minutes. Samples were dissolved in $CHCl_3$:MeOH, 1:1. Peaks were detected at λ= 254 nm. For the UV inactive compounds, peaks were detected at λ= 215 nm.

7.1.3. Procedures

7.1.3.1. Imidazopyridine amides (IPA)

7.1.3.1.1. Synthesis of Imidazo[1,2-a]pyridine-3-carboxylic acid Scaffold (1-15c)

2-Ethylimidazo[1,2-a]pyridine-3-carboxylic acids

A solution of NBS (1.2 equiv.) dissolved in H_2O (5 mL) was heated to 80 ºC, and then ethyl-3-oxo-pentanoate (1.05 equiv.) was added with a syringe and left to stir for 30 min. After complete addition, the colour of the solution changed from yellow to colourless. Afterwards 1 equiv. 2-aminopyridine was added and stirred for 30 min. to 1 h at 80 ºC. To stop the reaction, saturated Na_2CO_3 solution was added and the mixture was extracted three times with EtOAc. The organic phase was dried over anhydrous $MgSO_4$. After evaporation of the solvent, the product was purified by flash column chromatography (gradient mobile phase, heptane:EtOAc from 90:1 to 66:34) to give a pale-yellow solid (**1-8b**, **Scheme 1A**).[114] The yield ranged from 15% to 30% depending on the substituents on the pyridine.

The purified ester was dissolved in absolute Ethanol (30 mL) followed by the addition of an aqueous solution of LiOH (10 mL). The ratio of EtOH:H_2O was 3:1 v/v. The reaction mixture was left to reflux overnight. After evaporating EtOH on the Rotavap, 1N HCl was added dropwise until pH dropped to 4. The formed pale solid residue was filtered and washed with water and then dried in the desiccator to give **1-8c**.[105] The yield obtained was up to 90%.

2-Methylimidazo[1,2-a]pyridine-3-carboxylic acids

Ethyl-2-chloroacetoacetate was added to 25 mL EtOH, followed by 2-aminopyridine (1 equiv.). The reaction was left to reflux (80 ºC) overnight. The solvent was evaporated and 20 ml EtOAc was added. The organic phase was extracted three times with H_2O and dried over anhydrous $MgSO_4$. The product was purified by flash column chromatography (heptane:EtOAc, 4:1) to give a solid (**9-15b, scheme 1A**)[102]. The ester hydrolysis was done the same way as mentioned above (**9-15c**).[105]

Ethyl-6-bromo-2-ethylimidazo[1,2-a]pyridine-3-carboxylate **(1b)**

$C_{12}H_{13}BrN_2O_2$, yellow solid, 17% yield, ESI-MS: *m/z* 295.06 $[M-H]^-$, R_f= 0.26 (EtOAc: heptane, 1:2), ^{1}H NMR (400 MHz, Chloroform-*d*) δ 9.51 (dd, *J* = 1.9, 0.9 Hz, 1H), 7.52 (dd, *J* = 9.4, 0.9 Hz, 1H), 7.44 (dd, *J* = 9.4, 1.9 Hz, 1H), 4.44 (q, *J* = 7.1 Hz, 2H), 3.10 (q, *J* = 7.5 Hz, 2H), 1.44 (t, *J* = 7.1 Hz, 3H), 1.35 (t, *J* = 7.5 Hz, 3H).

6-Bromo-2-ethylimidazo[1,2-a]pyridine-3-carboxylic acid **(1c)**

$C_{10}H_9BrN_2O_2$, beige powder, 70%, ESI-MS: *m/z* 271.23 $[M+H]^+$, ^{1}H NMR (400 MHz, Methanol-d_4) δ 9.60 (dd, *J* = 1.9, 0.9 Hz, 1H), 7.68 (dd, *J* = 9.4, 1.9 Hz, 1H), 7.59 (dd, *J* = 9.4, 0.9 Hz, 1H), 3.16 (q, *J* = 7.6 Hz, 2H), 1.36 (t, *J* = 7.6 Hz, 3H).

Ethyl-7-bromo-2-ethylimidazo[1,2-a]pyridine-3-carboxylate **(2b)**

$C_{12}H_{13}BrN_2O_2$, yellow solid, APCI-MS: *m/z* 297, 299 (^{79}Br,^{81}Br) $[M+H]^+$, this compound was directly taken to the next step without further purification.

7-Bromo-2-ethylimidazo[1,2-a]pyridine-3-carboxylic acid **(2c)**

$C_{10}H_9BrN_2O_2$, white powder, 74% yield, APCI-MS: *m/z* 269.1, 271.1 (^{79}Br,^{81}Br) $[M+H]^+$, ^{1}H NMR (500 MHz, Methanol-d_4) δ 9.31 (d, *J* = 7.4 Hz, 1H), 7.85 (dd, *J* = 2.0, 0.8 Hz, 1H), 7.30 (dd, *J* = 7.4, 2.0 Hz, 1H), 3.13 (q, *J* = 7.6 Hz, 2H), 1.33 (t, *J* = 7.6 Hz, 3H).

Ethyl-6-(trifluoromethyl)-2-ethylimidazo[1,2-a]pyridine-3-carboxylate **(3b)**

$C_{13}H_{13}F_3N_2O_2$, white solid, 27% yield, APCI-MS: *m/z* 287.0 $[M+H]^+$, ^{1}H NMR (400 MHz, Chloroform-*d*) δ 9.81 (dt, *J* = 2.1, 1.1 Hz, 1H), 7.93 (d, *J* = 9.3 Hz, 1H), 7.64 (dd, *J* = 9.1, 1.7 Hz, 1H), 4.49 (q, *J* = 7.1 Hz, 2H), 3.20 (q, *J* = 7.6 Hz, 2H), 1.47 (t, *J* = 7.1 Hz, 3H), 1.41 (t, *J* = 7.6 Hz, 3H).

6-(Trifluoromethyl)-2-ethylimidazo[1,2-a]pyridine-3-carboxylic acid **(3c)**

$C_{11}H_9F_3N_2O_2$, white solid, 88% yield, APCI-MS: *m/z* 259.1 $[M+H]^+$, ^{1}H NMR (400 MHz, cd_3od) δ 9.82 (dp, *J* = 2.3, 1.2 Hz, 1H), 7.78 (dt, *J* = 9.4, 0.9 Hz, 1H), 7.72 (dd, *J* = 9.4, 1.9 Hz, 1H), 3.16 (q, *J* = 7.6 Hz, 2H), 1.34 (t, *J* = 7.6 Hz, 3H).

Ethyl-7-(trifluoromethyl)-2-ethylimidazo[1,2-a]pyridine-3-carboxylate **(4b)**

$C_{13}H_{13}F_3N_2O_2$, white solid, 28% yield, APCI-MS: *m/z* 287.0 $[M+H]^+$, ^1H NMR (400 MHz, Chloroform-*d*) δ 9.44 (dt, *J* = 7.3, 0.8 Hz, 1H), 7.93 (dp, *J* = 1.9, 1.0 Hz, 1H), 7.14 (dd, *J* = 7.3, 1.9 Hz, 1H), 4.46 (q, *J* = 7.1 Hz, 2H), 3.15 (q, *J* = 7.5 Hz, 2H), 1.45 (t, *J* = 7.1 Hz, 3H), 1.36 (t, *J* = 7.5 Hz, 3H).

7-(Trifluoromethyl)-2-ethylimidazo[1,2-a]pyridine-3-carboxylic acid **(4c)**

$C_{11}H_9F_3N_2O_2$, white powder, 93% yield, APCI-MS: *m/z* 259.1 $[M+H]^+$, ^1H NMR (400 MHz, Methanol-d_4) δ 9.55 (dt, *J* = 7.2, 0.9 Hz, 1H), 7.93 (dt, *J* = 2.1, 1.0 Hz, 1H), 7.33 (dd, *J* = 7.3, 1.9 Hz, 1H), 3.16 (q, *J* = 7.5 Hz, 2H), 1.34 (t, *J* = 7.5 Hz, 3H).

Ethyl 6-(trifluoromethoxy)-2-ethylimidazo[1,2-a]pyridine-3-carboxylate **(5b)**

$C_{13}H_{13}F_3N_2O_3$, pale yellow, 22% yield, APCI-MS: *m/z* 303.0 $[M+H]^+$, ^1H NMR (400 MHz, Chloroform-*d*) δ 9.44 (dt, *J* = 2.3, 0.8 Hz, 1H), 7.65 (dd, *J* = 9.7, 0.8 Hz, 1H), 7.34 (ddd, *J* = 9.7, 2.3, 1.0 Hz, 1H), 4.45 (q, *J* = 7.1 Hz, 2H), 3.13 (q, *J* = 7.5 Hz, 2H), 1.44 (t, *J* = 7.1 Hz, 3H), 1.36 (t, *J* = 7.5 Hz, 3H).

6-(Trifluoromethoxy)-2-ethylimidazo[1,2-a]pyridine-3-carboxylic acid **(5c)**

$C_{11}H_9F_3N_2O_3$, white powder, 73% yield, APCI-MS: *m/z* 275.1 $[M+H]^+$, ^1H NMR (400 MHz, Methanol-d_4) δ 9.53 (dt, *J* = 2.4, 0.9 Hz, 1H), 7.71 (dd, *J* = 9.7, 0.8 Hz, 1H), 7.58 (ddd, *J* = 9.7, 2.3, 1.0 Hz, 1H), 3.15 (q, *J* = 7.6 Hz, 2H), 1.34 (t, *J* = 7.6 Hz, 3H).

Ethyl 7-(trifluoromethoxy)-2-ethyl-imidazo[1,2-a]pyridine-3-carboxylate **(6b).**

$C_{13}H_{13}F_3N_2O_3$, pale yellow, 17% yield, APCI-MS: *m/z* 303.0 $[M+H]^+$, ^1H NMR (400 MHz, Chloroform-*d*) δ 9.36 (dd, *J* = 7.6, 0.8 Hz, 1H), 7.48 (d, *J* = 2.2 Hz, 1H), 6.89 (dd, *J* = 7.4, 2.4 Hz, 1H), 4.45 (q, *J* = 7.1 Hz, 2H), 3.12 (q, *J* = 7.5 Hz, 2H), 1.44 (t, *J* = 7.1 Hz, 3H), 1.36 (t, *J* = 7.6 Hz, 3H).

2-Ethyl-7-(trifluoromethoxy)imidazo[1,2-a]pyridine-3-carboxylic acid **(6c).**

$C_{11}H_9F_3N_2O_3$, white powder, 42% yield, APCI-MS: *m/z* 275.1 $[M+H]^+$, ^1H NMR (400 MHz, Methanol-d_4) δ 9.47 (dd, *J* = 7.6, 0.8 Hz, 1H), 7.48 (tt, *J* = 2.4, 1.2 Hz, 1H), 7.12 (ddd, *J* = 7.6, 2.6, 0.8 Hz, 1H), 3.13 (q, *J* = 7.6 Hz, 2H), 1.33 (t, *J* = 7.6 Hz, 3H).

Ethyl-6-chloro-2-ethylimidazo[1,2-a]pyridine-3-carboxylate **(7b)**

$C_{12}H_{13}ClN_2O_2$, pale yellow solid, 28% yield, ESI-MS: *m/z* 253.2 $[M+H]^+$, ^{1}H NMR (400 MHz, Chloroform-*d*) δ 9.41 (dd, *J* = 2.1, 0.8 Hz, 1H), 7.57 (dd, *J* = 9.5, 0.8 Hz, 1H), 7.34 (dd, *J* = 9.5, 2.1 Hz, 1H), 4.44 (q, *J* = 7.1 Hz, 2H), 3.10 (q, *J* = 7.5 Hz, 2H), 1.44 (t, *J* = 7.1 Hz, 3H), 1.35 (t, *J* = 7.5 Hz, 3H).

6-Chloro-2-ethylimidazo[1,2-a]pyridine-3-carboxylic acid **(7c)**

$C_{10}H_9ClN_2O_2$, white powder, 42% yield, ESI-MS: *m/z* 223.11 $[M-H]^-$, ^{1}H NMR (500 MHz, Methanol-d_4) δ 9.51 (dd, *J* = 2.1, 0.8 Hz, 1H), 7.61 (dd, *J* = 9.5, 0.8 Hz, 1H), 7.54 (dd, *J* = 9.5, 2.0 Hz, 1H), 3.15 (q, *J* = 7.6 Hz, 2H), 1.34 (t, *J* = 7.6 Hz, 3H).

Ethyl 2-ethylimidazo[1,2-a]pyridine-3-carboxylate **(8b)**

$C_{12}H_{14}N_2O_2$, orange solid, 5% yield, APCI-MS: *m/z* 219.0 $[M+H]^+$, ^{1}H NMR (400 MHz, Chloroform-*d*) δ 9.33 (dt, *J* = 7.0, 1.2 Hz, 1H), 7.66 (dt, *J* = 8.9, 1.2 Hz, 1H), 7.37 (ddd, *J* = 8.9, 6.8, 1.3 Hz, 1H), 6.97 (td, *J* = 6.9, 1.3 Hz, 1H), 4.43 (q, *J* = 7.1 Hz, 2H), 3.13 (q, *J* = 7.5 Hz, 2H), 1.44 (t, *J* = 7.1 Hz, 3H), 1.36 (t, *J* = 7.5 Hz, 3H).

2-Ethylimidazo[1,2-a]pyridine-3-carboxylic acid **(8c)**

$C_{10}H_{10}N_2O_2$, orange solid, 90% yield, ESI-MS: *m/z* 189.17 $[M-H]^-$, ^{1}H NMR (400 MHz, Methanol-d_4) δ 9.65 (d, *J* = 6.9 Hz, 2H), 8.13 (ddd, *J* = 8.5, 7.0, 1.1 Hz, 1H), 8.06 (d, *J* = 8.9 Hz, 1H), 7.67 (td, *J* = 7.0, 1.3 Hz, 1H), 3.34 – 3.26 (m, 2H), 1.43 (t, *J* = 7.6 Hz, 4H).

Ethyl-6-bromo-2-methylimidazo[1,2-a]pyridine-3-carboxylate **(9b)**

$C_{11}H_{11}BrN_2O_2$, pale yellow solid, 39% yield, APCI-MS: *m/z* 283.1 $[M+H]^+$, ^{1}H NMR (400 MHz, Chloroform-*d*) δ 9.49 (dd, *J* = 1.9, 0.9 Hz, 1H), 7.52 – 7.46 (m, 1H), 7.44 (dd, *J* = 9.4, 1.9 Hz, 1H), 4.44 (q, *J* = 7.1 Hz, 2H), 2.70 (s, 3H), 1.44 (t, *J* = 7.1 Hz, 3H).

6-Bromo-2-methylimidazo[1,2-a]pyridine-3-carboxylic acid **(9c)**

$C_9H_7BrN_2O_2$, beige solid, 65% yield, APCI-MS: *m/z* 255.1 $[M+H]^+$, ^{1}H NMR (400 MHz, Methanol-d_4) δ 9.60 (dd, *J* = 2.0, 0.8 Hz, 1H), 7.61 (dd, *J* = 9.5, 2.0 Hz, 1H), 7.52 (dd, *J* = 9.4, 0.8 Hz, 1H), 2.68 (s, 3H).

Ethyl-7-bromo-2-methylimidazo[1,2-a]pyridine-3-carboxylate **(10b)**

$C_{11}H_{11}BrN_2O_3$, pale yellow solid, 18% yield, APCI-MS*: m/z* 283.0, 285.0 (^{79}Br,^{81}Br) $[M+H]^+$. This compound was taken directly to the next step without further purification.

7-Bromo-2-methylimidazo[1,2-a]pyridine-3-carboxylic acid **(10c)**

$C_{10}H_7BrN_2O_2$, white solid, 70% yield, APCI-MS: *m/z* 255.1, 257.1(^{79}Br,^{81}Br) $[M]^+$, ^{1}H NMR (400 MHz, Methanol-d_4) δ 9.29 (dd, *J* = 7.4, 0.8 Hz, 1H), 7.81 (dd, *J* = 2.0, 0.8 Hz, 1H), 7.27 (dd, *J* = 7.4, 2.0 Hz, 1H), 2.68 (s, 3H).

Ethyl-6-(trifluoromethyl)-2-methylimidazo[1,2-a]pyridine-3-carboxylate **(11b)**

$C_{12}H_{11}F_3N_2O_2$, beige powder, 22%, APCI-MS: *m/z* 273.4 $[M+H]^+$, ^{1}H NMR (400 MHz, Methanol-d_4) δ 9.79 – 9.70 (m, 1H), 7.84 – 7.75 (m, 1H), 7.74 (dd, *J* = 9.4, 1.8 Hz, 1H), 4.47 (q, *J* = 7.1 Hz, 2H), 2.72 (s, 3H), 1.45 (t, *J* = 7.1 Hz, 3H).

6-(Trifluoromethyl)-2-methylimidazo[1,2-a]pyridine-3-carboxylic acid **(11c)**

$C_{12}H_{11}BrN_2O_2F_3$, light orange solid, 82% yield, APCI-MS: *m/z* 273.4 $[M+H]^+$, ^{1}H NMR (400 MHz, Methanol-d_4) δ 9.91 – 9.74 (m, 1H), 7.82 – 7.78 (m, 1H), 7.76 (dd, *J* = 9.4, 1.8 Hz, 1H), 2.76 (s, 3H).

Ethyl-7-(trifluoromethyl)-2-methylimidazo[1,2-a]pyridine-3-carboxylate **(12b)**

$C_{12}H_{11}F_3N_2O_2$, white solid,17% yield, APCI-MS*:* *m/z* 272.9 $[M]^+$,^{1}H NMR (400 MHz, Chloroform-*d*) δ 9.42 (dt, *J* = 7.3, 0.9 Hz, 1H), 7.89 (dt, *J* = 1.9, 1.0 Hz, 1H), 7.14 (dd, *J* = 7.3, 1.9 Hz, 1H), 4.45 (q, *J* = 7.1 Hz, 2H), 2.74 (s, 3H), 1.45 (t, *J* = 7.1 Hz, 3H).

7-(Trifluoromethyl)-2-methylimidazo[1,2-a]pyridine-3-carboxylate **(12c)**

$C_{10}H_7F_3N_2O_2$, pale yellow, 65% yield, APCI-MS: *m/z* 272.9 $[M]^+$, ^{1}H NMR (400 MHz, Methanol-d_4) δ 9.69 (d, *J* = 7.3 Hz, 1H), 8.10 (s, 1H), 7.56 (dd, *J* = 7.3, 2.0 Hz, 1H), 2.82 (s, 3H).

Ethyl-6-(trifluoromethoxy)-2-methylimidazo[1,2-a]pyridine-3-carboxylate **(13b)**

$C_{12}H_{11}F_3N_2O_3$, white powder, 21% yield, APCI-MS: *m/z* 289.1$[M+H]^+$. This compound was taken directly to the next step without further purification.

6-(Trifluoromethoxy)-2-methylimidazo[1,2-a]pyridine-3-carboxylic acid **(13c)**

$C_{10}H_7F_3N_2O_3$, white solid, 85% yield, APCI-MS: *m/z* 261.1 $[M+H]^+$, ^{1}H NMR (400 MHz, Methanol-d_4) δ 9.51 (dt, *J* = 2.5, 0.8 Hz, 1H), 7.69 (dd, *J* = 9.7, 0.8 Hz, 1H), 7.62 – 7.53 (m, 1H), 2.71 (s, 3H).

Ethyl-2-methyl-7-(trifluoromethoxy)imidazo[1,2-a]pyridine-3-carboxylate **(14b)**

$C_{12}H_{11}F_3N_2O_3$, white powder, 22% yield, APCI-MS: *m/z* 288.9 $[M+H]^+$. This compound was taken directly to the next step without further purification.

2-Methyl-7-(trifluoromethoxy)imidazo[1,2-a]pyridine-3-carboxylic acid **(14c)**

$C_{10}H_7F_3N_2O_3$, white solid, 43% yield, APCI-MS: *m/z* 261.1 $[M+H]^+$,^{1}H NMR (500 MHz, Methanol-d_4) δ 9.52 (d, *J* = 7.7 Hz, 1H), 7.55 (s, 1H), 7.23 (d, *J* = 7.6 Hz, 1H), 2.73 (s, 3H).

Ethyl-2,7-dimethylimidazo[1,2-a]pyridine-3-carboxylate **(15b)**

$C_{12}H_{14}N_2O_2$, pale yellow solid, 17%, APCI-MS: *m/z* 219.0 $[M+H]^+$, ^{1}H NMR (400 MHz, Chloroform-*d*) δ 9.14 (dd, *J* = 7.0, 0.9 Hz, 1H), 7.34 (dt, *J* = 2.0, 1.0 Hz, 1H), 6.78 (dd, *J* = 7.1, 1.8 Hz, 1H), 4.40 (q, *J* = 7.1 Hz, 2H), 2.67 (s, 3H), 2.44 – 2.39 (m, 6H), 1.41 (t, *J* = 7.1 Hz, 3H).

2,7-Dimethylimidazo[1,2-a]pyridine-3-carboxylic acid **(15c)**

$C_{12}H_{14}N_2O_2$, white solid, 39% yield, ESI-MS: *m/z* 191.28 $[M+H]^+$, ^{1}H NMR (400 MHz, Methanol-d_4) δ 9.45 (dd, *J* = 7.1, 0.8 Hz, 1H), 7.63 (dt, *J* = 1.9, 1.0 Hz, 1H), 7.33 (dd, *J* = 7.1, 1.7 Hz, 1H), 2.76 (s, 3H), 2.66 – 2.49 (m, 3H).

7.1.3.1.2. Synthesis of 2-substituted 1,3-benzoxazole-5-methylamine (Scheme 1B)

2-(4-Chlorophenyl)-1,3-benzoxazole-5-carbonitrile **(1d)**

To a suspension of 3-amino-4-hydroxybenzonitrile (5.7 mmol) in dioxane, 4-chlorobenzoylchloride (5.7 mmol) was added. The mixture was stirred at 100 ºC, and then Methanesulfonic acid (17.1 mmol, 3 equiv.) was added carefully. The reaction was stirred at 100 ºC overnight. After the evaporation of dioxane, a saturated solution of $NaHCO_3$ was added carefully (~ 5 mL). Effervescence was observed due to the release of CO_2. The formed brown precipitate was filtered and washed thoroughly with H_2O. This precipitate was recrystallized using hot isopropanol (70%) to get 1y in the form of reddish-brown crystals [121]. $C_{14}H_7ClN_2O$, 54% yield, APCI-MS: *m/z* 255.3 $[M+H]^+$, ^{1}H NMR (400 MHz, Chloroform-*d*) δ 8.19 (d, *J* = 8.6 Hz, 2H), 8.08 (d, *J* = 1.1 Hz, 1H), 7.67 (d, *J* = 1.4 Hz, 2H), 7.58 – 7.49 (m, 2H). ^{13}C NMR (101 MHz, Chloroform-*d*) δ 164.2, 153.1, 142.5, 138.9, 129.5, 129.3, 129.2, 124.6, 124.5, 118.6, 111.9, 108.8.

2-(4-Chlorophenyl)-1,3-benzoxazole-5-methylamine **(1e)**

1y (0.208 mmol) was suspended in dry MeOH (10 mL). Di-*tert*-butyl-dicarbonate (0.416 mmol, 2 equiv.) and $NiCl_2.6H_2O$ (0.02 mmol, 0.1 equiv.) were added. After cooling the mixture to 0 ºC, $NaBH_4$ (0.93 mmol, 4.5 equiv.) was added portion-wise and left to stir vigorously at room temperature overnight. 300 µL of diethylenetriamine was added before the evaporation of the solvent. The mixture was then diluted with ethyl acetate and washed with 10% citric acid, saturated $NaHCO_3$ and Brine. The organic phase was dried over anhydrous $MgSO_4$, concentrated and then purified with column chromatography using EtOAc: heptane (1:2) as the mobile phase. To the purified **1eBoc**, 4M HCl in dioxane was added (3-5 mL). The mixture was stirred for 2 h. As a workup, diethyl ether was added the formed precipitate was filtered and dried to give a greyish-white solid.[122] $C_{14}H_{12}ClN_2O^+$, 90% yield, ESI-MS: *m/z* 259.16 $[M+H]^+$, ^{1}H NMR (400 MHz, Methanol-d_4) δ 8.32 – 8.18 (m, 2H), 7.88 (dd, *J* = 1.8, 0.6 Hz, 1H), 7.78 (dd, *J* = 8.4, 0.6 Hz, 1H), 7.74 – 7.56 (m, 3H), 7.54 (dd, *J* = 8.4, 1.8 Hz, 1H), 4.28 (s, 3H).

2-(4-(Trifluoromethoxy)phenyl)-1,3-benzoxazole-5-carbonitrile **(2d)**

Under Argon 4-(trifluoromethoxy)benzoic acid (4.85 mmol) was suspended in dry DCM (20 mL), then a catalytic amount of DMF (3 drops) was added followed by thionyl chloride (2 equiv.). The colourless suspension was left to stir at room temperature for 2 h. The solvent was co-evaporated with toluene to get rid of excess remaining thionyl chloride.[185] The produced 4-(trifluoromethoxy)benzoyl chloride oil was directly added to a suspension of 3-amino-4-hydroxybenzonitrile (4.85 mmol, 1 equiv.) in dioxane. The procedure continues the same as mentioned above for (1y), however, **2d** crystals were paler and gave a lower yield (~30%). $C_{15}H_7F_3N_2O_2$, APCI-MS: *m/z* 305 $[M+H]^+$, ^{1}H NMR (400 MHz, Chloroform-*d*) δ 8.42 – 8.19 (m, 2H), 8.09 (t, *J* = 1.1 Hz, 1H), 7.73 – 7.64 (m, 2H), 7.45 – 7.26 (m, 2H). ^{13}C NMR (101 MHz, Chloroform-*d*) δ 163.8, 153.1, 152.2 (q, **C**OCF_3, $^2J_{CF}$ = 1.7 Hz), 142.5, 129.8, 129.35, 124.7, 124.5, 121.6, 120.2 (q, O**C**F_3, $^1J_{CF}$= 265 Hz), 118.8, 111.9, 108.8.

2-(4-(Trifluoromethoxy)phenyl)-1,3-benzoxazole-5-methylamine **(2e)**

2d (0.208 mmol) was suspended in dry MeOH (10 mL). Di-*tert*-butyl-dicarbonate (0.416, 2 equiv.) and $NiCl_2.6H_2O$ (0.02 mmol, 0.1 equiv.) were added. After cooling the mixture to 0 ºC, $NaBH_4$ (0.93 mmol, 4.5 equiv.) was added portion-wise and left to stir vigorously at room temperature overnight. 300 µL of diethylenetriamine was added before the evaporation of the solvent. The mixture was then diluted with ethyl acetate and washed with 10% citric acid,

saturated $NaHCO_3$ and Brine. The organic phase was dried over anhydrous $MgSO_4$, concentrated and then 4M HCl in dioxane was added (3-5 mL). The mixture was stirred for 2 h. As a workup, diethyl ether was added, the formed precipitate was filtered and dried to give a grey precipitate (**2e.HCl**).[122] $C_{15}H_{12}F_3N_2O_2^+$, 73% yield, ESI-MS: *m/z* 309.32 $[M+H]^+$, ^1H NMR (400 MHz, Methanol-*d*$_4$) δ 8.43 – 8.27 (m, 2H), 7.90 (dd, *J* = 1.8, 0.6 Hz, 1H), 7.79 (dd, *J* = 8.4, 0.6 Hz, 1H), 7.56 (d, *J* = 1.8 Hz, 1H), 7.54 – 7.51 (m, 2H), 4.29 (s, 2H).

7.1.3.1.3. General procedure for the synthesis of alkyl amines[127] (Scheme 3)

2-((2E,6E)-3,7,11-trimethyldodeca-2,6,10-trien-1-yl)isoindoline-1,3-dione **(1f)**

In a 100 mL round-bottom flask (*E*)-farnesol, phthalimide (1.2 equiv.), and Ph_3P (1.3 equiv.) were stirred in anhydrous THF (25 mL) in the dark. 1.3 equivalent DIAD was added dropwise, and then the mixture was left stirring at room temperature for 4 h. H_2O (100 mL) was added and the aqueous phase was extracted with heptane (3x 50 mL). The collected organic phases were washed with brine before drying over anhydrous Na_2SO_4 and then filtered. *N*-farnesylphthalimide (**1f**) was isolated by flash column chromatography (gradient elution, heptane:EtOAc, 100:0 to 50:50). $C_{23}H_{29}NO_2$, Colourless oil, 72 % yield, APCI-MS: *m/z* 352.1 $[M+H]^+$, ^1H NMR (500 MHz, Chloroform-*d*) δ 7.83 (dd, *J* = 5.4, 3.0 Hz, 2H), 7.72 – 7.62 (m, 2H), 5.28 (tq, *J* = 7.1, 1.3 Hz, 1H), 5.09-5.02 (m, 2H), 4.28 (d, *J* = 7.1 Hz, 2H), 2.11 – 1.87 (m, 8H), 1.84 (d, *J* = 1.3 Hz, 3H), 1.66 (d, *J* = 1.3 Hz, 3H), 1.57 (dd, *J* = 2.7, 1.3 Hz, 6H). ^{13}C NMR (126 MHz, Chloroform-*d*) δ 168.1, 140.6, 135.3, 133.7, 132.3, 131.2, 124.3, 123.6, 123.1, 118.0, 39.6, 39.5, 35.8, 26.7, 26.2, 25.6, 17.6, 16.3, 15.9.

(2E,6E)-3,7,11-trimethyldodeca-2,6,10-trien-1-amine **(1g)**

The purified **1f** was dissolved in MeOH, and then hydrazine hydrate (50% w/w) was added. The solution was left to stir overnight at room temperature. The reaction mixture was then diluted with an equal amount of H_2O, acidified with conc. HCl (pH<2) and washed with diethyl ether. The organic phase was discarded. The aqueous phase was basified with solid KOH to pH >10 and extracted with diethyl ether (3x). The combined organic phases were washed with brine, dried over anhydrous Na_2SO_4 and concentrated under vacuum. The resulting oil was passed through a silica gel plug with a mobile phase of 3% MeOH: DCM to give **1g**. $C_{15}H_{27}N$, Colourless oil, APCI-MS: *m/z* 222.1 $[M+H]^+$, ^1H NMR (500 MHz, Chloroform-*d*) δ 5.25 (tp, *J* = 6.8, 1.3 Hz, 1H), 5.13-5.05 (m, 2H), 3.27 (d, *J* = 6.8 Hz, 2H), 2.10 – 1.92 (m, 8H), 1.67 (d, *J* = 1.3 Hz, 3H), 1.62 (d, *J* = 1.3 Hz, 3H), 1.59 (d, *J* = 1.3 Hz, 6H).

2-(2E)-3,7-dimethylocta-2,6-dien-1-yl)isoindoline-1,3-dione (**2f**)

In a 100 mL round-bottom flask geraniol, phthalimide (1.2 equiv.), and Ph_3P (1.3 equiv.) were stirred in anhydrous THF (25 mL) in the dark. 1.3 equivalent DIAD was added dropwise, and then the mixture was left stirring at room temperature for 4 h. H_2O (100 mL) was added and the aqueous phase was extracted with heptane (3x 50 mL). The collected organic phases were washed with brine before drying over anhydrous Na_2SO_4 and then filtered. *N*-geranylphthalimide (**2f**) was isolated by flash column chromatography (gradient elution, heptane:EtOAc, 100:0 to 50:50). $C_{18}H_{21}NO_2$, Colourless oil, 87 % yield, APCI-MS: *m/z* 284.1 $[M+H]^+$, ^1H NMR (500 MHz, Methanol-*d*4) δ 7.89 – 7.86 (m, 2H), 7.84 – 7.81 (m, 2H), 5.28 (tq, *J* = 7.2, 1.2 Hz, 1H), 5.11 – 5.03 (m, 1H), 4.29 (dq, *J* = 7.1, 0.8 Hz, 2H), 2.16 – 2.09 (m, 2H), 2.09 – 2.01 (m, 2H), 1.86 (d, *J* = 1.6 Hz, 3H), 1.61 (d, *J* = 1.3 Hz, 3H), 1.58 (d, *J* = 1.3 Hz, 3H).

(2E)-3,7-dimethylocta-2,6-dien-1-amine (**2g**)

The purified **2f** was dissolved in MeOH, and then hydrazine hydrate (50% w/w) was added. The solution was left to stir overnight at room temperature. The reaction mixture was then diluted with an equal amount of H_2O, acidified with conc. HCl (pH<2) and washed with diethyl ether. The organic phase was discarded. The aqueous phase was basified with solid KOH to pH >10 and extracted with diethyl ether (3x). The combined organic phases were washed with brine, dried over anhydrous Na_2SO_4 and concentrated under vacuum. The resulting oil was passed through a silica gel plug with a mobile phase of 3% MeOH:DCM to give **2g**. $C_{10}H_{19}N$, Colourless oil, 66 % yield, APCI-MS: *m/z* 154.2 $[M+H]^+$, ^1H NMR (400 MHz, Chloroform-*d*) δ 5.30 – 5.21 (m, 1H), 5.15 – 5.05 (m, 1H), 3.27 (d, *J* = 6.8 Hz, 2H), 2.09 (m, 2H), 1.99 (m, 2H), 1.68 (s, 3H), 1.63 (s, 3H), 1.60 (s, 3H), 1.33 (s, NH_2, 2H).

2-(3,7-dimethyloctyl)isoindoline-1,3-dione (**3f**)

In a 100 mL round-bottom flask 3,7-dimethyl-1-octanol, phthalimide (1.2 equiv.), and Ph_3P (1.3 equiv.) were stirred in anhydrous THF (30 mL) in the dark. 1.3 equivalent DIAD was added dropwise, and then the mixture was left stirring at room temperature for 4 h. H_2O (100 mL) was added and the aqueous phase was extracted with heptane (3x 50 mL). The collected organic phases were washed with brine before drying over anhydrous Na_2SO_4 and then filtered **3f** was taken to the next step without further purification. $C_{18}H_{25}NO_2$, APCI-MS: *m/z* 288.0 $[M+H]^+$.

3,7-dimethyloctan-1-amine (**3g**)

The purified **3f** was dissolved in MeOH, and then hydrazine hydrate (50% w/w) was added. The solution was left to stir overnight at room temperature. The reaction mixture was then diluted with an equal amount of H_2O, acidified with conc. HCl (pH<2) and washed with diethyl ether. The organic phase was discarded. The aqueous phase was basified with solid KOH to pH >10 and extracted with diethyl ether (3x). The combined organic phases were washed with brine, dried over anhydrous Na_2SO_4 and concentrated under vacuum. The resulting oil was purified by column chromatography using a mobile phase of DCM:8% MeOH:1-3% NH_4OH to give **3g**. $C_{10}H_{23}N$, Colourless oil, 49 % yield, APCI-MS: *m/z* 158.2 $[M+H]^+$, ^1H NMR (500 MHz, Chloroform-*d*) δ 2.80 – 2.59 (m, 2H), 1.57 – 1.40 (m, 6H), 1.33 – 1.19 (m, 4H), 1.15 – 1.08 (m, 2H), 0.87 – 0.85 (m, 9H).

7.1.3.1.4. Synthesis of imidazopyridine amide analogues (1-30)

Method A:

In a round bottom flask covered with Aluminum foil (for light exclusion), **1c/2c/9c/10c**, **1e** or **2e** (1 equiv.) and DIPEA (5 equiv.) were dissolved in DMF (~10 mL) under Argon. PyBOP (1.1 equiv.), dissolved in DMF, was added through a septum over 30 min. and the reaction was left to stir overnight at room temperature. The mixture was diluted with H_2O to stop the reaction. The desired product crushed out and was filtered and washed with H_2O several times to get rid of DMF. (**1-5**)

Method B:

Under an inert atmosphere, **1-15c** and DIPEA (5 equiv.) were dissolved in anhydrous DMF. The yellow solution was left to stir for 10 min before adding HATU (1.1 equiv.). The solution got darker in colour as it stirred for 30 min. **1e/2e/1g/2g** (1 equiv.) was added and the reaction was stirred at room temperature for 1 h. Brine (50 mL) was added to precipitate the product. The filtered product was washed several times with water, EtOAc and one time with MeOH to get rid of DMF and impurities. (**6-30**)

6-Bromo-2-ethyl-N-((2-(4-chlorophenyl)-1,3-benzoxazol-5-yl)methyl)imidazo[1,2a]pyridine-3-carboxamide **(1)**

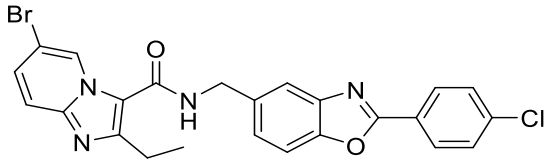

$C_{24}H_{18}BrClN_4O_2$, beige solid, 29% yield, m.p 260-262 ºC, calculated monoisotopic mass *m/z* 508.03017, ESI-HRMS: *m/z* 509.0379, 511.0354 (^{79}BrCl, ^{81}BrCl) $[M+H]^+$, ^{1}H NMR (500 MHz, Chloroform-*d*) δ 9.63 (dd, CH (IPA), *J* = 1.9, 0.9 Hz, 1H), 8.22 – 8.08 (m, 2 CH, 2H), 7.75 (dd, CH, *J* = 1.7, 0.7 Hz, 1H), 7.57 (dd, CH, *J* = 8.3, 0.6 Hz, 1H), 7.53 – 7.47 (m, 2CH, 2H), 7.48 (dd, CH (IPA), *J* = 9.5, 0.9 Hz, 1H), 7.41 (dd, CH, *J* = 8.5, 1.8 Hz, 1H), 7.38 (dd, CH (IPA), *J* = 9.5, 1.8 Hz, 1H), 6.18 (t, NH, *J* = 5.8 Hz, 1H), 4.81 (d, C**H$_2$**NH, *J* = 5.8 Hz, 2H), 2.98 (q, C**H$_2$**CH$_3$, *J* = 7.6 Hz, 2H), 1.40 (t, CH_3, *J* = 7.5 Hz, 3H). ^{13}C NMR (126 MHz, Chloroform-*d*) δ 162.8, 161.1, 151.29, 150.31, 144.6, 142.6, 137.9, 135.1, 130.4, 129.3, 128.9, 128.4, 125.5, 125.1, 119.1, 117.2, 114.8, 110.9, 108.1, 43.6, 23.6, 13.2. R_f= 0.44 (DCM: 3% MeOH).

6-Bromo-2-methyl-N-((2-(4-chlorophenyl)-1,3-benzoxazol-5-yl)methyl)imidazo[1,2a]pyridine-3-carboxamide **(2)**

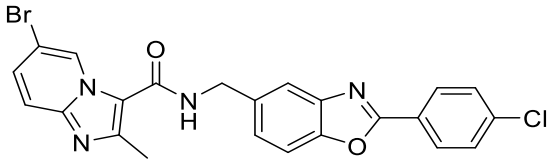

$C_{23}H_{16}BrClN_4O_2$, beige solid, 40% yield, m.p. 285-288 ºC, calculated monoisotopic mass *m/z* 494.01452, ESI-HRMS: *m/z* 495.52, 497.019 (^{79}BrCl, ^{81}BrCl) $[M+H]^+$, ^{1}H NMR (400 MHz, Chloroform-*d*) δ 9.67 (dd, CH (IPA), *J* = 1.9, 0.9 Hz, 1H), 8.23 – 8.14 (m, 2CH, 2H), 7.77 (dd, CH, *J* = 1.6, 0.7 Hz, 1H), 7.58 (d, CH, *J* = 8.3 Hz, 1H), 7.55 – 7.49 (m, 2CH, 2H), 7.47 (dd, CH (IPA), *J* = 9.4, 0.9 Hz, 1H), 7.45 – 7.37 (m, 2CH, 2H), 6.17 (t, NH *J* = 5.7 Hz, 1H), 4.83 (d, C**H$_2$**NH, *J* = 5.8 Hz, 2H), 2.69 (s, CH_3, 3H). ^{13}C NMR (101 MHz, Chloroform-*d*) δ 162.8, 161.1, 150.3, 144.5, 142.6, 137.9, 135.1, 130.5, 129.3, 128.8, 128.4, 125.5, 125.1, 119.04, 117.01, 110.9, 108.2, 43.5, 16.8. R_f= 0.22 (DCM:2% MeOH).

6-Bromo-2-ethyl-N-((2-(4-(trifluoromethoxy)phenyl)-1,3-benzoxazol-5yl)methyl)imidazo[1, 2a]pyridine-3-carboxa-mide **(3)**

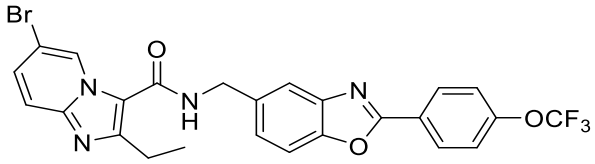

$C_{25}H_{18}BrF_3N_4O_3$, pale pink solid, 70% yield, m.p. 228-232 ºC, calculated monoisotopic mass *m/z* 558.05144, ESI-HRMS: *m/z* 559.0577, 561.0559 (^{79}Br, ^{81}Br) $[M+H]^+$, ^{1}H NMR (400 MHz, Chloroform-*d*) δ 9.65 (dd, CH (IPA), *J* = 1.9, 0.9 Hz, 1H), 8.34 – 8.25 (m, 2CH, 2H), 7.78 (dd, CH, *J* = 1.8, 0.7 Hz, 1H), 7.59 (dd, CH, *J* = 8.4, 0.6 Hz, 1H), 7.50 (dd, CH (IPA), *J* = 9.5, 0.9 Hz, 1H), 7.46 – 7.41 (m, 2CH, 2H), 7.40 – 7.35 (m, 2CH, 2H), 6.2 (t, NH, *J* = 5.8 Hz, 1H), 4.83 (d, C**H**$_2$NH, *J* = 5.8 Hz, 2H), 3.00 (q, C**H**$_2$CH$_3$, *J* = 7.6 Hz, 2H), 1.42 (t, CH$_3$, *J* = 7.6 Hz, 3H). ^{13}C NMR (101 MHz, Chloroform-*d*) δ 162.5, 161.1, 151.3, 150.3, 144.6, 142.5, 137.8, 135.1, 130.4, 129.4, 128.4, 124.2 (q, O**C**F$_3$, $^1J_{CF}$ = 267 Hz), 125.2, 122.4, 121.1, 119.1, 117.2, 116.5, 110.9, 108.1, 43.5, 23.6, 13.2. R_f= 0.23 (CHCl3:1% MeOH).

6-Bromo-2-methyl-N-((2-(4-(trifluoromethoxy)phenyl)-1,3-benzoxazol-5-yl)methyl)imidazo[1,2a]pyridine-3-carbo-xamide **(4).**

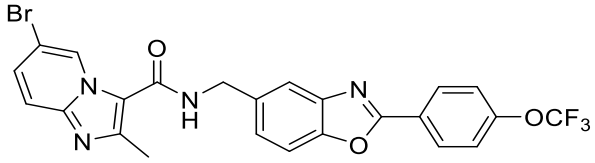

$C_{24}H_{16}BrF_3N_4O_3$, pale pink solid, 20% yield, m.p. 251-255 ºC, calculated monoisotopic mass *m/z* 544.03579, ESI-HRMS: *m/z* 545.32, 547.0411 (^{79}Br, ^{81}Br) $[M+H]^+$, ^{1}H NMR (500 MHz, Chloroform-*d*) δ 9.77 – 9.48 (m, CH (IPA), 1H), 8.37 – 8.19 (m, 2CH, 2H), 7.82 – 7.75 (m, CH, 1H), 7.60 (d, CH, *J* = 8.3 Hz, 1H), 7.53 (d, CH (IPA), *J* = 9.3 Hz, 1H), 7.47 (d, CH (IPA), *J* = 9.3 Hz, 1H), 1H), 7.43 (dd, CH, *J* = 8.3, 1.8 Hz, 1H), 7.41 – 7.31 (m, 2H), 6.28 (s, NH, 1H), 4.84 (d, *J* = 5.7 Hz, 2H), 2.72 (s, 3H). ^{13}C NMR (101 MHz, Chloroform-*d*) δ 162.5, 161.1, 151.6 (q, *J* = 1.8 Hz), 150.3, 145.8, 144.5, 142.5, 135.2, 130.6, 129.4, 128.4, 125.5, 125.2, 121.6, 121.1, 119.1, 116.9, 115.5, 110.9, 108.2, 43.5, 16.8. R_f= 0.28 ($CHCl_3$:2% MeOH).

7-Bromo-2-ethyl-N-((2-(4-chlorophenyl)-1,3-benzoxazol-5-yl)methyl)imidazo[1,2a]pyridine-3-carboxamide **(5)**

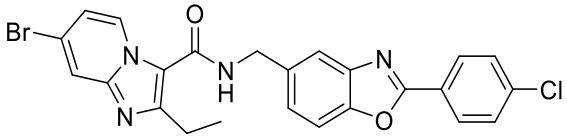

$C_{24}H_{18}BrClN_4O_2$, white solid, 50% yield, m.p.294-296 ºC, calculated monoisotopic mass *m/z* 508.03017, ESI-HRMS: *m/z* 509.0374, 511.0351, 513.0325 (^{79}BrCl, ^{81}BrCl, $^{81}Br^{37}$Cl) $[M+H]^+$, ^{1}H NMR (500 MHz, Chloroform-*d*) δ 9.33 (dd, *J* = 7.4, 0.8 Hz, 1H), 8.24 – 8.18 (m, 2H), 7.80 (dd, *J* = 2.0, 0.8 Hz, 1H), 7.78 (dd, *J* = 1.7, 0.7 Hz, 1H), 7.59 (dd, *J* = 8.3, 0.6 Hz, 1H), 7.55 – 7.50 (m, 2H), 7.42 (dd, *J* = 8.4, 1.7 Hz, 1H), 7.04 (dd, *J* = 7.4, 2.0 Hz, 1H), 6.19 (s, 1H), 4.83 (d, *J* = 5.7 Hz, 2H), 3.00 (q, *J* = 7.5 Hz, 2H), 1.41 (t, *J* = 7.6 Hz, 3H). ^{13}C NMR (126 MHz, Chloroform-*d*) δ 162.3, 161.1, 142.6, 135.1, 129.3, 128.9, 128.4, 128.1, 125.5, 125.1, 121.2, 119.1, 117.0, 110.9, 43.6, 23.6, 13.2. R_f= 0.1 (EtOAc:heptane:DCM, 1:1:1).

7-Bromo-2-methyl-N-((2-(4-chlorophenyl)-1,3-benzoxazol-5-yl)methyl)imidazo[1,2a]pyridine-3-carboxamide **(6)**

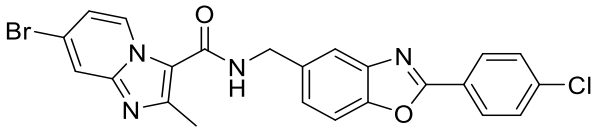

$C_{23}H_{16}BrClN_4O_2$, white solid, 7% yield, m.p. 281-285 ºC, calculated monoisotopic mass *m/z* 494.01452, ESI-HRMS: *m/z* 495.0227, 497.0202 (^{79}BrCl, ^{81}BrCl) $[M+H]^+$, ^{1}H NMR (400 MHz, Chloroform-*d*) δ 9.35 (d, *J* = 7.4 Hz, 1H), 8.22-8.17 (m, 2H), 7.81 – 7.75 (m, 1H), 7.59 (d, *J* = 8.1 Hz, 1H), 7.56 – 7.51 (m, 2H), 7.44-7.39 (m, 2H), 7.06 (dd, *J* = 7.4, 1.9 Hz, 1H), 6.16 (t, *J* = 5.7 Hz, 1H), 4.82 (d, *J* = 5.8 Hz, 2H), 2.69 (s, 3H). ^{13}C NMR (126 MHz, Chloroform-*d*) δ 162.8, 161.1, 150.3, 142.6, 138.00, 135.1, 129.3, 128.9, 128.4, 125.5, 125.1, 121.4, 119.1, 118.8, 117.1, 110.9, 43.5, 16.8. (purified by preparative HPLC), R_f= 0.15 (DCM:2% MeOH).

7-Bromo-2-ethyl-N-((2-(4-(trifluoromethoxy)phenyl)-1,3-benzoxazol-5-yl)methyl)imidazo[1, 2a]pyridine-3-carbox-amide **(7)**

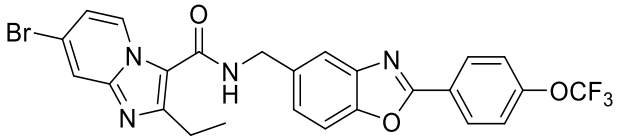

$C_{25}H_{18}BrF_3N_4O_3$, white solid, 77% yield, m.p. 266-270 ºC, calculated monoisotopic mass *m/z* 558.05144, ESI-HRMS: *m/z* 559.0582, 561.0561 (^{79}Br, ^{81}Br) $[M+H]^+$, ^{1}H NMR (500 MHz, Chloroform-*d*) δ 9.33 (dd, *J* = 7.4, 0.8 Hz, 1H), 8.33 – 8.26 (m, 2H), 7.80 (dd, *J* = 2.1, 0.8 Hz, 1H), 7.79 (dd, *J* = 1.7, 0.7 Hz, 1H), 7.59 (dd, *J* = 8.3, 0.6 Hz, 1H), 7.42 (dd, *J* = 8.4, 1.8 Hz, 1H), 7.40 – 7.35 (m, 2H), 7.04 (dd, *J* = 7.4, 2.1 Hz, 1H), 6.19 (s, 1H), 4.83 (d, *J* = 5.7 Hz, 2H), 2.99 (q, *J* = 7.6 Hz, 2H), 1.41 (t, *J* = 7.6 Hz, 3H). ^{13}C NMR (126 MHz, Chloroform-*d*) δ 161.1, 142.5, 135.1, 129.4, 128.4, 125.2, 121.1, 119.1, 119.1, 117.1, 110.9, 43.5, 23.5, 13.2. (purified by preparative HPLC). R_f=0.3 (DCM:1% MeOH).

7-Bromo-2-methyl-N-((2-(4-(trifluoromethoxy)phenyl)-1,3-benzoxazol-5-yl)methyl)imidazo[1,2a]pyridine-3-carbx-amide **(8)**

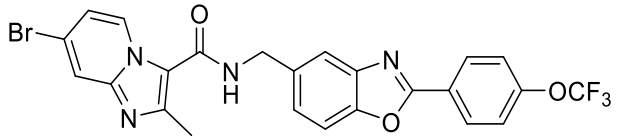

$C_{24}H_{16}BrF_3N_4O_3$, white solid, 22% yield, m.p. 272-275 ºC, calculated monoisotopic mass *m/z* 544.03579, ESI-HRMS: *m/z* 545.0422, 547.0401 (^{79}Br, ^{81}Br) $[M+H]^+$, ^{1}H NMR (500 MHz, Chloroform-*d*) δ 9.33 (d, *J* = 7.4 Hz, 1H), 8.38 – 8.23 (m, 2H), 7.88 (br s, 1H), 7.81 (d, *J* = 1.6 Hz, 1H), 7.59 (d, *J* = 8.3 Hz, 1H), 7.44 (dd, *J* = 8.3, 1.7 Hz, 1H), 7.42-7.38 (m, 2H), 7.20 – 7.06 (m, 1H), 6.58 (s, 1H), 4.83 (d, *J* = 5.5 Hz, 2H), 2.74 (s, 3H). ^{13}C NMR (126 MHz, Chloroform-*d*) δ 162.5, 151.6 (q, *J* = 1.8 Hz), 150.4, 142.5, 135.0, 129.4, 128.5, 125.5, 125.3, 124.5 (q, O**C**F_3, $^1J_{CF}$ = 271.1 Hz), 121.4, 121.1, 119.3, 110.9, 43.6, 11.5. 92% purity (HPLC), R_f= 0.1 ($CHCl_3$:1% MeOH). For the purification of this compound, a column was done using mobile phase $CHCl_3$:MeOH (99:1). This compound was not further purified as it did not show activity in biochemical and *in vitro* assays.

6-Trifluoromethyl-2-ethyl-N-((2-(4-chlorophenyl)-1,3-benzoxazol-5-yl)methyl)imidazo[1,2a] pyridine-3-carbox-amide **(9)**

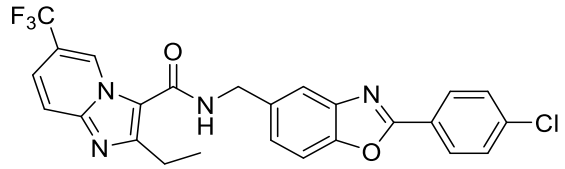

$C_{25}H_{18}ClF_3N_4O_2$, white solid, 6% yield, m.p. 255-257 ºC, calculated monoisotopic mass *m/z* 498.10704, ESI-HRMS: *m/z* 499.1144 [M+H], ^{1}H NMR (500 MHz, Chloroform-*d*) δ 9.89 (dq, *J* = 2.1, 1.2 Hz, 1H), 8.27 – 8.11 (m, 2H), 7.78 (dd, *J* = 1.8, 0.6 Hz, 1H), 7.71 (dt, *J* = 9.4, 0.9 Hz, 1H), 7.59 (dd, *J* = 8.4, 0.6 Hz, 1H), 7.54 – 7.50 (m, 2H), 7.50 – 7.46 (m, 1H), 7.42 (dd, *J* = 8.4, 1.8 Hz, 1H), 6.24 (t, *J* = 5.4 Hz, 1H), 4.85 (d, *J* = 5.8 Hz, 2H), 3.03 (q, *J* = 7.6 Hz, 2H), 1.43 (t, *J* = 7.5 Hz, 3H). ^{13}C NMR (126 MHz, Chloroform-*d*) δ 162.8, 160.9, 152.4, 150.3, 146.0, 142.6, 138.01, 134.8, 129.3, 128.9, 127.4 (q, $^3J_{CF}$ = 5.7 Hz), 125.4, 125.1, 123.5 (q, $^1J_{CF}$ = 271.4 Hz), 122.9 (q, $^4J_{CF}$ = 2.6 Hz), 119.1, 117.6 (q, $^2J_{CF}$ = 34.2 Hz), 117.3, 115.6, 110.9, 43.6, 23.6, 13.1.

6-Trifluoromethyl-2-methyl-N-((2-(4-chlorophenyl)-1,3-benzoxazol-5-yl)methyl)imidazo[1,2 a]pyridine-3-carbox-amide **(10)**

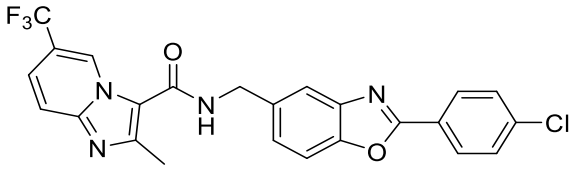

$C_{24}H_{16}ClF_3N_4O_2$, white solid, 39% yield, m.p. 251-254 ºC, calculated monoisotopic mass *m/z* 484.09139, ESI-HRMS: *m/z* 485.0989 $[M+H]^+$, ^{1}H NMR (500 MHz, Chloroform-*d*) δ 10.01 – 9.84 (m, 1H), 8.25 – 8.16 (m, 2H), 7.79 (dd, *J* = 1.7, 0.7 Hz, 1H), 7.69 (d, *J* = 9.3 Hz, 1H), 7.59 (dd, *J* = 8.4, 0.6 Hz, 1H), 7.55 – 7.51 (m, 2H), 7.51 – 7.48 (m, 1H), 7.43 (dd, *J* = 8.4, 1.7 Hz, 1H), 6.28 – 6.16 (m, 1H), 4.85 (d, *J* = 5.8 Hz, 2H), 2.74 (s, 3H).^{13}C NMR (126 MHz, Chloroform-*d*) δ 162.8, 160.9, 150.3, 146.9, 142.6, 138.0, 134.9, 129.3, 128.9, 125.4, 125.1, 123.4 (q, $^1J_{CF}$ = 274.6 Hz), 123.1 (q, $^4J_{CF}$ = 2.7 Hz), 119.1, 117.6 (q, $^2J_{CF}$ = 34.2 Hz), 117.1, 110.9, 43.6, 16.8.

6- Trifluoromethyl -2-ethyl-N-((2-(4-(trifluoromethoxy)phenyl)-1,3-benzoxazol-5-yl)methyl)imidazo[1,2a]pyridine-3-carboxamide **(11)**

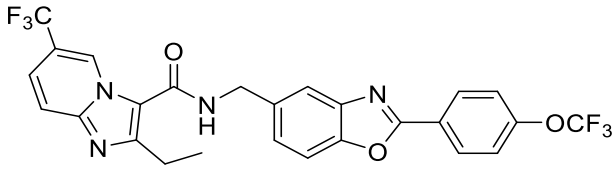

$C_{26}H_{18}F_6N_4O_3$, beige solid, 73% yield, m.p. 234-236 ºC, calculated monoisotopic mass *m/z* 548.12831, ESI-HRMS: *m/z* 549.1363 [M+H], ^{1}H NMR (400 MHz, Chloroform-*d*) δ 9.88 (dt, CH (IPA) *J* = 2.2, 1.1 Hz, 1H), 8.38 – 8.25 (m, 2CH, 2H), 7.82 – 7.75 (m, CH, 1H), 7.71 (d, CH (IPA), *J* = 9.4 Hz, 1H), 7.60 (d, CH, *J* = 8.4 Hz, 1H), 7.49 (dd, CH (IPA), *J* = 9.4, 1.9 Hz, 1H), 7.43 (dd, CH, *J* = 8.4, 1.7 Hz, 1H), 7.40 – 7.31 (m, 2CH, 2H), 6.25 (t, NH, *J* = 5.6 Hz, 1H), 4.85 (d, CH_2NH, *J* = 5.8 Hz, 2H), 3.03 (q, CH_2CH_3, *J* = 7.6 Hz, 3H), 1.43 (t, CH_3, *J* = 7.6 Hz, 3H). ^{13}C NMR (101 MHz, Chloroform-*d*) δ 162.5, 160.9, 152.4, 151.6 (q, *J* = 1.6 Hz), 150.4, 146.0, 142.6, 134.9, 129.4, 127.5 (q, $^3J_{CF}$ = 5.7 Hz), 125.5, 125.2, 123.5 (q, $^1J_{CF}$ = 272.6 Hz), 122.9 (q, $^4J_{CF}$ = 2.6 Hz), 121.1, 119.1, 117.6 (q, $^2J_{CF}$ = 34.6 Hz), 117.3, 115.6, 111.0, 43.6, 23.6, 13.1. R_f= 0.25 (DCM:2% MeOH).

6-Trifluoromethyl-2-methyl-N-((2-(4-(trifluoromethoxy)phenyl)-1,3-benzoxazol-5-yl)methyl)imidazo[1,2a]pyridine-3-carboxamide **(12)**

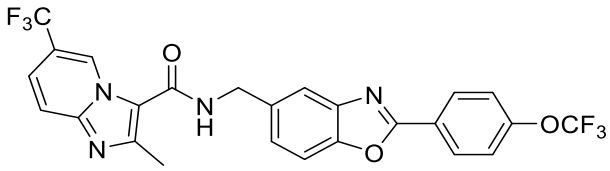

$C_{25}H_{16}F_6N_4O_3$, pale pink solid, 71% yield, m.p. 199-202 ºC, calculated monoisotopic mass *m/z* 534.11266, ESI-HRMS: *m/z* 535.1191 $[M+H]^+$, ^{1}H NMR (400 MHz, Chloroform-*d*) δ 9.89 (br s, CH (IPA), 1H), 8.34 – 8.22 (m, 2H), 7.79 (br s, 1H), 7.70 (d, CH (IPA) *J* = 9.3 Hz, 1H), 7.59 (d, *J* = 8.3 Hz, 1H), 7.52 (d, CH (IPA), *J* = 9.0 Hz, 1H), 7.43 (d, *J* = 8.4 Hz, 1H), 7.40 – 7.32 (m, 2H), 6.40 (s, NH, 1H), 4.84 (d, *J* = 4.3 Hz, 2H), 2.74 (s, 3H). ^{13}C NMR (101 MHz, Chloroform-*d*) δ 162.5, 160.7, 151.6 (q, *J* = 1.7 Hz), 150.4, 142.5, 134.9, 129.4, 127.4 (q, $^3J_{CF}$ = 5.7 Hz), 125.5, 125.2, 123.3 (q, $^1J_{CF}$ = 273.5 Hz), 123.5 (q, $^3J_{CF}$ = 4.1 Hz), 120.5 (q, OCF_3, $^1J_{CF}$ = 261.2 Hz), 121.1, 119.2, 118.0 (q, $^2J_{CF}$ = 35.0 Hz), 116.9, 110.9, 43.6, 16.6. R_f= 0.12 ($CHCl_3$:1% MeOH).

7-Trifluoromethyl-2-ethyl-N-((2-(4-chlorophenyl)-1,3-benzoxazol-5-yl)methyl)imidazo[1,2a] pyridine-3-carbox-amide **(13)**

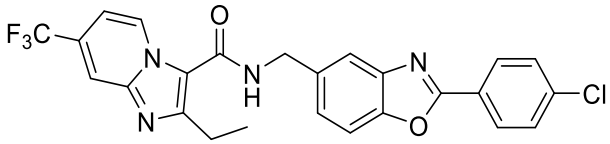

This compound was synthesized following method A. $C_{25}H_{18}ClF_3N_4O_2$, beige solid, 70% yield, m.p. 265-268 ºC, calculated monoisotopic mass *m/z* 498.10704, ESI-HRMS: *m/z* 499.1134 $[M+H]^+$, ^{1}H NMR (400 MHz, Chloroform-*d*) δ 9.55 (dt, CH (IPA), *J* = 7.4, 2.0, 1.2 Hz, 1H), 8.28 – 8.10 (m, 2CH, 2H), 7.92 (dt, CH (IPA), *J* = 2.0, 1.1 Hz, 1H), 7.81 – 7.68 (m, CH, 1H), 7.59 (d, CH, *J* = 8.2 Hz, 1H), 7.55 – 7.49 (m, 2CH, 2H), 7.41 (dd, CH, *J* = 8.4, 1.8 Hz, 1H), 7.10 (dd, CH (IPA) *J* = 7.4, 1.9 Hz, 1H), 6.23 (t, NH, *J* = 4.6 Hz, 1H), 4.84 (d, **C**H_2NH, *J* = 5.7 Hz, 2H), 3.03 (q, **C**H_2CH_3, *J* = 7.5 Hz, 2H), 1.43 (t, CH_3, *J* = 7.6 Hz, 3H). ^{13}C NMR (101 MHz, Chloroform-*d*) δ 171.1, 160.9, 160.7, 152.5, 150.3, 149.8, 142.6, 138.0, 129.3, 129.0, 128.9, 125.4, 125.1, 119.1, 117.5 (q, $^1J_{CF}$ = 279.2 Hz), 117.4, 116.1, 114.5 (q, $^3J_{CF}$ = 3.7 Hz),112.9, 110.9, 108.9 (q, $^4J_{CF}$ = 1.9 Hz), 43.6, 23.5, 13.1. R_f= 0.25 (DCM:1% MeOH).

7-Trifluoromethyl-2-methyl-N-((2-(4-chlorophenyl)-1,3-benzoxazol-5-yl)methyl)imidazo[1,2 a]pyridine-3-carbox-amide **(14)**

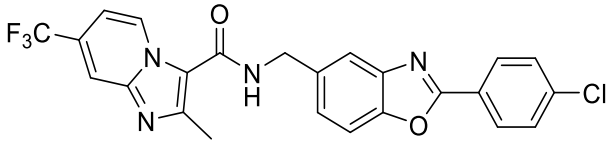

$C_{24}H_{16}ClF_3N_4O_2$, white solid, 3% yield, m.p. 257-260 ºC, calculated monoisotopic mass *m/z* 484.09139, ESI-HRMS: *m/z* 485.0978 $[M+H]^+$, ^{1}H NMR (400 MHz, Chloroform-*d*) δ 9.58 (d, *J* = 7.3 Hz, 1H), 8.19 (d, *J* = 8.2 Hz, 2H), 7.88 (s, 1H), 7.78 (s, 1H), 7.59 (d, *J* = 8.4 Hz, 1H), 7.51 (d, *J* = 8.3 Hz, 2H), 7.42 (d, *J* = 8.4 Hz, 1H), 7.11 (d, *J* = 7.3 Hz, 1H), 6.23 (s, 1H), 4.84 (d, *J* = 5.8 Hz, 2H), 2.73 (s, 3H). ^{13}C NMR (126 MHz, Chloroform-*d*) δ 162.9, 160.9, 150.3, 146.9, 142.6, 138.0, 134.9, 129.3, 128.95, 128.9, 125.4, 125.1, 119.1, 117.6 (q, $^1J_{CF}$ = 280.0 Hz), 114.3 (q, $^3J_{CF}$ = 4.9 Hz), 110.9, 109.0 (q, $^3J_{CF}$ = 3.1 Hz), 43.6, 16.8. R_f= 0.24 (DCM:1% MeOH).

7-Trifluoromethyl-2-ethyl-N-((2-(4-(trifluoromethoxy)phenyl)-1,3-benzoxazol-5-yl)methyl)imidazo[1,2a]pyridine-3-carboxamide **(15)**

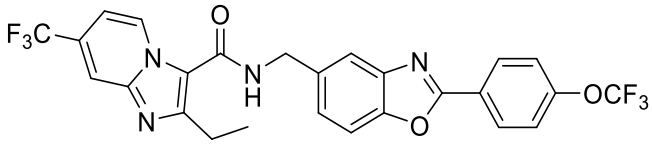

$C_{26}H_{18}F_6N_4O_3$, white solid, 47% yield, m.p. 258-261 ºC, calculated monoisotopic mass *m/z* 548.12831, ESI-HRMS: *m/z* 549.1348 $[M+H]^+$, ^{1}H NMR (400 MHz, TFA/DMSO) δ 9.39 (d, *J* = 7.2 Hz, 1H), 8.50 – 8.40 (m, 2H), 8.27 – 8.18 (m, 1H), 8.04 (d, *J* = 1.6 Hz, 1H), 7.94 (d, *J* = 8.7 Hz, 1H), 7.86 (dd, *J* = 8.8, 1.6 Hz, 1H), 7.74 (dd, *J* = 7.4, 1.7 Hz, 1H), 7.62 – 7.54 (m, 2H), 5.01 (s, 1H), 3.27 (q, *J* = 7.6 Hz, 2H), 1.47 (t, *J* = 7.6 Hz, 3H). ^{13}C NMR (126 MHz, TFA/DMSO) δ 166.5, 161.9, 158.9 (q, *J* = 1.8 Hz), 150.8, 145.8, 141.2, 140.6, 133.7, 132.5, 131.6, 131.1, 123.4, 119.5, 118.3 (q, $^2J_{CF}$ = 34.6 Hz), 117.1, 117.1, 116.7, 115.7, 115.6 (q, $^1J_{CF}$ = 282.8 Hz), 115.24, 45.91, 21.12, 12.85. Some signals are covered by the solvent signal. R_f = 0.21 (DCM:1% MeOH).

7-Trifluoromethyl-2-methyl-N-((2-(4-(trifluoromethoxy)phenyl)-1,3-benzoxazol-yl)methyl)imidazo[1,2a]pyridine-3-carboxamide **(16)**

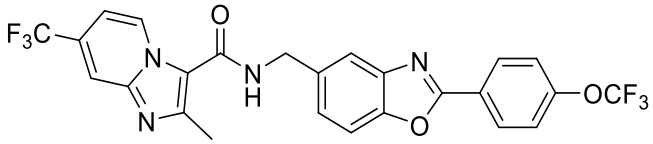

$C_{25}H_{16}F_6N_4O_3$, white solid, 80% yield, m.p. 276-277 ºC, calculated monoisotopic mass *m/z* 534.11266, ESI-HRMS: *m/z* 535.1192 $[M+H]^+$, ^{1}H NMR (500 MHz, Chloroform-*d*) δ 9.59 (dt, *J* = 7.3, 0.8 Hz, 1H), 8.34 – 8.26 (m, 2H), 7.88 (dt, *J* = 1.8, 1.0 Hz, 1H), 7.80 (dd, *J* = 1.7, 0.7 Hz, 1H), 7.62 – 7.57 (m, 1H), 7.43 (dd, *J* = 8.4, 1.7 Hz, 1H), 7.41 – 7.35 (m, 2H), 7.12 (dd, *J* = 7.4, 1.9 Hz, 1H), 6.24 (s, 1H), 4.85 (d, *J* = 5.8 Hz, 2H), 2.74 (s, 3H). ^{13}C NMR (126 MHz, Chloroform-*d*) δ 162.5, 160.9, 150.4, 146.9, 144.3, 142.6, 134.9, 129.4, 128.9, 125.2, 121.9, 121.1 (q, $^4J_{CF}$ = 1.2 Hz), 119.2, 117.6 (q, $^1J_{CF}$ = 275.3 Hz), 116.5, 114.3 (q, $^3J_{CF}$ = 5.0 Hz), 111.0, 109.0 (q, $^3J_{CF}$ = 3.0 Hz), 43.6, 16.8. 100% purity (HPLC, the compound was purified using preparative HPLC). R_f= 0.2 (DCM:2% MeOH).

6-Trifluoromethoxy-2-ethyl-N-((2-(4-chlorophenyl)-1,3-benzoxazol-5-yl)methyl)imidazo[1,2a]pyridine-3-carbox-amide **(17)**

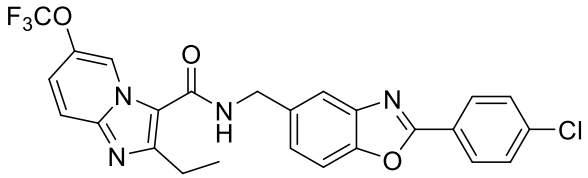

$C_{25}H_{18}ClF_3N_4O_3$, white solid, 10% yield, m.p. 264-266 ºC, calculated monoisotopic mass *m/z* 514.10195, ESI-HRMS: *m/z* 515.1093 $[M+H]^+$, ^{1}H NMR (400 MHz, Chloroform-*d*) δ 9.64 – 9.58 (m, 1H), 8.21 – 8.13 (m, 2H), 7.77 (dd, *J* = 1.7, 0.6 Hz, 1H), 7.65 (d, *J* = 9.7 Hz, 1H), 7.58 (dd, *J* = 8.3, 0.6 Hz, 1H), 7.53 – 7.48 (m, 2H), 7.42 (dd, *J* = 8.4, 1.7 Hz, 1H), 7.33 (dd, *J* = 9.6, 2.5 Hz, 1H), 6.30 – 6.13 (m, 1H), 4.83 (d, *J* = 5.7 Hz, 2H), 3.01 (q, *J* = 7.6 Hz, 2H), 1.42 (t, *J* = 7.5 Hz, 3H). ^{13}C NMR (101 MHz, Chloroform-*d*) δ 162.8, 160.9, 150.3, 142.6, 138.0, 134.9, 129.3, 128.9, 125.4, 125.1, 124.1(q, $^1J_{CF}$ = 260.8 Hz), 122.3, 119.1, 116.8, 110.9, 43.6, 23.6, 13.1. R_f= 0.23 ($CHCl_3$: 1% MeOH).

6-Trifluoromethoxy-2-methyl-N-((2-(4-chlorophenyl)-1,3-benzoxazol-5-yl)methyl)imidazo[1,2a]pyridine-3-carbox-amide **(18)**

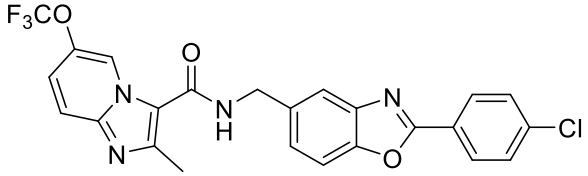

$C_{24}H_{16}ClF_3N_4O_3$, white solid, 42% yield, m.p. 256-260 ºC, calculated monoisotopic mass *m/z* 500.08630, ESI-HRMS: *m/z* 501.0937 $[M+H]^+$, ^{1}H NMR (500 MHz, Chloroform-*d*) δ 9.71 – 9.53 (m, 1H), 8.23 – 8.09 (m, 2H), 7.84 – 7.71 (m, 1H), 7.60 (dd, *J* = 9.6, 0.8 Hz, 1H), 7.58 (dd, *J* = 8.4, 0.5 Hz, 1H), 7.54 – 7.48 (m, 2H), 7.42 (dd, *J* = 8.4, 1.8 Hz, 1H), 7.33 (ddd, *J* = 9.6, 2.4, 1.0 Hz, 1H), 6.20 (s, 1H), 4.84 (d, *J* = 5.7 Hz, 2H), 2.72 (s, 3H). ^{13}C NMR (126 MHz, Chloroform-*d*) δ 162.9, 161.0, 150.3, 146.7, 144.3, 142.6, 138.6 (q, *J* = 2.5 Hz), 138.0, 135.0, 129.3, 128.9, 127.8, 125.4, 125.1, 122.8, 122.2, 120.5 (q, $^1J_{CF}$ = 263.1 Hz), 119.06, 116.74, 110.95, 43.51, 16.89. R_f= 0.12 ($CHCl_3$:1% MeOH).

6-Trifluoromethoxy-2-ethyl-N-((2-(4-(trifluoromethoxy)phenyl)-1,3-benzoxazol-5-yl)methyl)imidazo[1,2a]pyridine-3-carboxamide **(19)**

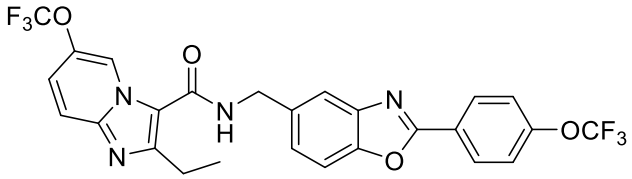

$C_{26}H_{18}F_6N_4O_4$, white solid, 60% yield, m.p. 248-251 ºC, calculated monoisotopic mass *m/z* 564.12322, ESI-HRMS: *m/z* 565.13 $[M+H]^+$, ^1H NMR (400 MHz, Chloroform-*d*) δ 9.61 (s, 1H), 8.29 (d, *J* = 8.4 Hz, 2H), 7.78 (s, 1H), 7.62 (d, *J* = 9.7 Hz, 1H), 7.59 (d, *J* = 8.3 Hz, 1H), 7.42 (d, *J* = 8.4 Hz, 1H), 7.38 (d, *J* = 8.2 Hz, 2H), 7.32 (d, *J* = 9.7 Hz, 1H), 6.22 (s, 1H), 4.84 (d, *J* = 5.7 Hz, 2H), 3.01 (q, *J* = 7.5 Hz, 2H), 1.42 (t, *J* = 7.5 Hz, 3H). ^{13}C NMR (126 MHz, Chloroform-*d*) δ 162.5, 161.0, 152.2, 151.6 (q, *J* = 1.8 Hz), 150.4, 144.5, 142.6, 138.6 (q, *J* = 2.6 Hz), 135.0, 129.4, 125.5, 125.2, 122.7, 122.3, 121.6 (q, $^1J_{CF}$ = 261.4 Hz), 121.4 (q, $^1J_{CF}$ = 258.5 Hz), 121.1, 119.1, 116.9, 115.7, 110.9, 43.5, 23.7, 13.2. R_f= 0.37 ($CHCl_3$:2% MeOH).

6-Trifluoromethoxy-2-methyl-N-((2-(4-(trifluoromethoxy)phenyl)-1,3-benzoxazol-5-yl)meth yl)imidazo[1,2a]pyridine-3-carboxamide **(20)**

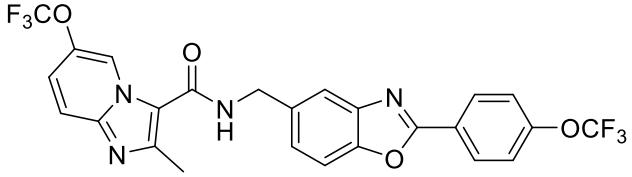

$C_{25}H_{16}F_6N_4O_4$, white solid, 55% yield, m.p. 239-240 ºC, calculated monoisotopic mass *m/z* 550.10757, ESI-HRMS: *m/z* 551.1141 $[M+H]^+$, ^1H NMR (400 MHz, Chloroform-*d*) δ 9.62 (s, CH (IPA), 1H), 8.35 – 8.18 (m, 2CH, 2H), 7.80 (s, CH, 1H), 7.69 (d, CH (IPA), *J* = 9.6 Hz, 1H), 7.59 (d, CH, *J* = 8.2 Hz, 1H), 7.44 (d, CH, *J* = 8.2 Hz, 1H), 7.40 (d, CH (IPA), *J* = 9.6 Hz, 1H), 7.38 – 7.33 (m, 2CH, 2H), 6.47 (s, NH, 1H), 4.84 (s, CH_2NH, 2H), 2.76 (s, CH_3, 3H). ^{13}C NMR (101 MHz, Chloroform-*d*) δ 162.5, 160.6, 150.4, 142.6, 134.9, 129.4, 125.5, 125.3, 123.7, 122.3, 121.1, 119.2, 116.2, 114.1, 110.9, 43.6, 16.4. R_f= 0.3 ($CHCl_3$:1% MeOH).

7-Trifluoromethoxy-2-methyl-N_((2-(4_chlorophenyl)-1,3-benzoxazol-5-yl)methyl)imidazo[1,2a]pyridine-3-carbox-amide **(21)**

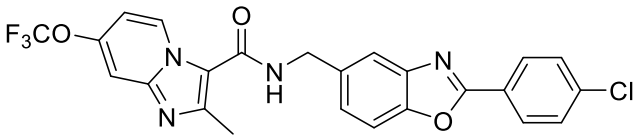

$C_{24}H_{16}ClF_3N_4O_3$, beige solid, 40% yield, m.p. 261-263 ºC, calculated monoisotopic mass *m/z* 500.08630, ESI-HRMS: *m/z* 501.0926 $[M+H]^+$, ^1H NMR (500 MHz, Chloroform-*d*) δ 9.51 (dd, *J* = 7.6, 0.8 Hz, 1H), 8.26 – 8.11 (m, 2H), 7.78 (dd, *J* = 1.7, 0.7 Hz, 1H), 7.59 (dd, *J* = 8.3, 0.6 Hz, 1H), 7.55 – 7.48 (m, 2H), 7.44 – 7.38 (m, 2H), 6.86 (dd, *J* = 7.5, 2.5 Hz, 1H), 6.17 (t, *J* = 5.5, 5.1 Hz, 1H), 4.84 (d, *J* = 5.8 Hz, 2H), 2.70 (s, 3H). ^{13}C NMR (126 MHz, Chloroform-*d*) δ 162.9, 161.1, 150.3, 148.0 (q, *J* = 1.8 Hz), 146.6, 146.0, 138.0, 135.1, 129.6, 129.3, 128.9, 125.5, 125.1, 119.1, 110.9, 107.9, 106.1, 43.5, 16.8. R_f = 0.086 ($CHCl_3$:1% MeOH).

7-Trifluoromethoxy-2-ethyl-N-((2-(4-(trifluoromethoxy)phenyl)-1,3-benzoxazol-5-yl)methyl)imidazo[1,2a]pyridine-3-carboxamide **(22)**

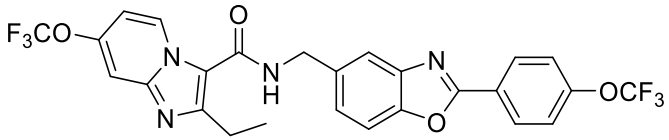

$C_{26}H_{18}F_6N_4O_4$, white solid, 50% yield, m.p. 251-255 ºC, calculated monoisotopic mass *m/z* 564.12322, ESI-HRMS: *m/z* 565.1303 $[M+H]^+$, ^1H NMR (400 MHz, Chloroform-*d*) δ 9.48 (d, CH (IPA), *J* = 7.6 Hz, 1H), 8.29 (d, 2CH, *J* = 8.5 Hz, 2H), 7.78 (s, CH, 1H), 7.59 (d, CH, *J* = 8.4 Hz, 1H), 7.44 (d, CH, *J* = 8.5 Hz, 1H), 7.40 (d, CH (IPA), *J* = 7.6 Hz, 1H), 7.37 (d, 2CH, *J* = 8.4 Hz, 2H), 6.85 (d, CH (IPA), *J* = 7.9 Hz, 1H), 6.20 (t, NH, *J* = 6.3 Hz, 1H), 4.83 (d, CH_2NH, *J* = 5.7 Hz, 2H), 3.00 (q, CH_2CH_3, *J* = 7.5 Hz, 2H), 1.42 (t, CH_3, *J* = 7.5 Hz, 3H).^{13}C NMR (101 MHz, Chloroform-*d*) δ 161.1, 151.6 (q, *J* = 1.6 Hz), 150.3, 148.0 (q, *J* = 2.9 Hz), 146.0, 142.6, 135.1, 129.6, 129.4, 125.5, 125.2, 121.5, 121.1, 119.1, 114.9, 110.9, 107.9, 106.1, 43.5, 23.5, 13.1. R_f = 0.24 ($CHCl_3$:1% MeOH).

7-Trifluoromethoxy-2-methyl-N-((2-(4-(trifluoromethoxy)phenyl)-1,3-benzoxazol-5-yl)methyl)imidazo[1,2a]pyridine-3-carboxamide **(23)**

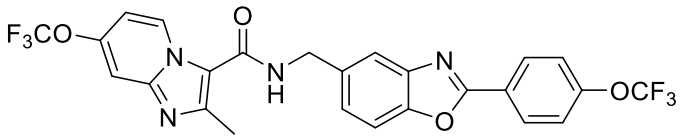

$C_{25}H_{16}F_6N_4O_4$, white solid, 25% yield, m.p. 255-259 ºC, calculated monoisotopic mass *m/z* 550.10757, ESI-HRMS: *m/z* 551.1152 $[M+H]^+$, ^{1}H NMR (400 MHz, Chloroform-*d*) δ 9.51 (d, *J* = 7.6 Hz, 1H), 8.32 – 8.25 (m, 2H), 7.79 (s, 1H), 7.59 (d, *J* = 8.3 Hz, 1H), 7.47 – 7.40 (m, 2H), 7.37 (d, *J* = 8.4 Hz, 2H), 6.89 (d, *J* = 7.6 Hz, 1H), 6.28 (s, 1H), 4.83 (d, *J* = 5.4 Hz, 2H), 2.72 (s, 3H). ^{13}C NMR (126 MHz, Chloroform-*d*) δ 162.5, 161.1, 151.6 (q, *J* = 1.8 Hz), 150.4, 142.6, 135.1, 129.6, 129.4, 125.5, 125.2, 121.4 (q, $^1J_{CF}$ = 255.9 Hz), 121.3 (q, $^1J_{CF}$ = 259.4 Hz), 121.1, 119.1, 110.9, 107.9, 106.0, 43.5, 16.8.

6-Chloro-2-ethyl-N-((2-(4-(trifluoromethoxy)phenyl)-1,3-benzoxazol-5-yl)methyl)imidazo[1,2a]pyridine-3-carbox-amide **(24)**[86]

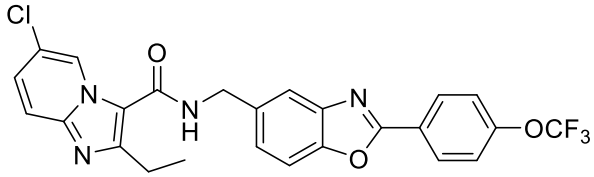

$C_{25}H_{18}ClF_3N_4O_3$, pale pink solid, 29% yield, m.p. 240-242 ºC, calculated monoisotopic mass *m/z* 514.10195, ESI-HRMS: *m/z* 515.1089 $[M+H]^+$, ^{1}H NMR (400 MHz, Chloroform-*d*) δ 9.56 (dd, *J* = 2.1, 0.9 Hz, 1H), 8.32 – 8.26 (m, 2H), 7.78 (t, *J* = 2.8 Hz, 1H), 7.61 – 7.49 (m, 2H), 7.42 (dt, *J* = 8.3, 2.5 Hz, 1H), 7.39 – 7.34 (m, 2H), 7.31 (dd, *J* = 9.5, 2.1 Hz, 1H), 6.19 (s, 1H), 4.83 (d, *J* = 5.8 Hz, 2H), 3.08 – 2.92 (m, 2H), 1.41 (td, *J* = 7.6, 1.5 Hz, 3H). ^{13}C NMR (^{13}C NMR (101 MHz, Chloroform-*d*) δ 161.1, 150.3, 144.5, 142.5, 135.3, 133.9, 133.0, 129.4, 128.9, 128.3, 126.2, 125.5, 125.2, 121.6, 121.1, 119.1, 116.9, 111.0, 43.5, 23.6, 13.1.

N-benzyl-2,7-dimethylimidazo[1,2a]pyridine-3-carboxamide **(25)**[112]

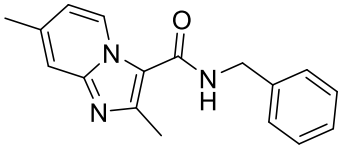

$C_{17}H_{17}N_3O$, white solid, m.p. 169-170ºC, calculated monoisotopic mass *m/z* 279.13716, ESI-HRMS: *m/z* 280.144 $[M+H]^+$, ^{1}H NMR (400 MHz, Chloroform-*d*) δ 9.31 (dd, *J* = 7.1, 0.9 Hz, 1H), 7.40 – 7.36 (m, 4H), 7.34 – 7.30 (m, 2H), 6.76 (dd, *J* = 7.2, 1.8 Hz, 1H), 4.70 (d, *J* = 5.7 Hz, 2H), 2.66 (s, 3H), 2.42 (d, *J* = 1.0 Hz, 3H). ^{13}C NMR (101 MHz, Chloroform-*d*) δ 161.5, 146.5, 145.3, 138.3, 128.8, 127.6, 127.3, 115.7, 115.0, 43.4, 21.3, 16.8. R_f= 0.17 (DCM:2% MeOH).

2-Ethyl-*N*-((2-(4-(trifluoromethoxy)phenyl)-1,3-benzoxazol-5-yl)methyl)imidazo[1,2a]pyridine-3-carboxamide **(26)**

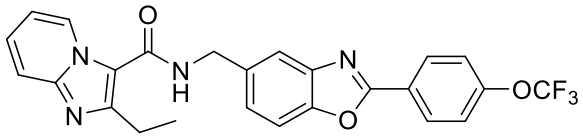

$C_{25}H_{19}F_3N_4O_3$, white solid, 25% yield, m.p. 229-233 ºC, calculated monoisotopic mass *m/z* 480.14092, ESI-HRMS: *m/z* 481.1476 $[M+H]^+$, ^{1}H NMR (500 MHz, Chloroform-*d*) δ 9.43 (dt, *J* = 7.0, 1.2 Hz, 1H), 8.32 – 8.24 (m, 2H), 7.81 – 7.76 (m, 1H), 7.61 (dt, *J* = 8.9, 1.2 Hz, 1H), 7.58 (d, *J* = 8.3 Hz, 1H), 7.43 (dd, *J* = 8.4, 1.8 Hz, 1H), 7.39 – 7.34 (m, 2H), 7.33 (ddd, *J* = 9.0, 6.9, 1.4 Hz, 1H), 6.93 (td, *J* = 6.9, 1.2 Hz, 1H), 6.18 (d, *J* = 6.2 Hz, 1H), 4.84 (d, *J* = 5.7 Hz, 2H), 3.01 (q, *J* = 7.6 Hz, 2H), 1.42 (t, *J* = 7.6 Hz, 3H). ^{13}C NMR (126 MHz, Chloroform-*d*) δ 162.4, 161.5, 151.6 (q, *J* = 1.8 Hz), 150.9, 150.3, 146.3, 142.5, 135.3, 129.4, 128.2, 126.9, 125.5, 125.2, 121.1, 120.3 (q, $^1J_{CF}$ = 259.0 Hz), 119.1, 116.7, 114.6, 113.2, 110.9, 43.5, 23.6, 13.3. R_f= 0.33 ($CHCl_3$:2% MeOH).

6-Chloro-2-ethyl-*N*-((2*E*,6*E*)-3,7,11-trimethyldodeca-2,6,10-trien-1-yl)imidazo[1,2a]pyridine -3-carboxamide **(27)**

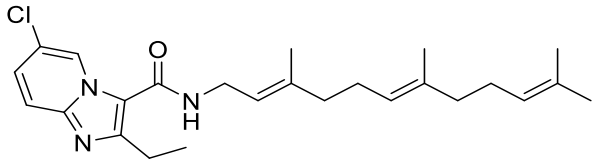

$C_{25}H_{34}ClN_3O$, white solid, 8% yield, m.p. 101-106 ºC, calculated monoisotopic mass *m/z* 427.23904, ESI-HRMS: *m/z* 428.2459 $[M+H]^+$, ^{1}H NMR (500 MHz, Chloroform-*d*) δ 9.48 (dd, *J* = 2.1, 0.9 Hz, 1H), 7.52 (dd, *J* = 9.4, 0.9 Hz, 1H), 7.28 (dd, *J* = 9.5, 2.1 Hz, 1H), 5.70 (t, *J* = 5.2 Hz, 1H), 5.33 (tq, *J* = 7.0, 1.3 Hz, 1H), 5.13 – 5.04 (m, 2H), 4.10 (t, *J* = 5.8 Hz, 2H), 2.98 (q, *J* = 7.6 Hz, 2H), 2.15 – 1.95 (m, 8H), 1.76 (d, *J* = 1.3 Hz, 3H), 1.67 (d, *J* = 1.3 Hz, 3H), 1.60 (d, *J* = 1.3 Hz, 3H), 1.58 (d, *J* = 1.3 Hz, 3H), 1.43 (t, *J* = 7.6 Hz, 3H). ^{13}C NMR (126 MHz, Chloroform-*d*) δ 160.9, 151.0, 144.3, 140.9, 135.5, 131.3, 127.9, 126.1, 124.2, 123.6, 121.4, 119.5, 116.8, 115.3, 39.7, 39.5, 37.4, 26.7, 26.3, 25.6, 23.4, 17.6, 16.4, 16.0, 13.2. R_f= 0.35 ($CHCl_3$:1% MeOH).

6-chloro-*N*-((2*E*)-3,7-dimethylocta-2,6-dien-1-yl)-2-ethylimidazo[1,2-a]pyridine-3-carboxam -ide **(28)**

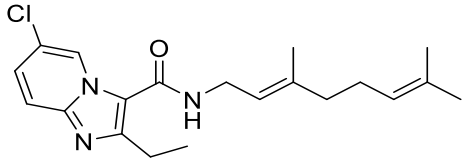

$C_{20}H_{26}ClN_3O$, white powder, 50% yield, m.p. 117-120 ºC, calculated monoisotopic mass *m/z* 359.17644, ESI-HRMS: *m/z* 360.1838, 362.1810 (^{35}Cl, ^{37}Cl) $[M+H]^+$, ^{1}H NMR (500 MHz, Chloroform-*d*) δ 9.49 (dd, *J* = 2.1, 0.8 Hz, 1H), 7.55 (dd, *J* = 9.5, 0.9 Hz, 1H), 7.29 (dd, *J* = 9.4, 2.1 Hz, 1H), 5.74 (d, *J* = 6.2 Hz, 1H), 5.34 (tp, *J* = 6.9, 1.3 Hz, 1H), 5.10 (ddp, *J* = 6.8, 5.6, 1.4 Hz, 1H), 4.11 (ddt, *J* = 7.1, 5.3, 0.9 Hz, 2H), 3.00 (q, *J* = 7.6 Hz, 2H), 2.17 – 2.00 (m, 4H), 1.76 (d, *J* = 1.3 Hz, 3H), 1.69 (q, *J* = 1.3 Hz, 3H), 1.62 (s, 2H), 1.44 (t, *J* = 7.6 Hz, 3H). ^{13}C NMR (126 MHz, Chloroform-*d*) δ 160.89, 150.78, 144.13, 140.9, 131.9, 128.2, 126.1, 123.7, 121.5, 119.5, 116.7, 115.4, 39.5, 37.4, 26.4, 25.7, 23.3, 17.7, 16.4, 13.2.

N-benzyl-6-chloro-2-ethylimidazo[1,2-a]pyridine-3-Carboxamide **(29)**

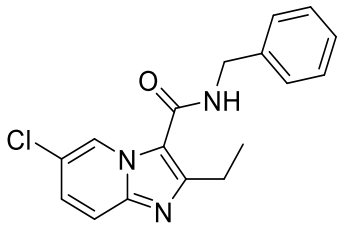

$C_{17}H_{16}ClN_3O$, white solid, 71% yield, m.p. 135-137 ºC, calculated monoisotopic mass *m/z* 313.09819, ESI-HRMS: *m/z* 314.1056 $[M+H]^+$. ^1H NMR (500 MHz, Chloroform-*d*) δ 9.53 (dd, *J* = 2.1, 0.8 Hz, 1H), 7.55 (dd, *J* = 9.5, 0.8 Hz, 1H), 7.39 (d, *J* = 4.4 Hz, 4H), 7.37 – 7.27 (m, 2H), 6.15 (d, *J* = 6.5 Hz, 1H), 4.71 (d, *J* = 5.7 Hz, 2H), 2.99 (q, *J* = 7.6 Hz, 2H), 1.41 (t, *J* = 7.6 Hz, 3H). ^{13}C NMR (126 MHz, Chloroform-*d*) δ 161.1, 151.3, 144.4, 137.9, 128.9, 128.2, 127.7, 127.6, 126.2, 121.5, 116.8, 115.1, 43.6, 23.5, 13.2.

6-chloro-*N*-[(4-chlorophenyl)methyl]-2-ethylimidazo[1,2-a]pyridine-3-carboxamide **(30)**

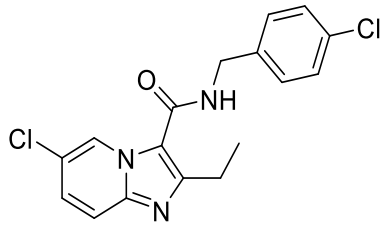

$C_{17}H_{15}Cl_2N_3O$, beige solid, 29% yield, m.p. 200-205 ºC, calculated monoisotopic mass *m/z* 347.05922, ESI-HRMS: *m/z* 348.0665, 350.0636 ($^{35}Cl^{35}Cl$, $^{37}Cl^{35}Cl$) $[M+H]^+$. ^1H NMR (400 MHz, Chloroform-*d*) δ 9.46 (dd, *J* = 2.1, 0.9 Hz, 1H), 7.64 (dd, *J* = 9.5, 0.8 Hz, 1H), 7.38 (dd, *J* = 9.4, 2.1 Hz, 1H), 7.34 (s, 4H), 4.66 (d, *J* = 5.9 Hz, 2H), 3.03 (q, *J* = 7.5 Hz, 2H), 1.40 (t, *J* = 7.6 Hz, 3H). ^{13}C NMR (101 MHz, Chloroform-*d*) δ 160.7, 136.6, 133.7, 129.3, 129.2, 126.4, 116.2, 43.1, 23.0, 13.3.

7.1.3.2. Cytochrome *bd* inhibitor

7.1.3.2.1. Synthesis of ethyl 2-heptylacetoacetate (1h)

To a suspension of NaH (60% in oil, 125 mmole) in dry THF, ethyl acetoacetate (1 equiv.) was added dropwise. The mixture was stirred for 30 min at room temperature. Heptyl bromide (1 equiv.) was added dropwise and the reaction was stirred under reflux for 12 h. After cooling, saturated NH_4Cl (125 mL) was added. The aqueous phase was separated and extracted with 200 mL EtOAc (3x). The organic phases were dried over Na_2SO_4 and concentrated under vacuum. The crude product was purified twice by column chromatography (gradient elutione, heptane:EtOAc, 100:0 to 20:1).[186] The compound was further purified using preparative HPLC. $C_{13}H_{24}O_3$, yellow oil, 12% yield, APCI-MS: *m/z* 229.1 $[M+H]^+$, ^{1}H NMR (400 MHz, Chloroform-*d*) δ 4.28 – 4.10 (m, 2H), 3.37 (t, *J* = 7.4 Hz, 1H), 2.20 (s, 3H), 1.89 – 1.77 (m, 2H), 1.26 (td, *J* = 7.1, 6.5, 2.9 Hz, 13H), 0.93 – 0.80 (m, 3H).

7.1.3.2.2. Synthesis of 3-Heptyl-2-methylquinolin-4(1H)-one (31) [131, 132, 187]

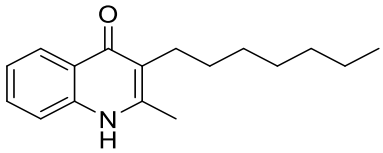

Aniline (0.473 mmole), **1h** (10 equiv.), glacial acetic acid (1 drop) and toluene were added to an oven-dried round-bottom flask connected to a Dean-stark apparatus with a reflux condenser. The mixture was heated at 100 °C until no more water was separated. After the evaporation of toluene, the produced imine was taken directly to the next step. The imine was added rapidly through a dropping funnel to biphenyl ether, which was stirred at 250 °C (Reflux). Refluxing continued for 10 to 15 min. until no more ethanol was separated in the Dean-Stark trap. The mixture was then left to cool to room temperature. The formed precipitate was then filtered and washed with heptane and acetone. $C_{17}H_{23}NO$, white solid, 14% yield, m.p. 230-235 °C, calculated monoisotopic mass *m/z* 257.17796, ESI-HRMS: *m/z* 258.1853 $[M+H]^+$, ^{1}H NMR (400 MHz, DMSO-d_6) δ 11.32 (s, 1H), 8.04 (dd, *J* = 8.2, 1.5 Hz, 1H), 7.56 (ddd, *J* = 8.4, 6.9, 1.6 Hz, 1H), 7.49 – 7.40 (m, 1H), 7.23 (ddd, *J* = 8.1, 6.9, 1.1 Hz, 1H), 2.68 (t, *J* = 1.9 Hz, 1H), 2.38 (s, 3H), 2.34 (t, *J* = 1.9 Hz, 1H), 1.47 – 1.17 (m, 10H), 0.90 – 0.81 (m, 3H). ^{13}C NMR (101 MHz, DMSO-d_6) δ 175.9, 146.1, 139.6, 131.3, 125.5, 123.8, 122.6, 119.6, 117.8, 31.8, 29.7, 29.2, 29.1, 25.3, 22.6, 17.9, 14.4.

7.1.3.3. EMB analogues

7.1.3.3.1. Synthesis of symmetric EMB analogues having N-atoms as substituents on aromatic systems (Scheme 5 and Scheme 6).

N[1],*N*[2]-bis(5-chloro-2-methoxyphenyl)ethane-1,2-diamine **(32)**

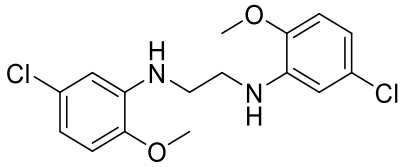

Under an inert atmosphere, dibromoethane (DBE, 6.34 mmole) was added dropwise to a solution of 5-chloro-2-methoxyaniline (4 equiv.) in dry DMF. $CaCO_3$ (1.66 equiv.) was added and the mixture was stirred vigorously at 100 ºC for 2h.[147] After the removal of DMF under vacuum, the mixture was extracted three times with DCM and dried over Na_2SO_4. The crude oil was purified by column chromatography (*tert*-butylmethylether:heptane, 1:2 +1% TFA). $C_{16}H_{18}Cl_2N_2O_2$, White solid, 15% yield, m.p. 135-136 ºC, calculated monoisotopic mass *m/z* 340.07453, ESI-HRMS: *m/z* 341.0814 $[M+H]^+$, ^{1}H NMR (500 MHz, Chloroform-*d*) δ 6.64 (d, *J* = 8.3 Hz, 2H), 6.63 (dd, *J* = 8.3, 2.2 Hz, 2H), 6.58 (d, *J* = 2.2 Hz, 2H), 4.77 – 4.72 (m, 2H), 3.81 (s, 6H), 3.40 (s, 4H). ^{13}C NMR (126 MHz, Chloroform-*d*) δ 145.5, 138.9, 126.4, 115.9, 110.2, 109.8, 55.6, 42.7.

N[1],*N*[2]-bis(5-chloro-2-hydroxyphenyl)ethane-1,2-diamine **(33)**

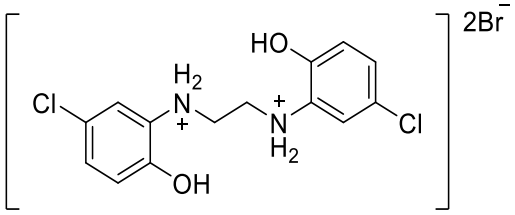

To cleave the ether, 5 equiv. of BBr_3 (1M in DCM) was slowly added to (**32)** and left to stir at 0 ºC -room temperature for 5h**.**[188] The reaction progress was monitored by the disappearance of the start signal in the APCI-MS. MeOH was added to quench the reaction and after the evaporation of the solvent, the pure **33** was obtained without further purification. $C_{14}H_{16}Cl_2N_2O_2^{2+}$, brown solid, 78% yield, m.p. 135-136 ºC, calculated monoisotopic mass *m/z* 312.04323, ESI-HRMS: *m/z* 311.0366 $[M-H]^-$,392.9605 $[M+Br]^-$, 313.0506 $[M+H]^+$, 392.9588 $[M+Br]^+$. ^{1}H NMR (400 MHz, Methanol-*d*4) δ 7.18 (d, *J* = 2.5 Hz, 2H), 7.08 (dd, *J* = 8.7, 2.5 Hz, 2H), 6.90 (d, *J* = 8.6 Hz, 2H), 3.65 (s, 4H). ^{13}C NMR (101 MHz, Methanol-d_4) δ 147.5, 127.6, 126.0, 124.4, 119.0, 116.4, 44.4.

N[1],*N*[2]-di((2-hydroxyphenyl)ethyl)ethane-1,2-diamine.2HBr **(35)**

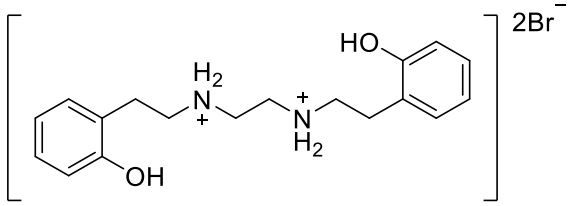

An aqueous solution HBr (48%, excess) was added carefully to **34**[44]. The mixture was left to stir for 3 h at 130 ºC and then overnight at room temperature. The reaction was monitored with thin-layer chromatography (TLC, $CHCl_3$:MeOH 2%:NH_4OH 0.05%). Water was evaporated under vacuum and the solid was purified by preparative HPLC. $C_{18}H_{26}N_2O_2^{2+}$, grey solid, 23% yield, melts with decomposition at 250 ºC, calculated monoisotopic mass *m/z* 302.19943, ESI-HRMS: *m/z* 301.1912 ($C_{18}H_{25}N_2O_2$) $[M+H]^+$, ^{1}H NMR (400 MHz, Deuterium Oxide) δ 7.33 (t, *J* = 7.8 Hz, 2H), 6.95 – 6.84 (m, 6H), 3.46 (s, 4H), 3.42 (t, *J* = 7.3 Hz, 4H), 3.03 (t, *J* = 7.3 Hz, 4H). ^{13}C NMR (101 MHz, Deuterium Oxide) δ 155.9, 137.9, 130.5, 120.9, 115.7, 114.3, 49.0, 43.1, 31.6.

7.1.3.3.2. Synthesis of EMB analogues with alkyl side chains (Scheme 7) [142]

1. Synthesis of the silyl-protected amino alcohol (1-2i)

TBDSiCl (1.1 equiv.) was added dropwise to a mixture of imidazole (1.1 equiv.) in DCM at 0 ºC. After stirring for 15 min, (*s*)-(+) amino alcohol was added. The solution was left to stir for 16 h at room temperature before pouring into a saturated $NaHCO_3$ solution. The pH was kept below 12 to avoid the cleavage of the *tert*-butyldiphenylsilane. The organic phase was extracted with DCM (3x) and the collected organic phases were dried over $MgSO_4$. DCM was evaporated under vacuum and the crude oil was purified by column chromatography (DCM:1% MeOH + drops of NH_4OH) to give **1-2i** oil.

[(2*S*)-2-aminobutoxy](*tert*-butyl)diphenylsilane **(1i)**

$C_{20}H_{29}NOSi$, 77% yield, APCI-MS: *m/z* 328.3 $[M+H]^+$, ^{1}H NMR (400 MHz, Chloroform-*d*) δ 7.72 – 7.63 (m, 4H), 7.48 – 7.33 (m, 6H), 3.63 (dd, *J* = 9.9, 4.1 Hz, 1H), 3.43 (dd, *J* = 9.8, 7.1 Hz, 1H), 2.85 – 2.74 (m, 1H), 1.52 – 1.36 (m, 2H), 1.07 (s, 9H), 0.89 (t, *J* = 7.5 Hz, 3H).

[(2*S*)-2-aminobut-3-en-1-yl)oxy](*tert*-butyl)diphenylsilane **(2i)**

An additional 0.4 equiv. of imidazole was added after leaving the reaction mixture to stir for few hours. $C_{20}H_{27}NOSi$, 91% yield, ESI-MS: *m/z* 326.4 $[M+H]^+$, ^1H NMR (400 MHz, Chloroform-*d*) δ 7.70 – 7.62 (m, 4H), 7.47 – 7.33 (m, 6H), 5.89 – 5.74 (m, 1H), 5.25 – 5.01 (m, 2H), 3.69 – 3.61 (m, 1H), 3.55 – 3.45 (m, 2H), 1.07 (s, 9H).

2. Synthesis of Chloracetamide scaffold (1-2j)

Chloroacetyl chloride (1.1 equiv.) was added dropwise to a cooled solution (0 °C) of **1i/2i** and DIPEA (2 equiv.) in DCM. The solution was left to stir overnight at room temperature. Water was added to quench the reaction. The organic phase was extracted with EtOAc (3x) and dried over $MgSO_4$. After the evaporation of the solvent, flash chromatography (*tert*-butylmethylether:heptane, 1:2) was done to get the pure **1j/2j.**

N-[(2*S*)-1-[(*tert*-butyldiphenylsilyl)oxy]butan-2-yl]-2-chloroacetamide **(1j)**

$C_{22}H_{30}ClNO_2Si$, 50% yield, APCI-MS: *m/z* 404.2 $[M]^+$, ^1H NMR (400 MHz, Chloroform-*d*) δ 7.70 – 7.60 (m, 4H), 7.50 – 7.33 (m, 6H), 6.96 – 6.89 (m, 1H), 4.12 – 3.96 (m, 2H), 3.98 – 3.85 (m, 1H), 3.70 (d, *J* = 3.3 Hz, 2H), 1.79 – 1.56 (m, 2H), 1.12 – 1.05 (m, 9H), 0.95 – 0.81 (m, 3H).

N-[(2*S*)-1-[(*tert*-butyldiphenylsilyl)oxy]but-3-en-2-yl]-2-chloroacetamide **(2j)**

$C_{22}H_{28}ClNO_2Si$, 73% yield, APCI-MS: *m/z* 401.9 $[M]^+$, ^1H NMR (500 MHz, Chloroform-*d*) δ 7.71 – 7.62 (m, 4H), 7.49 – 7.32 (m, 6H), 7.11 (d, *J* = 8.5 Hz, 1H), 5.97 – 5.80 (m, 1H), 5.30 – 5.19 (m, 2H), 4.61 – 4.50 (m, 1H), 4.14 – 4.01 (m, 2H), 3.82 – 3.70 (m, 2H), 1.07 (s, 9H).

3. Synthesis of the amino acetamide scaffold (1-4k)

A second amino alcohol (1 equiv.) was added to a cooled solution (0 °C) of **1j/2j** and DIPEA (3 equiv.) in DMF. The reaction was stirred at 70 °C for 14 h before quenching with water. The organic phase was extracted with $CHCl_3$ and brine (3x) to get rid of DIPEA and DMF. The collected organic phases were dried over $MgSO_4$. Flash chromatography ($CHCl_3$: MeOH +1% NH_4OH, 0 → 5%) yielded **1k/2k.**

2g or **3g** was added to a cooled solution (0 °C) of **1j** and DIPEA (3 equiv.) in DMF. The reaction was stirred at 70 °C for 14 h before quenching with water. The organic phase was extracted with $CHCl_3$ and brine (3x) to get rid of DIPEA and DMF. The collected organic phases were dried over $MgSO_4$. Flash chromatography (heptane:EtOAc, 100% to 50:50) yielded **3k/4k.**

N-[(2*S*)-1-[(*tert*-butyldiphenylsilyl)oxy]butan-2-yl]-2-[(4,4,4-trifluoro-1-hydroxybutan-2-yl)-amino]acetamide **(1k)**

$C_{26}H_{37}F_3N_2O_3Si$, orange oil, 40% yield, APCI-MS: *m/z* 510.3 $[M]^+$, ^{1}H NMR (400 MHz, Chloroform-*d*) δ 7.64 (dq, *J* = 8.0, 1.8 Hz, 4H), 7.49 – 7.33 (m, 7H), 7.15 (d, *J* = 9.3 Hz, 1H), 7.03 (d, *J* = 9.1 Hz, 1H), 3.97 – 3.85 (m, 1H), 3.76 – 3.59 (m, 3H), 3.48 (dd, *J* = 11.1, 4.8 Hz, 1H), 3.26 (d, *J* = 1.7 Hz, 2H), 3.00 – 2.88 (m, 1H), 2.45 (s, 1H), 2.41 – 2.12 (m, 2H), 1.76 – 1.46 (m, 2H), 1.07 (s, 9H), 0.86 (td, *J* = 7.5, 2.7 Hz, 3H).

N-[(2*S*)-1-[(*tert*-butyldiphenylsilyl)oxy]but-3-en-2-yl]-2-[(4,4,4-trifluoro-1-hydroxybutan-2-yl)-amino]acetamide **(2k)**

The (S)-2-aminobut-3-en-1-ol was dissolved in DMF and stirred with DIPEA at 0 °C, before the dropwise addition of **2j**. $C_{26}H_{36}F_3N_2O_3Si$, yellow oil, 5% yield, APCI-MS: *m/z* 453.0 $[M+H]^+$. The low yield is due to several trials of purification using flash column chromatography (EtOAc:heptane, gradient elution, 100:0 to 80:20). The ^{1}H NMR spectrum could not confirm the purity of the compound. However, direct mass measurements of the TLC spots suggested that all the spots were isomers (*m/z* 453.0) and thus, the compound was taken to the next step.

(12E)-3,3-dicyclohexyl-6-ethyl-2,2,13,17-tetramethyl-4-oxa-7,10-diaza-3-silaoctadeca-12,16-diene (**3k**)

$C_{32}H_{48}N_2O_2Si$, orange oil, 30% yield, APCI-MS: *m/z* 520.4 $[M]^+$, ^{1}H NMR (400 MHz, Chloroform-*d*) δ 7.67 – 7.62 (m, 4H), 7.45 – 7.34 (m, 6H), 5.26 – 5.15 (m, 1H), 5.07 (tt, *J* = 6.8, 1.5 Hz, 1H), 3.99 – 3.81 (m, 1H), 3.73 – 3.62 (m, 2H), 3.25 – 3.18 (m, 3H), 2.30 (s, 1H), 2.12 – 1.95 (m, 4H), 1.68 (q, *J* = 1.4 Hz, 3H), 1.62 (d, *J* = 1.4 Hz, 3H), 1.59 (d, *J* = 1.2 Hz, 3H), 1.55 – 1.53 (m, 4H), 1.07 (s, 9H), 0.91 – 0.86 (m, 3H).

6-ethyl-2,2,13,17-tetramethyl-3,3-diphenyl-4-oxa-7,10-diaza-3-silaoctadecane (**4k**)

$C_{32}H_{52}N_2O_2Si$, orange oil, 35% yield, APCI-MS: *m/z* 524.3 $[M]^+$, ^{1}H NMR (400 MHz, Chloroform-*d*) δ 7.64 (dq, *J* = 6.6, 1.3 Hz, 4H), 7.46 – 7.33 (m, 6H), 3.97 – 3.88 (m, 1H), 3.70 – 3.64 (m, 2H), 3.27 – 3.20 (m, 2H), 2.68 – 2.52 (m, 2H), 1.75 – 1.57 (m, 4H), 1.55 – 1.43 (m, 2H), 1.32 – 1.18 (m, 4H), 1.16 – 1.09 (m, 2H), 1.07 (s, 9H), 0.90 – 0.83 (m, 12H).

4. Synthesis of the ethylene diamine scaffold (Reduction of the amino acetamide) (37-38) [44]

A 2-necked round-bottom flask was dried and flushed with Argon. $LiAlH_4$ (6 equiv.) was suspended in dry dioxane and cooled to 0 ^{0}C. **1-4k** (1 equiv.) was diluted in a small amount of dry dioxane before adding it dropwise to the suspension. The mixture was then left to stir under Reflux (100 ^{o}C) overnight. For workup, the reaction flask was cooled to 0 ^{0}C and H_2O (H_2O: $LiAlH_4$, 1:1), NaOH 15% aq. Solution (NaOH:$LiAlH_4$, 1:1), and H_2O (H_2O:$LiAlH_4$, 3:1) were cautiously added and left to stir overnight at room temperature. The solids were removed by vacuum filtration and the filtrate was concentrated under reduced pressure.

4,4,4-trifluoro-2-[(2-{[(2S)-1-hydroxybutan-2-yl]amino}ethyl)amino]butan-1-ol **(37)**

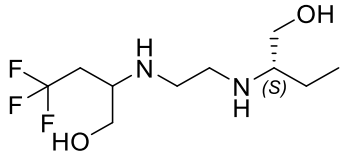

The crude oil was dissolved in $CHCl_3$ then drops of heptane were added until **37** crushed out as a white precipitate. It was filtered and left overnight in the desiccator to dry. $C_{10}H_{21}F_3N_2O_2$, white solid, 9% yield, m.p. 118-120 ^{o}C, calculated monoisotopic mass *m/z* 258.15551, ESI-HRMS: *m/z* 281.1448 $[M+Na]^+$, ^{1}H NMR (400 MHz, Methanol-d_4) δ 3.71 – 3.60 (m, 2H), 3.53 (dd, *J* = 11.2, 5.7 Hz, 1H), 3.45 (dd, *J* = 11.0, 6.6 Hz, 1H), 2.94 (m, 1H), 2.82 – 2.68 (m, 4H), 2.52 (tt, *J* = 6.8, 5.0 Hz, 1H), 2.46 – 2.25 (m, 2H), 1.63 – 1.39 (m, 2H), 0.97 (t, *J* = 7.5 Hz, 3H). ^{13}C NMR (101 MHz, Methanol-d_4) δ 126.9 (q, CF_3, $^1J_{CF}$ = 275.9 Hz), 62.6, 62.4 (d, $^4J_{CF}$ = 1.2 Hz), 60.6 – 60.5 (m), 53.9 (q, $^3J_{CF}$ = 2.4 Hz), 46.0, 45.8, 34.9 (q, $^2J_{CF}$ = 27.2 Hz), 23.4, 9.3. 89% purity (HPLC).

7.2. Solubility assays for IPAs

First, equidistant and logarithmic predilutions were prepared in a round-bottomed 96-well plate using 10 mM stock solutions of the compounds and DMSO. Then, 5 µL of each predilution

was added to 245 µL of PBS buffer in a straight-bottomed 96 well-plate. Quadruplicates were prepared for the blank (DMSO+PBS) and final concentrations tested (one plate/compound). The final concentrations measured ranged from 200 µM to 0.3125 µM. A nephelometer (NEPHELOstar^{plus}) was used to measure solubilities and Omega-Data Analysis software was used to evaluate the results.

7.3. *In silico*

7.3.1. Structure-activity relationship (SAR) of Q203-*Msmeg* $CIII_2CIV_2$

The electron cryomicroscopy generated 3D structure of the *Msmeg* $CIII_2CIV_2$ bound to Q203[‡‡‡‡‡] (PDB:7rh7) was used to study the protein-ligand interactions. Protein preparation wizard of Schrödinger software (Schrödinger Release 2019-1: Protein Preparation Wizard; Epik, Schrödinger, LLC, New York, NY, 2019; Impact, Schrödinger, LLC, New York, NY; Prime, Schrödinger, LLC, New York, NY, 2019) was used to prepare the protein for modelling. First, the structure was split into chains and then chains F (QcrB and ligand 'Q203'), I (QcrC) and Y (QcrA) were merged. Merged chains were pre-processed to add missing H-atoms, fill in missing side chains, and adjust the ionization and tautomeric states of the ligand. The next step was optimizing H-bond networks between the protein's amino acids and the ligand. For example, reorientation of the amino acids side chains (His, Asn, Asp, Glu, Gln,…) and prediction of their ionization and tautomeric states.[189] Finally, structure refinement to remove any atomic clashes (geometry minimization, force field: OPLS3e[§§§§§]).[190]

The crystal structure of *Msmeg* $CIII_2CIV_2$ bound to Q203 (PDB:7rh7) was used for docking. The protein preparation wizard with Schrödinger software (Schrödinger Suite 2022-3, Schrödinger, New York, USA, NY, 2021) was used to prepare the protein for modeling. This time structure was refined through an energy minimization step using OPLS4[191] force field.
The receptor grid was generated using the receptor grid generator panel without any constraints, assigning the co-crystallized ligand (Q203) as the center of the grid. Ligands were prepared using the LigPrep (LigPrep, Schrödinger, LLC, New York, NY, 2021.) using default settings. The protonation states were generated using Epik[192, 193] (Epik, Schrödinger, LLC, New

[‡‡‡‡‡] The electron cryomicroscopy structure was determined by David Yanofsky in the Lab of Prof. John Rubinstein, Hospital for Sick Children, Toronto, Canada.

[§§§§§] Optimized potential liquid simulation.

York, NY, 2021). Following this step, bioactive conformers (maximum of 20) of the prepared ligands were generated using the Confgen[194] panel (ConfGen, Schrödinger, LLC, New York, NY, 2021). Glide[195–197] (Glide, Schrödinger, LLC, New York, NY, 2021.) was used for docking: the precision mode was set to standard precision (SP) and no constraints were applied. Q203 was re-docked as well for validation and the RMSD calculated was < 2.

7.3.2. SAR of EMB and synthesized analogues

The 3D structure of the *Mtb* EmbA-EmbB bound to EMB (PDB:7bvf) was used to study the protein-ligand interactions. Protein preparation wizard of Schrödinger software (Schrödinger Release 2019-1: Protein Preparation Wizard; Epik, Schrödinger, LLC, New York, NY, 2019; Impact, Schrödinger, LLC, New York, NY; Prime, Schrödinger, LLC, New York, NY, 2019) was used to prepare the protein for modelling. First, the structure was split into chains and only chain B (EmbB-EMB) was used. Chain B was pre-processed to add missing H-atoms, fill in missing side chains, and adjust the ionization and tautomeric states of the ligand. The next step was optimizing H-bond networks between the protein's amino acids and the ligand. For example, reorientation of the amino acids side chains (His, Asn, Asp, Glu, Gln,…) and prediction of their ionization and tautomeric states.[189] Finally, structure refinement to remove any atomic clashes (geometry minimization, force field: OPLS3e*).[190]

The minimized chain B was used for docking compounds **32-37**. EMB was re-docked for validation. the receptor grid was generated using the receptor grid generator panel without any constraints, assigning the co-crystallized EMB as the center of the grid. Ligands were prepared using LigPrep (LigPrep, Schrödinger, LLC, New York, NY, 2019) and pH was adjusted to 5 to insure the ionization of the amino groups. The protonation states were generated using Epik[192, 193] (Epik, Schrödinger, LLC, New York, NY, 2019). Following this step, bioactive conformers (maximum of 20) of the prepared ligands were generated using the Confgen[194] panel (ConfGen, Schrödinger, LLC, New York, NY, 2019). Glide[195–197] (Glide, Schrödinger, LLC, New York, NY, 2019) was used for docking: the precision mode was set to XP and no constraints were applied. Docking using XP precision mode gave better results than SP (standard precision) mode (rmsd < 2).

7.4. Biological evaluation

7.4.1. Biochemical assays for IPAs

7.4.1.1. *M. smegmatis* growth, cell lysis, and protein purification

The protocol followed was the same as described previously.[107] An *M. smegmatis* strain[******] with a 3×FLAG tag at the C terminus of subunit QcrB was grown on 7H9+hygromycin plates for two days at 30 ºC. A colony from the plate was transferred to a 20 mL preculture of 7H9 (Sigma) supplemented with TDS (10 g/L, tryptone, 2 g/L dextrose, 0.8 g/L NaCl) and grown for two days in the dark at 30 ºC and 180 rpm before inoculating in a 6 L culture and growing under the same conditions for 48 hours. Cells were harvested by centrifugation for 20 min at 4 ºC, and then cell pellets were frozen in liquid nitrogen and stored at -80 ºC. Thawed cell pellets were resuspended in ~150 mL lysis buffer (50 mM Tris-HCl pH 7.5, 100 mM NaCl, 0.5 mM EDTA) and homogenized first with a Dounce homogenizer, then filtered with cheesecloth before using an Avestin homogenizer at 20 kpsi. Lysed cells were centrifuged at 39000 ×g for 30 min to remove cell debris. The supernatant was then centrifuged at 149,000 ×g for 60 min (Type 70Ti Beckmann rotor) to isolate the membranes. Membrane pellets were resuspended in lysis buffer (12 mL/g membranes) before aliquoting in falcon tubes, freezing, and storing at -80 ºC. To isolate and purify $CIII_2CIV_2$, thawed membranes were solubilized with 1% (w/v) dodecyl maltoside detergent (DDM), stirring for 45 minutes at 4 ºC. Following addition of 117 detergent, the solution was centrifuged at 149,000 ×g for 50 min to remove insoluble material. The supernatant was filtered (0.45 µm) before loading onto a columnof 1.5 mL Anti-FLAG M2 Affinity gel (Sigma). The column was washed with DTBS buffer (50 mM Tris-HCl pH 7.4, 100 mM NaCl, 0.02% DDM) and eluted with 6× 500 µL 150 µg/mL 3×FLAG peptide. The purified protein was exchanged into 50 mM Tris-HCl pH 7.4, 100 mM NaCl, and 0.003% (w/v) glyco-diosgenin (GDN) with a 100 kDa molecular weight cut-off concentrator (Sigma).[107]

[******] The *M. smegmatis* QcrB-3xFLAG was generated by colleagues in the group of Prof. John Rubinstein, Hospital for Sick Children, Toronto, Canada.

7.4.1.2. NDH-2 purification from *Caldalalibacillus thermarum* strain TA2.A1

C41 (DE3) cells were transformed with the ppTRC99A-ndh vector[52] and grown on LB + 100 µg/ml ampicillin plates overnight. A single colony was selected and grown in a 20 mL preculture in LB + 100 µg/ml ampicillin at 220 rpm overnight which was used to inoculate a 1L growth. The 1L culture was grown under the same conditions as the preculture until the OD600 ~ 0.6 when the cells were induced with 1mM of isopropyl ß-D-thiogalactopyranoside (IPTG) and grown for 4 hours before being harvested by centrifugation at 6,5000 ×g for 20 min then were frozen.†††††† Cells were thawed and resuspended in 20 mL NDH-2 lysis buffer (50 mM Tris-HCl pH 7.5, 2mM $MgCl_2$, 0.001% PMSF) and sonicated (Q Sonica Q500) for 10 min with 2 sec pulses and 2 sec pause between pulses and an amplitude of 30%. After lysis, cell debris was spun down at 10,000 ×g for 15 min. Membranes from the supernatant were then harvested at 125,000 ×g for 1 h and resuspended in buffer A (50 mM Tris-HCl pH 8.0, 20 mM imidazole, 150 mM NaCl, 0.05% w/v DDM, 0.001% (w/v) PMSF). Membranes were solubilized with 1% DDM at 4 ºC for 2 h. This solubilization was followed by ultracentrifugation at 125,000 ×g for 1 h to remove insoluble material. The supernatant was filtered (0.45 µm) before loading on a HisTrap column (5 mL) previously equilibrated with 50 mL of buffer A before loading the sample at 1 mL/min. then washed with 25 mL of buffer A to remove the unbound sample. To elute, 55% buffer B (50 mM Tris-HCl pH 8.0, 500 mM imidazole, 150 mM NaCl, 0.05% (w/v) DDM, 0.001% (w/v) PMSF) was applied over 10 column volumes. Fractions with high absorbance at 280 nm were pooled and dialyzed against 50 mM Tris-HCl pH 8.0, 150 mM NaCl, and 0.05% w/v DDM to remove imidazole.

7.4.1.3. Sub-mitochondrial particle (SMP) preparation

Bovine hearts were kept on ice and all subsequent steps were carried out at 4°C. Fat, blood vessels and connective tissues were removed from the hearts and the remaining material was cut into ~2 cm^3 pieces before being ground with a meat grinder. For each minced heart, 1400 mL buffer A (250 mM sucrose, 10 mM Tris-HCl pH 7.8, 2-mercaptoethanol) was added. The buffer was squeezed out of the mince through muslin. Buffer B (1600 mL per heart; 250 mM sucrose, 10 mM Tris-HCl pH 7.8, 5mM 2-mercaptoethanol, 0.2 mM EDTA, and 1mM Tris-

†††††† The cell transformation and *C. thermarum* growth were done by colleagues in the group of Prof. John Rubinstein, Hospital for Sick Children, Toronto, Canada.

succinate) was added and 25 mL Tris (not pH adjusted) was added per heart. The suspension was blended for 30 s on high setting. Cell debris was removed by centrifugation at 1,600 × g for 15 min. The supernatant was filtered through muslin cloth and mitochondria from the filtrate were harvested at 18,542 ×g for 27 min. The mitochondria were resuspended in 3600 mL buffer B per heart and harvested again at 18,542 ×g for 27 min. A total of ~30 mL of mitochondria was obtained per heart were flash frozen in liquid nitrogen and stored at -80 ^{o}C. ‡‡‡‡‡‡ In a falcon tube, 0.5 mL of bovine heart mitochondria were added to 4 mL of the isotonic buffer (0.25 M sucrose, 10 mM MOPS, 2mM EDTA pH 8). To form SMPs, the sample was sonicated while keeping the tube in a beaker of ice mixed with NaCl. The sonicator (Q Sonica Q500) was adjusted to provide ten 5 sec pulses with a 30 sec pause between pulses and an amplitude of 20%. SMPs were then centrifuged at 16000 ×g for 10 min at 4 ^{o}C to remove mitochondrial debris.[198, 199]

7.4.1.4. Oxygen Consumption assays

All oxygen consumption assays were done using an Oxygraph Clark-type electrode (Hansatech). For assay of *M. smegmatis* purified proteins with inhibitors, 500 nM superoxide dismutase (SOD, Sigma), 25 nM purified $CIII_2CIV_2$ (SC), 114 nM NADH-dehydrogenase type II (NDH-2, purification described above), 100 µM 2,3-dimethyl[1,4]naphthoquinone (DMW, sigma), and 10 µM of inhibitor in DMSO or DMSO alone (blank) were incubated in a 500 µL reaction (GTBS: 50 mM Tris-HCl pH 7.4, 100 mM NaCl, and 0.003% (w/v) glyco-diosgenin, GDN) at room temperature for 1 h. The reaction was initiated by injecting 1 mM NADH. To account for the effect of autoxidation of $DMWH_2$, a baseline oxygen consumption was measured by monitoring oxygen consumption without the addition of $CIII_2CIV_2$. The rate of oxygen consumption was calculated using a custom Python Script§§§§§§ where the baseline was subtracted.

To calculate the half-maximal inhibitory concentrations (IC_{50}) of Q203 and compound **27**, different concentrations of the two compounds (10 µM, 1 µM, 0 .1 µM, 0.01 µM, and blank)

‡‡‡‡‡‡ The handling of bovine heart and harvesting mitochondria were done by colleagues in the group of Prof. John Rubinstein, Hospital for Sick Children, Toronto, Canada.

§§§§§§ All Python Scripts were written by Dr. Justin M. Di Trani in the group of Prof. John Rubinstein, Hospital for Sick Children, Toronto, Canada.

were tested using the above protocol. The assays were repeated four times on different days and using different batches of purified $CIII_2CIV_2$. The IC_{50}s were calculated with a custom Python script and errors were estimated using Monte Carlo simulations.[200] Briefly, the overall standard deviation σ_{data} of the data was estimated by taking the average standard deviation of all the inhibitor concentrations. The best fit curve was calculated and simulated data sets were created using the best-fit parameters. Random errors $N(0,\ \sigma_{data})$ (normal random numbers with standard deviation = σ_{data}) were added to each data point and the simulated data with errors was fit to extract an IC_{50}. The addition of random errors and fitting was repeated 10,000 times and the standard deviation of the 10,000 best-fit parameters was taken to be the standard deviation of the IC_{50}. The Python matplotlib library was used to generate plots for figures.

To establish the specificity of compounds **27** and Q203, oxygen consumption was measured with bovine heart SMPs. In 500 µL reaction buffer (0.25 M sucrose, 10 mM 3-(N-morpholino) propanesulfonic acid) (MOPS) pH 8.0, 2 mM EDTA) 200 µL SMPs were incubated at room temperature with different concentrations (10 µM, 1 µM) for 1 h. The reaction was initiated by adding 10 mM NADH. Rotenone, KCN and Antimycin A were used as positive controls for inhibition.

7.4.1.5. NDH-2 activity assay

To confirm that Q203 and the analogues that were synthesized do not inhibit the NDH-2 used in oxygen consumption assays, the oxidation of NADH to NAD^+ was monitored spectrophotometrically at λ= 340 nm for 1.5 h. In a 96-well plate, 500 nM SOD, 3.15 nM NDH-2, 100 µM DMW, and 10 µM of one of the putative inhibitors (28 in total) were added to each well. The plate was loaded into a Synergy neo2 multi-mode plate reader and 100 µM NADH (100 µL) was injected to start the reaction (Total volume = 200 µL).

7.4.1.6. *Bos taurus* complex I activity assay

In a 96-well plate, SMPs (1/5 of the total volume of the reaction), 10 µM of positive control (Rotenone, Antimycin A or KCN) or inhibitor (Q203 or 27) were added to each well. 200 µM NADH was injected to start the reaction (Total volume = 200 µL). The oxidation of NADH was monitored spectrophotometrically for 8 min at λ= 340 nm.

7.4.1.7. *Candida albicans* complex III activity assay[*******]

The isolation and purification of $CIII_2$ followed the protocol described previously.[201] The reduction of cytochrome *c* was followed spectrophotometrically at λ= 550 nm to measure the activity of *C. albicans* complex III. In a 96-well plate, 50 µL reaction mixture containing ~25 nM purified cytochrome bc_1, 150 µM equine cytochrome *c* in reaction buffer (50 mM KPi pH 7.4, 100 mM KCl, 0.1 mM EDTA, 0.01% GDN, 0.5 mM KCN) was added to each well. Q203, **24**, and **27** were each dispensed from 376 µM DMSO stock to their final concentrations (10 µM and 1µM). The final DMSO concentration was 2.66%. After 10 min of incubation at room temperature, 100 µL of 120 µM DBH_2 (decylubiquinol) in reaction buffer was added column by column in the well plate to start the reaction. After shaking for 5 min, absorbance was recorded every 15 seconds for 15 minutes. Inz-5, a cytochrome bc_1 inhibitor was used as a positive control for complex III inhibition.[201]

7.4.2. *In vitro* mycobacterial growth inhibition assays (IPAs and EMB)

7.4.2.1. *M. tuberculosis*

7.4.2.1.1. Testing of IPAs [†††††††]

M. tuberculosis strain H37Rv, harbouring the red fluorescent protein (RFP)-expressing plasmid pTEC27, was used for measuring growth. The plasmid confers resistance to hygromycin. *M. tuberculosis* was grown in 7H9 broth (Difco Middlebrook) supplemented with 10 % (v/v) OADC (5% bovine albumin fraction, 2% dextrose, 0.004% catalase, 0.05% oleic acid, and 0.8% NaCl) and 0.05 % (v/v) Tween-80 at 37 °C in standing cultures. Hygromycin B was added to the medium at a final concentration of 50 µg/mL to suppress/inhibit the growth of non-transformed (non-plasmid containing) *Mtb* strains.

MIC_{90} determination: MIC_{90}s were determined by the broth microdilution method using flat-bottom 96-well Corning Costar plates. In the first well in each row, two times the desired highest concentration (50 µM) of each compound was added in growth medium 7H9 medium

[*******] This assay was performed by Zhong Liu in the Lab of Leah E. Cowen, Department of Molecular Genetics, The University of Toronto, Toronto, Canada.

[†††††††] The assay was done by Dr. Henok Sahile in the laboaratory of Prof. Yossef Av Gay, Department of Medicine and Microbiology and Immunology, University of British Columbia, Vancouver, Canada.

supplemented with 10% OADS, and 0.05% Tween 80 and hygromycin (50 µg/ mL). Each well was then diluted 2-fold in a 10-point serial dilution. Subsequently, 100 µL of the bacterial inoculum was added to each well to give a final volume of 200 µL. The concentration of the inoculum of 5×10^5 cells/mL (OD_{600}, 0.1 = 0.33×10^8 CFU/mL) was prepared from a starting inoculum that was diluted from a preculture at the mid-log phase (OD_{600}, 0.3 to 0.7). In each plate, a negative control (1% dimethyl sulfoxide [DMSO]) and a positive control (4 µM bedaquiline) were included. The plates were sealed with parafilm, placed in a container with moist tissue, and incubated for 6 days at 37 °C. After incubation, the fluorescence intensity (signal) of each well was measured (Synergy H4 plate reader (BioTek), excitation 530 nm, emission 590 nm) and the growth inhibition was calculated with the following equation:

$$\%\ growth\ inhibition\ = (-100)\ x\ \frac{(\ Signal_{sample} - Signal_{DMSO})}{(Signal_{DMSO} - Signal_{sample})}$$

MIC_{90} was calculated as the concentration of the compound that caused more than 90% growth reduction. Each test was done in duplicate.

7.4.2.1.2. Testing of EMB analogues ‡‡‡‡‡‡‡

M. tuberculosis (*Mtb*) strain H37Rv (ATCC 25618) carrying a mCherry-expressing plasmid (pCherry10)[202] was cultured in 7H9 complete medium (BD Difco; Becton Dickinson) supplemented with oleic acid-albumin-dextrose-catalase (OADC, 10%; BD), 0.2% glycerol, and 0.05% polysorbate 80 as previously described. At the mid-log phase (OD600 = 0.4) cultures were harvested and frozen in aliquots at −80 °C.[203] Frozen aliquots of mCherry-*Mtb* H37Rv were thawed and centrifuged (3700×g, 10 minutes). Supernatants were discarded and bacteria were thoroughly resuspended in 7H9 medium (10% OADC) in the absence of glycerol and Tween80 by use of a syringe and a 26-gauge syringe needle. The bacterial suspension was passed in and out of the syringe about 10 times. Compounds were tested in 2-fold dilutions starting at 64 µM in triplicates (2×10e6 bacteria, volume 100 µl) for their anti-tubercular activity using 96-well flat clear bottom black polystyrene microplates (Corning® CellBIND®, New York, USA). Each plate was prepared with rifampicin (National Reference Center, Borstel) as a reference compound. Plates were sealed with an air-permeable membrane (Porvair Sciences, Wrexham, UK) in a 37◦C incubator with mild agitation (TiMix5, Edmund Bühler, Germany), as previously described[204]. Bacterial growth was measured as relative light units (RLU) from the fluorescence intensity obtained at an excitation wavelength of 575 nm and

‡‡‡‡‡‡‡ *Mtb* assays were done in the laboratory of PD Dr. Norbert Reiling, Research Center Borstel.

emission wavelength of 635 nm (microplate reader, Synergy 2, BioTek Instruments, Vermont, USA) at the indicated time points. Obtained values were normalized to RLU values of the solvent control (DMSO)-treated bacteria set to 100%) and MIC_{95} of each compound was determined. MIC_{95} was defined as the minimum concentration of the compound required to achieve a reduction in fluorescence by 95%. Obtained MIC values were validated by a visual Resazurin microtiter assay (REMA)[205] by adding 30 µL of 0,02% Resazurin (Cayman) solution to each well followed by another 20 h of culture without agitation.

7.4.2.2. *M. intacellulare, M. smegmatis* and *M. abscessus*

7.4.2.2.1. Bacterial cells and culture media

M. intracellulare ATCC 35761, *M.abscessus* ATCC19977 or *M. smegmatis mc² 155* pTEC27, expressing RFP tdTomato were used for the activity assays. Stocks of the bacteria grown in complete 7H9 broth were stored in approximately 15% glycerol at -80°C. Using an inoculation loop, bacteria were spread on 7H10 plates (containing 400 mg/mL hygromycin) and grown in an incubator at 37°C.

Bacteria were grown in 7H9 broth supplemented with 10% ADS (0.8% sodium chloride, 5.0% bovine serum albumin, and 2.0% dextrose), 0.05% Tween 80 and hygromycin (400 mg/mL). The culture volume was 10 mL in a 50-mL Falcon tube. The tubes were covered to protect the photosensitive hygromycin and shaken in an incubator at 37°C.

7.4.2.2.2. MIC determination

In 7H9 medium

MICs were determined against *M. intracellulare* ATCC 35761, *M.abscessus* ATCC19977 or *M. smegmatis mc² 155* pTEC27, the broth microdilution method. 96-Well flat bottom tissue culture plates (Sarstedt, 83.3924.500) were used. In the fourth well of each row two times of the desired highest concentration of the tested compound was added in 7H9 medium. Each compound was diluted twofold in a ten-point serial dilution. The concentration of the starting inoculum was 5×10^5 cells ml^{-1}. The starting inoculum was diluted from a preculture at the mid-log phase (OD_{600} 0.2 to 0.8, mid-log phase) and an OD_{600} of 0.1 was correlated to 1×10^8 CFU ml^{-1}. The plates were sealed with parafilm, placed in a container with moist tissue and incubated at 37 °C. The incubation period for *M. intracellulare* is five days, the incubation period for *M. smegmatis* and *M.abscessus* is three days. Row three of the 96-Well plate included eight negative controls (1% dimethyl sulfoxid [DMSO]) and row two eight positive

controls (100 µM amikacin). After incubation, the plates were monitored by RFP measurement (λ_{ex} = 544 nm λ_{em} = 590 nm) (BMG labtech Fluostar Optima). The assay was performed in duplicate and results were validated by OD measurement.

Every assay plate contained eight wells with 1% DMSO as the negative control, which corresponds to 100% bacterial growth and eight wells with the respective inhibitor as a positive control in which 100 % inhibition of bacterial growth was reached. Controls were used to monitor the assay quality through the determination of the Z' score. The Z' factor was calculated as follows:

$$Z' = 1 - \frac{3(SD_{inhibitor} + SD_{DMSO})}{M_{inhibitor} - M_{DMSO}}$$

(SD = standard deviation, M = mean)

The percentage of growth inhibition was calculated by the equation:

$$\%\ \text{growth inhibition} = -100\ \% \times \frac{RFP_{signal}(\text{sample}) - RFP_{signal}(\text{DMSO})}{RFP_{signal}(\text{DMSO}) - RFP_{signal}(\text{inhibitor})}$$

Medium with Oleic acid

For the glucose-free Medium (7H9, 0.05% T80, 0.01% oleic acid) oleic acid solution (1.8% oleic acid: 120 mL double distilled water, 2.4 mL 6M NaOH, 2,2 mL Oleic acid) was used. Bacteria were grown to mid-log phase (OD 0.2 to 0.8) and adapted to the new media for 24 h before the bacteria were used.[183] The liquid culture assay in 96-well plates in glucose-free media was performed after the method described above.

7.4.2.2.3. MBC determination

After 3 days of incubation (*M. smegmatis*), wells were selected for MBC determination. Subsequently, the MBC was determined by CFU counting: For this, Petri dishes with three sections were used, each petri dish was filled with 25 mL 7H10 agar supplemented with 0.5% glycerol, 10% ADS and 400 µg/mL hygromycin. From the selected drug concentrations of the microplate dilution assay, 10 µL of the respective dilution was plated in one section of the plate. The colonies were counted after 3 days of incubation at 37°C for *M. smegmatis* or 10-14 days for *M. intracellulare*. Based on the result, the concentration of CFUs per mL was calculated. The number of CFUs was also determined in the inoculum at day 0 before the incubation time.

The MBC_{90}, MBC_{99}, and $MBC_{99.9}$ were defined as the lowest concentrations of drug that reduced the number of CFUs per millilitre by 10-fold, 100-fold, and 1,000-fold, respectively, relative to the day 0 value.

8. References

(1) Stop TB Partnership. The Potential Impact of the Covid-19 Response on Tuberculosis in High-Burden Countries: A Modelling Analysis. *Dev. by Stop TB Partnersh. Collab. with Imp. Coll. Avenir Heal. Johns Hopkins Univ. USAID.* **2020**, 1–7.

(2) *Global Tuberculosis Report 2021. Geneva: World Health Organization; 2021. Licence: CC BY-NC-SA 3.0 IGO.*; Geneva, Switzerland.

(3) United States, Department of Health and Human Services, C. for D. C. and P. Tuberculosis (TB): Data and Statistics https://www.cdc.gov/tb/statistics/tbcases.html.

(4) RKI. Report on the Epidemiology of Tuberculosis in Germany (2020) https://www.rki.de/EN/Content/infections/epidemiology/inf_dis_Germany/TB/summary_2020.html.

(5) World Bank. Incidence of tuberculosis https://data.worldbank.org/indicator/SH.TBS.INCD.

(6) Vergne, I.; Chua, J.; Singh, S. B. Cell Biology of Mycobacterium. *Rev. Lit. Arts Am.* **2004**.

(7) Glaziou, P. Predicted Impact of the COVID-19 Pandemic on Global Tuberculosis Deaths in 2020. *medRxiv* **2021**, *000*, 2020.04.28.20079582.

(8) Fekadu, G.; Bekele, F.; Tolossa, T.; Fetensa, G.; Turi, E.; Getachew, M.; Abdisa, E.; Assefa, L.; Afeta, M.; Demisew, W.; et al. Impact of COVID-19 Pandemic on Chronic Diseases Care Follow-up and Current Perspectives in Low Resource Settings: A Narrative Review. *Int. J. Physiol. Pathophysiol. Pharmacol.* **2021**, *13* (3), 86–93.

(9) Hogan, A. B.; Jewell, B. L.; Sherrard-Smith, E.; Vesga, J. F.; Watson, O. J.; Whittaker, C.; Hamlet, A.; Smith, J. A.; Winskill, P.; Verity, R.; et al. Potential Impact of the COVID-19 Pandemic on HIV, Tuberculosis, and Malaria in Low-Income and Middle-Income Countries: A Modelling Study. *Lancet Glob. Heal.* **2020**, *8* (9), e1132–e1141. https://doi.org/10.1016/S2214-109X(20)30288-6.

(10) Thomson, R.; Tolson, C.; Carter, R.; Coulter, C.; Huygens, F.; Hargreaves, M. Isolation of Nontuberculous Mycobacteria (NTM) from Household Water and Shower Aerosols in Patients with Pulmonary Disease Caused by NTM. *J. Clin. Microbiol.* **2013**, *51* (9), 3006–3011. https://doi.org/10.1128/JCM.00899-13.

(11) Wallace, R. J.; Iakhiaeva, E.; Williams, M. D.; Brown-Elliott, B. A.; Vasireddy, S.; Vasireddy, R.; Lande, L.; Peterson, D. D.; Sawicki, J.; Kwait, R.; et al. Absence of

Mycobacterium Intracellulare and Presence of Mycobacterium Chimaera in Household Water and Biofilm Samples of Patients in the United States with Mycobacterium Avium Complex Respiratory Disease. *J. Clin. Microbiol.* **2013**, *51* (6), 1747–1752. https://doi.org/10.1128/JCM.00186-13.

(12) Daley, C. L.; Iaccarino, J. M.; Lange, C.; Cambau, E.; Wallace, R. J.; Andrejak, C.; Böttger, E. C.; Brozek, J.; Griffith, D. E.; Guglielmetti, L.; et al. Treatment of Nontuberculous Mycobacterial Pulmonary Disease: An Official ATS/ERS/ESCMID/IDSA Clinical Practice Guideline. *Eur. Respir. J.* **2020**, *56* (1). https://doi.org/10.1183/13993003.00535-2020.

(13) Martiniano, S. L.; Nick, J. A.; Daley, C. L. Nontuberculous Mycobacterial Infections in Cystic Fibrosis. *Clin. Chest Med.* **2022**, *43* (4), 697–716. https://doi.org/10.1016/J.CCM.2022.06.010.

(14) Adelman, M. H.; Addrizzo-Harris, D. J. Management of Nontuberculous Mycobacterial Pulmonary Disease. *Curr. Opin. Pulm. Med.* **2018**, *24* (3), 212–219. https://doi.org/10.1097/MCP.0000000000000473.

(15) Schiff, H. F.; Jones, S.; Achaiah, A.; Pereira, A.; Stait, G.; Green, B. Clinical Relevance of Non-Tuberculous Mycobacteria Isolated from Respiratory Specimens: Seven Year Experience in a UK Hospital. *Sci. Rep.* **2019**, *9* (1), 6–11. https://doi.org/10.1038/s41598-018-37350-8.

(16) Kim, B. R.; Kim, B. J.; Kook, Y. H.; Kim, B. J. Mycobacterium Abscessus Infection Leads to Enhanced Production of Type 1 Interferon and NLRP3 Inflammasome Activation in Murine Macrophages via Mitochondrial Oxidative Stress. *PLoS Pathog.* **2020**, *16* (3), 1–26. https://doi.org/10.1371/journal.ppat.1008294.

(17) Kam, J. Y.; Hortle, E.; Krogman, E.; Warner, S. E.; Wright, K.; Luo, K.; Cheng, T.; Manuneedhi Cholan, P.; Kikuchi, K.; Triccas, J. A.; et al. Rough and Smooth Variants of Mycobacterium Abscessus Are Differentially Controlled by Host Immunity during Chronic Infection of Adult Zebrafish. *Nat. Commun.* **2022**, *13* (1). https://doi.org/10.1038/s41467-022-28638-5.

(18) Clary, G.; Sasindran, S. J.; Nesbitt, N.; Mason, L.; Cole, S.; Azad, A.; McCoy, K.; Schlesinger, L. S.; Hall-Stoodley, L. Mycobacterium Abscessus Smooth and Rough Morphotypes Form Antimicrobial-Tolerant Biofilm Phenotypes but Are Killed by Acetic Acid. *Antimicrob. Agents Chemother.* **2018**, *62* (3). https://doi.org/10.1128/AAC.01782-17.

(19) Abdalla, M. Y.; Ahmad, I. M.; Switzer, B.; Britigan, B. E. Induction of Heme Oxygenase-1 Contributes to Survival of Mycobacterium Abscessus in Human Macrophages-like THP-1 Cells. *Redox Biol.* **2015**, *4*, 328–339. https://doi.org/10.1016/j.redox.2015.01.012.

(20) Victoria, L.; Gupta, A.; Gómez, J. L.; Robledo, J. Mycobacterium Abscessus Complex: A Review of Recent Developments in an Emerging Pathogen. *Front. Cell. Infect. Microbiol.* **2021**, *11* (April), 1–8. https://doi.org/10.3389/fcimb.2021.659997.

(21) Lopeman, R. C.; Harrison, J.; Desai, M.; Cox, J. A. G. Mycobacterium Abscessus: Environmental Bacterium Turned Clinical Nightmare. *Microorganisms* **2019**, *7* (3). https://doi.org/10.3390/microorganisms7030090.

(22) Van Ingen, J.; Turenne, C. Y.; Tortoli, E.; Wallace, R. J.; Brown-Elliott, B. A. A Definition of the Mycobacterium Avium Complex for Taxonomical and Clinical Purposes, a Review. *Int. J. Syst. Evol. Microbiol.* **2018**, *68* (11), 3666–3677. https://doi.org/10.1099/ijsem.0.003026.

(23) Bhatia, A.; Shah, H.; Mehra, D.; Ogunjemilusi, O. Disseminated Mycobacterium Avium Intracellulare Infection With Concurrent Small Bowel Obstruction: Case, Pathophysiology, and Clinical Considerations. *Cureus* **2021**, *13* (2), 7–9. https://doi.org/10.7759/cureus.13469.

(24) Zheng, H. W.; Pang, Y.; He, G. X.; Song, Y. Y.; Zhao, Y. L. Comparing the Genotype and Drug Susceptibilities between Mycobacterium Avium and Mycobacterium Intracellulare in China. *Biomed. Environ. Sci.* **2017**, *30* (7), 517–525. https://doi.org/10.3967/bes2017.068.

(25) Lin, S.; Hua, W.; Wang, S.; Zhang, Y.; Chen, X.; Liu, H.; Shao, L.; Chen, J.; Zhang, W. In Vitro Assessment of 17 Antimicrobial Agents against Clinical Mycobacterium Avium Complex Isolates. *BMC Microbiol.* **2022**, *22* (1), 1–10. https://doi.org/10.1186/s12866-022-02582-2.

(26) Koh, W. J.; Jeong, B. H.; Jeon, K.; Lee, N. Y.; Lee, K. S.; Woo, S. Y.; Shin, S. J.; Kwon, O. J. Clinical Significance of the Differentiation Between Mycobacterium Avium and Mycobacterium Intracellulare in M Avium Complex Lung Disease. *Chest* **2012**, *142* (6), 1482–1488. https://doi.org/10.1378/CHEST.12-0494.

(27) Sonawane, V. V.; Ruth, M. M.; Pennings, L. J.; Svensson, E. M.; Wertheim, H. F. L.; Hoefsloot, W.; van Ingen, J. An in Vitro Perspective on What Individual Antimicrobials Add to Mycobacterium Avium Complex Therapies. *Antimicrob. Agents Chemother.*

2021, *65* (8), 1–9. https://doi.org/10.1128/AAC.02730-20.

(28) Villemagne, B.; Crauste, C.; Flipo, M.; Baulard, A. R.; Déprez, B.; Willand, N. Tuberculosis: The Drug Development Pipeline at a Glance. *Eur. J. Med. Chem.* **2012**, *51*, 1–16. https://doi.org/10.1016/j.ejmech.2012.02.033.

(29) Zhang, Y.; Mitchison, D.; Shi, W.; Zhang, W. Mechanisms of Pyrazinamide Action and Resistance. *Microbiol. Spectr.* **2014**, *2* (4), 1–12. https://doi.org/10.1128/microbiolspec.MGM2-0023-2013.

(30) Timmins, G. S.; Deretic, V. MicroReview Mechanisms of Action of Isoniazid. **2006**, *62* (October), 1220–1227. https://doi.org/10.1111/j.1365-2958.2006.05467.x.

(31) Zhang, Y. The Magic Bullets and Tuberculosis Drug Targets. *Annu. Rev. Pharmacol. Toxicol.* **2005**, *45* (2), 529–564. https://doi.org/10.1146/annurev.pharmtox.45.120403.100120.

(32) Ma, Z.; Ginsberg, A. M.; Spigelman, M.; Alliance, G.; Development, D.; York, N. 7.24 Antimycobacterium Agents. **2007**, 699–730.

(33) Makarov, V.; Lechartier, B.; Zhang, M.; Neres, J.; van der Sar, A. M.; Raadsen, S. A.; Hartkoorn, R. C.; Ryabova, O. B.; Vocat, A.; Decosterd, L. A.; et al. Towards a New Combination Therapy for Tuberculosis with next Generation Benzothiazinones. *EMBO Mol. Med.* **2014**, *6* (3), 372–383. https://doi.org/10.1002/emmm.201303575.

(34) Williams, K. N.; Stover, C. K.; Zhu, T.; Tasneen, R.; Tyagi, S.; Grosset, J. H.; Nuermberger, E. Promising Antituberculosis Activity of the Oxazolidinone PNU-100480 Relative to That of Linezolid in a Murine Model. *Antimicrob. Agents Chemother.* **2009**, *53* (4), 1314–1319.

(35) Ma, Z.; Lienhardt, C. Toward an Optimized Therapy for Tuberculosis? Drugs in Clinical Trials and in Preclinical Development. *Clin. Chest Med.* **2009**, *30* (4), 755–768.

(36) Almeida, D.; Converse, P. J.; Li, S. Y.; Upton, A. M.; Fotouhi, N.; Nuermberger, E. L. Comparative Efficacy of the Novel Diarylquinoline TBAJ-587 and Bedaquiline against a Resistant Rv0678 Mutant in a Mouse Model of Tuberculosis. *Antimicrob. Agents Chemother.* **2021**, *65* (12). https://doi.org/10.1128/AAC.01412-21.

(37) Lee, B. S.; Pethe, K. Telacebec: An Investigational Antibacterial for the Treatment of Tuberculosis (TB). *Expert Opin. Investig. Drugs* **2022**, *31* (2), 139–144. https://doi.org/10.1080/13543784.2022.2030309.

(38) Pipeline | Working Group for New TB Drugs https://www.newtbdrugs.org/pipeline/clinical (accessed Feb 26, 2023).

(39) Singh, R.; Manjunatha, U.; Boshoff, H. I. M.; Ha, Y. H.; Niyomrattanakit, P.; Ledwidge, R.; Dowd, C. S.; Lee, I. Y.; Kim, P.; Zhang, L. PA-824 Kills Nonreplicating Mycobacterium Tuberculosis by Intracellular NO Release. *Science (80-.).* **2008**, *322* (5906), 1392–1395.

(40) Matsumoto, M.; Hashizume, H.; Tomishige, T.; Kawasaki, M.; Tsubouchi, H.; Sasaki, H.; Shimokawa, Y.; Komatsu, M. OPC-67683, a Nitro-Dihydro-Imidazooxazole Derivative with Promising Action against Tuberculosis in Vitro and in Mice. *PLoS Med.* **2006**, *3* (11), e466.

(41) Zumla, A.; Nahid, P.; Cole, S. T. Advances in the Development of New Tuberculosis Drugs and Treatment Regimens. *Nat. Rev. Drug Discov.* **2013**, *12* (5), 388–404. https://doi.org/10.1038/nrd4001.

(42) Li, K.; Schurig-Briccio, L. A.; Feng, X.; Upadhyay, A.; Pujari, V.; Lechartier, B.; Fontes, F. L.; Yang, H.; Rao, G.; Zhu, W.; et al. Multitarget Drug Discovery for Tuberculosis and Other Infectious Diseases. *J. Med. Chem.* **2014**, *57* (7), 3126–3129. https://doi.org/10.1021/jm500131s.

(43) Gawad, J.; Bonde, C. Current Affairs, Future Perspectives of Tuberculosis and Antitubercular Agents. *Indian J. Tuberc.* **2017**, *65* (1), 15–22. https://doi.org/10.1016/j.ijtb.2017.08.011.

(44) Abdelaziz, R. Design and Synthesis of Ethambutol Analogues and Their Testing as Antimycobacterial Agents, 2018.

(45) Shetye, G. S.; Franzblau, S. G.; Cho, S. New Tuberculosis Drug Targets, Their Inhibitors, and Potential Therapeutic Impact. *Transl. Res.* **2020**, *220*, 68–97. https://doi.org/10.1016/j.trsl.2020.03.007.

(46) Foo, C. S. Y.; Pethe, K.; Lupien, A. Oxidative Phosphorylation-an Update on a New, Essential Target Space for Drug Discovery in Mycobacterium Tuberculosis. *Appl. Sci.* **2020**, *10* (7). https://doi.org/10.3390/app10072339.

(47) Black, P. A.; Warren, R. M.; Louw, G. E.; Van Helden, P. D.; Victor, T. C.; Kana, B. D. Energy Metabolism and Drug Efflux in Mycobacterium Tuberculosis. *Antimicrob. Agents Chemother.* **2014**, *58* (5), 2491–2503. https://doi.org/10.1128/AAC.02293-13.

(48) Wiseman, B.; Nitharwal, R. G.; Fedotovskaya, O.; Schäfer, J.; Guo, H.; Kuang, Q.; Benlekbir, S.; Sjöstrand, D.; Ädelroth, P.; Rubinstein, J. L.; et al. Structure of a Functional Obligate Complex III2IV2 Respiratory Supercomplex from Mycobacterium Smegmatis. *Nat. Struct. Mol. Biol.* **2018**, *25* (12), 1128–1136.

https://doi.org/10.1038/s41594-018-0160-3.

(49) Prochaska, L. J.; Cvetkov, T. L. Mitochondrial Electron Transport. In *Encyclopedia of Biophysics*; Roberts, G. C. K., Ed.; Springer Berlin Heidelberg: Berlin, Heidelberg, 2013; pp 1539–1544. https://doi.org/10.1007/978-3-642-16712-6_25.

(50) Shi, L.; Sohaskey, C. D.; Kana, B. D.; Dawes, S.; North, R. J.; Mizrahi, V.; Gennaro, M. L. Changes in Energy Metabolism of Mycobacterium Tuberculosis in Mouse Lung and under in Vitro Conditions Affecting Aerobic Respiration. *Proc. Natl. Acad. Sci. U. S. A.* **2005**, *102* (43), 15629–15634. https://doi.org/10.1073/pnas.0507850102.

(51) Hards, K.; Cook, G. M. Targeting Bacterial Energetics to Produce New Antimicrobials. *Drug Resist. Updat.* **2018**, *36* (June 2017), 1–12. https://doi.org/10.1016/j.drup.2017.11.001.

(52) Heikal, A.; Nakatani, Y.; Dunn, E.; Weimar, M. R.; Day, C. L.; Baker, E. N.; Lott, J. S.; Sazanov, L. A.; Cook, G. M. Structure of the Bacterial Type II NADH Dehydrogenase: A Monotopic Membrane Protein with an Essential Role in Energy Generation. *Mol. Microbiol.* **2014**, *91* (5), 950–964. https://doi.org/10.1111/mmi.12507.

(53) Bald, D.; Villellas, C.; Lu, P.; Koul, A. Targeting Energy Metabolism in Mycobacterium Tuberculosis, a New Paradigm in Antimycobacterial Drug Discovery. *Am. Soc. Microbiol.* **2017**, *8* (2), 1–11.

(54) Vilchèze, C.; Weinrick, B.; Leung, L. W.; Jacobs, W. R. Plasticity of Mycobacterium Tuberculosis NADH Dehydrogenases and Their Role in Virulence. *Proc. Natl. Acad. Sci. U. S. A.* **2018**, *115* (7), 1599–1604. https://doi.org/10.1073/pnas.1721545115.

(55) Rao, S. P. S.; Alonso, S.; Rand, L.; Dick, T.; Pethe, K. The Protonmotive Force Is Required for Maintaining ATP Homeostasis and Viability of Hypoxic, Nonreplicating Mycobacterium Tuberculosis. *Proc. Natl. Acad. Sci. U. S. A.* **2008**, *105* (33), 11945–11950. https://doi.org/10.1073/pnas.0711697105.

(56) Pecsi, I.; Hards, K.; Ekanayaka, N.; Berney, M.; Hartman, T.; Jacobs, W. R.; Cook, G. M. Essentiality of Succinate Dehydrogenase in Mycobacterium Smegmatis and Its Role in the Generation of the Membrane Potential under Hypoxia. *MBio* **2014**, *5* (4). https://doi.org/10.1128/mBio.01093-14.

(57) Hartman, T.; Weinrick, B.; Vilchèze, C.; Berney, M.; Tufariello, J.; Cook, G. M.; Jacobs, W. R. Succinate Dehydrogenase Is the Regulator of Respiration in Mycobacterium Tuberculosis. *PLoS Pathog.* **2014**, *10* (11). https://doi.org/10.1371/journal.ppat.1004510.

(58) Watanabe, S.; Zimmermann, M.; Goodwin, M. B.; Sauer, U.; Barry, C. E.; Boshoff, H. I. Fumarate Reductase Activity Maintains an Energized Membrane in Anaerobic Mycobacterium Tuberculosis. *PLoS Pathog.* **2011**, *7* (10). https://doi.org/10.1371/journal.ppat.1002287.

(59) Sassetti, C. M.; Boyd, D. H.; Rubin, E. J. Genes Required for Mycobacterial Growth Defined by High Density Mutagenesis. *Mol. Microbiol.* **2003**, *48* (1), 77–84. https://doi.org/10.1046/j.1365-2958.2003.03425.x.

(60) Eoh, H.; Rhee, K. Y. Multifunctional Essentiality of Succinate Metabolism in Adaptation to Hypoxia in Mycobacterium Tuberculosis. *Proc. Natl. Acad. Sci. U. S. A.* **2013**, *110* (16), 6554–6559. https://doi.org/10.1073/pnas.1219375110.

(61) Upadhyay, A.; Fontes, F. L.; Gonzalez-Juarrero, M.; McNeil, M. R.; Crans, D. C.; Jackson, M.; Crick, D. C. Partial Saturation of Menaquinone in Mycobacterium Tuberculosis: Function and Essentiality of a Novel Reductase, MenJ. *ACS Cent. Sci.* **2015**, *1* (6), 292–302. https://doi.org/10.1021/acscentsci.5b00212.

(62) Mascolo, L.; Bald, D. Cytochrome Bd in Mycobacterium Tuberculosis: A Respiratory Chain Protein Involved in the Defense against Antibacterials. *Prog. Biophys. Mol. Biol.* **2020**, *152* (xxxx), 55–63. https://doi.org/10.1016/j.pbiomolbio.2019.11.002.

(63) Safarian, S.; Rajendran, C.; Müller, H.; Preu, J.; Langer, J. D.; Ovchinnikov, S.; Hirose, T.; Kusumoto, T.; Sakamoto, J.; Michel, H. Structure of a Bd Oxidase Indicates Similar Mechanisms for Membraneintegrated Oxygen Reductases. *Science (80-.).* **2016**, *352* (6285), 583–586. https://doi.org/10.1126/science.aaf2477.

(64) Shiba, T.; Kido, Y.; Sakamoto, K.; Inaoka, D. K.; Tsuge, C.; Tatsumi, R.; Takahashi, G.; Balogun, E. O.; Nara, T.; Aoki, T.; Honma, T.; et al. Structure of the Trypanosome Cyanide-Insensitive Alternative Oxidase. *Proc. Natl. Acad. Sci. U. S. A.* **2013**, *110* (12), 4580–4585. https://doi.org/10.1073/pnas.1218386110.

(65) Cook, G. M.; Berney, M.; Gebhard, S.; Heinemann, M.; Cox, R. A.; Danilchanka, O.; Niederweis, M. Physiology of Mycobacteria. Advances in Microbial Physiology. Academic Press, 2009; Vol. 55, pp 81–319. https://doi.org/https://doi.org/10.1016/S0065-2911(09)05502-7.

(66) Tran, S. L.; Cook, G. M. The F1Fo-ATP Synthase of Mycobacterium Smegmatis Is Essential for Growth. *J. Bacteriol.* **2005**, *187* (14), 5023–5028. https://doi.org/10.1128/JB.187.14.5023-5028.2005.

(67) Datta, S.; Krishna, R.; Ganesh, N.; Chandra, N. R.; Muniyappa, K.; Vijayan, M. Crystal

Structures of Mycobacterium Smegmatis RecA and Its Nucleotide Complexes. *J. Bacteriol.* **2003**, *185* (14), 4280–4284. https://doi.org/10.1128/JB.185.14.4280-4284.2003.

(68) Gong, H.; Li, J.; Xu, A.; Tang, Y.; Ji, W.; Gao, R.; Wang, S.; Yu, L.; Tian, C.; Li, J.; Yen, H. Y.; et al. An Electron Transfer Path Connects Subunits of a Mycobacterial Respiratory Supercomplex. *Science (80-.).* **2018**, *362* (6418). https://doi.org/10.1126/science.aat8923.

(69) Ädelroth, P.; Svensson Ek, M.; Mitchell, D. M.; Gennis, R. B.; Brzezinski, P. Glutamate 286 in Cytochrome Aa3 from Rhodobacter Sphaeroides Is Involved in Proton Uptake during the Reaction of the Fully-Reduced Enzyme with Dioxygen. *Biochemistry* **1997**, *36* (45), 13824–13829. https://doi.org/10.1021/bi9629079.

(70) Gygli, S. M.; Borrell, S.; Trauner, A.; Gagneux, S. Antimicrobial Resistance in Mycobacterium Tuberculosis: Mechanistic and Evolutionary Perspectives. *FEMS Microbiol. Rev.* **2017**, *41* (3), 354–373. https://doi.org/10.1093/femsre/fux011.

(71) Calgin, M. K.; Sahin, F.; Turegun, B.; Gerceker, D.; Atasever, M.; Koksal, D.; Karasartova, D.; Kiyan, M. Expression Analysis of Efflux Pump Genes among Drug-Susceptible and Multidrug-Resistant Mycobacterium Tuberculosis Clinical Isolates and Reference Strains. *Diagn. Microbiol. Infect. Dis.* **2013**, *76* (3), 291–297. https://doi.org/10.1016/j.diagmicrobio.2013.02.033.

(72) Burian, J.; Ramón-García, S.; Howes, C. G.; Thompson, C. J. WhiB7, a Transcriptional Activator That Coordinates Physiology with Intrinsic Drug Resistance in Mycobacterium Tuberculosis. *Expert Rev. Anti. Infect. Ther.* **2012**, *10* (9), 1037–1047. https://doi.org/10.1586/eri.12.90.

(73) Grzegorzewicz, A. E.; De Sousa-D'Auria, C.; McNeil, M. R.; Huc-Claustre, E.; Jones, V.; Petit, C.; Angala, S. K.; Zemanová, J.; Wang, Q.; Belardinelli, J. M.; et al. Assembling of the Mycobacterium Tuberculosis Cell Wall Core. *J. Biol. Chem.* **2016**, *291* (36), 18867–18879. https://doi.org/10.1074/jbc.M116.739227.

(74) Jankute, M.; Cox, J. A. G.; Harrison, J.; Besra, G. S. Assembly of the Mycobacterial Cell Wall. *Annu. Rev. Microbiol.* **2015**, *69* (1), 405–423. https://doi.org/10.1146/annurev-micro-091014-104121.

(75) Mishra, A. K.; Driessen, N. N.; Appelmelk, B. J.; Besra, G. S. Lipoarabinomannan and Related Glycoconjugates: Structure, Biogenesis and Role in Mycobacterium Tuberculosis Physiology and Host-Pathogen Interaction. *FEMS Microbiol. Rev.* **2011**,

35 (6), 1126–1157. https://doi.org/10.1111/j.1574-6976.2011.00276.x.

(76) Gilleron, M.; Nigou, J.; Nicolle, D.; Quesniaux, V.; Puzo, G. The Acylation State of Mycobacterial Lipomannans Modulates Innate Immunity Response through Toll-like Receptor 2. *Chem. Biol.* **2006**, *13* (1), 39–47. https://doi.org/10.1016/j.chembiol.2005.10.013.

(77) Hoffmann, C.; Leis, A.; Niederweis, M.; Plitzko, J. M.; Engelhardt, H. Disclosure of the Mycobacterial Outer Membrane: Cryo-Electron Tomography and Vitreous Sections Reveal the Lipid Bilayer Structure. *Proc. Natl. Acad. Sci.* **2008**, *105* (10), 3963–3967.

(78) Park, S.-H.; Bendelac, A. CD1-Restricted T-Cell Responses and Microbial Infection. *Nature* **2000**, *406* (6797), 788.

(79) Tan, Y. Z.; Rodrigues, J.; Keener, J. E.; Zheng, R. B.; Brunton, R.; Kloss, B.; Giacometti, S. I.; Rosário, A. L.; Zhang, L.; Niederweis, M.; Clarke, O. B.; Lowary, T. L.; Marty, M. T.; Archer, M.; Potter, C. S.; Carragher, B.; Mancia, F. Cryo-EM Structure of Arabinosyltransferase EmbB from Mycobacterium Smegmatis. *Nat. Commun.* **2020**, *11* (1), 1–10. https://doi.org/10.1038/s41467-020-17202-8.

(80) Zhang, L.; Zhao, Y.; Gao, Y.; Wu, L.; Gao, R.; Zhang, Q.; Wang, Y.; Wu, C.; Wu, F.; Gurcha, S. S.; et al. Structures of Cell Wall Arabinosyltransferases with the Anti-Tuberculosis Drug Ethambutol. *Science (80-.).* **2020**, *368* (6496), 1211–1219. https://doi.org/10.1126/science.aba9102.

(81) Tan, Y. Z.; Zhang, L.; Rodrigues, J.; Zheng, R. B.; Giacometti, S. I.; Rosário, A. L.; Kloss, B.; Dandey, V. P.; Wei, H.; Brunton, R.; et al. Cryo-EM Structures and Regulation of Arabinofuranosyltransferase AftD from Mycobacteria. *Mol. Cell* **2020**, *78* (4), 683-699.e11. https://doi.org/10.1016/j.molcel.2020.04.014.

(82) Alderwick, L. J.; Birch, H. L.; Krumbach, K.; Bott, M.; Eggeling, L.; Besra, G. S. AftD Functions as an A1 → 5 Arabinofuranosyltransferase Involved in the Biosynthesis of the Mycobacterial Cell Wall Core. *Cell Surf.* **2018**, *1*, 2–14. https://doi.org/10.1016/j.tcsw.2017.10.001.

(83) Pettersen, E. F.; Goddard, T. D.; Huang, C. C.; Couch, G. S.; Greenblatt, D. M.; Meng, E. C.; Ferrin, T. E. UCSF Chimera--a Visualization System for Exploratory Research and Analysis. *J. Comput. Chem.* **2004**, *25* (13), 1605–1612. https://doi.org/10.1002/jcc.20084.

(84) Safi, H.; Lingaraju, S.; Amin, A.; Kim, S.; Jones, M.; Holmes, M.; McNeil, M.; Peterson, S. N.; Chatterjee, D.; Fleischmann, R.; et al. Evolution of High-Level

Ethambutol-Resistant Tuberculosis through Interacting Mutations in Decaprenylphosphoryl-β-D-Arabinose Biosynthetic and Utilization Pathway Genes. *Nat. Genet.* **2013**, *45* (10), 1190–1197. https://doi.org/10.1038/ng.2743.

(85) Pethe, K.; Bifani, P.; Jang, J.; Kang, S.; Park, S.; Ahn, S.; Jiricek, J.; Jung, J.; Jeon, H. K.; Cechetto, J. Discovery of Q203, a Potent Clinical Candidate for the Treatment of Tuberculosis. *Nat. Med.* **2013**, *19* (9), 1157.

(86) Kang, S.; Kim, Y. M.; Jeon, H.; Park, S.; Seo, M. J.; Lee, S.; Park, D.; Nam, J.; Lee, S.; Nam, K.; et al. Synthesis and Structure-Activity Relationships of Novel Fused Ring Analogues of Q203 as Antitubercular Agents. *Eur. J. Med. Chem.* **2017**, *136*, 420–427. https://doi.org/10.1016/j.ejmech.2017.05.021.

(87) Kim, J.; Choi, J.; Kang, H.; Ahn, J.; Hutchings, J.; van Niekerk, C.; Park, D.; Kim, J.; Jeon, Y.; Nam, K.; et al. Safety, Tolerability, and Pharmacokinetics of Telacebec (Q203), a New Antituberculosis Agent, in Healthy Subjects. *Antimicrob. Agents Chemother.* **2022**, *66* (1). https://doi.org/10.1128/AAC.01436-21.

(88) TB Drug monographs http://www.tbdrugmonographs.co.uk/isoniazid.html.

(89) Pethe, K.; Bifani, P.; Jang, J.; Kang, S.; Park, S.; Ahn, S.; Jiricek, J.; Jung, J.; Jeon, H. K.; Cechetto, J.; et al. Discovery of Q203, a Potent Clinical Candidate for the Treatment of Tuberculosis. *Nat. Med.* **2013**, *19* (9), 1157–1160. https://doi.org/10.1038/nm.3262.

(90) Asif, M. An Overview of Various Heterocyclic Imidazopyridine, Triazolopyridine and Quinoline Derivatives and Their Biological Significances. *Moroccan J. Chem.* **2017**, *5* (2), 317–324.

(91) Enguehard-Gueiffier, C.; Gueiffier, A. Recent Progress in the Pharmacology of Imidazo[1,2-a]Pyridines. *Mini Rev. Med. Chem.* **2007**, *7* (9), 888–899. https://doi.org/10.2174/138955707781662645.

(92) L.S. Kishbaugh, T. Pyridines and Imidazopyridines with Medicinal Significance. *Curr. Top. Med. Chem.* **2016**, *16* (28), 3274–3302. https://doi.org/10.2174/1568026616666160506145141.

(93) Chitti, S.; Singireddi, S. R.; Santosh Kumar Reddy, P.; Trivedi, P.; Bobde, Y.; Kumar, C.; Rangan, K.; Ghosh, B.; Sekhar, K. V. G. C. Design, Synthesis and Biological Evaluation of 2-(3,4-Dimethoxyphenyl)-6 (1,2,3,6-Tetrahydropyridin-4-Yl)Imidazo[1,2-a]Pyridine Analogues as Antiproliferative Agents. *Bioorganic Med. Chem. Lett.* **2019**, *29* (18), 2551–2558. https://doi.org/10.1016/j.bmcl.2019.08.013.

(94) Dymińska, L. Imidazopyridines as a Source of Biological Activity and Their

Pharmacological Potentials - Infrared and Raman Spectroscopic Evidence of Their Content in Pharmaceuticals and Plant Materials. *Bioorganic Med. Chem.* **2015**, *23* (18), 6087–6099. https://doi.org/10.1016/j.bmc.2015.07.045.

(95) Mali, S. N.; Pandey, A. Recent Developments in Medicinal and In Silico Applications of Imidazopyridine Derivatives: Special Emphasis on Malaria, Trypanosomiasis, and Tuberculosis. *Chem. Africa* **2022**, *5* (5), 1215–1236. https://doi.org/10.1007/s42250-022-00462-w.

(96) Anaflous, A.; Benchat, N.; Mimouni, M.; Abouricha, S.; Ben-Hadda, T.; El-Bali, B.; Hakkou, A.; Hacht, B. Armed Imidazo [1, 2-a] Pyrimidines (Pyridines): Evaluation of Antibacterial Activity. *Lett. Drug Des. Discov.* **2004**, *1* (3), 224–229.

(97) Nilsson, M. T.; Krajewski, W. W.; Yellagunda, S.; Prabhumurthy, S.; Chamarahally, G. N.; Siddamadappa, C.; Srinivasa, B. R.; Yahiaoui, S.; Larhed, M.; Karlén, A.; et al. Structural Basis for the Inhibition of Mycobacterium Tuberculosis Glutamine Synthetase by Novel ATP-Competitive Inhibitors. *J. Mol. Biol.* **2009**, *393* (2), 504–513. https://doi.org/10.1016/j.jmb.2009.08.028.

(98) Nordqvist, A.; Nilsson, M. T.; Lagerlund, O.; Muthas, D.; Gising, J.; Yahiaoui, S.; Odell, L. R.; Srinivasa, B. R.; Larhed, M.; Mowbray, S. L.; et al. Synthesis, Biological Evaluation and X-Ray Crystallographic Studies of Imidazo[1,2-a]Pyridine-Based Mycobacterium Tuberculosis Glutamine Synthetase Inhibitors. *Medchemcomm* **2012**, *3* (5), 620–626. https://doi.org/10.1039/c2md00310d.

(99) Moraski, G. C.; Markley, L. D.; Hipskind, P. A.; Boshoff, H.; Cho, S.; Franzblau, S. G.; Miller, M. J. Advent of Imidazo[1,2-a]Pyridine-3-Carboxamides with Potent Multi- and Extended Drug Resistant Antituberculosis Activity. *ACS Med. Chem. Lett.* **2011**, *2* (6), 466–470. https://doi.org/10.1021/ml200036r.

(100) Miller, M. J.; Moraski, G. C.; Markley, L. D.; Davis, George, E. Imidazo[1,2-a]Pyridine Compounds, Synthesis Thereof, And Methods Of Using Same. WO 2011/057145 A2, 2011.

(101) Moraski, G. C.; Chang, M.; Villegas-Estrada, A.; Franzblau, S. G.; Möllmann, U.; Miller, M. J. Structure-Activity Relationship of New Anti-Tuberculosis Agents Derived from Oxazoline and Oxazole Benzyl Esters. *Eur. J. Med. Chem.* **2010**, *45* (5), 1703–1716. https://doi.org/10.1016/j.ejmech.2009.12.074.

(102) Moraski, G. C.; Markley, L. D.; Cramer, J.; Hipskind, P. A.; Boshoff, H.; Bailey, M. A.; Alling, T.; Ollinger, J.; Parish, T.; Miller, M. J. Advancement of Imidazo[1,2-

a]Pyridines with Improved Pharmacokinetics and NM Activity vs. Mycobacterium Tuberculosis. *ACS Med. Chem. Lett.* **2013**, *4* (7), 675–679. https://doi.org/10.1021/ml400088y.

(103) No, Z.; Kim, J.; Brodin, P. B.; Seo, M. J.; Kim, Y. M.; Cechetto, J.; Jeon, H.; Genovesio, A.; Lee, S.; Kang, S.; et al. Anti-Infective Compounds. WO 2011/113606 A1, 2011.

(104) No, Z.; Kim, J.; Brodin, P. B.; Seo, M. J.; Kim, Y. M.; Cechetto, J.; Jeon, H.; Genovesio, A.; Lee, S.; Kang, S.; et al. Anti-Infective Compounds. US 2013/0065884, 2013.

(105) Kang, S.; Kim, R. Y.; Seo, M. J.; Lee, S.; Kim, Y. M.; Seo, M.; Seo, J. J.; Ko, Y.; Choi, I.; Jang, J.; et al. Lead Optimization of a Novel Series of Imidazo[1,2-a]Pyridine Amides Leading to a Clinical Candidate (Q203) as a Multi- and Extensively-Drug- Resistant Anti-Tuberculosis Agent. *J. Med. Chem.* **2014**, *57* (12), 5293–5305. https://doi.org/10.1021/jm5003606.

(106) Malík, I.; Čižmárik, J.; Kováč, G.; Pecháčová, M.; Hudecova, L. Telacebec (Q203): Is There a Novel Effective and Safe Anti-Tuberculosis Drug on the Horizon? *Ces. a Slov. Farm. Cas. Ces. Farm. Spol. a Slov. Farm. Spol.* **2021**, *70* (5), 164–171. https://doi.org/10.5817/CSF2021-5-164.

(107) Yanofsky, D. J.; Di Trani, J. M.; Król, S.; Abdelaziz, R.; Bueler, S. A.; Imming, P.; Brzezinski, P.; Rubinstein, J. L. Structure of Mycobacterial CIII2CIV2 Respiratory Supercomplex Bound to the Tuberculosis Drug Candidate Telacebec (Q203). *Elife* **2021**, *10*. https://doi.org/10.7554/eLife.71959.

(108) Kang, S.; Kim, Y. M.; Kim, R. Y.; Seo, M. J.; No, Z.; Nam, K.; Kim, S.; Kim, J. Synthesis and Structure-Activity Studies of Side Chain Analogues of the Anti-Tubercular Agent, Q203. *Eur. J. Med. Chem.* **2017**, *125*, 807–815. https://doi.org/10.1016/j.ejmech.2016.09.082.

(109) Wu, Z.; Lu, Y.; Li, L.; Zhao, R.; Wang, B.; Lv, K.; Liu, M.; You, X. Identification of N-(2-Phenoxyethyl)Imidazo[1,2-a]Pyridine-3-Carboxamides as New Antituberculosis Agents. *ACS Med. Chem. Lett.* **2016**, *7* (12), 1130–1133. https://doi.org/10.1021/acsmedchemlett.6b00330.

(110) Lv, K.; Li, L.; Wang, B.; Liu, M.; Wang, B.; Shen, W.; Guo, H.; Lu, Y. Design, Synthesis and Antimycobacterial Activity of Novel Imidazo[1,2-a]Pyridine-3-Carboxamide Derivatives. *Eur. J. Med. Chem.* **2017**, *137*, 117–125. https://doi.org/10.1016/j.ejmech.2017.05.044.

(111) Wang, A.; Wang, H.; Geng, Y.; Fu, L.; Gu, J.; Wang, B.; Lv, K.; Liu, M.; Tao, Z.; Ma,

C.; et al. Design, Synthesis and Antimycobacterial Activity of Less Lipophilic Q203 Derivatives Containing Alkaline Fused Ring Moieties. *Bioorganic Med. Chem.* **2019**, *27* (5), 813–821. https://doi.org/10.1016/j.bmc.2019.01.022.

(112) O'Malley, T.; Alling, T.; Early, J. V.; Wescott, H. A.; Kumar, A.; Moraski, G. C.; Miller, M. J.; Masquelin, T.; Hipskind, P. A.; Parish, T. Imidazopyridine Compounds Inhibit Mycobacterial Growth by Depleting ATP Levels. *Antimicrob. Agents Chemother.* **2018**, *62* (6), 1–8. https://doi.org/10.1128/AAC.02439-17.

(113) Elliott, A. J.; Guzik, H.; Soler, J. R. On the Reaction of 2-aminopyridines with Alpha-halocarbonyl Compounds. *Journal of Heterocyclic Chemistry*. 1982, pp 1437–1440. https://doi.org/10.1002/jhet.5570190636.

(114) Bhagat, S. B.; Telvekar, V. N. NBS Mediated Protocol for the Synthesis of N-Bridged Fused Heterocycles in Water. *Tetrahedron Lett.* **2017**, No. August. https://doi.org/10.1016/j.tetlet.2017.08.017.

(115) Li, Z.; Khaliq, M.; Zhou, Z.; Post, C. B.; Kuhn, R. J.; Cushman, M. Design, Synthesis, and Biological Evaluation of Antiviral Agents Targeting Flavivirus Envelope Proteins. *J Med Chem* **2008**, *51* (15), 4660–4671. https://doi.org/10.1021/jm800412d.

(116) Lu, F.-L.; Naguib, Y. M. A.; Kitadani, M.; Chow, Y. L. An Investigation of the Photodecomposition of N -Bromosuccinimide; the Generation and Reactivity of Succinimidyl Radical . *Can. J. Chem.* **1979**, *57* (15), 1967–1976. https://doi.org/10.1139/v79-315.

(117) Incremona, J. H.; Martin, J. C. N-Bromosuccinimide. Mechanisms of Allylic Bromination and Related Reactions. *J. Am. Chem. Soc* **1970**, *92* (3), 627–634.

(118) Lindström, U. M.; Andersson, F. Hydrophobically Directed Organic Synthesis. *Angew. Chemie - Int. Ed.* **2006**, *45* (4), 548–551. https://doi.org/10.1002/anie.200502882.

(119) Li, C. J.; Chen, L. Organic Chemistry in Water. *Chem. Soc. Rev.* **2006**, *35* (1), 68–82. https://doi.org/10.1039/b507207g.

(120) Kumar, R. V. Synthetic Strategies towards Benzoxazole Ring Systems: A Review. *Asian J. Chem.* **2004**, *16* (3–4), 1241–1260. https://doi.org/10.1002/chin.200528243.

(121) Kumar, D.; Rudrawar, S.; Chakraborti, A. K. One-Pot Synthesis of 2-Substituted Benzoxazoles Directly from Carboxylic Acids. *Aust. J. Chem.* **2008**, *61* (11), 881–887. https://doi.org/10.1071/CH08193.

(122) Caddick, S.; Judd, D. B.; Lewis, A. K. D. K.; Reich, M. T.; Williams, M. R. V. A Generic Approach for the Catalytic Reduction of Nitriles. *Tetrahedron* **2003**, *59* (29), 5417–

5423. https://doi.org/10.1016/S0040-4020(03)00858-5.

(123) Khurana, J. M.; Kukreja, G. Rapid Reduction of Nitriles to Primary Amines with Nickel Boride at Ambient Temperature. *Synth. Commun.* **2002**, *32* (8), 1265–1269. https://doi.org/10.1081/SCC-120003619.

(124) Paquette, L. A. *Encyclopedia of Reagents for Organic Synthesis, Volume 6, N- Sin*; John Wiley & Sons, 1995.

(125) Ganem, B.; Osby, J. O. Synthetically Useful Reactions with Metal Boride and Aluminide Catalysts. *Chem. Rev.* **1986**, *86* (5), 763–780. https://doi.org/10.1021/cr00075a003.

(126) Yin, B. L.; Cai, C. B.; Lai, J. Q.; Zhang, Z. R.; Huang, L.; Xu, L. W.; Jiang, H. F. Sodium Borohydride-Nickel Chloride-Methanol Catalytic System for Regioselective Reduction of Electron-Rich Conjugated Dienes and Reductive Cleavage of Allyl Esters Involving π-Allylnickel Intermediates. *Adv. Synth. Catal.* **2011**, *353* (18), 3319–3324. https://doi.org/10.1002/adsc.201100612.

(127) Stephanie E. Sen, S. L. R. A Convenient Two-Step Procedure for the Synthesis of Substituted Allylic Amines from Allylic Alcohols. *Thieme E-Journals* **1995**, No. 7, 756–758. https://doi.org/10.1055/s-1995-4012.

(128) Hoelke, B.; Gieringer, S.; Arlt, M.; Saal, C. Comparison of Nephelometric, UV-Spectroscopic, and HPLC Methods for High-Throughput Determination of Aqueous Drug Solubility in Microtiter Plates. *Anal. Chem.* **2009**, *81* (8), 3165–3172. https://doi.org/10.1021/ac9000089.

(129) Bevan, C. D.; Lloyd, R. S. A High-Throughput Screening Method for the Determination of Aqueous Drug Solubility Using Laser Nephelometry in Microtiter Plates. *Anal. Chem.* **2000**, *72* (8), 1781–1787. https://doi.org/10.1021/ac9912247.

(130) Radloff, M.; Elamri, I.; Grund, T. N.; Witte, L. F.; Hohmann, K. F.; Nakagaki, S.; Goojani, H. G.; Nasiri, H.; Hideto Miyoshi; Bald, D.; et al. Short-Chain Aurachin D Derivatives Are Selective Inhibitors of E. Coli Cytochrome Bd-I and Bd-II Oxidases. *Sci. Rep.* **2021**, *11* (1), 1–9. https://doi.org/10.1038/s41598-021-03288-7.

(131) Friedrich, T.; Wohlwend, D.; Borisov, V. B. Recent Advances in Structural Studies of Cytochrome Bd and Its Potential Application as a Drug Target. *Int. J. Mol. Sci.* **2022**, *23* (6). https://doi.org/10.3390/ijms23063166.

(132) Cross, R. M.; Monastyrskyi, A.; Mutka, T. S.; Burrows, J. N.; Kyle, D. E.; Manetsch, R. Endochin Optimization: Structure-Activity and Structure-Property Relationship

Studies of 3-Substituted 2-Methyl-4(1 H)-Quinolones with Antimalarial Activity. *J. Med. Chem.* **2010**, *53* (19), 7076–7094. https://doi.org/10.1021/jm1007903.

(133) Jean-Cristophe Brouet; Shen Gu; Peet, N. P.; John D. Williams. A Survey of Solvents for the Conrad-Limpach Synthesis of 4- Hydroxyquinolones. *Synth. Commun.* **2009**, *39* (9), 5193–5196. https://doi.org/10.1080/00397910802542044.A.

(134) Brouet, J. C.; Gu, S.; Peet, N. P.; Williams, J. D. A Survey of Solvents for the Conrad-Limpach Synthesis of 4-Hydroxyquinolones. *Synth. Commun.* **2009**, *39* (9), 5193. https://doi.org/10.1080/00397910802542044.

(135) Shepherd, R. G.; Baughn, C.; Cantrall, M. L.; Goodstein, B.; Thomas, J. P.; Wilkinson, R. G. Structure-activity Studies Leading to Ethambutol, a New Type of Antituberculous Compound. *Ann. N. Y. Acad. Sci.* **1966**, *135* (1), 686–710.

(136) Wilkinson, R. G.; Cantrall, M. B.; Shepherd, R. G. Antituberculous Agents. III. (+)-2,2-(Ethylenediimino)-Di-1-Butanol and Some Analogs. **1962**, *5* (4), 835–845.

(137) Brown-Elliott, B. A.; Nash, K. A.; Wallace, R. J. Antimicrobial Susceptibility Testing, Drug Resistance Mechanisms, and Therapy of Infections with Nontuberculous Mycobacteria. *Clin. Microbiol. Rev.* **2012**, *25* (3), 545–582.

(138) Kang, Y. A.; Koh, W. J. Antibiotic Treatment for Nontuberculous Mycobacterial Lung Disease. *Expert Rev. Respir. Med.* **2016**, *10* (5), 557–568. https://doi.org/10.1586/17476348.2016.1165611.

(139) Asif, M. Anti-Tubercular Potential of Ethylenediamine Derivatives : A Short Review. *Discov. Chem.* **2015**, *1* (1), 49–54.

(140) Carr, R. E.; Henkind, P. Ocular Manifestations of Ethambutol: Toxic Amblyopia after Administration of an Experimental Antituberculous Drug. *Arch. Ophthalmol.* **1962**, *67* (5), 566–571.

(141) Trebucq, A. Should Ethambutol Be Recommended for Routine Treatment of Tuberculosis in Children? A Review of the Literature. *Int. J. Tuberc. Lung Dis.* **1997**, *1* (1), 12–15.

(142) Yendapally, R.; Lee, R. E. Design, Synthesis, and Evaluation of Novel Ethambutol Analogues. *Bioorganic Med. Chem. Lett.* **2008**, *18* (5), 1607–1611. https://doi.org/10.1016/j.bmcl.2008.01.065.

(143) Lee, R. E.; Protopopova, M.; Crooks, E.; Slayden, R. A.; Terrot, M.; Barry, C. E. Combinatorial Lead Optimization of [1,2]-Diamines Based on Ethambutol as Potential Antituberculosis Preclinical Candidates. *J. Comb. Chem.* **2003**, *5* (2), 172–187.

https://doi.org/10.1021/cc020071p.

(144) Nava-Zuazo, C.; Estrada-Soto, S.; Guerrero-Álvarez, J.; León-Rivera, I.; Molina-Salinas, G. M.; Said-Fernández, S.; Chan-Bacab, M. J.; Cedillo-Rivera, R.; Moo-Puc, R.; Mirón-López, G.; et al. Design, Synthesis, and in Vitro Antiprotozoal, Antimycobacterial Activities of N-{2-[(7-Chloroquinolin-4-Yl)Amino]Ethyl}ureas. *Bioorganic Med. Chem.* **2010**, *18* (17), 6398–6403. https://doi.org/10.1016/j.bmc.2010.07.008.

(145) Häusler, H.; Kawakami, R. P.; Mlaker, E.; Severn, W. B.; Stütz, A. E. Ethambutol Analogues as Potential Antimycobacterial Agents. *Bioorganic Med. Chem. Lett.* **2001**, *11* (13), 1679–1681. https://doi.org/10.1016/S0960-894X(01)00258-X.

(146) Brennan, P.; Crick, D. The Cell-Wall Core of Mycobacterium Tuberculosis in the Context of Drug Discovery. *Curr. Top. Med. Chem.* **2007**, *7* (5), 475–488. https://doi.org/10.2174/156802607780059763.

(147) Vaughan, O. J.; Gibson, J. F. Coordination Chemistry of N,N′-Bis(2-Hydroxyphenyl)Ethylenediamine-N,N′-Diacetic Acid and Some Related Ligands. *Polyhedron* **1990**, *9* (13), 1593–1601. https://doi.org/10.1016/S0277-5387(00)86578-X.

(148) Ranu, B. C.; Bhar, S. Dealkylation of Ethers. A Review. *Org. Prep. Proced. Int.* **1996**, *28* (4), 371–409. https://doi.org/10.1080/00304949609356549.

(149) Soukup-Hein, R. J.; Remsburg, J. W.; Dasgupta, P. K.; Armstrong, D. W. A General, Positive Ion Mode ESI-MS Approach for the Analysis of Singly Charged Inorganic and Organic Anions Using a Dicationic Reagent. *Anal. Chem.* **2007**, *79* (19), 7346–7352. https://doi.org/10.1021/ac071102b.

(150) Yuan, B.; Benskin, J. P.; Chen, C. E. L.; Bergman, Å. Determination of Chlorinated Paraffins by Bromide-Anion Attachment Atmospheric-Pressure Chemical Ionization Mass Spectrometry. *Environ. Sci. Technol. Lett.* **2018**, *5* (6), 348–353. https://doi.org/10.1021/acs.estlett.8b00216.

(151) Cai, Y.; Cole, R. B. Stabilization of Anionic Adducts in Negative Ion Electrospray Mass Spectrometry. *Anal. Chem.* **2002**, *74* (5), 985–991. https://doi.org/10.1021/ac0108818.

(152) Breitbach, Z. S.; Wanigasekara, E.; Dodbiba, E.; Schug, K. A.; Armstrong, D. W. Mechanisms of ESI-MS Selectivity and Sensitivity Enhancements When Detecting Anions in the Positive Mode Using Cationic Pairing Agents. *Anal. Chem.* **2010**, *82* (21), 9066–9073. https://doi.org/10.1021/ac102115w.

(153) Patschinski, P. Chemoselective Silylation of Alcohols Through Lewis Base-Catalyzed

Reactions Experimental and Theoretical Studies. *Thesis* **2015**, 1–263.

(154) Corey, E. J.; Venkateswarlu, A. Protection of Hydroxyl Groups as Tert-Butyldimethylsilyl Derivatives. *J. Am. Chem. Soc.* **1972**, *94* (17), 6190–6191. https://doi.org/10.1021/ja00772a043.

(155) Kim, K. S.; Kimball, S. D.; Misra, R. N.; Rawlins, D. B.; Hunt, J. T.; Xiao, H. Y.; Lu, S.; Qian, L.; Han, W. C.; Shan, W.; et al. Discovery of Aminothiazole Inhibitors of Cyclin-Dependent Kinase 2: Synthesis, x-Ray Crystallographic Analysis, and Biological Activities. *J. Med. Chem.* **2002**, *45* (18), 3905–3927. https://doi.org/10.1021/jm0201520.

(156) Onajole, O. K.; Belewa, X. V.; Coovadia, Y.; Govender, T.; Kruger, H. G.; Maguire, G. E. M.; Naidu, D.; Benesh, S.; Singh, N.; Govender, P. SQ109 Analogues as Potential Antimicrobial Candidates. https://doi.org/10.1007/s00044-010-9490-3.

(157) Tahlan, K.; Wilson, R.; Kastrinsky, D. B.; Arora, K.; Nair, V.; Fischer, E.; Barnes, S. W.; Walker, J. R.; Alland, D.; Barry, C. E. SQ109 Targets MmpL3, a Membrane Transporter of Trehalose Monomycolate Involved in Mycolic Acid Donation to the Cell Wall Core of Mycobacterium Tuberculosis. *Antimicrob. Agents Chemother.* **2012**, *56* (4), 1797–1809.

(158) Zhou, S.; Wang, W.; Zhou, X.; Zhang, Y.; Lai, Y.; Tang, Y.; Xu, J.; Li, D.; Lin, J.; Yang, X.; et al. Structure of Mycobacterium Tuberculosis Cytochrome Bcc in Complex with Q203 and Tb47, Two Anti-Tb Drug Candidates. *Elife* **2021**, *10*, 1–24. https://doi.org/10.7554/eLife.69418.

(159) Rastogi, N.; Goh, K. S.; Bryskier, A.; Devallois, A. Spectrum of Activity of Levofloxacin against Nontuberculous Mycobacteria and Its Activity against the Mycobacterium Avium Complex in Combination with Ethambutol, Rifampin, Roxithromycin, Amikacin, and Clofazimine. *Antimicrob. Agents Chemother.* **1996**, *40* (11), 2483–2487. https://doi.org/10.1128/aac.40.11.2483.

(160) Alcaide, F.; Pfyffer, G. E.; Telenti, A. Role of EmbB in Natural and Acquired Resistance to Ethambutol in Mycobacteria. *Antimicrob. Agents Chemother.* **1997**, *41* (10), 2270–2273. https://doi.org/10.1128/aac.41.10.2270.

(161) T, J. A. S.; J, R.; Rajan, A.; Shankar, V. Features of the Biochemistry of Mycobacterium Smegmatis, as a Possible Model for Mycobacterium Tuberculosis. *J. Infect. Public Health* **2020**, *13* (9), 1255–1264. https://doi.org/10.1016/j.jiph.2020.06.023.

(162) Namouchi, A.; Cimino, M.; Favre-Rochex, S.; Charles, P.; Gicquel, B. Phenotypic and

Genomic Comparison of Mycobacterium Aurum and Surrogate Model Species to Mycobacterium Tuberculosis: Implications for Drug Discovery. *BMC Genomics* **2017**, *18* (1), 25–28. https://doi.org/10.1186/s12864-017-3924-y.

(163) Lelovic, N.; Mitachi, K.; Yang, J.; Lemieux, M. R.; Ji, Y.; States, U.; Sciences, B.; Avenue, C.; States, U. HHS Public Access. **2020**, *73* (11), 780–789. https://doi.org/10.1038/s41429-020-0320-7.Application.

(164) Kao, W. C.; Kleinschroth, T.; Nitschke, W.; Baymann, F.; Neehaul, Y.; Hellwig, P.; Richers, S.; Vonck, J.; Bott, M.; Hunte, C. The Obligate Respiratory Supercomplex from Actinobacteria. *Biochim. Biophys. Acta - Bioenerg.* **2016**, *1857* (10), 1705–1714. https://doi.org/10.1016/j.bbabio.2016.07.009.

(165) Munday, R. Autoxidation of Naphthohydroquinones: Effects of PH, Naphthoquinones and Superoxide Dismutase. *Free Radic. Res.* **2000**, *32* (3), 245–253. https://doi.org/10.1080/10715760000300251.

(166) Fieser, L. F. The Reduction Potentials of Various Phenanthrenequinones. *J. Am. Chem. Soc.* **1929**, *51* (10), 3101–3111. https://doi.org/10.1021/ja01385a032.

(167) Jackson, W. R.; Zurqiyah, A. 985. The Occurrence of 1,2- or 1,4-Addition in the Reduction of Some α,β-Unsaturated Ketones with Metal Hydrides. *J. Chem. Soc.* **1965**, No. 0, 5280–5287. https://doi.org/10.1039/JR9650005280.

(168) Masesane, I. B.; Mazimba, O. NaBH4-Mediated Complete Reduction of the α,β-Unsaturated Ketone Units of Chalcones in the Synthesis of Flavans. In: Gupta Bhowon, M., Jhaumeer-Laulloo, S., Li Kam Wah, H., Ramasami, P. (eds) *Chemistry: The Key to our Sustainable Future.* Springer Netherlands: Dordrecht, 2014; pp 229–235.

(169) Lu, P.; Asseri, A. H.; Kremer, M.; Maaskant, J.; Ummels, R.; Lill, H.; Bald, D. The Anti-Mycobacterial Activity of the Cytochrome Bcc Inhibitor Q203 Can Be Enhanced by Small-Molecule Inhibition of Cytochrome Bd. *Sci. Rep.* **2018**, *8* (1), 1–7. https://doi.org/10.1038/s41598-018-20989-8.

(170) Jang, J.; Kim, R.; Woo, M.; Jeong, J.; Kim, G.; Delorme, V. Efflux Attenuates the Antibacterial Activity of Q203 in Mycobacterium Tuberculosis. *Antimicrob. Agents Chemother.* **2017**, *61* (7), 1–8.

(171) Sorayah, R.; Manimekalai, M. S. S.; Shin, S. J.; Koh, W. J.; Grüber, G.; Pethe, K. Naturally-Occurring Polymorphisms in QcrB Are Responsible for Resistance to Telacebec in Mycobacterium Abscessus. *ACS Infect. Dis.* **2019**, *5* (12), 2055–2060. https://doi.org/10.1021/acsinfecdis.9b00322.

(172) Jumper, J.; Evans, R.; Pritzel, A.; Green, T.; Figurnov, M.; Ronneberger, O.; Tunyasuvunakool, K.; Bates, R.; Žídek, A.; Potapenko, A.; et al. Highly Accurate Protein Structure Prediction with AlphaFold. *Nature* **2021**, *596* (7873), 583–589. https://doi.org/10.1038/s41586-021-03819-2.

(173) Varadi, M.; Anyango, S.; Deshpande, M.; Nair, S.; Natassia, C.; Yordanova, G.; Yuan, D.; Stroe, O.; Wood, G.; Laydon, A.; et al. AlphaFold Protein Structure Database: Massively Expanding the Structural Coverage of Protein-Sequence Space with High-Accuracy Models. *Nucleic Acids Res.* **2022**, *50* (D1), D439–D444. https://doi.org/10.1093/nar/gkab1061.

(174) Zhou, S.; Wang, W.; Zhou, X.; Zhang, Y.; Lai, Y.; Tang, Y.; Xu, J.; Yang, X.; Guddat, L. W.; Wang, Q.; et al. Structure of Mycobacterial Cytochrome Bcc in Complex with Q203 and TB47, Two Anti-TB Drug Candidates 2 3. https://doi.org/10.1101/2021.06.15.448498.

(175) Altschul, S. F.; Gish, W.; Miller, W.; Myers, E. W.; Lipman, D. J. Basic Local Alignment Search Tool. *J. Mol. Biol.* **1990**, *215* (3), 403–410. https://doi.org/10.1016/S0022-2836(05)80360-2.

(176) Madeira, F.; Pearce, M.; Tivey, A. R. N.; Basutkar, P.; Lee, J.; Edbali, O.; Madhusoodanan, N.; Kolesnikov, A.; Lopez, R. Search and Sequence Analysis Tools Services from EMBL-EBI in 2022. *Nucleic Acids Res.* **2022**, gkac240. https://doi.org/10.1093/nar/gkac240.

(177) Waterhouse, A. M.; Procter, J. B.; Martin, D. M. A.; Clamp, M.; Barton, G. J. Sequence Analysis Jalview Version 2-a Multiple Sequence Alignment Editor and Analysis Workbench. *Bioinforma. Appl. NOTE* **2009**, *25* (9), 1189–1191. https://doi.org/10.1093/bioinformatics/btp033.

(178) Wang, J.; Jing, W.; Shi, J.; Huo, F.; Shang, Y.; Wang, F.; Chu, N.; Pang, Y. Bipolar Distribution of Minimum Inhibitory Concentration of Q203 Across Mycobacterial Species. *Microb. Drug Resist.* **2021**, *27* (8), 1013–1017.

(179) Taneja, N. K.; Tyagi, J. S. Resazurin Reduction Assays for Screening of Anti-Tubercular Compounds against Dormant and Actively Growing Mycobacterium Tuberculosis, Mycobacterium Bovis BCG and Mycobacterium Smegmatis. *J. Antimicrob. Chemother.* **2007**, *60* (2), 288–293. https://doi.org/10.1093/jac/dkm207.

(180) Parish, T.; Stoker, N. G. *Mycobacteria Protocols*; 1998. https://doi.org/10.1385/0896034712.

(181) Chauhan, P.; van der Meulen, S. A.; Simões Caetano, J. M.; Goojani, H. G.; Botman, D.; van Spanning, R.; Lill, H.; Bald, D. Response of Mycobacterium Smegmatis to the Cytochrome Bcc Inhibitor Q203. *Int. J. Mol. Sci.* **2022**, *23* (18). https://doi.org/10.3390/ijms231810331.

(182) Hards, K.; Robson, J. R.; Berney, M.; Shaw, L.; Bald, D.; Koul, A.; Andries, K.; Cook, G. M. Bactericidal Mode of Action of Bedaquiline. *J. Antimicrob. Chemother.* **2015**, *70* (7), 2028–2037. https://doi.org/10.1093/jac/dkv054.

(183) Koul, A.; Vranckx, L.; Dhar, N.; Göhlmann, H. W. H.; Özdemir, E.; Neefs, J. M.; Schulz, M.; Lu, P.; Mørtz, E.; McKinney, J. D.; et al. Delayed Bactericidal Response of Mycobacterium Tuberculosis to Bedaquiline Involves Remodelling of Bacterial Metabolism. *Nat. Commun.* **2014**, *5*, 3369. https://doi.org/10.1038/ncomms4369.

(184) Dammann, M.; Stahlecker, J.; Zimmermann, M. O.; Klett, T.; Rotzinger, K.; Kramer, M.; Coles, M.; Stehle, T.; Boeckler, F. M. Screening of a Halogen-Enriched Fragment Library Leads to Unconventional Binding Modes. *J. Med. Chem.* **2022**. https://doi.org/10.1021/acs.jmedchem.2c00951.

(185) Gao, X. hui; Liu, L. bo; Liu, H. ran; Tang, J. jing; Kang, L.; Wu, H.; Cui, P.; Yan, J. Structure–Activity Relationship Investigation of Benzamide and Picolinamide Derivatives Containing Dimethylamine Side Chain as Acetylcholinesterase Inhibitors. *J. Enzyme Inhib. Med. Chem.* **2018**, *33* (1), 110–114. https://doi.org/10.1080/14756366.2017.1399885.

(186) Kou, X.; Shao, Q.; Ye, C.; Yang, G.; Zhang, W. Asymmetric Aza-Wacker-Type Cyclization of N-Ts Hydrazine-Tethered Tetrasubstituted Olefins: Synthesis of Pyrazolines Bearing One Quaternary or Two Vicinal Stereocenters. *J. Am. Chem. Soc* **2018**, *140* (24), 7587–7597. https://doi.org/10.1021/jacs.8b02865.

(187) Miyoshi, H.; Takegami, K.; Sakamoto, K.; Mogi, T.; Iwamura, H. Characterization of the Ubiquinol Oxidation Sites in Cytochromes Bo and Bd from Escherichia Coli Using Aurachin C Analogues. *J. Biochem.* **1999**, *125* (1), 138–142. https://doi.org/10.1093/oxfordjournals.jbchem.a022250.

(188) Schaefer, M.; Perner-storfer, J.; Kadereit, D.; Strobel, H.; Czechtizky, W.; Chen, L., C.; Safarova, A.; Weichsel, A.; Patek, M. Acylamino-Substituted Fused Cyclopentanecarboxylic Acid Derivatives as EDG-2 Receptor Inhibitors and Their Preparation. WO 2009/135590 A1, 2009.

(189) Olsson, M. H. M.; Søndergaard, C. R.; Rostkowski, M.; Jensen, J. H. PROPKA3:

Consistent Treatment of Internal and Surface Residues in Empirical PKa Predictions. *J. Chem. Theory Comput.* **2011**, *7* (2), 525–537. https://doi.org/10.1021/ct100578z.

(190) Roos, K.; Wu, C.; Damm, W.; Reboul, M.; Stevenson, J. M.; Lu, C.; Dahlgren, M. K.; Mondal, S.; Chen, W.; Wang, L.; et al. OPLS3e: Extending Force Field Coverage for Drug-Like Small Molecules. **2019**. https://doi.org/10.1021/acs.jctc.8b01026.

(191) Lu, C.; Wu, C.; Ghoreishi, D.; Chen, W.; Wang, L.; Damm, W.; Ross, G. A.; Dahlgren, M. K.; Russell, E.; Von Bargen, C. D.; et al. OPLS4: Improving Force Field Accuracy on Challenging Regimes of Chemical Space. *Cite This J. Chem. Theory Comput* **2021**, *17*, 4300. https://doi.org/10.1021/acs.jctc.1c00302.

(192) Greenwood, J. R.; Calkins, D.; Sullivan, A. P.; Shelley, J. C. Towards the Comprehensive, Rapid, and Accurate Prediction of the Favorable Tautomeric States of Drug-like Molecules in Aqueous Solution. *J. Comput. Aided Mol. Des.* **2010**, *24*, 591–604.

(193) Shelley, J.C.; Cholleti, A.; Frye, L; Greenwood, J.R.; Timlin, M.R.; Uchimaya, M. Epik: A Software Program for PKa Prediction and Protonation State Generation for Drug-like Molecules. *J. Comp.-Aided Mol. Des.* **2007**, *21*, 681–691.

(194) Watts, K.S.; Dalal, P.; Murphy, R.B.; Sherman, W.; Friesner, R.A.; Shelley, J. C. ConfGen: A Conformational Search Method for Efficient Generation of Bioactive Conformers. *J. Chem. Inf. Model* **2010**, *50*, 543–546.

(195) Friesner, R. A.; Murphy, R. B.; Repasky, M. P.; Frye, L. L.; Greenwood, J. R.; Halgren,T. A.; Sanschagrin, P. C.; Mainz, D. T. Extra Precision Glide: Docking and Scoring Incorporating a Model of Hydrophobic Enclosure for Protein-Ligand Complexes. *J. Med. Chem* **2006**, *49*, 6177–6196.

(196) Halgren, T. A.; Murphy, R. B.; Friesner, R. A.; Beard, H. S.; Frye, L. L.; Pollard, W. T.; Banks, J. L. Glide: A New Approach for Rapid, Accurate Docking and Scoring. 2. Enrichment Factors in Database Screening. *J. Med. Chem* **2004**, *47*, 1750–1759.

(197) Friesner, R. A.; Banks, J. L.; Murphy, R. B.; Halgren, T. A.; Klicic, J. J.; Mainz, D. T.; Repasky, M. P.; Knoll, E. H.; Shaw, D. E.; Shelley, M.; et al. Glide: A New Approach for Rapid, Accurate Docking and Scoring. 1. Method and Assessment of Docking Accuracy. *J. Med. Chem* **2004**, *47*, 1739–1749.

(198) Zulfiya Orynbayeva. PhD Thesis, Drexel University College of Medicine, 2018.

(199) Panov A. *Practical Mitochondriology. Pitfalls and Problems in Studies of Mitochondria. ISBN-10: 1483963853*; 2013.

(200) Koehler, E.; Brown, E.; Haneuse, S. J. P. A. On the Assessment of Monte Carlo Error in Simulation-Based Statistical Analyses. *Am. Stat.* **2009**, *63* (2), 155–162. https://doi.org/10.1198/tast.2009.0030.

(201) Di Trani, J. M.; Liu, Z.; Whitesell, L.; Brzezinski, P.; Cowen, L. E.; Rubinstein, J. L. Rieske Head Domain Dynamics and Indazole-Derivative Inhibition of Candida Albicans Complex III. *Structure* **2022**, *30* (1), 129-138.e4. https://doi.org/10.1016/j.str.2021.08.006.

(202) Zelmer, A.; Carroll, P.; Andreu, N.; Hagens, K.; Mahlo, J.; Redinger, N.; Robertson, B. D.; Wiles, S.; Ward, T. H.; Parish, T.; et al. A New in Vivo Model to Test Anti-Tuberculosis Drugs Using Fluorescence Imaging. *J. Antimicrob. Chemother.* **2012**, *67* (8), 1948–1960. https://doi.org/10.1093/jac/dks161.

(203) Kolbe, K.; Möckl, L.; Sohst, V.; Brandenburg, J.; Engel, R.; Malm, S.; Bräuchle, C.; Holst, O.; Lindhorst, T. K.; Reiling, N. Azido Pentoses: A New Tool To Efficiently Label Mycobacterium Tuberculosis Clinical Isolates. *ChemBioChem* **2017**, *18* (13), 1172–1176. https://doi.org/10.1002/cbic.201600706.

(204) Jumde, R. P.; Guardigni, M.; Gierse, R. M.; Alhayek, A.; Zhu, D.; Hamid, Z.; Johannsen, S.; Elgaher, W. A. M.; Neusens, P. J.; Nehls, C.; et al. Hit-Optimization Using Target-Directed Dynamic Combinatorial Chemistry: Development of Inhibitors of the Anti-Infective Target 1-Deoxy-d-Xylulose-5-Phosphate Synthase. *Chem. Sci.* **2021**, *12* (22), 7775–7785. https://doi.org/10.1039/d1sc00330e.

(205) Franzblau, S. G.; Degroote, M. A.; Cho, S. H.; Andries, K.; Nuermberger, E.; Orme, I. M.; Mdluli, K.; Angulo-Barturen, I.; Dick, T.; Dartois, V.; et al. Comprehensive Analysis of Methods Used for the Evaluation of Compounds against Mycobacterium Tuberculosis. *Tuberculosis* **2012**, *92* (6), 453–488. https://doi.org/10.1016/j.tube.2012.07.003.

Curriculum Vitae (CV)

Education

2019-present	Ph.D. student in Pharmaceutical Chemistry. Martin Luther University, Halle-Wittenberg (MLU).
October 2016- July 2018	M.Sc. in Pharmaceutical Chemistry. German university in Cairo (GUC). GPA: 0.88 (Excellent with Highest Honors). *GPA Scale Max. = 0.7 and Min.= 5.*
October 2011- July 2016	B.Sc. in Pharmacy. German University in Cairo (GUC), Egypt. GPA: 0.8 (Excellent with Highest Honors). *GPA Scale Max. = 0.7 and Min.= 5.*
September 2008- July 2011	Secondary School, General high school certificate. Al-Bashaer School, Cairo, Egypt. Grade: 99.1%.

Research Experience

November 2021-February 2022	Research stay in Prof. John L. Rubinstein's research lab, Department of Biochemistry
2019-present	Ph.D. student in Pharmaceutical Chemistry.
October 2016- July 2018	M.Sc. in Pharmaceutical Chemistry. Thesis title: Design and Synthesis of Ethambutol Analogues and their Testing as Antimycobacterial Agents. Supervisor: Dr. Mohammad Abdel-Halim, Lecturer in Pharmaceutical Chemistry, German University in Cairo (GUC) in collaboration with Prof. Dr. Peter Imming.
June- August 2015	Trainee in Prof. Dr. Peter Imming's Research lab, Head of the Department of Pharmaceutical Chemistry and Clinical Pharmacy, Martin-Luther University, Halle-Wittenberg.
June 2014	Synthesis of organic compounds. Prof. Dr. Ashraf Abadi lab, Pharmaceutical Chemistry Department, German University in Cairo (GUC), Egypt.

Teaching Experience

2019-present	Scientific assistant, Pharmaceutical Chemistry Department, Institute of pharmacy, Martin Luther University, Halle Wittenberg. ○ Organic chemistry practical course (in German)
September 2016-January 2019	Teaching assistant, Pharmaceutical Chemistry Department. German University in Cairo, (GUC). <u>Courses:</u> ○ Chemistry for engineering (Basic Chemistry; Theory only) ○ Physical chemistry (Chemical Kinetics, Thermodynamics, Spectroscopy) ○ Instrumental analysis (Mass spectrometry, Structure Elucidation, Electroanalytical Methods) ○ Pharmaceutical chemistry (Drug metabolism, Antibiotics)

Scholarships and Awards

November 2021-February 2022	Four months fund from the German Academic Exchange Service (DAAD, Project ID: 57556281). Partial funding from the Canada Foundation for Ph.D. Students. (Stiftung für Kanada-Studien, Project no.: T0191/38098/2021).
July-December 2017	Six months fund from the GUC/DAAD/BMBF M.Sc. Projects Scholarship.
2016-2018	Master fellowship from The German University in Cairo (GUC).
2012	DAAD Scholarship for a German course in Ulm.

Languages

Arabic	Fluent (Mother tongue).
English	Fluent (C1).
German	Good (B2).
French	Fair.

Internship

September 2014	Trainee in Future access, patient support program (PSP), SANOFI.
August 2014	Trainee as a retail pharmacist at el Salam pharmacy.

Skills

Research skills
Teaching skills
Communication and Presentation Skills.
Microsoft Office (Word, PowerPoint, Excel).

Extra-Curricular Activity

2016-present	Member in Rotaract Cairo North Club (NGO).
2018-2019	Secretary at Rotaract Cairo North Club (NGO).

Rana Abdelaziz

List of Publications

Abdelaziz, R; Di Trani, J. M; Sahile, H; Mann, L; Richter, A; Liu, Z; Bueler, S. A; Cowen, L. E; Rubinstein, J. L; Imming, P. Imidazopyridine amides: Synthesis, *Mycobacterium smegmatis* $CIII_2CIV_2$ supercomplex binding and *in vitro* antimycobacterial activity. *ACS omega* **2023**. https://doi.org/10.1021/acsomega.3c02259. (Accepted in ACS omega, April 2023)

Yanofsky, D. J., Di Trani, J. M., Krol, S., Abdelaziz, R., Bueler, S. A., Imming, P., Brzezinski, P., & Rubinstein, J. L. (2021). Structure of mycobacterial CIII2CIV2 respiratory supercomplex bound to the tuberculosis drug candidate telacebec (Q203). ELife, 10, 1–18. https://doi.org/10.7554/eLife.71959.

Publications not connected to the thesis

Lang, M.; Ganapathy, U. S.; Mann, L.; Abdelaziz, R.; Seidel, R. W.; Goddard, R.; Sequenzia, I.; Hoenke, S.; Schulze, P.; Aragaw, W. W.; Csuk, R.; Dick, T.; Richter, A. Synthesis and Characterization of Phenylalanine Amides Active against Mycobacterium Abscessus and Other Mycobacteria. *J. Med. Chem.* **2023**. https://doi.org/10.1021/acs.jmedchem.3c00009.

Mann, L.; Ganapathy, U. S.; Abdelaziz, R.; Lang, M.; Zimmerman, M. D.; Dartois, V.; Dick, T.; Richter, A. *In Vitro* Profiling of the Synthetic RNA Polymerase Inhibitor MMV688845 against Mycobacterium Abscessus. *Microbiol. Spectr.* **2022**, *10* (6), e02760-22. https://doi.org/10.1128/spectrum.02760-22.

Tan, Y. Z.; Keon, K. A.; Abdelaziz, R.; Imming, P.; Schulze, W.; Schumacher, K.; Rubinstein, J. L. Structure of V-ATPase from Citrus Fruit. *Structure* **2022**, *30* (10), 1403-1410.e4. https://doi.org/10.1016/J.STR.2022.07.006.

Conference presentations

Presentation at the Pharma research day, Martin Luther University, Halle-Wittenberg, Germany, **June 2019**: An overview on the projects in our research group**:** Antimycobacterial Compounds, NIR Spectroscopy, African Anti-infective Plants.

Poster presentations

Abdelaziz, R; Yanofsky, D. J; Di Trani, J. M; Krol, S; Bueler, S. A; Brezinski, P; Rubinstein, J. L; Imming, P. Analysis of the binding of the antimycobacterial imidazopyridine telacebec to the mycobacterial CIII2CIV2 respiratory supercomplex. Colorado *Mycobacteria* Conference 2022: Focus on NTM **31.05.2022–03.06.2022***;* Fort Collins; Colorado; USA.

Abdelaziz, R; Yanofsky, D. J, Di Trani, J. M; Krol, S; Bueler, S. A; Brezinski, P; Rubinstein, J. L; Imming, P. Analysis of the binding of the antimycobacterial imidazopyridine telacebec to the mycobacterial CIII2CIV2 respiratory supercomplex. Pharma research day **05.07.2022**, Martin Luther University, Halle-Wittenberg, Germany.

Abdelaziz, R; Di Trani, J. M; Sahile, H; Mann, L; Richter, A; Liu, Z; Bueler, S. A; Cowen, L. E; Rubinstein, J. L; Imming, P. Analysis of the binding of imidazopyridine amides to the *Mycobacterium smegmatis* $CIII_2CIV_2$ respiratory supercomplex. Annual conference of the association for Canadian Studies (GKS), **03.03.2023-05.03.2023**, Grainau, Germany.

Abdelaziz, R; Di Trani, J. M; Sahile, H; Mann, L; Richter, A; Liu, Z; Bueler, S. A; Cowen, L. E; Rubinstein, J. L; Imming, P. Analysis of the binding of imidazopyridine amides to the *Mycobacterium smegmatis* $CIII_2CIV_2$ respiratory supercomplex. Gordon research conference: Tuberculosis Drug Discovery and Development (GRS and GRC) **22.07.2023-28.07.2023**, Rey Don Jaime Grand Hotel, Barcelona, Spain. (Abstract accepted).

Eidesstattliche Erklärung

Hiermit erkläre ich, dass ich diese Arbeit selbstständig und nur unter Verwendung der angegebenen Hilfsmittel und Quellen verfasst habe.

Alle Passagen und Abbildungen, die wörtlich oder inhaltlich aus Publikationen übernommen wurden, sind als solche gekennzeichnet. Ferner versichere ich, dass ich diese Arbeit bei keiner anderen Institution eingereicht habe.

Mir ist bekannt, dass bei falschen Angaben die Prüfung als nicht bestanden gilt. Mit meiner Unterschrift bestätige ich die Richtigkeit dieser Angaben und erkenne die Rechtsgrundlage an.

Rana Abdelaziz
Halle (Saale) 02.05.2023